Université de Lille, Faculté des Sciences et Technologies

École Graduée de Biologie Santé de Lille

THESE DE DOCTORAT

En vue de l'obtention du titre de Docteur de l'Université de Lille

Discipline Aspects moléculaires et cellulaires de la biologie

Characterization of LESV and ESV1, two proteins involved in starch metabolism in potato tubers (*Solanum tuberosum*)

Caractérisation de LESV et ESV1, deux protéines impliquées dans le métabolisme de l'amidon des tubercules de pomme de terre

Présentée le 23 octobre 2025

par **Camille LOCQUET**

Pr. Ikram EL YAZIDI	Pr. Université de Lille	Présidente
Pr. Gabrielle POTOCKI-VERONESE	DR, INRAE Toulouse	Rapportrice
Pr. Jérôme PELLOUX	Pr. UPJV, Amiens	Rapporteur
Dr. Cécile RAYNAUD	DR, CNRS, Paris-Saclay	Examinatrice
Dr. David SEUNG	Group leader, JIC, Norwich	Examinateur
Dr. Fabrice WATTEBLED	MCf, HDR, Université de Lille	Directeur de thèse
Dr. Nicolas SZYDLOWSKI	CR, CNRS, Lille	Encadrant de thèse
Dr. Pierre DEVAUX	Directeur Recherche et Innovation, Florimond Desprez, HDR	Encadrant de l'entreprise

REMERCIEMENTS – ACKNOWLEDGMENTS

La réalisation de ce travail de thèse a été un long cheminement personnel, marqué par des apprentissages, des doutes, mais aussi de très belles rencontres. Ce parcours n'aurait pas été possible sans le soutien, la bienveillance et l'implication de nombreuses personnes, à qui je souhaite ici adresser toute ma gratitude.

Je tiens tout d'abord à exprimer ma reconnaissance aux membres du jury : au Pr. Ikram EL YAZIDI, ainsi qu'au Pr. Jérôme Pelloux et au Dr. Gabrielle POTOCKI-VERONESE en qualité de rapporteurs de ce travail, et au Pr. Cécile RAYNAUD et au Dr. David SEUNG en qualité d'examinateurs. Merci à vous tous pour le temps consacré à l'évaluation de cette thèse et pour l'intérêt que vous y avez porté. Thank you all for your time and interest in evaluating this thesis.

Ce projet a vu le jour grâce à la collaboration entre l'équipe « Plant Storage Polysaccharides » et l'entreprise Florimond Desprez Veuve et Fils dirigée par Bruno DESPREZ. Je leur suis reconnaissante d'avoir cru en moi pour ce projet et pour avoir permis de concrétiser ce travail. Merci également à M. Pierre DEVAUX dont les conseils pertinents et la présence bienveillante ont jalonné ces trois années.

Je souhaite ensuite témoigner toute ma gratitude au Dr. Fabrice WATTEBLED, qui a dirigé cette thèse avec patience et bienveillance. Ton écoute, ton soutien dans les moments de doute et ta capacité à trouver les mots justes ont été déterminants pour moi. Je suis certaine que je ne serais pas parvenue à la fin de ces trois années sans ton soutien. Pour cela et pour tout le temps que tu m'as consacré, je tiens à t'adresser un immense merci. Cela a été un honneur pour moi de te battre (presque) chaque jour aux mots fléchés !

Un mot également pour le Dr. Nicolas SZYDLOWSKI, qui a été mon co-encadrant de thèse tout au long de ces trois années. Merci pour ton accompagnement, ta rigueur scientifique, mais aussi pour ta capacité à toujours garder ton calme, même dans les moments où moi, je ne l'étais pas ! Merci aussi pour ta confiance et pour avoir su créer un cadre de travail bienveillant.

Je dois également beaucoup au Pr. Christophe D'HULST. Merci de m'avoir fait confiance lors de mon arrivée au laboratoire, moi qui n'avais alors que peu d'expérience après mon

master. Tes conseils, ta rigueur scientifique et ton humour (même si certains jeux de mots me dépassent encore…) ont été pour moi une source d'inspiration. J'ai énormément appris à tes côtés. Merci également pour tes recommandations de livre et de série, et j'espère que tu prendras la relève des debriefs de Koh-Lanta après mon départ.

Ces années au sein du laboratoire ont été enrichies par toutes les personnes que j'ai eu la chance d'y croiser. À l'ancienne équipe « Plant Storage Polysaccharides », merci pour votre accueil, vos échanges et les moments partagés : Mara BERTI, Coralie BOMPARD, Thibault BOSCART, Adeline COURSEAUX, David DAUVILLEE, Stanislas HELLE, Rayan OSMAN, Pierre OTUSZEWSKI, Claudine RAZANABOAHIRANA, Xavier ROUSSEL et François SEVESTRE. Un merci particulier à Mélanie BOSSU, qui a toujours été une oreille attentive et bienveillante lors de nos pauses café, et à Océane GEORGE, ma « binôme », avec qui j'ai partagé plein de bons moments, entre nos debriefs de week-end, les films de Noël, les pauses café et les virées à la friperie !

Depuis la réorganisation de l'équipe en « Integrative Biology of Storage Polysaccharides », j'ai également eu la chance de côtoyer Jules BEAUVOIS, Anne-Sophie BLERVACQ, Ugo CENCI, Malika CHABI, Christophe COLLEONI, Anne CREACH, Isabelle FABRIZI, Léa FERMONT, Estelle GOULAS et Peggy MISTARZ. Merci à tous pour votre bonne humeur, votre soutien et les échanges enrichissants.

Merci également à l'ensemble du personnel administratif, et en particulier à Laurence, qui m'a aidé à organiser mes déplacements durant ma thèse.

I would like to sincerely thank Dr. David SEUNG, who is a member of this committee, for his warm welcome during my two-month stay at JIC in Norwich. Thank you for the enriching discussions, for making this opportunity possible, and for organizing my visit with such care and attention. It was a truly wonderful experience and I learned a lot during my time there. A special thanks also goes to Carol HUANG, Nitin KAMBLE, Rose MCNELLY, Ciara O'BRIEN, Thomas NAVARRO, Farrukh MAKHAMADJONOV, Petros ZAFEIRIOU, Jinjin DING, and Georgia YIASOUMI for their warm welcome and their help with my experiments.

Je n'oublie pas non plus les séjours à l'INRAE de Nantes, qui m'ont permis d'approfondir mes connaissances sur les propriétés physicochimiques de l'amidon. Merci au Dr. Denis

LOURDIN, à Catherine GARNIER, ainsi qu'à Hyazann HULIN et Lèna BRIONNE pour leur accompagnement.

Merci également à Fabrice BRAY et Stéphanie FLAMENT du laboratoire MSAP pour leur accompagnement en spectrométrie de masse, ainsi qu'à Corentin SPRIET, Thomas BANCE et Nicolas BAROIS de la plateforme BiCeL pour leur aide précieuse en microscopie.

Je souhaite également saluer le suivi attentif et les conseils apportés par le Dr. Jean-Philippe RAL et le Dr. Fabien NOGUE lors de mes CSI. Merci pour vos recommandations.

Mes remerciements vont également à Murielle LOMMEL, Glenda WILLEMS, et Hilde VAN HOUTTE de l'entreprise SESVANDERHAVE, pour nos échanges autour du projet de greffe, et pour leur accueil chaleureux lors de mon séjour à Tirlemont.

Enfin, je voudrais dire quelques mots aux personnes qui me sont les plus chères.

À mes parents, pour leur amour inconditionnel, leur confiance, et leur présence à chaque étape de ma vie : merci papa et maman de m'avoir toujours encouragée à suivre ma voie et m'avoir aidé à grandir. Je vous aime énormément. Merci à mes sœurs, Florine et Noémie, pour leur soutien et leur humour. J'espère que ce manuscrit suffira à vous convaincre que je n'ai pas passé mes journées à regarder des patates pousser ! À Juliette et Martin, merci d'être une filleule et un neveu aussi adorables. Merci également à ma belle-famille, pour sa présence bienveillante tout au long de ces années.

Et surtout, à Romain, l'homme merveilleux qui partage ma vie depuis 8 ans maintenant. Merci à toi d'être un soutien inconditionnel, d'être l'épaule sur laquelle je peux me reposer. Ton amour, ta patience et ta confiance en moi, même dans les moments où je doute de tout sont tellement précieux. Rien de tout cela n'aurait eu la même saveur sans toi à mes côtés.

Ma dernière pensée va à mes grands-parents qui ne sont malheureusement plus de ce monde. J'aurais tant aimé partager cette nouvelle étape de ma vie avec vous, et je sais que j'aurais reçu tout votre soutien et votre amour. Pas un jour ne passe sans que je pense à vous. J'espère que, d'où vous êtes, votre petite-fille vous rend fiers.

TABLE OF CONTENTS

ABSTRACT **12**

RESUME **14**

ABBREVIATONS **17**

INTRODUCTION **19**

CHAPTER 1. POTATO **20**

1. INTRODUCTION TO POTATO 20

1.1. Historical background 20

1.2. Economic importance of potato 21

2. BOTANICAL DESCRIPTION 22

3. GENETICS AND BREEDING 25

4. AGRONOMY AND CULTIVATION PRACTICES 27

CHAPTER 2. STARCH **28**

1. INDUSTRIAL APPLICATIONS 28

2. COMPOSITION AND STRUCTURE 30

2.1. Glucans 30

2.1.1. Amylose 30

2.1.2. Amylopectin 31

2.2. Crystallinity and organization 33

2.3. Other components 35

3. MORPHOLOGY 37

4. DISTRIBUTION OF STARCH IN PLANTS 39

CHAPTER 3. STARCH METABOLISM **40**

1. SYNTHESIS 40

1.1. ADP-Glc synthesis 40

1.2. Amylose synthesis requires the major enzyme GBSS 41

1.3. The complex process of amylopectin synthesis 42

1.3.1. Implication of soluble starch synthases 42

1.3.2. Formation of the α-1,6 linkages by branching enzymes 44

1.3.3. Debranching enzymes play a role in the maturation of the glucans 45
2. DEGRADATION 47
2.1. Initiation of Starch Degradation: The Role of Phosphorylation 47
2.2. Hydrolysis of amylose and amylopectin: the role of Amylases and Debranching Enzymes 49
2.3. Dephosphorylation 49
2.4. The role of DPE 49
2.5. Phosphorylases 50
3. INITIATION 52
3.1. SS4, the central initiating enzyme 52
3.2. PII1/MRC and MFP1: structural regulators of localization 54
3.3. PTST2 and PTST3 are involved in primers delivery 57
3.4. SS5 : a noncanonical modulator 59
3.5. Protein-protein interactions 60
3.6. The role of isoamylases in suppressing excessive granule initiation 63
3.7. Suspected implication of Pho1 in granule initiation 64
4. ESV1 AND LESV: TWO RECENTLY IDENTIFIED PROTEINS INFLUENCING STARCH METABOLISM 67
4.1. ESV1 and LESV structure 67
4.2. ESV1 and LESV localization 70
4.3. ESV1 and LESV conservation in plant kingdom 72
4.4. ESV1 and LESV deficient and overexpressing plants 73
4.5. ESV1 and LESV expression promote insoluble glucan accumulation 77
4.6. LESV and ESV1 promote and stabilize amylopectin phase transition 80
4.7. LESV is involved in ISA1 targeting to starch in rice 83
4.8. LESV and ESV1 influence in vitro activities of enzymes involved in starch metabolism 84
4.9. ESV1 is involved in the gravitropism perception 86
CHAPTER 4. PROBLEMATIC AND OBJECTIVES OF THIS WORK 87

MATERIAL AND METHODS 88

PLANT MATERIAL AND GROWTH CONDITIONS 89
SELECTION OF TARGETS AND PLASMIDS CONSTRUCTS 89
***AGROBACTERIUM*-MEDIATED TRANSFORMATION 90**
CHARACTERIZATION OF INDUCED MUTATIONS 91
STARCH EXTRACTION 91
STARCH, GLUCOSE AND WATER-SOLUBLE POLYSACCHARIDES CONTENT 92

COLOR EVALUATION AFTER FRYING **92**
GRANULOMORPHOMETRY **93**
SCANNING ELECTRON MICROSCOPY **93**
ASSAY OF PHOSPHORYLATED GLUCOSE RESIDUES IN STARCH **93**
LABEL-FREE QUANTITATIVE PROTEOMICS **94**
OPTICAL AND SCANNING ELECTRON MICROSCOPY **94**
WIDE-ANGLE X-RAY SCATTERING **95**
SMALL-ANGLE X-RAY SCATTERING (SAXS) **95**
MAXIMUM WAVELENGTH OF STARCH/IODINE COMPLEX **95**
DETERMINATION OF AMYLOSE CONTENT **96**
CHAIN LENGTH DISTRIBUTION **96**
***IN VITRO* ENZYMATIC HYDROLYSIS OF STARCH** **97**
PASTING PROPERTIES **97**
DIFFERENTIAL SCANNING CALORIMETRY **97**
FILTER FRACTIONATION OF STARCH GRANULES **98**
PROTEIN-PROTEIN INTERACTION ASSAYS **98**
UNTARGETED APPROACH: IMMUNOPRECIPITATION ON TUBERS AND MASS SPECTROMETRY 98
TARGETED APPROACH: TRANSIENT EXPRESSION OF PROTEINS IN *NICOTIANA BENTHAMIANA* AND IMMUNOPRECIPITATION 99
YEAST-TWO HYBRID ASSAYS 99
PREPARATION OF LEAF SECTIONS FOR MICROSCOPY OBSERVATION **100**

RESULTS **101**

1. PRODUCTION OF *LESV* AND *ESV1* MUTANTS **102**
1.1. TARGETED MUTAGENESIS OF *LESV* AND *ESV1* GENE USING THE CRISPR/CAS9 APPROACH 102
1.2. MUTATION VERIFICATION BY GENOTYPING 104
2. CHARACTERIZATION OF MUTANTS AT THE PLANT LEVEL **107**
2.1. IMPACT OF MUTATIONS ON PLANT DEVELOPMENT 107
2.2. CARBOHYDRATE CONTENT IN MUTANT LINES 108
2.3. IMPACT OF MUTATIONS ON COLD-INDUCED SWEETENING 109
3. INFLUENCE OF *LESV* AND *ESV1* INACTIVATION ON STARCH GRANULE MORPHOLOGY AND STRUCTURE **112**
3.1. STARCH GRANULE MORPHOLOGY IS DRASTICALLY AFFECTED IN *LESV* MUTANTS 112
3.2. STARCH ULTRASTRUCTURE IS UNAFFECTED IN BOTH *LESV* AND *ESV1* MUTANTS 116
3.3. *LESV* AND *ESV1* MUTATIONS AFFECT STARCH PHOSPHATE CONTENT 118

4. PHYSICOCHEMICAL PROPERTIES OF STARCH 120
4.1. A-AMYLOLYSIS OF STARCH GRANULES 120
4.2. PASTING PROPERTIES 120
4.3. DIFFERENTIAL SCANNING CALORIMETRY 122
5. PROTEOMICS AND PROTEIN INTERACTIONS 124
5.1. STARCH GRANULE PROTEOME 124
5.2. PROTEIN-PROTEIN INTERACTIONS STUDIES 126
5.2.1. Untargeted approach: immunoprecipitation from tubers and mass spectrometry 126
5.2.2. Transient expression of LESV and ISA1 proteins for pairwise immunoprecipitation 129
5.2.3. Yeast two hybrid assay 131
6. COMPLEMENTARY ANALYSES TO FURTHER EXPLORE THE *LESV* AND *ESV1* PHENOTYPE 134
6.1. GRANULE SIZE-BASED SEPARATION AND FRACTION CHARACTERIZATION 134
6.2. GRANULE MORPHOLOGICAL EVOLUTION ALONG TUBER DEVELOPMENT 137
6.3. STARCH GRANULES IN *LESV* AND *ESV1* LEAVES 139
6.4. CHARACTERIZATION OF *SS5* KNOCK-OUT MUTANTS 142

DISCUSSION AND PERSPECTIVES 145

***LESV* MUTATION ALTERS THE REGULATION OF STARCH INITIATION IN POTATO TUBER 146**
DIVERGENCE IN THE CONTROL OF STARCH GRANULE INITIATION ACROSS ORGANS AND SPECIES 153
SS5 QUANTITY IS STRONGLY INCREASED IN GRANULES OF *LESV* MUTANTS 160
***LESV* MUTATION ALTERS STARCH PHOSPHORYLATION AND FUNCTIONAL PROPERTIES 161**
***ESV1* MUTANTS HAVE A WILD-TYPE PHENOTYPE 163**

ANNEX PROJECT 1: PRODUCTION OF HERITABLE TRANSGENE FREE GENE EDITED PLANTS 166

1. INTRODUCTION 167
2. MATERIAL AND METHODS 170
PLASMID CONSTRUCT 170
DESIGN OF THE GRNAS TARGETING *GBSS* 171
GRAFTING PROCEDURE 172
3. RESULTS 172
3.1. DESIGN OF THE GRNAS 172
3.2. PRODUCTION OF THE TRANSGENIC SCION 174
3.3. GRAFTING OF TRANSGENIC SCIONS ON WILD-TYPE ROOTSTOCKS 175

4. DISCUSSION 176

ANNEX PROJECT 2 : ENZYMATIC CHARACTERIZATION OF SS6 179

1. INTRODUCTION 180

2. A CAPILLARY ELECTROPHORESIS METHOD FOR DETERMINING STARCH-SYNTHASE ACTIVITIES 182

2.1. INTRODUCTION 182

2.2. METHODS 183

3. PRODUCTION, PURIFICATION AND ENZYMATIC CHARACTERIZATION OF SS6 PROTEIN 186

3.1. MATERIAL AND METHODS 186

Bacterial material 186

Production of SS6 recombinant protein 187

Purification of SS6 recombinant protein 187

SDS-PAGE and native gel 188

Enzymatic characterization - General Conditions 188

3.2. RESULTS 191

3.2.1. PRODUCTION OF THE SS6-HIS-TAG RECOMBINANT PROTEIN 191

3.2.2. ENZYMATIC CHARACTERIZATION OF SS6 RECOMBINANT PROTEIN 192

4. DISCUSSION 194

LITERATURE 196

LIST OF FIGURES 220

LIST OF TABLES 224

ANNEXES 225

ABSTRACT

Potato (*Solanum tuberosum*) is the world's fourth most important food crop, widely used for various industrial applications due to its high starch content and functional properties. Despite significant advances in understanding starch biosynthesis and degradation, the molecular mechanisms underlying starch granule initiation remain poorly understood, particularly in tuber-forming species such as potato.

This thesis investigates the roles of two non-enzymatic proteins, LESV (Like Early Starvation 1) and ESV1 (Early Starvation 1), in potato starch metabolism. Both proteins were previously identified in the starch granule proteome, and homologs in *Arabidopsis thaliana* are known to be involved in the regulation of transient starch. CRISPR/Cas9 genome editing was used to generate *lesv* and *esv1* mutant lines, which were characterized at the phenotypic, structural, biochemical, and proteomic levels.

In *lesv* mutants, starch granule size was significantly reduced, and granules frequently appeared as small, tightly packed aggregates, a phenotype not observed in wild-type tubers. This indicates a major role for LESV in the initiation of starch granules in potato. In contrast, starch from *lesv* mutant leaves displayed minor or opposite trends, suggesting organ-specific differences in LESV function and a more dominant role in tubers. Yeast two-hybrid assays revealed that potato LESV interacts with the debranching enzyme ISA1, raising the hypothesis that this interaction facilitates targeting of the ISA1/ISA2 complex to the starch granule, thereby contributing to granule initiation. Interestingly, SS5 levels were significantly increased in starch granules of *lesv* mutants, despite the absence of any phenotype in *ss5* mutants, suggesting a possible compensatory mechanism that remains to be explored.

Furthermore, *lesv* starch displayed increased phosphate content (notably at C6 positions), enhanced susceptibility to enzymatic hydrolysis, and altered functional properties including reduced gelatinization temperature and higher viscosity. These are directly related to the diminution of the starch granule diameter.

Altogether, these findings position LESV as a key regulator of starch granule initiation in potato tubers, potentially acting via protein–protein interactions rather than enzymatic activity.

By contrast, *esv1* mutants did not show any major changes in starch granule morphology or size under the tested conditions. However, changes were observed in their functional properties: a decrease in paste viscosity and phosphate content along with an increased susceptibility to enzymatic hydrolysis. These findings suggest the presence of subtle structural defects in the starch that are not detectable by conventional analytical methods. While ESV1 does not appear to be essential for granule initiation in potato tubers, it may contribute to the internal organization or architecture of amylopectin, possibly influencing the crystalline or branching structure.

The presence of LESV in *esv1* mutant plants could partially compensate for the loss of ESV1, explaining the mild phenotype. This idea is reinforced by the highly conserved C-terminal domain shared by LESV and ESV1, hinting at potential functional redundancy.

This work sheds light on poorly understood aspects of starch metabolism and opens new perspectives for biotechnological applications aimed at modulating starch properties for industrial uses.

RESUME

Titre : Caractérisation de LESV et ESV1, deux protéines impliquées dans le métabolisme de l'amidon des tubercules de pomme de terre

La pomme de terre (*Solanum tuberosum*) est la quatrième culture la plus importante au monde derrière le maïs, le blé et le riz. En raison de son contenu élevé en amidon, de son haut rendement par unité de surface et de ses propriétés épaississantes uniques, elle joue un rôle clé dans diverses industries, notamment la papeterie, le textile, le secteur énergétique et la pharmacie. L'amidon constitue également la source principale de glucides pour l'alimentation humaine et du bétail. La culture de la pomme de terre revêt une importance particulière dans le Nord et l'Est de la France, où elle alimente l'industrie agroalimentaire. Malgré les progrès réalisés dans la compréhension de la biosynthèse et de la dégradation de l'amidon, de nombreux aspects de son métabolisme demeurent mal compris.

L'amidon est une réserve essentielle de glucides dans les plantes, stockée principalement sous forme de grains dans les plastes des cellules. Les mécanismes moléculaires régissant la formation et l'initiation des grains d'amidon ne sont que partiellement élucidés, notamment dans les tubercules de pomme de terre. Cette thèse vise à approfondir la compréhension du rôle de plusieurs protéines dans ce phénomène et, plus largement, dans le métabolisme de l'amidon. Des études récentes sur le protéome de l'amidon de pomme de terre ont permis l'identification de deux protéines importantes : ESV1 (Early Starvation 1) et LESV (Like Early Starvation 1), bien qu'aucun site catalytique n'ait été identifié dans ces protéines. Des travaux menés sur *Arabidopsis thaliana* ont montré que LESV et ESV1 jouent un rôle dans la régulation de l'amidon transitoire. Leur présence dans le grain d'amidon, ainsi que la forte abondance de LESV, laissent à penser que ces protéines pourraient jouer un rôle important dans le métabolisme de l'amidon chez la pomme de terre.

L'objectif principal de cette thèse est donc d'étudier le rôle de LESV et ESV1 dans le métabolisme de l'amidon chez la pomme de terre. Pour ce faire, des lignées mutantes ont été produites en utilisant l'approche CRISPR/Cas9. LESV se révèle être un acteur clé dans l'initiation des grains d'amidon, un processus qui varie selon les espèces et les organes étudiés. Alors que dans *Arabidopsis thaliana*, la protéine SS4 joue un rôle majeur dans l'initiation des grains d'amidon des feuilles, LESV semble assumer cette fonction dans les

tubercules de pomme de terre. Cette divergence entre espèces souligne la complexité des mécanismes de formation des grains d'amidon.

Nos résultats montrent que les mutants *lesv* présentent une diminution significative de la taille des grains d'amidon, accompagnée d'une accumulation de petits grains formant des agrégats. Cela suggère que la protéine LESV est indispensable au bon déroulement de l'initiation des grains d'amidon. A l'inverse, l'analyse préliminaire des mutants *lesv* dans les feuilles de pomme de terre a montré des changements moins prononcés et même contraires à ceux observés dans les tubercules, suggérant que LESV joue un rôle secondaire dans le métabolisme de l'amidon des feuilles.

Nous avons également observé, grâce à des expérimentations de double hybride dans la levure, qu'à l'instar du riz, la protéine LESV de pomme de terre est capable d'interagir avec l'enzyme de débranchement ISA1, Cette interaction pourrait être responsable de la fixation à l'amidon du complexe ISA1/ISA2, qui joue un rôle dans l'initiation des grains d'amidon.

Une autre découverte intéressante de cette thèse est l'augmentation significative de l'abondance de SS5 dans les grains d'amidon des mutants *lesv*, bien que les mutants *ss5* ne présentent aucun phénotype visible dans les mêmes conditions expérimentales. Cette observation suggère que SS5 pourrait compenser l'absence de LESV dans l'initiation des grains d'amidon. Toutefois, le rôle exact de SS5 dans ce contexte nécessite de plus amples recherches. Ces résultats ouvrent la voie à de futures investigations sur l'interaction potentielle entre LESV et SS5, ainsi que sur les mécanismes régulant l'initiation des grains d'amidon dans les tubercules de pomme de terre.

Concernant la phosphorylation de l'amidon, les mutants *lesv* présentent une augmentation marquée des niveaux de phosphates, notamment au niveau des résidus O-6-phosphoester. Cette modification semble être liée à la diminution de la taille des grains. Ce phénomène est accompagné d'une accélération notable de la vitesse d'hydrolyse de l'amidon, probablement pour la même raison, facilitant l'accès des enzymes. Enfin, l'étude des mutants *lesv* et *esv1* a également révélé des différences intéressantes dans les propriétés fonctionnelles de l'amidon, comme une température de gélatinisation réduite et une viscosité plus élevée pour l'amidon du mutant *lesv.* En revanche, le mutant *esv1* présente une viscosité réduite, ce qui indique des défauts dans la structure du grain ou l'architecture de

l'amylopectine, défauts qui n'ont pas été détectés par les méthodes utilisées dans cette étude. De telles modifications pourraient avoir d'intéressantes applications industrielles.

En conclusion, cette thèse met en évidence le rôle majeur de LESV dans l'initiation des grains d'amidon dans les tubercules de pomme de terre et suggère que ce mécanisme pourrait être modulé par des interactions avec d'autres protéines. Bien que les mécanismes précis restent à élucider, les résultats obtenus ouvrent de nouvelles perspectives pour la compréhension d'initiation du grain d'amidon et de sa régulation dans les tubercules de pomme de terre. Ces travaux pourraient également avoir des applications pratiques dans le domaine de la biotechnologie, notamment pour la modification des propriétés fonctionnelles de l'amidon destiné à des fins industrielles.

J'ai personnellement généré l'ensemble des données présentées ici, à l'exception de la production initiale des mutants *lesv* et *esv1* réalisée par M. Berti, des analyses de spectrométrie de masse effectuées par F. Bray (MSAP), des images de microscopie électronique à balayage produites en collaboration avec N. Barois (Plateforme BiCeL), ainsi que des analyses de diffraction des rayons X réalisées en collaboration avec H. Hulin de l'unité BIA à l'INRAE de Nantes et G. Stoclet de l'UMR 8207 – UMET à l'Université de Lille.

ABBREVIATONS

AD	Activation Domain
APTS	8-Aminopyrene-1,3,6-Trisulfonic Acid
BD	DNA-Binding Domain
BE	Branching Enzyme
Cefo	Cefotaxime
CIS	Cold Induced Sweetening
CRISPR/Cas9	Clustered Regularly Interspaced Short Palindromic Repeats/CRISPR associated 9
cv.	Cultivar
DBE	Debranching Enzyme
DDO	Double Dropout medium
DNA	Deoxyribonucleic Acid
DP	Degree of Polymerization
DSC	Differential Scattering Calorimetry
DTT	Dithiothreitol
eFASP	enhanced Filter Aided Sample Preparation
ESV1	EARLY STARVATION 1
G3P	Glucose-3-P
G6P	Glucose-6-P
GA3	Gibberellic Acid
Genta	Gentamicin
Glc	Glucose
IAA	Indole-3-Acetic Acid
Indel	Insertion/deletion
IPTG	Isopropyl β-D-1-thiogalactopyranoside
ISA	Isoamylase
gRNA	guide RNA
Kan	Kanamycin
KO	Knock-Out
LB medium	Lysogeny Broth
LESV	LIKE EARLY STARVATION 1

LFQ	Label Free Quantification
MFP	Mar-binding Filament-like Protein 1
MRC	Myosin Resembling Chloroplast protein
MS medium	Murashig & Skoog medium
MS	Mass Spectrometry
PAM	Protospacer Adjacent Motif
PCR	Polymerase Chain Reaction
PII1	Protein Involved in starch Initiation 1
PTST	Protein Targeting To Starch
QDO	Quadruple Dropout medium
RVA	Rapid Visco Analyzer
Rif	Rifampicin
RVA	Rapid Visco Analyzer
SAXS	Small Angle X-ray Scattering
SDS	Sodium Dodecyl Sulfate
SEM	Scanning Electron Microscopy
SS	Starch Synthase
TFA	Trifluoro Acetic Acid
Tim	Timentin
WAXS	Wide Angle X-ray Scattering
X-Gal	X-Galactose
Y2H	Yeast Two Hybrid
ZR	Zeatin-Riboside

INTRODUCTION

Chapter 1. Potato

1. Introduction to potato

The potato significance as a global food crop, coupled with its unique starch properties, makes it an ideal subject for exploring starch metabolism. This research project aims to contribute to our understanding of starch metabolism in potato, a fundamental aspect of tuber quality and food processing. By investigating starch metabolism pathways, this research intents to clarify the mechanisms involved in granule initiation, providing data that could be used in potato varietal improvement programs.

1.1. Historical background

The history of potato begins in high-altitude regions of South America, where it was first domesticated. Archeological evidences suggest that hundreds of potato varieties began to be cultivated 8000 years ago (Reader, 2008). In the Andes, potato was not only a food source but was also central to the culture. The potato remained a South American crop until the 16th century.

After the Spanish conquest of the Inca Empire, potato was brought to Europe (Rousselle & Robert, 1996). Several reasons prevented its spread for a long time. First, because of its similarities to other toxin-producing species belonging to the *Solanaceae* family (e.g. mandrake, datura, belladonna), it was assimilated to the other plants of this family (Salaman, 1949). Second, the Andean varieties that were initially introduced in Europe were better adapted to short-day conditions. The progressive adaptation to long-day conditions took almost two hundred years, with a work of selection and with the introduction of Chilean varieties, better adapted to long-day conditions (Rousselle & Robert, 1996). Third, the agricultural system of the 16th century was strongly regulated and did not allow the introduction of new species in the three-year rotation system, mainly based on cereals (Rousselle & Robert, 1996). It was necessary to wait the second half of the 18th century and the French Revolution, to see the rules of a “New Agriculture” emerging, defended by philosophers of the Age of Enlightenment. A complete remodeling of the landscape appeared in order to feed a growing urban population. Finally, the potato’s underground growth also

contributed to reluctance to adopt it as a food source. During the Middle Ages, crops growing into the soil were often considered impure by popular religious superstition (Salaman, 1949).

Over time, the potato began to spread across Europe. Its advantages as a high-calorie and easy-to-grow crop were recognized during periods of food shortages. In the 18th century, the popularity of potato increased in Europe, due to the efforts of persons like Antoine Augustin Parmentier in France, who defended its benefits (Reader, 2008). The crop played a crucial role in times of war and poor harvests, and its cultivation contributed to significant population growth.

However, reliance on the potato as a primary food source also had consequences. In Ireland, where it became the main staple food, a catastrophic event known as the Great Irish Famine happened in the middle of the 19th century. The famine was caused by a potato disease called *Phytophthora infestans*, commonly referred to as potato blight (Salaman, 1949). This fungal disease devastated potato crops across Ireland, leading to mass starvation and emigration.

By the 18th century, potato had already spread beyond Europe, reaching other parts of the world. Spanish and Portuguese sailors took it to Asia. By the 19th century, potato was also cultivated in Africa and North America, where it was initially introduced by European settlers (Reader, 2008). Potato has become a dietary staple in many parts of the world and is used boiled, baked, fried, mashed, and processed into food products.

1.2. Economic importance of potato

The cultural, economic, social and environmental importance of potato and its contribution to food security and nutrition are essential. Nowadays, potato is a pillar of agriculture. The cultivated diversity of *Solanum tuberosum* is considerable. In Europe alone, more than 6000 registered potato cultivars are listed in the European Cultivated Potato Database (ECPD, https://www.europotato.org/). On a global scale, the International Potato Center (CIP) based in Peru conserves over 7,000 accessions in its gene bank (CIP, https://cipotato.org/) including cultivated varieties, landraces, and wild relatives, making it the most comprehensive collection of potato genetic resources worldwide, and offering a genetic wealth to combat pests, diseases, and impacts of climate change. The cultural and

economic significance of the potato has importantly increased over time, becoming an essential component of global agriculture. In the past decade, global production of potatoes has increased by 10 percent, leading to higher incomes, making the potato the fourth largest crop worldwide with an estimated production of over 374 million tons (Mt) in 2022, ranking behind maize (1163 Mt), wheat (808 Mt) and rice (776 Mt) (https://www.fao.org/faostat/en/#data).

Parmentier, who popularized the potato by demonstrating its nutritional value during times of famine, laid the foundation for the widespread adoption of the potato as a staple food in France. Today, France is one of the largest producers of potatoes in Europe, with most of its production concentrated in the northern regions such as Hauts-de-France, where climatic conditions are ideal for potato cultivation. The country produces over 8 million tons of potatoes annually, with around 60% of production concentrated in the region Hauts-de-France (https://www.fao.org/faostat/en/#data).

2. Botanical description

Potato is a member of the Solanaceae family which also includes tomato, tobacco, eggplant, and pepper. This family is known for its species that produce both food crops and some toxic plants, rich in alkaloids. The term “potato” refers to hundreds of different species. The most common, *Solanum tuberosum*, is highly cultivated for its tubers that grows underground and serves as energy storage organ for the plant (Rousselle & Robert, 1996). The tubers are rich in starch, making them a valuable source of energy for both humans and animals.

The potato plant can reproduce both sexually through seeds and vegetatively via tubers. Sexual reproduction via seeds, resulting from potato flowers, is rare in agriculture but can be used in breeding programs to develop new varieties. Farmers typically plant "seed potatoes", which are pieces of tubers with buds that sprout and grow into new plants. Its reproduction is then ensured by the tuber, a reserve organ rich in water and nutrients.

Potato plant grows up to 60 cm tall. The above-ground part of the plant consists of branching stems and leaves, with compound leaves made of leaflets (Figure 1). The stems of

the potato plant produce stolons that extend underground, from which the tubers develop (Figure 1).

After planting the mother tuber (Figure 1), its sprouts elongate until they reach soil level (Rousselle & Robert, 1996). At the same time the roots, that grow close to the soil surface, begin to elongate. During this period, the plant is dependent of the reserves of the mother tuber. Potato has both above-ground and below-ground stems. The above-ground stems are green branching stems that produce leaves and flowers (Figure 1). Potato flowers can vary in color (white, purple, pink, or blue) depending on the variety and the petals form a star shape, characteristic of the *Solanaceae* family. Above-ground stems are photosynthetic and essential for capturing energy from sunlight. After flowering, some potato plants develop small, green, tomato-like fruits, which contain seeds. However, these berries are not edible because they contain toxic alkaloids. As the plant approaches the end of its life cycle, leaves and stems begin to fade, and tubers reach full size.

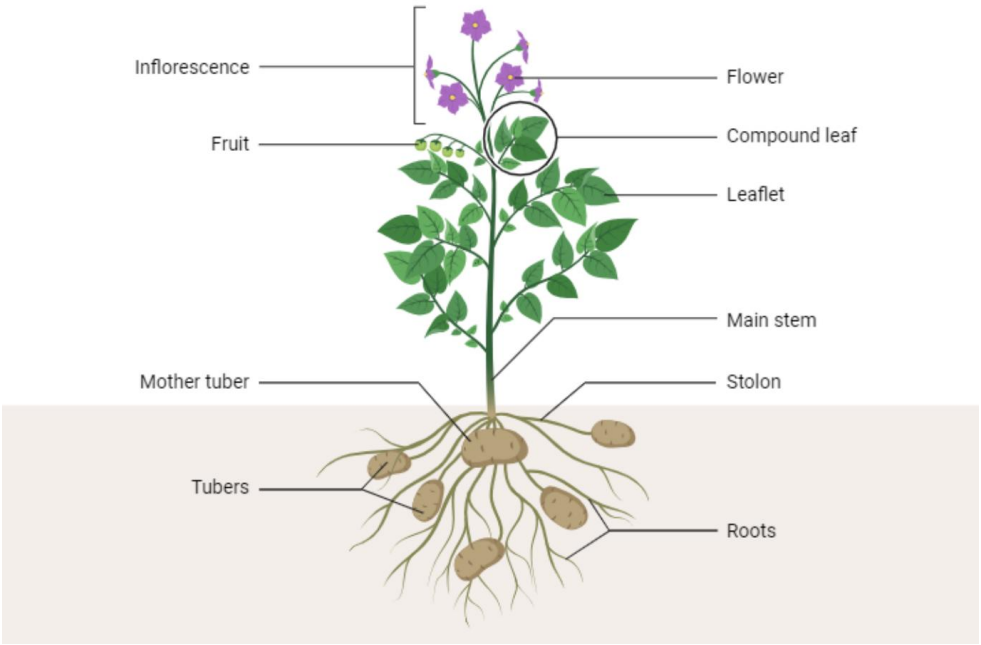

Figure 1: Potato plant anatomy. (Kim, S. (2023). Potato Plant Anatomy. (https://app.biorender.com/biorender-templates/figures/all/t-65539435ba8e0fbd36a182e3-potato-plant-anatomy))

Below the soil, the plant forms stolons, which are horizontal underground stems (Figure 1). After a certain time, the tubers are formed at the ends of the underground stolons,

which enlarge as starch and nutrients accumulate. The formation of tuber primordia usually occurs in a very short time (1 to 2 weeks) for most varieties. All tubers formed by a plant are therefore approximately the same age, regardless of their size at the time of harvest. The differences in growth rate and final size observed between tubers of a plant are due to inter-plant and intra-plant competition.

Tubers function as storage organs for nutrients. This storage capacity not only helps the plant survive hard conditions but also makes potato a valuable food crop for humans. Each tuber has multiple “eyes”, which are nodes with small buds capable of sprouting new shoots. Potato can be propagated by planting tuber sections, as each eye can produce a new plant. Potato varieties show a wide range of morphological traits (e.g., tuber size, shape, skin color, flesh color), resulting from selective breeding and genetic diversity. This diversity supports breeding programs that are aimed at improving yield, pest resistance, and other desirable traits.

Tubers are primarily composed of carbohydrates, mostly in the form of starch, making it a significant source of energy (Rousselle & Robert, 1996). A high level of resistant starch can develop when potatoes are cooked and then cooled. Unlike grains, potato is naturally gluten-free and is an important food option for people with gluten sensitivities.

Potato is also a source of fiber, highly present in its periderm (skin). Although potato is not high in protein (about 2g per 100g), the protein quality is considered good due to a balanced amino acid profile. It includes essential amino acids, especially lysine, which is often lacking in cereal-based diets. Potato is an excellent source of vitamin C: one medium potato can provide up to 30% of the recommended daily intake of vitamin C. Potato also contains B vitamins, such as pyridoxine (B6), thiamin (B1), niacin (B3), and folate (B9). Moreover, a medium potato can provide up to 20% of the recommended daily potassium intake.

Potato contains various antioxidants, including carotenoids and flavonoids (Rousselle & Robert, 1996). Colored potatoes, such as red and purple varieties, have higher antioxidant levels due to anthocyanins. Glycoalkaloids like solanine and chaconine can have potential health benefits when consumed in moderation (Friedman, 2006). However, high levels can be toxic, which is why green or sprouted potatoes should be avoided.

In summary, potato constitutes an important source of energy and contains essential nutrients.

3. Genetics and breeding

With the rapid increase in the global population, potato plays a key role in food supply. These aspects led scientists to genetically engineer potato for yield and nutrition improvement. However, potato is genetically complex. While most wild species are diploid, the world's main cultivated species grown worldwide, *Solanum tuberosum*, is an autotetraploid that contains 48 chromosomes. This polyploidy increases genetic diversity and adaptability but also complicates breeding.

Breeding can offer several advantages (Campos & Ortiz, 2020). Increasing tuber size, number and yield or improving resistance to diseases (e.g. late blight disease, caused by *Phytophthora infestans*) and virus are primary objectives, particularly to meet the global demand for potatoes. Breeding also aims to develop varieties with natural pest resistance, reducing the need for chemical control. Developing varieties that can tolerate climate changes is also an objective. Additionally, biofortification efforts focus on increasing the nutrient content of potatoes. Breeding for reduced browning, low sugar accumulation during storage, and suitability for frying or baking helps improve the commercial value of potato. Traits like reduced glycoalkaloid content are also targeted to ensure safety and quality.

However, the tetraploid nature of most cultivated potatoes complicates breeding efforts, as four copies of each chromosome must be managed. This complexity makes it challenging to predict how traits will be inherited and expressed in new generations. Moreover, potato breeding is time-consuming due to its long-life cycle and the need for field trials. Developing a new variety can take 10 to 15 years.

Recent advances in potato genomics have accelerated breeding efforts. The sequencing of the potato genome, completed in 2011, has opened the way for understanding genes related to key traits, such as disease resistance, tuber yield, and stress tolerance. Access to the potato genome has accelerated breeding efforts and allowed for more targeted trait selection. However, producing knock-out mutants in potato remains challenging because of the tetraploid nature of potato and the high heterozygosity of this species.

In parallel, the development of gene-editing technologies like CRISPR/Cas brought new possibilities for precisely modifying potato genes. The CRISPR/Cas technique, originally discovered as a natural defense mechanism in bacteria, has revolutionized genetic engineering by allowing precise and efficient DNA editing (Jinek et al., 2012). CRISPR (Clustered Regularly Interspaced Short Palindromic Repeats) works with the Cas (CRISPR-associated) protein, most commonly Cas9, to target specific genes within an organism genome. Guided by a customized RNA sequence (gRNA for guide RNA), the Cas protein locates and cuts the DNA at the desired site, enabling the addition or deletion of nucleic acid bases with high precision. This technology has been widely used since its discovery in 2012.

Studies have demonstrated efficient targeted mutagenesis in potato using the CRISPR/Cas9 system in various applications (Chincinska et al., 2023; del Mar Martínez-Prada et al., 2021; Tiwari et al., 2022). Improving tuber quality and starch metabolism in potato through CRISPR/Cas genome editing has also been the subject of much work, with various studies highlighting its potential. Notably, the Cas9 system has been used to generate a range of tuber starch phenotypes by targeting starch-branching enzymes, which play a critical role in starch synthesis (Tuncel et al., 2019). Veillet et al. (2019) also explored the application of CRISPR/Cas for inactivation the expression of *GBSS* gene, essential for amylose synthesis. Similarly, Sevestre et al. (2020) demonstrated the use of CRISPR/Cas technology to modify genes involved in starch metabolism and proposed a Single Nucleotide Polymorphisms (SNPs) map to facilitate gene editing in *Solanum tuberosum*. Furthermore, the manipulation of the *Pho1a* gene, essential to starch metabolism has resulted in the successful knockout of all four alleles, significantly altering tuber starch (S. Sharma et al., 2023). These studies underscore the effectiveness of CRISPR/Cas technology in modifying starch metabolism, opening the way for the development of potato varieties with improved properties.

Breeding plays an essential role in enhancing potato production, from improving yield and disease resistance to adapting to climate change. Modern genetic tools are transforming traditional breeding, making it faster, more precise, and better suited to address both global food security challenges and consumer preferences.

4. Agronomy and cultivation practices

Potato varieties can be grouped into early and late varieties. Early varieties require are typically photoperiod-sensitive and require long days, which make them particularly suited for spring or summer cultivation in temperate regions. On the contrary, late varieties are less sensitive to photoperiod and can tuberize under both long and short day conditions (Rousselle & Robert, 1996).

After harvest, good storage conditions are essential, to prevent losses due to dehydration, sprouting and sweetening. Proper storage conditions maintain tuber quality, extending their shelf life and availability throughout all the year. Ideal storage temperatures for fresh potatoes are typically between 4-10°C. Temperatures above 10°C promote sprouting and encourage the growth of bacteria and fungi. The recent prohibition of chlorpropham (CIPC) in Europe, used to control tuber sprouting, has forced the industrial to lower the tubers storage temperature. Low temperatures (around 4°C) are used for long-term storage, but at these temperatures, starch can be converted into sugars (glucose and fructose). This reaction, called “cold-induced sweetening”, can cause browning when the potatoes are fried due to the Maillard reaction and may lead to higher levels of acrylamide, a recognized carcinogen.

Through this chapter, we have explored the importance of potato, from its origins to becoming a global food staple, examining its cultural, nutritional and agricultural interests. Despite initial resistance, potato have become essential to food security due to its nutritional profile, including high starch content and essential nutrients. Recent advances in genetics, especially through genome sequencing and CRISPR/Cas9 technology, have opened new perspectives for improving yield, disease resistance, and tuber quality.

The following chapters will explore starch industrial applications, as well as its morphology and structure, with a particular focus on starch metabolism. These sections will highlight the importance of starch metabolism both in the role of potato as a staple crop and in its industrial applications.

Chapter 2. Starch

1. Industrial applications

Potato is an economically significant crop cultivated worldwide for its high starch content and nutritional values. It has traditionally been used as a staple food in the human diet. However, technological advances have expanded its utility, significantly contributing to various industrial applications that make starch a valuable resource not just for nutrition (Adewale et al., 2022; Nsanzabera et al., 2023).

Potato is widely used for its starch-rich tubers, with starch representing up to 80% of the dry weight and standing as a vital reserve of carbohydrates that supports plant sprouting (Coleman, 1987). The abundance of starch in tubers, combined with a high yield per cultivated area, make it an interesting resource for diverse industrial applications. Starch derived from potato is widely used in various sectors including food processing, biotechnologies, pharmaceuticals, biofuel production, paper and textile industries, particularly for its high viscosity and unique thickening properties.

In the paper and textile industries, potato starch is an important binding and sizing agent (Adewale et al., 2022; Nsanzabera et al., 2023; Rousselle & Robert, 1996). It also finds applications in the construction sector, where it enhances the properties of paints, plasters, and adhesives. Its unique properties also make it valuable in the pharmaceutical industry, where it acts as a binder and filler. Due to its biodegradable properties, the research on utilization of potato starch in the delivery of therapeutic agents and as a material for drug encapsulation is developing. Potato starch is also used as a sustainable alternative to plastics. Starch-based films can be used for various packaging, including food. These biobased plastics are increasingly employed as sustainable alternatives to conventional packaging materials, reducing plastic waste and environmental impact.

In this perspective, potato has also been explored as a renewable resource for biofuel production due to their high carbohydrate content (Adewale et al., 2022; Nsanzabera et al., 2023; Rousselle & Robert, 1996). Ethanol, produced by the fermentation of potato starch, might serves as a component in biofuels. This ethanol is also widely used in the beverage

industry, most notably in the production of vodka. Additionally, potato processing waste, such as peels and pulp, provides raw material for biogas production through anaerobic digestion.

Besides these varied non-food applications, 53% of the starch production found its utilization is the food industry in 2021. Indeed, starch holds a significant importance as the primary source of carbohydrates in both human and cattle diets. In France, starchy foods contribute, on average, to 33% (for women) to 55% (for men) of daily dietary intake (Szabo De Edelenyi et al., 2014). Potato provides a source of energy consumed as it is, or starch is also commonly used in the food industry as a thickening, gelling, and stabilizing agent, essential for the preparation of processed foods.

With its high yield and gluten-free source of carbohydrates, potato is an interesting choice for the food industry. This highlights the major role of potato starch not only in industrial applications, but also in sustaining nutritional needs across various sectors of our society.

2. Composition and structure

The numerous properties of potato starch, such as thickening, binding and gelling are related to different parameters. Understanding starch composition and structure is essential, because it directly impacts these properties. Starch is composed of two types of polyglucans, amylose and amylopectin, and forms a semi-crystalline granule that is insoluble in cold water. Other minor components, such as protein, lipids, and phosphate, represent less than 1% of the starch weight. The composition and organization of starch will be described in the following paragraphs.

2.1. Glucans

Starch is a polysaccharide composed of two distinct polyglucans: amylose and amylopectin. In potato starch, amylopectin accounts for approximately 80% of the total starch weight (Banks & Greenwood, 1975; Fredriksson et al., 1998). While amylose is mainly linear, amylopectin is highly branched, and together they arrange to form a semi-crystalline granule.

2.1.1. Amylose

Amylose is a predominantly linear polysaccharide composed of glucose residues linked by α-1,4 O-glycosidic bonds (Figure 2 and Figure 4a). Despite being the minor component of starch, it is present in all non-mutant starch granules and constitutes between 5% and 35% of the carbohydrate content in most starches (Kram et al., 1993; Seung, 2020) In potato starch, its proportion typically ranges from 17% to 21% (Seung, 2020).

The degree of polymerization (DP) of amylose varies between 500 and 6000 glucose residues, corresponding to a molecular weight of approximately 10^6 kDa (Buléon et al., 1998). Amylose contains very few branching points, with less than 1% of its glycosidic bonds being α-1,6 linkages, in contrast to amylopectin, which contains 4% to 6% of such linkages (Buléon et al., 1998; Hizukuri et al., 1981; Manners, 1989).

It is now known that amylose itself is not required for the formation of starch granules. Some plant species, such as *Arabidopsis thaliana*, contain only a small proportion of amylose, while mutants lacking GBSS activity (an enzyme responsible for amylose synthesis), known as

"waxy" starches, completely lack amylose (Nelson & Tsai, 1964; Weatherwax, 1922). The role of amylose within the starch granule remains incompletely understood and is still under investigation.

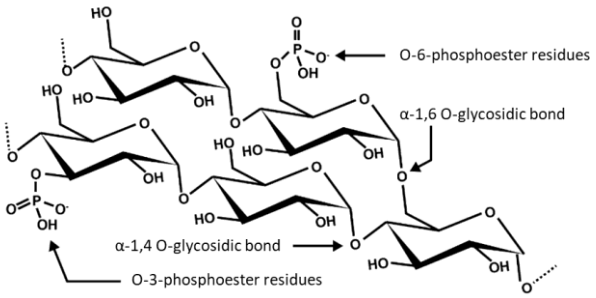

Figure 2 : Schematic representation of the primary structure of O-glycosidic bonds between glucose residues of starch, including phosphate residues (Modified from Helle, 2020).

2.1.2. Amylopectin

Amylopectin is a branched polysaccharide composed of glucose residues connected primarily by α-1,4 O-glycosidic bonds, with branching points formed by α-1,6 linkages, which constitute 4% to 6% of the total glycosidic bonds (Figure 2). Due to its high molecular weight and its peculiar organization, amylopectin is structurally more complex than amylose (Figure 4a). The synthesis and degradation of amylose and amylopectin molecules which includes dozens of different proteins will be detailed in Chapter 3.

The degree of polymerization of amylopectin ranges from 10^5 to 10^6 glucose units, corresponding to a molecular weight of approximately 10^8 kDa (Manners, 1989). Its branched structure is composed of different types of chains, classified according to their length and degree of branching (Bertoft, 1991; Hizukuri, 1986; Peat et al., 1956) (Figure 4a). A chains are the shortest and most external, with a maximum DP of 15, and do not contain additional branching points beyond their connection to the rest of the amylopectin cluster. B chains are of intermediate length (DP 10 to >40) and carry other B or A chains. They are further classified into B1 chains, the shortest, located at the periphery and carrying only A chains and B2 and B3 chains, which are longer and can carry both A and B chains (Figure 3a). Finally, the amylopectin contains a single C chain, which is the longest and contain the only reducing end

of the amylopectin molecule. Although comprehensive structural models of full amylopectin and amylose molecules are still missing, two main models have been proposed to describe amylopectin architecture: the cluster model and the building block backbone model. Both agree that the double helices are arranged perpendicularly to the starch granule surface. However, they diverge in their interpretation of the orientation of the long chains. In the building block backbone model, long chains are aligned perpendicular to the double helices and form the backbone of each amorphous lamella (Bertoft, 2015; Vamadevan & Bertoft, 2015) (Figure 3b). In contrast, the cluster model proposes that long chains run parallel to the double helices and can extend across multiple crystalline layers (Hizukuri, 1986) (Figure 3c).

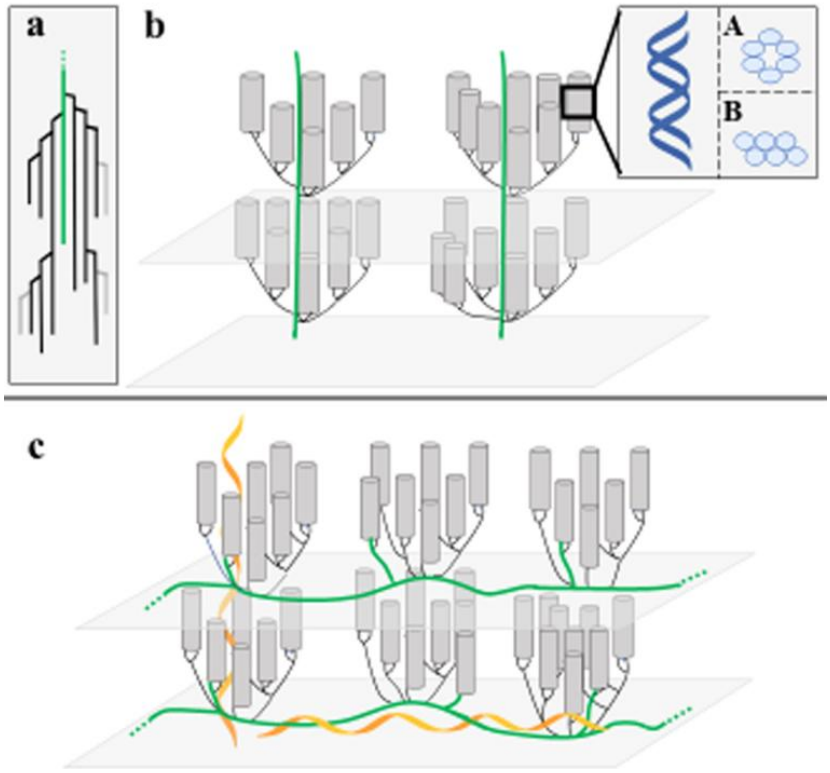

Figure 3 : Starch structure. A cross-section of a starch granule showing the typical growth rings with crystalline and amorphous lamellae (9 nm repeat distance), the structure of amylopectin and the possible positions of amylose. The chains from amylopectin can subdivided into A (light grey), B (black), and C (green) chains according to their length (ordered from short to long; subfigure a). The double helices (depicted as cylinders) with a vicinal intramolecular position formed by short side chains (A and partly B chains). Double helices can be organized as A-type and B-type allomorph (zoom in is illustrated in b). The orientation of the long chains (C chains; green) can be either perpendicularly to the double helices according to the building block backbone model (c) or parallel as described in the cluster concept (b). The possible location of amylose (yellow helices) is also shown in figure c. However, basically both or mixture of orientations is conceivable (modified from Apriyanto et al., 2022).

The semi-crystalline nature of starch granules is primarily attributed to amylopectin. Its highly branched and ordered organization facilitates the formation of secondary and tertiary structures, resulting in a highly ordered architecture that will be detailed in the next subchapter.

2.2. Crystallinity and organization

The assembly of amylose and amylopectin results in a semicrystalline starch granule, insoluble in cold water. Amylopectin primarily contributes to the crystallinity of the starch granule. Amylopectin branch points are not uniformly distributed within the molecule but are clustered in specific regions (French, 1972; Robin et al., 1974). The clustering of amylopectin chains contributes to the partial crystallinity of starch. The heterogeneity of branching point distribution leads to the formation of amylopectin clusters, consisting of amorphous lamellae, where most branch points are located, and crystalline lamellae, where linear glucan chains form parallel double helices (Hizukuri, 1986) (Figure 4a). X-ray diffraction analysis has identified two crystalline allomorphs, A and B, which differ in the packing of double helices and the positioning of water molecules within the formed structure (Figure 4a). Type A crystals, found primarily in cereal storage starches, have a densely packed structure with minimal space for water molecules. In contrast, type B crystals, common in hydrated tissues such as leaves and tubers, exhibit a looser hexagonal structure that contain more water molecules (Imberty & Perez, 1988; Pérez & Bertoft, 2010).

One amylopectin cluster consists of one amorphous and one crystalline lamella, with a periodicity of 9 to 10 nm, regardless of the botanical origin of the starch, giving the starch its semicrystalline nature (Jenkins & Donald, 1995). The amorphous lamella measures approximately 3 nm, while the crystalline lamella measures 6 nm.

Amylopectin clusters form super helices that further organize into larger structures called "blocklets," ranging in size from 20 to 500 nm (Gallant et al., 1997) (Figure 4b). These structures, initially observed in potato starch using electron microscopy, may consist of left-handed superhelices of crystalline lamellae (Gallant et al., 1997; Oostergetel & Van Bruggen, 1993). However, the existence of these blocklets remains debated, as some researchers

suggest they may be artifacts caused by sample preparation, particularly starch dehydration, leading to aggregation of amylopectin (Ridout et al., 2003).

Amylopectin molecules, structured into amorphous and crystalline lamellae and possibly forming blocklets, ultimately arrange into concentric layers, forming the starch granule (Figure 4b). These layers exhibit radial symmetry with amylopectin chains organized perpendicular to the granule surface. This arrangement is evidenced by the Maltese cross pattern observed under polarized light, regardless of the botanical origin of the starch (Ziegler et al., 2005). The layers originate from the granule center, called the hilum, and grow outward, forming growth rings that vary in thickness from 100 to 400 nm (Pérez & Bertoft, 2010; Yamaguchi et al., 1979). These growth rings alternate between amorphous regions, which appear electron-lucent under electron microscopy, and semicrystalline regions, which appear electron-dense (Yamaguchi et al., 1979). The composition of the hilum remains poorly understood due to the difficulty in studying its structure, but it appears to contain amylose-like glucans or slightly branched intermediate materials (Ziegler et al., 2005). Semicrystalline growth rings are more resistant to hydrolysis than amorphous growth rings.

The composition of the amorphous regions of starch remains poorly understood. These regions may contain amylose, or loosely packed amylopectin. The exact location of amylose within growth rings is still unknown, but the most widely accepted hypothesis suggests that amylose exists as individual chains intertwined with amylopectin clusters, helping to stabilize the structure (Pérez & Bertoft, 2010). In waxy starch, which lacks amylose, gelatinization occurs more rapidly and easily upon heating, suggesting that amylose helps maintaining amylopectin compactness (Hsieh et al., 2019). This hypothesis is supported by cross-linking experiments on amylose and amylopectin in maize, demonstrating that amylose does not interact with itself but with amylopectin chains (Kasemsuwan & Jane, 1994). If the blocklet hypothesis is valid, amylose may form a network around amylopectin to stabilize the blocklet structures (Ridout et al., 2003).

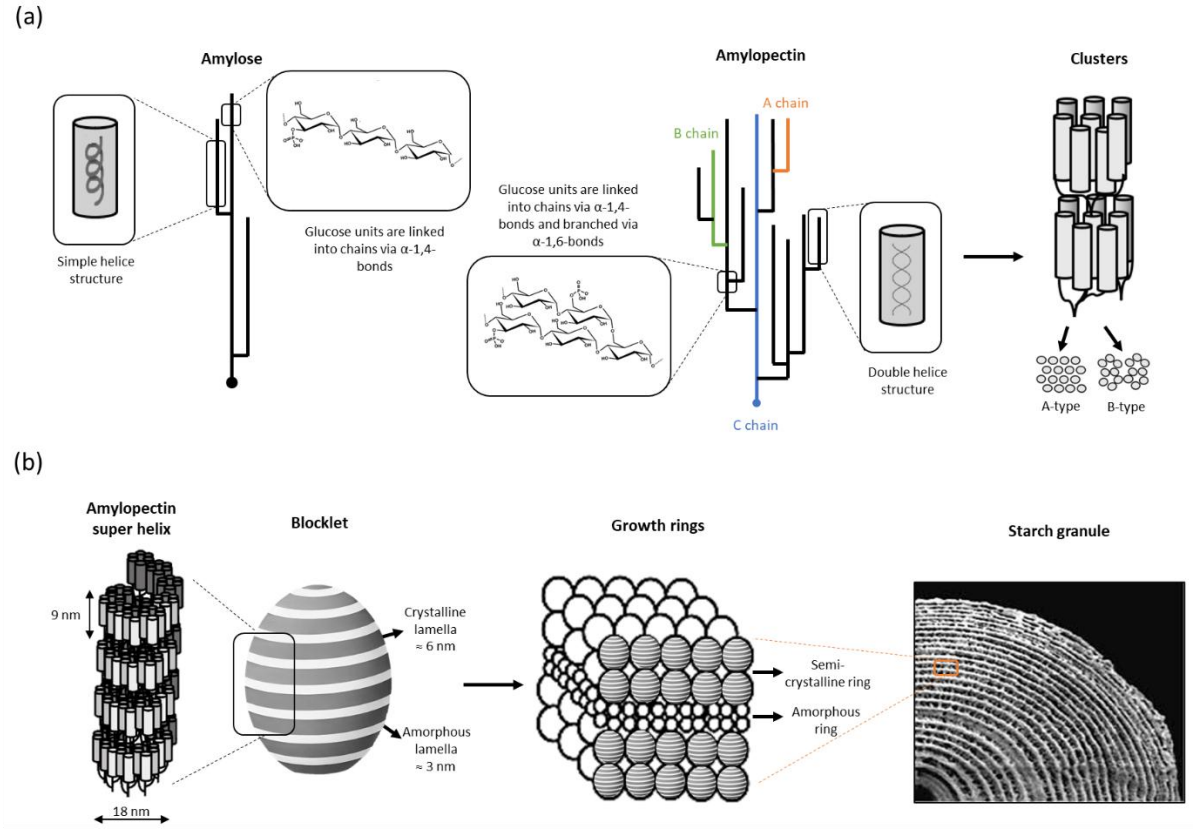

Figure 4: Composition and structure of starch granules. (a) Schematic representation of amylose and amylopectin, and the structures adopted by the constituent chains. (b) Relationship between the starch granule and amylopectin structure. Amylopectin clusters form super helices that further arrange into blocklets, consisting of crystalline and amorphous lamellae alternation. Amylopectin molecules, possibly forming blocklets, ultimately arrange into concentric layers named growth rings, forming the starch granule. (Adapted from Helle, 2020; Zeeman et al., 2010).

2.3. Other components

Although starch is primarily composed of polysaccharides, other macromolecules, such as proteins, lipids and minerals, are also present in small amounts. These components, despite their low abundance, play significant roles in starch properties and metabolism.

Proteins represent approximately 0.1% to 0.7% of the dry weight of starch granules, depending on the plants species (Biliaderis et al., 1979; Yusuph et al., 2003). Most of these proteins are involved in starch metabolism, such as the major enzyme Granule Bound Starch Synthase (GBSS), which is essential for amylose synthesis, as well as other enzymes associated with starch biosynthesis and degradation (Grimaud et al., 2008; Helle et al., 2018). Further details on the specific proteins involved in starch metabolism will be discussed in the next chapter.

The lipid content of starch varies depending on the plant species. In cereal endosperm starch, lipids can constitute up to 1.5% of the dry weight (Morrison et al., 1984). In contrast, tuber starch, such as that from potatoes, contains significantly lower amounts of lipids. These lipids influence the physicochemical properties of starch, particularly its gelatinization and retrogradation behavior.

Minerals found in starch are mainly in the form of phosphoesters covalently bound to amylopectin. Some amylopectin chains are phosphorylated at the C3 or C6 position of glucose residues (Ritte et al., 2006) (Figure 2). Among starches, potato starch has one of the highest phosphate contents (Blennow & Engelsen, 2010). These phosphate groups contribute to the destabilization of linear amylopectin chains, facilitating starch degradation. However, the degree of phosphorylation remains very low: starches rich in phosphate, such as those from potato tubers and turmeric, contain only about 0.1% of glucose-phosphate residues (Jane et al., 1994; Kasemsuwan & Jane, 1996; Verbeke et al., 2016). Digestion studies on potato starch *in vitro* suggest that phosphate residues are predominantly located at the center of B chains in amylopectin, approximately nine residues away from a branching point (Compart et al., 2023; Takeda & Hizukuri, 1982).

3. Morphology

Granule morphology is thought to have a great importance on physicochemical properties of starch (Li et al., 2021; Lindeboom et al., 2004). For example, large granules such as potato starch granules, have a high swelling power, but are not suitable for extruded products (Lindeboom et al., 2004; Q. Liu, 2005). In contrast, small granules are often used for biodegradable plastics or in paper industry (Lindeboom et al., 2004). The size and shape of starch granules vary significantly depending on their botanical origin. Granule sizes range from as small as 1 µm, as observed in amaranth, to up to 100 µm in potato tubers, which have the largest starch granules among common starch sources (Jane et al., 1994) (Figure 5). Their morphology is also diverse, reflecting the structural and functional differences among plant species.

In *Arabidopsis thaliana* leaves, starch granules are typically lenticular and around 2 µm in size. In contrast, species such as rice, maize, and amaranth produce angular granules (Jane et al., 1994). Wheat starch consists of two distinct populations: large A-type granules, which range from 15 to 35 µm in size and have a flattened shape, begin to form around five days post-anthesis, whereas smaller B-type granules, spherical in shape and measuring between 2 and 10 µm, appear later, around 15 days post-anthesis (Tanaka et al., 2017). In potato tubers and peas, starch granules are predominantly ovoid. In the rice endosperm, each amyloplast produces compound granules consisting of several dozen polyhedral, sharp-edged and easily separable granules (Yun & Kawagoe, 2010).

The size of starch granules was shown to be influenced by the volume and structure of the plastids, which can vary between plant tissues or between species. For example, the transient starch synthesized in Arabidopsis is formed between chloroplasts, which could explain its small size and flattened shape due to the limited space between these membrane structures (Bürgy et al., 2021; Gámez-Arjona et al., 2014; M. Sharma et al., 2024). In contrast, potato tubers provide a much larger space within amyloplasts, allowing the formation of starch granules up to 100 µm in size. In wheat, A-type granules are formed earlier during grain development and have more space available within the amyloplast, allowing them to grow larger. In contrast, B-type granules are synthesized later, in extensions of the membrane named “stromules”, when much of the internal space is already occupied by A-type granules

(Tanaka et al., 2017). As a result, they are constrained to the peripheral regions of the amyloplast, leading to their smaller size.

Additionally, some proteins have been identified as playing a role in regulating granule size and morphology. The mechanisms involved in this regulation will be explored in more detail in Chapter 3.

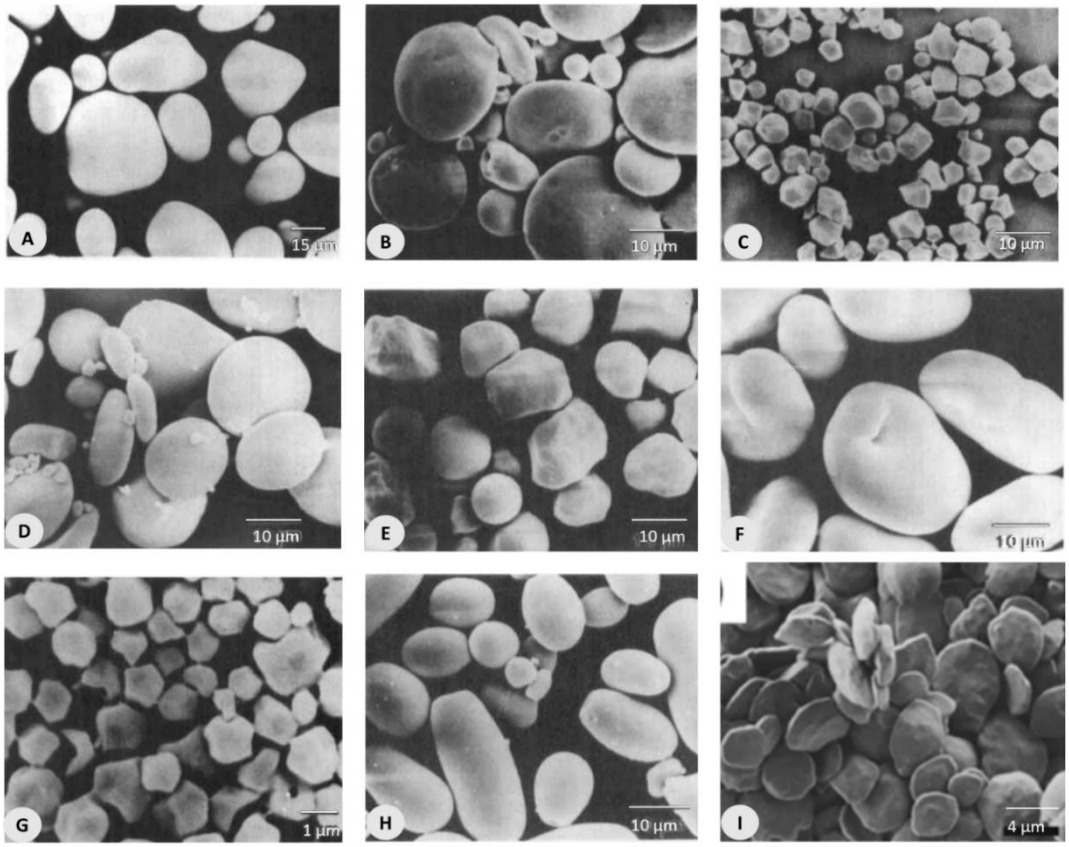

Figure 5 : Scanning electron microscopy of purified starch granules from different botanic origins. A: potato; B: wheat; C: rice; D: barley; E: waxy maize; F: green pea; G: amaranth; H: avocado; I: Arabidopsis thaliana (Adapted from Apriyanto et al., 2022; Jane et al., 1994)

4. Distribution of starch in plants

As previously described, the size, number, and morphology of starch granules vary significantly depending on the species and even the specific organ analyzed (Tetlow & Bertoft, 2020). In plants, starch is stored in the form of granules within plastids (S. G. Ball & Morell, 2003).

In photosynthetic tissues such as leaves, starch is synthesized within chloroplasts during the day and degraded at night to provide a readily available energy source (Geiger & Servaites, 1994). At night, this transient starch is broken down through respiration, providing the needed energy for the plant for its survival when photosynthesis is inactive.

In contrast, non-photosynthetic tissues, such as cereal grains, roots and tubers, contain amyloplasts, which specialize in long-term starch storage. This storage starch supports vegetative reproduction by providing energy for tuber sprouting and the emergence of new plants (Tyson & Ap Rees, 1988).

In potato, both transitory and storage starch coexist, depending on the tissue type. Additionally, starch granules are also found in roots within specialized amyloplasts known as statoliths, which are involved in gravity perception and help regulate plant growth orientation (Vandenbrink & Kiss, 2019).

Chapter 3. Starch metabolism

Despite the apparent simplicity of its composition, merely consisting of glucose units and two types of bonds, starch metabolism is in fact a complex process involving a wide range of catalytic and non-catalytic proteins.

1. Synthesis

Four major enzyme classes are involved in starch biosynthesis. First, ADP-glucose phosphorylase (AGPase) provides ADP-glucose (ADP-Glc), the basic unit of starch synthesis. The glucosyl units of ADP-Glc substrate are then used by soluble starch synthases (SSs) to elongate glucose polymer chains. Third, branching enzymes (BEs) create branching points from existing chains by transferring small glucan chains to the C6 position of another glucose unit in the glucan molecule. Fourth, debranching enzymes (DBEs or isoamylases) hydrolyze excess branches, allowing the crystallization of clusters (S. Ball et al., 1996; Brust et al., 2013). These processes are remarkably well conserved among different plant species. The steps catalyzed by SSs, BEs, and DBEs will be detailed below. Although presented in a sequential manner, it is important to keep in mind that they are interdependent and simultaneous processes that occur in a concerted manner.

1.1. ADP-Glc synthesis

The first step of starch synthesis in plants is the production of ADP-glucose, the unique precursor for starch biosynthesis. This glucosyl-nucleotide is synthesized by condensation of ATP and glucose-1-phosphate (Glc-1-P), with the release of inorganic pyrophosphate (PPi). This reaction is catalyzed by ADP-glucose pyrophosphorylase (AGPase), a heterotetrameric enzyme located in the stroma. In *Arabidopsis thaliana* mutants, the loss of AGPase completely blocks ADP-Glc synthesis, preventing its use by starch synthases (SSs) for glucan chain elongation (Bahaji et al., 2011). Once synthesized, ADP-glucose serves as the glucose donor for the elongation of amylose and amylopectin polymers. The availability of Glc-1-P for this process depends on gluconeogenesis, as it is derived from glyceraldehyde-3-phosphate (G3P),

an intermediate of the Calvin cycle. The synthesis of ADP-Glc is tightly regulated by the concentrations of 3-phosphoglycerate (3-PGA) and inorganic phosphate (Pi) in the stroma (Mugford et al., 2014). Potato AGPase is also under similar control (Ballicora et al., 1995; Hwang et al., 2008; Iglesias et al., 1993).

1.2. Amylose synthesis requires the major enzyme GBSS

Granule Bound Starch Synthase (GBSS), is essentially active when bound to the starch granule and is entirely responsible for amylose synthesis (Denyer, Waite, Edwards, et al., 1999; Denyer, Waite, Motawia, et al., 1999; Edwards et al., 1995; Shure et al., 1983). This has been demonstrated in several studies showing that mutants lacking GBSS do not produce amylose and exhibit a characteristic “waxy” phenotype due to the altered appearance of their starch granules (Okagaki & Wessler, 1988; Tsai, 1974). GBSS catalyzes amylose elongation by using ADP-glucose (ADP-Glc) as a substrate to extend amylose chains at their non-reducing ends (Rongine De Fekete et al., 1960).

In potato, GBSS has a molecular weight of approximately 66 kDa and possesses two glycosyltransferase (GT) domains, a feature common to other starch synthases. It also contains conserved catalytic amino acid residues essential for its enzymatic function (K-X-G-G-L and X-X-G-G-L). While GBSS is primarily responsible for amylose synthesis, it has also been shown to possess an elongation activity that allows the extension of amylopectin chains. However, this activity does not contribute to the final structure of amylopectin, as these elongated chains are subsequently debranched by debranching enzymes, leading to the formation of amylose chains (S. G. Ball et al., 1998; Pfister & Zeeman, 2016; Van De Wal et al., 1998).

GBSS represents approximately 95% of the total starch-bound protein content, highlighting its major role in starch granule formation (Helle et al., 2018). It is predominantly active when associated with starch granules, displaying only minimal activity in its soluble form (Dry et al., 1992; Rongine De Fekete et al., 1960). In wheat, two isoforms of GBSS have been identified: GBSS1, which is responsible for amylose synthesis in the endosperm, and GBSS2, which is involved in amylose synthesis in leaves (Vrinten & Nakamura, 2000).

Despite its high abundance in starch granules, GBSS does not possess any known carbohydrate-binding domain, which is surprising given its granule association. It has been demonstrated that GBSS is targeted to the starch granule via PTST1, a protein containing a CBM48 domain that facilitates interaction with starch (Bull et al., 2018; Seung et al., 2015). This interaction is mediated by the coiled-coil motifs present in GBSS (Seung et al., 2015). In Arabidopsis *ptst1* mutants, a strong reduction in starch-bound GBSS and amylose content has been observed, confirming the essential role of PTST1 in GBSS localization and function.

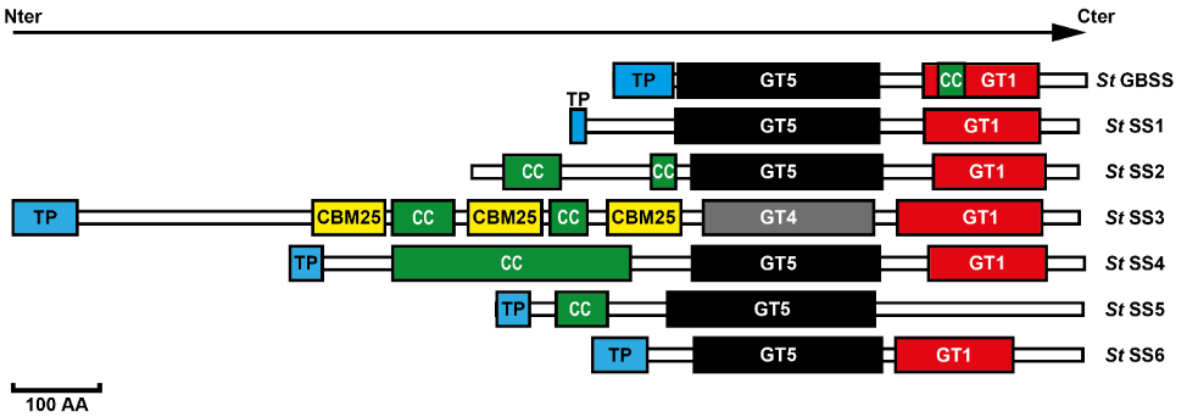

Figure 6 : Domain structure of Starch Synthases (SSs) from potato. Different structural domains are highlighted. Black and red boxes represent glycosyl-transferase domain (GT1, GT4 and GT5). Yellow boxes represent Carbohydrate Binding Domain (CBM). Green boxes represent coiled-coil (CC) regions, involved in protein-protein interaction. Blue boxes represent transit peptide signal. *St*: *Solanum tuberosum*, GBSS : Granule Bound Starch Synthase, SS : soluble Starch Synthase, AA : amino acids. (Helle et al., (2018)).

1.3. The complex process of amylopectin synthesis

1.3.1. Implication of soluble starch synthases

Starch Synthases (SSs) are key enzymes of the starch biosynthesis. They elongate glucan chains by catalyzing the transfer of the glucosyl moiety of ADP-glucose to the non-reducing end of a pre-existing α-1,4 glucan primer. In plants, at least six conserved gene classes encode SSs. Five of them are present in the soluble fraction and are responsible for amylopectin synthesis (SS1 to SS5), while the sixth (GBSS) is granule-bound and involved in amylose synthesis (Deschamps et al., 2008). A seventh class, named SS6, has been identified in potato (Helle et al., 2018).

Canonical SSs (SS1 to SS4 and GBSS) share a conserved C-terminal catalytic domain, which is further divided into a N-terminal and a C-terminal subdomains, named GT5 and GT1 respectively. The catalytic domain contain two conserved K-X-G-G-L and X-X-G-G-L motifs (Cao et al., 1999). SS3 differs from SS1 and SS2 by an extended N-terminal region containing three CBMs (Carbohydrate Binding Domains). SS isoforms differ significantly at their N-terminal moiety, with some containing predicted coiled-coil motifs (SS2, SS3 and SS4) or CBMs (SS3), while SS1 and GBSS exhibit a reduced N-terminal moiety, with no specific domain. Two additional isoforms, SS5 and SS6, have been identified in potato starch granules, implying a role in starch metabolism (Helle et al., 2018). SS5 from Arabidopsis is truncated compared to that of potato, and both lacks catalytic motifs. SS6 contains conserved starch synthase catalytic sites, suggesting a role in glucan chain elongation.

SS1, SS2 and SS3 contribute to amylopectin synthesis, their loss leading to an alteration of amylopectin structure. In potato, SS1 has a minimal impact on amylopectin synthesis, as RNAi lines and mutants show no major modification of amylopectin structure (Kossmann et al., 1999; Tyynelä & Schulman, 1993). This may be due to the low expression of SS1 in tubers (Kossmann et al., 1999). However, SS1 is highly expressed in leaves of this species. This expression pattern is also observed in rice, but amylopectin chain length distribution is altered in the rice endosperm of the corresponding mutant (Fujita et al., 2006; Hirose & Terao, 2004). The same phenotype is observed in *ss1* Arabidopsis mutants, with a reduction of short chains (DP8 to DP12) and an increase of chains with a DP between 12 and 23 glucose residues (Delvallé et al., 2005). From these results, it was proposed that SS1 is mainly involved in the synthesis of the small amylopectin chains.

SS2-deficient plants exhibit a consistent phenotype across species and tissues, characterized by decreased DP 12–30 glucan chains and increased shorter chains (Craig et al., 1998; Morell et al., 2003; Szydlowski et al., 2011a; X. Zhang et al., 2004). It was subsequently proposed that SS2 is responsible for the synthesis of intermediate glucan chains ($12 < DP < 30$).

The lack of SS3 led to similar phenotypes in deficient plants, including a reduced starch content, an increase of long glucan chains (DP 10-40) and an altered granule morphology (Abel et al., 1996; Fontaine et al., 1993; Gao et al., 1998; X. Zhang et al., 2005). In addition of

this elongation activity and only in absence of SS4, SS3 can compensate the loss of SS4 in the granule initiation (Szydlowski et al., 2009).

SS4 is required for granule initiation and control of granule number per plastid, but does not significantly contribute to amylopectin structure (Crumpton-Taylor et al., 2012; Crumpton-Taylor et al., 2013; K.-J. Lu et al., 2018; Roldán et al., 2007; Seung et al., 2017; Szydlowski et al., 2009). Similarly, SS5 lacks catalytic activity, and *ss5* mutants resemble *ss4* mutants, although less severe, suggesting a role in granule initiation (Abt et al., 2020).

1.3.2. Formation of the α-1,6 linkages by branching enzymes

Starch branching enzymes (BEs) catalyze the formation of α-1,6 bonds of amylopectin. Their activity was first identified in potato (Haworth et al., 1944). Most plants contain two to three isoforms of BEs, which cleave an α-1,4 bond in a pre-existing glucan chain and transfer it to an α-1,6 position. These isoforms are classified based on their amino acid sequences (Burton et al., 1995) but this classification also reflects their specificities. BE1 primarily acts on amylose and transfers longer chains, whereas BE2 is more active on amylopectin (Guan & Preiss, 1993; Takeda et al., 1993).

In potato BE1 is expressed in tuber and leaves and represents the major catalytic activity (S. A. . Jobling et al., 1999), whereas in cereal endosperms, BE2 accounts for the majority of measurable BE activity (Boyer & Preiss, 1981; Nishi et al., 2001; Regina et al., 2006). The function of BE1 is uncertain in maize, since *be1* mutants are similar to wild-type plants (Blauth et al., 2002), while in rice, a slight alteration of the amylopectin structure was observed (Nakamura, 2002; Satoh et al., 2003). Heterologous expression of different BE isoforms in yeast demonstrated that BE1 is unable to function in absence of other BE isoforms (Seo et al., 2002), a finding also supported by mutant studies in rice (Satoh et al., 2003). It has been suggested that BE1 acts downstream of BE2 in the amylopectin biosynthesis, but its precise function remains unclear.

In maize, barley and rice, two types of BE2 were identified, named BE2a and BE2b (Dang & Boyer, 1988; Fisher et al., 1996; Gao et al., 1996, 1997; Nishi et al., 2001; Sun et al., 1998; Yamanouchi & Nakamura, 1992). The expression of both genes is tissue specific. While BE2a is expressed in most organs, BE2b is restricted to the endosperm. As a result, BE2b-

deficient mutants produce an amylose-rich starch, with altered amylopectin structure in the endosperm but show no modification in leaves (Dang & Boyer, 1988; Gardwood et al., s. d.; Hedman & Boyer, 1982). In contrast, maize mutants lacking BE2a exhibit reduced amylopectin branching in leaves with an accelerated senescence, but no modification in the endosperm (Blauth et al., 2001). In potato, where only one BE2 isoform exists, *in vitro* studies indicate that BE2 preferentially acts on shorter chains (DP6) compared to BE1 (Rydberg et al., 2001). Overexpression of BE2 in potato leads to amylopectin structural alterations, notably increasing the proportion of short chains (DP≤12), particularly DP6 (Brummell et al., 2015). Unlike most plants, Arabidopsis lacks a BE1 ortholog but possesses two BE2 genes, BE2.1 (BE3) and BE2.2 (BE2), which are expressed in leaves and involved in transient starch synthesis (Fisher et al., 1996; Wychowski et al., 2017). Although their expression varies throughout the diurnal cycle, both enzymes appear to have redundant functions, as single mutants exhibit only a slight reduction of short chains (DP 5-8) associated to a slight increase in intermediate chains (DP 9-15), while the *be2 be3* double mutant completely lacks starch accumulation and displays severe growth retardation. These results indicate that BE2 is essential for amylopectin synthesis (Dumez et al., 2006).

The activity of branching enzymes is also regulated by post-translational modifications. In wheat, branching enzyme activity is regulated by phosphorylation and dephosphorylation (Tetlow et al., 2004). Dephosphorylation significantly reduces BEII activity, whereas BEI activity remains unaffected. This phosphorylation mechanism has also been observed in maize and barley (Ahmed et al., 2015; F. Liu et al., 2009).

1.3.3. Debranching enzymes play a role in the maturation of the glucans

DBEs specifically cleave α-1,6 bonds and are subdivided into two classes depending on their substrate specificity. Isoamylases (ISA) act on amylopectin and glycogen, while limit dextrinases (LDAs), also called pullulanases (PU) are active on amylopectin and pullulan (a highly branched polyglucan) but not on glycogen. Debranching enzymes are highly conserved, with three isoamylase genes (ISA1, ISA2 and ISA3) and one pullulanase gene (Deschamps et al., 2008). These proteins regulate both starch degradation and biosynthesis.

ISA1 and ISA2 are involved in granule synthesis, facilitating glucan polymer maturation and crystallization. ISA2 lacks catalytic activity in all organisms where it has been identified. However, it forms heteromultimers with ISA1 in all species, although ISA1 can also be active alone as homomultimer in some of them, such as maize or rice (Facon et al., 2013; Hussain et al., 2003; Kubo et al., 2010; Utsumi & Nakamura, 2006). ISA2 has been proposed to assist ISA1 in binding to the substrate in maize and potato. ISA1 and ISA2 form heteromultimers in potato, similar to Arabidopsis (Delatte et al., 2005; Hussain et al., 2003; Wattebled et al., 2005). In Arabidopsis leaves, both ISA1 and ISA2 are required, as mutants lacking ISA1 and/or ISA2 exhibit an 80% reduction in starch content at the end of the day and an accumulation of a highly branched soluble polysaccharide called phytoglycogen (Delatte et al., 2005; Wattebled et al., 2005; Zeeman et al., 1998). Additionally, these mutants produce significantly smaller starch granules than wild-type plants (Delatte et al., 2005). A similar phenotype was observed in barley, maize, and rice for *isa1* mutants. However, in these cereals, *isa2* mutants exhibit a wild-type starch phenotype, likely due to ISA1 ability to form homomultimers (Burton et al., 2002; Dinges et al., 2001; James et al., 1995; Kubo et al., 2010; Nakamura et al., 1996; Utsumi et al., 2011; Utsumi & Nakamura, 2006). In potato ISA1 and ISA2 antisense lines, granule morphology is strongly impaired, with an accumulation of small granules (Bustos et al., 2004).

ISA3 is mainly involved in transitory starch breakdown in Arabidopsis and rice leaves (Wattebled et al., 2005; Yun et al., 2011) but it can also partially compensate the loss of ISA1 and/or ISA2 in amylopectin synthesis. In potato, simultaneous antisense inhibition of ISA1, ISA2, and ISA3 significantly reduced tuber starch content (Ferreira et al., 2017). Granule morphology was also altered, with an increased proportion of smaller starch granules, consistent with previous findings in antisense lines with reduced ISA1 and ISA2 expression (Bustos et al., 2004; Ferreira et al., 2017).

The function of pullulanase (PU) remains less clearly defined. Single mutants typically display only mild phenotypes, and studies involving combined knockouts of multiple debranching enzymes suggest that PU may play a marginal role in both starch synthesis and degradation (Dinges et al., 2003; Wattebled et al., 2008).

2. Degradation

Plants rely on stored metabolites to maintain their metabolism at night. In leaves, transient starch is synthesized during the day and degraded at night to support growth and metabolism when photosynthesis is inactive while in storage organs such as tubers, starch is mobilized during sprouting to provide the energy required for new growth. This degradation process involves a coordinated set of enzymes acting on the starch granules to break down the complex polysaccharide into glucose residues (Streb & Zeeman, 2012; Zeeman et al., 2010) (Figure 7). Key enzymes include β- and α-amylases (BAM and AMY), debranching enzymes (DBE, typically isoamylase 3 - ISA3), and phosphorylation/dephosphorylation enzymes including Glucan Water Dikinase (GWD), Phosphoglucan Water Dikinase (PWD), Starch Excess 4 (SEX4), and Like Starch Excess Four 2 (LSF2).

2.1. Initiation of Starch Degradation: The Role of Phosphorylation

The semi-crystalline structure of amylopectin makes it resistant to enzymatic degradation. Phosphorylation by Glucan Water Dikinase (GWD) and Phosphoglucan Water Dikinase (PWD) facilitates starch breakdown by adding phosphate groups to glucan residues at C6 and C3 positions, respectively (Blennow & Engelsen, 2010; Kötting et al., 2005; Ritte et al., 2002). This modification disrupts the structure of amylopectin thus improving its accessibility to degrading enzymes (Figure 7). Since starch metabolism is a dynamic process, with alternating cycles of biosynthesis and degradation, some phosphate groups are not eliminated and remain present in the granule during its growth. These phosphate groups influence the rheological properties of starch (Zhou et al., 2021).

GWD phosphorylates glucose residues at the C6 position, allowing further phosphorylation by PWD at C3 (Blennow & Engelsen, 2010). The importance of these enzymes is evident in Arabidopsis *sex1* mutants, which lack GWD and exhibit excessive starch accumulation, increased amylose content, and reduced levels of phosphoester (Caspar et al., 1991; Stitt & Zeeman, 2012; Zeeman & Rees, 1999). GWD contains a nucleotide-binding domain for ATP interaction, a phosphohistidine domain for ATP β-phosphate transfer on a histidine residue, and a carbohydrate-binding module (CBM) for starch binding and phosphate transfer to C6 of a glucose residue (Kötting et al., 2005; Mikkelsen et al., 2004).

Similarly, PWD possesses a CBM, nucleotide-binding domain, and phosphohistidine domain. It follows the same catalytic mechanism as GWD but phosphorylates glucose on C3 (Baunsgaard et al., 2005; Kötting et al., 2005; Mikkelsen et al., 2004). Phosphorylation at the C3 position creates a structural conflict that destabilizes the amylopectin double helices. This leads to a decompaction of the amylopectin structure, making it more accessible to other degradative enzymes.

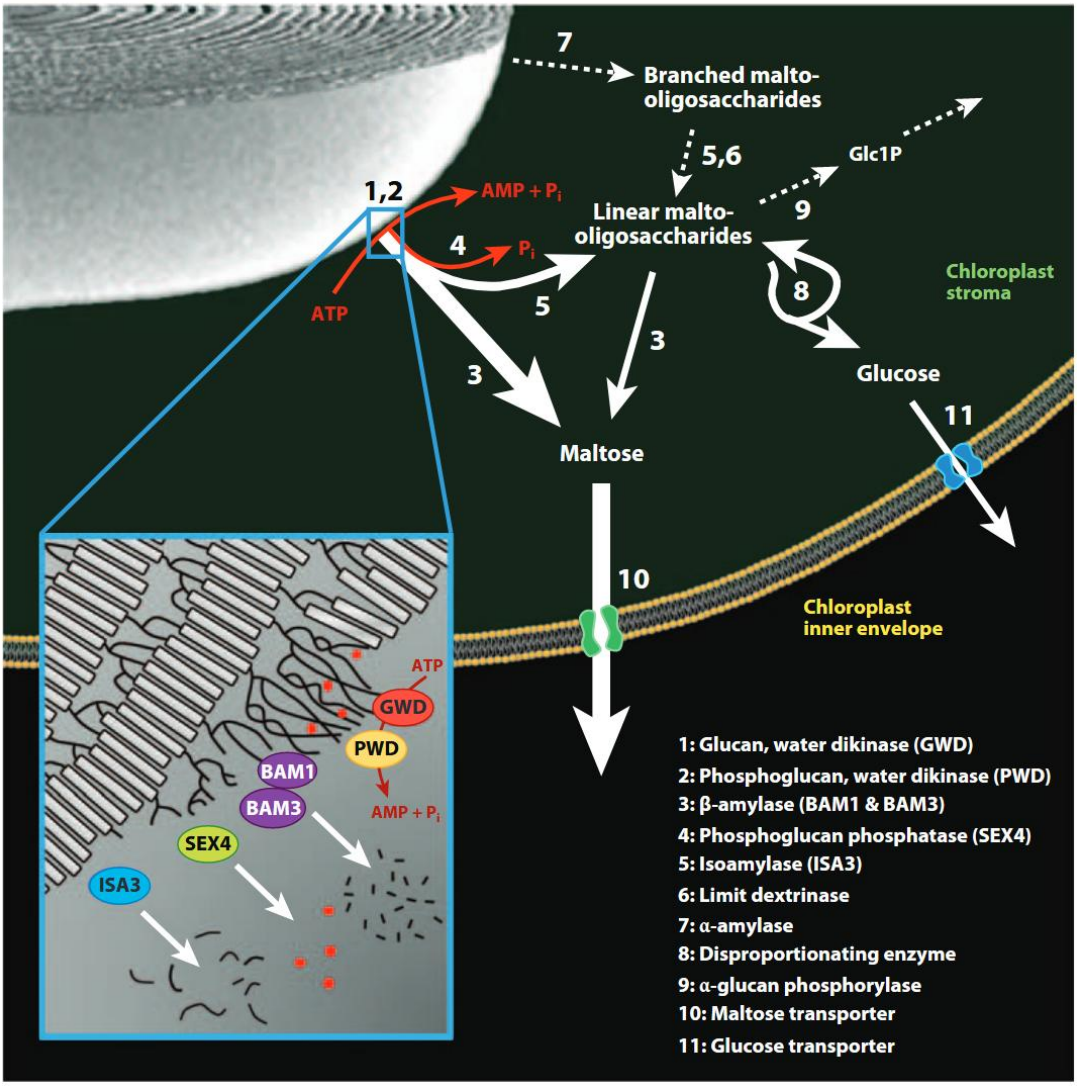

Figure 7 : The pathway of starch degradation in chloroplasts and the role of transient glucan phosphorylation. Maltose and malto-oligosaccharides are released from the surface of the starch granule during degradation. Maltooligosaccharides are metabolized in the stroma. Maltose and glucose are exported to the cytosol. Estimated fluxes are indicated by relative arrow size. Dashed arrows represent the minor steps in Arabidopsis (see text). Inset is a model depicting the role of phosphorylation by GWD and PWD in disrupting the packing of amylopectin double helices (gray boxes). This allows the release of maltose and malto-oligosaccharides (black lines) by β-amylases (BAMs) and DBE (ISA3). Phosphate (red dots) is concomitantly released by SEX4 to allow complete degradation (Zeeman et al., 2010)

2.2. Hydrolysis of amylose and amylopectin: the role of Amylases and Debranching Enzymes

Once phosphorylated, starch is more susceptible to hydrolysis by amylolytic enzymes. β-Amylases (BAMs) cleave maltose units from the non-reducing ends of glucan chains (Figure 7). In Arabidopsis, they play a key role in starch degradation at night (Fulton et al., 2008). α-Amylases (AMY) hydrolyze internal α-1,4 linkages, generating malto-oligosaccharides of varying lengths. AMY3 is the only plastid-targeted α-amylase in Arabidopsis and appears to participate in starch degradation (Yu et al., 2005). However, *amy3* mutants exhibit a wild-type phenotype, suggesting AMY3 is not essential for starch breakdown. It may act synergistically with other amylases (Thalmann et al., 2016).

Debranching enzymes (DBEs) hydrolyze the α-1,6 branch points in amylopectin, producing linear maltodextrins that are further degraded by amylases. These include isoamylases (mainly ISA3) and pullulanases.

2.3. Dephosphorylation

The breakdown of amylopectin glucans requires both phosphorylation and dephosphorylation (Smirnova et al., 2015). Starch Excess 4 (SEX4) and Like Starch-Excess Four 2 (LSF2) catalyze dephosphorylation (Figure 7), removing phosphate groups that would otherwise prevent β-amylase activity (Mahlow et al., 2016). SEX4 dephosphorylates both C6 and C3 positions, whereas LSF2 acts exclusively on C3 (Kötting et al., 2009; Santelia et al., 2011). Arabidopsis *sex4* mutants accumulate phosphorylated glucans and excess starch in plastids (Niittylä et al., 2006).

2.4. The role of DPE

Disproportionating enzymes (DPE) play an important role in starch degradation by preventing the accumulation of short MOS. They cleave a linear α-1,4-glucan chain and transfer the resulting fragment onto another linear glucan chain (Critchley et al., 2001) (Figure 7).

In potato, two isoforms of DPE have been identified: DPE1, which is plastidial, and DPE2, which is cytosolic (Lloyd et al., 2004; Takaha et al., 1993). Both enzymes contain a carbohydrate-binding module (CBM) and a glucanotransferase domain. Disproportionating enzyme 1 (DPE1) is essential for redistributing maltodextrins during starch degradation. It transfers glucosyl residues from small maltodextrins to larger chains, releasing one glucose residue and facilitating the conversion of starch breakdown products into metabolically useful sugars (Critchley et al., 2001). In the cytosol, DPE2 transfers one glucose from maltose on a heteroglycan, releasing the other one (Chia et al., 2004).

The role of DPE is closely linked to that of phosphorylases. Together, these enzymes elongate glucan chains that cannot be processed by other degradative enzymes while also contributing directly to degradation by releasing glucose or Glc-1-P. These products are then used for sucrose synthesis, facilitating energy transport and remobilization within the plant.

2.5. Phosphorylases

Starch phosphorylases are involved in starch metabolism, catalyzing the reversible transfer of glucose-1-phosphate (G-1-P) to α-1,4-glucan chains. In higher plants, two isoforms exist: the plastidial starch phosphorylase, named Pho1 (L-type), and the cytosolic form, Pho2 (H-type) (Albrecht et al., 2001; Brisson et al., 1989; Sonnewald et al., 1995). These enzymes contribute to both starch biosynthesis and degradation (Flores-Castellanos & Fettke, 2023; Hwang et al., 2010; Y. Lu et al., 2006; Satoh et al., 2008).

Pho1 is localized in plastids, where it plays a role in transitory starch metabolism and storage starch accumulation in reserve organs such as roots, tubers, and cereal grains (H.-M. Chen et al., 2002; Hwang et al., 2016; Nakamura et al., 2017; Schupp & Ziegler, 2004; Young et al., 2006). Pho2 is found in the cytosol, where it is involved in maltose metabolism resulting from starch degradation (Flores-Castellanos & Fettke, 2023; Hwang et al., 2010; Y. Lu et al., 2006; Satoh et al., 2008). Pho1 has been identified as a key player in transitory starch turnover and storage starch biosynthesis, maintaining plastidial maltodextrin pools (Hwang et al., 2016; Nakamura et al., 2017; Schupp & Ziegler, 2004; Young et al., 2006). Pho1 has been shown to interact with starch synthases (SS) and starch-branching enzymes (SBEs) in cereals such as wheat, rice, maize, and barley (Ahmed et al., 2015; Crofts et al., 2017; Hwang et al.,

2016; Kamble et al., 2023; F. Liu et al., 2009; Nakamura et al., 2012, 2017; Tetlow et al., 2004, 2008). Pho1 plays a role in the recycling of maltooligosaccharides (MOS) generated from pre-amylopectin trimming by debranching enzymes (DBEs) (Hwang et al., 2010, 2016; Y.-C. Lin et al., 2017; Satoh et al., 2008). It has been suggested that Pho1 could be involved in the granule initiation (Kamble et al., 2023; Mérida & Fettke, 2021). This aspect will be further detailed in the subchapter 3.7.

3. Initiation

While the role of proteins involved in the granule biosynthesis and degradation are well documented, the regulation of the granule initiation itself is an area where further investigation is needed. Unraveling the mysteries of starch granule initiation in potato tuber would not only advance our comprehension of starch metabolism but would also enhance industrial applications based on starch quality and yield of potato and other starch-rich tubers. In contrast to the well-understood synthesis and degradation pathways of amylose and amylopectin, starch granule initiation remains a complex and less elucidated aspect of starch metabolism across plant species. Variation in this process could explain the diversity of granule morphology and number between species and organs (Seung & Smith, 2019).

Recent work, mostly in Arabidopsis leaves, has discovered and characterized proteins involved in granule initiation and morphogenesis. It is now established that this initiation depends, at least in *Arabidopsis thaliana* leaves, of a major enzyme, Starch Synthase 4 (SS4). More recently, several proteins lacking enzymatic activity, and interacting with SS4, were found to be essential to the correct starch granule initiation. (Abt et al., 2020; Seung et al., 2017, 2018; M. Sharma et al., 2024; Szydlowski et al., 2009; Vandromme et al., 2019, 2023). However, the presence of a primary substrate at least a DP10, is required by this heteromultimeric complex to start the initiation (Seung et al., 2017).

In potato, despite its starch-rich tubers, the specific mechanisms governing granule initiation are still under investigation. The granule initiation has been less studied in storage organs, but some proteins, mentioned below, are suspected to be involved in this process (Seung & Smith, 2019).

3.1. SS4, the central initiating enzyme

The glucosyltransferase STARCH SYNTHASE 4 (SS4) is a critical enzyme involved in the granule initiation and morphogenesis in Arabidopsis. The chloroplasts of the wild-type Arabidopsis plants usually contain five to seven granules, this number being dependent of the chloroplast volume (Crumpton-Taylor et al., 2012). In contrast, mutants lacking SS4 exhibit a drastically reduced number of starch granules per chloroplast, often forming only one or none, which leads to an increase of granule size (Roldán et al., 2007). This highlights the

critical role of this enzyme in granule initiation (Mérida & Fettke, 2021; Seung & Smith, 2019). More precisely, in wild-type plants, immature leaves contain more starch granules per chloroplast than mature leaves, likely due to coalescence of the granules during leaf development (Bürgy et al., 2021; Crumpton-Taylor et al., 2012). However, *ss4* mutants failed to form starch granules until late in leaf development, and then a single starch granule is formed in each chloroplast (Crumpton-Taylor et al., 2013). Additionally, SS4 is essential for anisotropic growth of starch granules, which results in the characteristic flattened shape of granules in Arabidopsis leaves (Roldán et al., 2007). Mutants deficient in SS4 produce spherical granules due to isotropic growth, demonstrating SS4 necessity in shaping granules. Moreover, *ss4* mutants display a severe growth defect, with a modest but significant reduction in starch levels (Roldán et al., 2007). *ss4* mutants accumulate ADP-Glc, suggesting that other SS isoforms cannot efficiently use this substrate in absence of SS4 (Crumpton-Taylor et al., 2013). This accumulation of ADP-Glc in plants is likely the cause of the growth defect observed in *ss4* mutants (Ragel et al., 2013).

Despite these alterations, no modification of the granule internal structure was observed in *ss4* mutants, except for a slight but reproducible decrease in amylopectin short chains (Roldán et al., 2007). Normal starch metabolism was restored in *ss4* mutants plants by transgenic expression of SS4 at concentrations far below those in wild-type plants (Crumpton-Taylor et al., 2013). It is also interesting to note that starch granules in Arabidopsis *ss4* mutants are rounded with a distinct core (or hilum), resembling those in non-photosynthetic organs such as potato tubers, where SS4 is weakly expressed (Hochmuth et al., 2024; Roldán et al., 2007). This suggests that SS4 may play a minor role in granule initiation in storage organs, as supported by findings in rice, where an SS4b-deficient mutant exhibits only minor alterations in starch content and granule morphology (Toyosawa et al., 2016).

The role of SS4 in controlling the granule morphology and number has also been demonstrated in wheat. In wild type wheat, a single large A-type granule initiates during early grain development, whereas in mutants deficient in SS4, most amyloplasts formed compound granules due to multiple initiation points (Hawkins et al., 2021). This contrasts with Arabidopsis *ss4* mutants, where granule number is reduced rather than increased (Roldán et al., 2007).

SS4 contains a C-terminal glucosyltransferase domain, which promotes granule initiation, and a non-enzymatic N-terminal region, essential for its correct localization near the thylakoid membranes, which also influences anisotropic granule growth (Bürgy et al., 2021; Gámez-Arjona et al., 2014; K.-J. Lu et al., 2018). SS4 belongs to the GT5 family of glycosyltransferases within the Carbohydrate Active Enzyme (CAZy) database (Lombard et al., 2014), with highly conserved starch catalytic (GT5) and glycosyltransferase 1 (GT1) domains in its C-terminal region (Leterrier et al., 2008; H. Liu et al., 2015). The active form of SS4 appears to be a homodimer, with a conserved region between the coiled-coil and glycosyltransferase domains required for dimer formation (Raynaud et al., 2016).

Overall, SS4 is proposed to play an essential role in generating glucan primers necessary for starch granule initiation, based on three key observations. First, unlike mutants of other SS isoforms, *ss4* mutants show only minor changes in amylopectin structure but have a drastically reduced number of starch granules per chloroplast (Crumpton-Taylor et al., 2013; Roldán et al., 2007; Szydlowski et al., 2009). Second, *ss4* mutants accumulate high levels of ADP-glucose, suggesting that other SS isoforms have limited activity without SS4 and that SS4 acts upstream in granule initiation (Crumpton-Taylor et al., 2013). Finally, the ss4 phenotype is partially rescued when the glucan hydrolase AMY3 is inactivated, indicating that glucan primers can form without SS4 but are more susceptible to degradation (Seung et al., 2016).

Furthermore, in Arabidopsis, *ss3 ss4* double mutants display decreased starch synthesis compared to *ss4* single mutants (Szydlowski et al., 2009), suggesting that SS3 can partially compensate for SS4 loss. This redundancy is also observed in rice, where *ss3 ss4* double mutants exhibit aberrant granule morphology, unlike single mutants (Toyosawa et al., 2016).

While SS4 is crucial for starch granule formation and morphology in Arabidopsis, its precise mechanism of action—particularly its interaction with the initiation complex—remains to be fully elucidated.

3.2. PII1/MRC and MFP1: structural regulators of localization

PROTEIN INVOLVED IN THE STARCH INITIATION 1 (PII1), also named MRC for MYOSIN-RESEMBLING CHLOROPLAST PROTEIN (MRC), plays a central role in regulating starch granule

initiation, interacting with multiple other proteins. Like *ss4*, *pii1* mutants in *Arabidopsis thaliana* exhibit a reduction of granule number (Roldán et al., 2007; Seung et al., 2018; Vandromme et al., 2019). Indeed, mutants lacking PII1 exhibit one large lenticular granule per chloroplast, instead of the five to seven granules in wild-type plants. However, unlike s*s4*, no modification of the granule morphology was observed in *pii1* mutants, where the granules remain flattened like in wild-type plants. Additionally, no modification of growth rate and starch amount were observed in *pii1* mutants, and the amylopectin chain length distribution remained unchanged (Vandromme et al., 2019). The *pii1* phenotype appears less severe than that of *ss4*. It was suggested that the function of the C-terminal region (catalytic part) of SS4 was inactivated in absence of PII1 (leading to less starch granule per chloroplast), without affecting the function of the N-terminal part (anisotropic growth still occurs). PII1 could prevent the substrate degradation before SS4 action (Vandromme et al., 2019). Moreover, in absence of SS4, SS3 can partially fulfill its function (Szydlowski et al., 2009) but the additional loss of PII1 (*ss4 pii1*) further reduces the initiation of starch granules, with a phenotype more severe than that of the s*s4* simple mutant (Vandromme et al., 2023). This means that PII1 can help SS3 in the initiation step in absence of SS4.

While MRC/PII1 is also involved in granule initiation in wheat (*Triticum turgidum*), its role appears distinct from that previously described in *Arabidopsis thaliana* leaves. In wild-type wheat, large A-type starch granules are initiated early in grain development, whereas smaller B-type granules start forming approximately 10 to 15 days later. However, in TILLING mutants of tetraploid wheat lacking *MRC* expression, A-type granules were reduced in size, and B-type granules occupied a higher volume of the endosperm compared to the wild type. Additionally, B-type granules were observed earlier in development, emerging around 10 days post-anthesis rather than the typical 15 to 20 days in wild-type plants (J. Chen et al., 2024). These findings suggest that MRC regulates the timing of starch granule initiation by repressing the early formation of B-type granules highlighting a case of functional diversification among granule initiation proteins.

This protein was not detected in potato tubers, which could explain the presence of a single granule per amyloplast in the storage organs (Hochmuth et al., 2024). Surprisingly, the ectopic overexpression of MRC in the tubers led to a strong diminution of the granule size, the starch content and the tuber yield (Hochmuth et al., 2024). Moreover, the granule

morphology was altered in the MRC overexpression lines, with the presence of multiple initiation points.

MFP1 (MAR-BINDING FILAMENT-LIKE PROTEIN 1) is a thylakoid membrane-associated protein. Its N-terminal part is predicted to contain a plastid transit peptide, but also a thylakoid twin-arginine translocation (Tat) signal sequence, and a short transmembrane domain that allows its anchoring to thylakoid membranes. Its C-terminal part, consisting of long coiled-coil motifs, faces the plastid stroma (Jeong et al., 2003; M. Sharma et al., 2024). MFP1 can promote starch granule initiation without being associated to the thylakoid membrane, but is fully efficient when being associated to it (M. Sharma et al., 2024).

Arabidopsis mutants lacking MFP1 produce fewer, but larger, granules per chloroplast than the WT (Seung et al., 2018). A slight increase in the number of granule per chloroplast was observed in lines overexpressing MFP1 and no impact was observed on the granule morphology (M. Sharma et al., 2024). The impact of the MFP1 overexpression on the granule number and morphology is less severe than in the lines overexpressing PTST2 (Seung et al., 2017). No impact of the MFP1 overexpression was observed on the starch content. The simultaneous overexpression of MFP1 and PTST2 in Arabidopsis led to a strong increase of the granule number per chloroplast, greater than that of single-overexpressing plants, with more than twenty granules per chloroplast (M. Sharma et al., 2024). However, it appears unlikely that MFP1 and PTST2 may have a redundant role, because PTST2 can interact with short glucan chains thanks to its CBM48 domain and with the major initiation enzyme SS4, whereas MFP1, which is thylakoid associated, does not have CBM48 and appears to have more a undirect role, by guiding and localizing PTST2 and SS4 (Seung et al., 2017; M. Sharma et al., 2024).

The expression of MFP1 variants led to a modification of starch granule number and localization (M. Sharma et al., 2024). The absence of the transmembrane domain of MFP1 led to the formation of the starch granules at the periphery of the chloroplasts. In Arabidopsis, expression of MFP1 with a transmembrane domain anchoring it to the chloroplast membrane rather than the thylakoid membrane also altered the localization of PTST2 and SS4 to the periphery of the chloroplasts, demonstrating that MFP1 is required for the correct localization of PTST2 and SS4 (Seung et al., 2018; M. Sharma et al., 2024). Thus, MFP1 localization specifically determines the subchloroplast localization of the heteromultimeric initiation

complex and the formation of the starch granules. The correct localization of MFP1 could be the first step of granule initiation.

3.3. PTST2 and PTST3 are involved in primers delivery

Two homologs of PTST1 (responsible for GBSS localization), termed as PTST2 and PTST3, were identified in *Arabidopsis thaliana* in 2017 (Seung et al., 2017). Like PTST1, both proteins contain coiled-coil and a CBM48 domain, the latter being required for PTST2 function. Mutant studies highlight the distinct roles of these proteins: while accumulating ADP-Glc, *ptst2* mutants display either no granules or a single large granule per chloroplast, like *ss4* (Roldán et al., 2007). *ptst3* mutants showed only a slight reduction of granule numbers and wild-type ADP-Glc levels (Seung et al., 2017). The *ptst2 ptst3* double mutant produces a higher number of starchless chloroplasts than the *ptst2* single mutant, with granules displaying a more rounded morphology compared to the single mutants and the flattened shape of wild-type granules. Amylopectin structure was not altered in both *ptst2* and *ptst3* mutants. Consistent with the reduction of granule number, the ADP-Glc content was strongly increased in the double mutant (twice the *ptst2* level). Overexpression of PTST2 in Arabidopsis resulted in chloroplasts containing a high number of small granules, and this effect was dependent on the presence of SS4. Overall, these results indicate that PTST2 plays a significant role in starch granule initiation. Since the gene encoding PTST3 has been lost in several species during evolution and no particular difference with wild-type plants was observed in *ptst3* mutants, this protein might play a minor role. However, the phenotype of the *ptst2 ptst3* double mutant, more severe than the *ptst2* single mutant, suggests that PTST3 can partially compensate for the absence of PTST2 (Seung et al., 2017).

The study of different mutants indicates that the function of PSTS2 could be different depending on the species but also depending on the organs. An homolog to Arabidopsis PTST2, named FLO6, was found in rice and barley (Peng et al., 2014; Saito et al., 2018; Yan et al., 2024). Leaves of *flo6* mutants in rice displayed a reduced number of starch granules, whereas loss of this PTST2 ortholog in the endosperm resulted in heterogenous amyloplasts with highly variable numbers of initiations within each compound granule (Peng et al., 2014; L. Zhang et al., 2022).

In barley leaves, the loss of FLO6 resulted in fewer granules per chloroplast with reduced starch content (Watson-Lazowski *et al*., 2022). However, the lack of this protein in storage organs of the corresponding mutant (*Hvflo6)* resulted in the impossibility to produce B-type granules in the endosperm, and with the formation of an A-type granule displaying aberrant morphology (Suh et al., 2004).

The effect of the loss of BGC1, homolog to Arabidopsis PTST2, in wheat endosperm is similar to that of barley. Indeed, the lack of the protein in storage organs of the corresponding mutants (*Tabgc1, Tabgc2)* resulted in the absence of B-type granules in the endosperm and an aberrant morphology of A-type granules (Chia et al., 2020). In leaves, it caused fewer but larger starch granules per chloroplast with normal starch content (Watson-Lazowski *et al*., 2022).

In leaves of *Brachypodium*, the loss of PTST2 caused an almost complete loss of starch, with a severe growth alteration (Watson-Lazowski et al., 2022). On the contrary, in the *Brachypodium* endosperm of mutants defective in *ptst2,* compound starch granules were produced from supernumerary granule initiations per amyloplast, and no modification of starch content was observed (Watson-Lazowski *et al*., 2022). The strong alteration of the granule initiation in *Brachypodium* compared to other species can be explained by differences between species in their capacity to form granules in absence of PTST2. Indeed, in Arabidopsis*,* it was demonstrated that the fewer granules per chloroplast were observed in *ptst2 ptst3* or *ptst2 ss5* double mutants, compared to *ptst2* single mutant, suggesting a redundant role of PTST3 and SS5 (Abt et al., 2020; Seung et al., 2017). However, neither PTST3 or SS5 were detected in wheat, barley or *Brachypodium*. The slighter modification of phenotype in wheat and barley could be explained by the presence of other interacting proteins, such as PHS1 that interacts with BGC1 in wheat (Kamble et al., 2023).

Two isoforms of PTST2, named PTST2a and PTST2b, were recently identified in potato (Hochmuth et al., 2024). These genes have been found in other Solanaceae species, on different chromosomes, suggesting that they are paralogs. Some species, such as *Solanum melonga* and *Solanum lycopersicum* contain only PTST2a, but no species with only PTST2b have been identified. Unlike MRC, PTST2b is expressed in the tubers. While it has long been supposed that ellipsoid granule morphology results from the amyloplast physical space constraints, *ptst2b* mutants exhibit perfectly round shaped granules. Therefore, it appears

that granule morphology might be controlled by PTST2. Such effects of PTST2 on granule shape were unexpected, as in *Arabidopsis thaliana*, this protein only affects granules number and size.

3.4. SS5 : a noncanonical modulator

In Arabidopsis, STARCH SYNTHASE 5 (SS5) exists as a truncated version compared to potato SS5 and other Arabidopsis SS isoforms (Helle et al., 2018; Pfister & Zeeman, 2016). STARCH SYNTHASE 5 (SS5) appears different from the canonical starch synthases, responsible for starch biosynthesis. Bioinformatic study reveal that, unlike SS4 and other starch synthases, SS5 lacks catalytic glycosyltransferase activity (Abt et al., 2020; Helle et al., 2018). This lack of catalytic activity was confirmed *in vitro* and *in vivo.* However, the phenotypic characteristics of *ss5* mutants resemble those of *ss4* mutants, although less severe, displaying fewer but larger starch granules per plastid (Abt et al., 2020; Roldán et al., 2007). Interestingly, the granules exhibit an irregular lenticular shape, similar to those observed in *ss3* mutants (Szydlowski et al., 2009, 2011). Then, although not catalyzing a classic glucosyltransferase reaction, SS5 seems to be implied in the granule initiation. SS5 inactivation does not alter the amylopectin chain length distribution, suggesting that SS5 does not possess elongation activity (Abt et al., 2020). This is consistent with the suspected lack of catalytic activity in SS5. Furthermore, *ss4 ss5* double mutant revealed a greater number of empty chloroplasts than the *ss4* simple mutant, even though sporadic starch granule formation still occurs in some chloroplasts, likely due to the marginal activity of SS3. In the same way, the effect of PTST2 and PTST3 inactivation was more intense when combined with SS5 mutation.

This protein can interact with starch, thanks to an aliphatic patch on the surface of the GT5 subdomain, which is strongly conserved among SS5 orthologs (Abt et al., 2020). In potato tubers, SS5 has been found to be associated with starch granules (Helle et al., 2018). When incubated with waxy maize starch granules, recombinant At-SS5 effectively bound to starch (Abt et al., 2020). Overall, it was suggested that SS5 may promote granule initiation by binding and correctly localizing glucan substrates, via its interaction with protein partners (see p.60). Alternatively, SS5 may protect new forming granules from amylolytic degradation (Abt et al., 2020; Seung et al., 2016).

No orthologs of SS5 were identified in *Brachypodium distachyon,* wheat or barley, suggesting a relatively recent gene loss within the Pooideae family (Abt et al., 2020). SS5 has also been identified in starch granules of potato tubers (Helle et al., 2018). A very recent study using dihaploid lines reported marked changes in starch granule initiation upon SS5 disruption (Hu et al., 2025). These included a reduced granule size, increased number of starch granules per amyloplast (often forming compound granules), lower gelatinization temperatures and changes in amylose/amylopectin ratio. However, the significance of these observations could be discussed, as statistical analyses were not systematically provided to support these differences.

3.5. Protein-protein interactions

Beyond their individual functions, these proteins operate within multiprotein complexes. While the individual roles of these proteins provide important insights into starch metabolism, understanding how they interact reveals a more complete picture of the mechanisms regulating granule initiation. In *Arabidopsis thaliana*, these interactions form a coordinated network essential for this process.

SS4 interacts with multiple partners in Arabidopsis. By associating with PTST2 and PII1 (MRC), SS4 binds to maltooligosaccharides to elongate them (Seung et al., 2017; Vandromme et al., 2019). However, its role in *Solanum tuberosum* is poorly understood. SS4 expression was found to be very low in potato tubers (Hochmuth et al., 2024) and while it can interact with PTST2a, it does not associate with PTST2b, which is predominant in the tubers, indicating distinct specificities among the PTST2 isoforms regarding their partners.

PII1 contains long coiled-coil domains, usually involved in protein-protein interactions (Adamson et al., 1993). Indeed, using a yeast two-hybrid screen and BiFC (Bimolecular Fluorescence Complementation) experiments, it was demonstrated that PII1 can interact with SS4 (Vandromme et al., 2019). PII1 does not contain any carbohydrate binding module (CBM). It localizes with SS4 in specific points of the thylakoids, but their respective localization does not depend on each other (Vandromme et al., 2019). It was suggested that PII1 could prevent the substrate degradation before SS4 action or may be required for the correct folding of SS4 (Vandromme et al., 2019). PII1 also interacts with PTST2 (Seung et al., 2017, 2018) and SS5

(Abt et al., 2020). However, the function of these interactions in the granule initiation is not yet understood.

In Arabidopsis, PTST2 interacts directly with several proteins. Supporting this, PTST2 has been shown to copurify with SS4, PTST3, MRC/PII1, and MFP1 (Seung et al., 2017, 2018). Since CBM48 of PTST2 can bind to DP10 maltooligosaccharides (MOS), but not to shorter ones (DP7), it has been suggested that PTST2 facilitates granule initiation by delivering MOS primers to SS4 (which does not possess a CBM itself). This length is likely necessary because it allows the formation of a helical secondary structure required for recognition by PSTS2. This MOS is then used as the initial substrate for starch granule formation (Seung et al., 2017). Consistent with this model, several mutants in Arabidopsis with altered MOS levels have altered starch granule numbers (Malinova, Qasim, et al., 2018; Mérida & Fettke, 2021). An homolog to Arabidopsis PTST2, named FLO6, was found in rice (Peng et al., 2014). In this species, FLO6 interacts with ISA1 and more recently, it was found that it also interacts with FLO9, a protein ortholog to Arabidopsis LIKE EARLY STARVATION 1 protein (LESV) (Yan et al., 2024). No evidence of an interaction between PTST2 and ISA1 was found in Arabidopsis (Seung et al., 2017, 2018), which can be explained by a potential difference between species and between leaves and storage organs.

In Arabidopsis, SS5 interacts with itself and co-immunoprecipitation and co-expression assays revealed that it interacts as well as with MRC/PII1 (Abt et al., 2020; Seung et al., 2018; Vandromme et al., 2019, 2023). No difference could be observed between *ss5* and *ss5 mrc* double mutant, suggesting that SS5 influences starch granule initiation via the MRC protein (Abt et al., 2020).

It now appears that normal starch granule initiation in Arabidopsis leaves requires a heteromultimeric complex that forms a specific network, which includes SS4, PTST2, PTST3, MFP1, MRC/PII1 and SS5, and coordinates the process through protein-protein and protein-glucan interactions (Figure 8). All these proteins (except SS4) are proposed to act in granule formation by modulating SS4 activity, location and substrate availability, but they are unlikely to play a direct role in granule synthesis. SS4 is the major enzyme of this complex, as it provides the elongation activity necessary to initiate the starch granule formation. PTST2 appears to be a central node in this interaction network, as it connects with SS4, PTST3, PII1, and MFP1. Its interaction with MFP1 allows the correct localization of the complex within the

chloroplast (Seung et al., 2017; M. Sharma et al., 2024). It also can bind to glucans through its CBM48, useful for delivering long MOS primers to SS4, which are then used as the initial substrate for starch granule formation (Seung et al., 2017). PTST2 appears to plays an important role in coordinating these interactions. PII1 connects SS4, SS5, and PTST2, making it a potential linker between these proteins. SS5 appears more isolated, interacting only with itself and PII1, which could suggest a more specific or tightly regulated function.

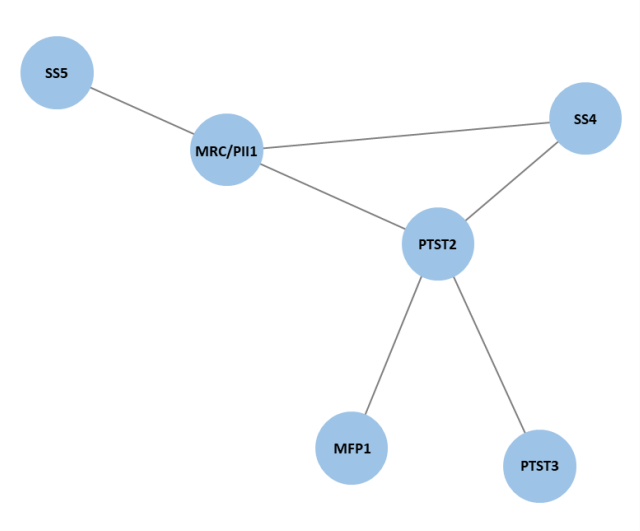

Figure 8 : Protein interaction network in *Arabidopsis thaliana* starch granule initiation. This network highlights the interdependency of enzymatic activity and structural organization in regulating granule initiation. SS4 is a key enzyme in starch granule initiation, and is involved in glucan elongation. PTST2 binds to maltooligosaccharides and facilitates their transfer to SS4. MFP1 is thought to contribute to granule initiation by influencing its spatial localization and anchoring. PII1/MRC is a potential regulator of SS4 activity. PTST3 is a carbohydrate-binding protein that may act redundantly or synergistically with PTST2 in starch granule initiation, although its precise function remains less well defined. SS5 is a recently identified non-catalytic protein that appears to contribute to starch granule initiation by interacting with SS4 and influencing granule number, possibly through regulatory or scaffolding functions.

All the observations presented in this chapter indicate that the proteins involved in granule initiation are conserved across species and organs. However, their roles may vary depending on the specific granule initiation patterns of a given species or tissue. Notably, some proteins (ISA1, ISA2, PHO1) known for their involvement in starch metabolism in Arabidopsis have been identified as playing a more specific role in granule initiation in potato tubers. These proteins will be discussed in detail in the following sections.

3.6. The role of isoamylases in suppressing excessive granule initiation

In potato tubers, isoamylase, a starch-debranching enzyme exists as a heterotetrameric complex comprising ISA1 and ISA2 subunits (Bustos et al., 2004). Comparative studies in *Arabidopsis* and maize demonstrate evolutionary divergence: dicotyledonous plants like potato require both ISA1 and ISA2 for granule regulation, whereas monocot ISA1 can function as a homomultimer (Facon et al., 2013; Q. Lin et al., 2013). The complex is responsible for hydrolyzing some of the α-1,6 linkages (branching points) that leads to distribution of branching points compatible with amylopectin phase transition (S. Ball et al., 1996) (see p.45).

Additionally, isoamylase plays a critical role in modulating starch granule initiation. Without sufficient isoamylase activity, soluble glucans (phytoglycogen) accumulate, but the primary defect lies in the loss of control over granule number. Antisense suppression of either subunit leads to a 5–10-fold increase in granule numbers, with transgenic lines accumulating small granules alongside normal-sized granules within the same amyloplast (Bustos et al., 2004). This phenotype suggests that isoamylase normally suppresses the initiation of excess glucan molecules that could crystallize into new granules. The presence of tiny granule clusters was also observed in the antisense lines (Figure 9). It was proposed that isoamylases trim poorly organized glucan branches, ensuring only structured glucans proceed to grow and form mature granules (Delatte et al., 2005). In *Arabidopsis*, the absence of isoamylases in *Atisa1* and *Atisa2* mutants leads to phytoglycogen accumulation and structurally altered amylopectin, a phenotype mirrored in potato (Bustos et al., 2004; Delatte et al., 2005; Streb et al., 2009; Wattebled et al., 2005, 2008). A phenotype similar to Arabidopsis was observed in barley mutants lacking isoamylase activity (Burton et al., 2002). Additionally, it was recently demonstrated in rice that ISA1 interacts with FLO6, a protein homolog to Arabidopsis PTST2, known to be involved in granule initiation (Peng et al., 2014). These findings highlight isoamylases conserved role across species in maintaining amylopectin crystallinity and regulating granule initiation. The proposed mechanism relies on the capacity of ISA1/ISA2 to regulate the number of starch granules per amyloplast by limiting the initiation of new glucans precursors.

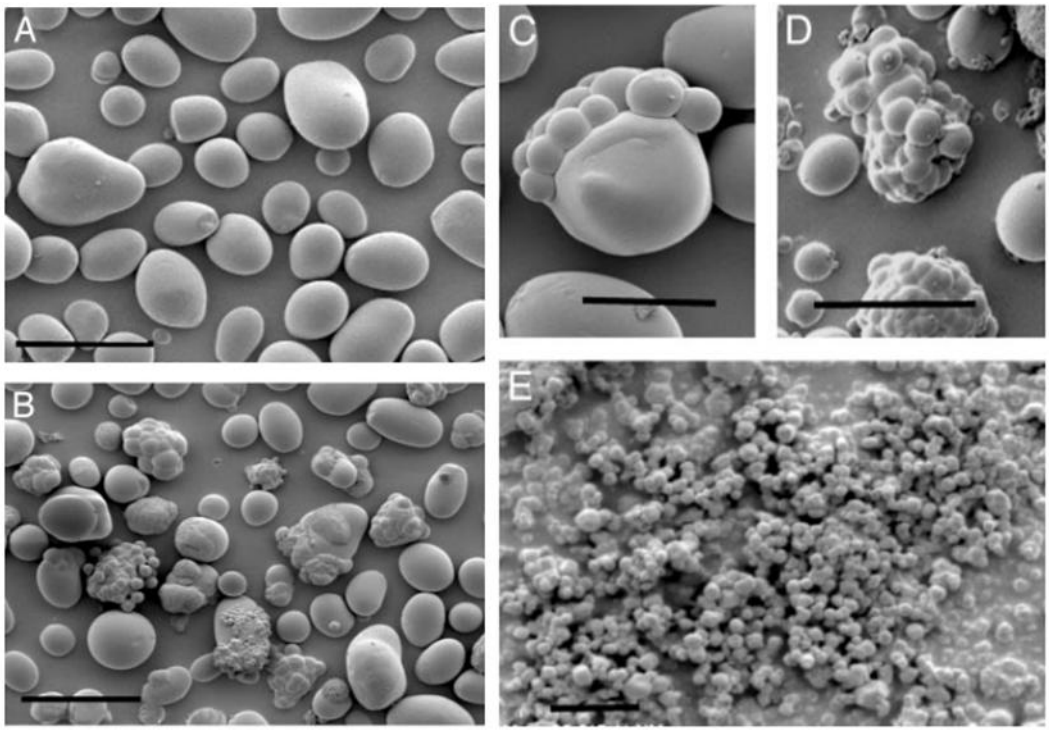

Figure 9 : Starch granules isolated from control and isoamylase mutant tubers. (A) Control line Stisa1.32. (Scale bar is 50 µm.) (B) Antisense line Stisa1.44. (Scale bar is 50 µm.) (C) Antisense line Stisa2.27. (Scale bar is 20 µm.) (D) Granule clusters from antisense line Stisa1.44. (Scale bar is 20 µm.) (E) Very small starch granules isolated from starch of antisense line Stisa1.37. (Scale bar is 2 µm.) No equivalent material was found in starch of control tubers (Adapted from Bustos et al., 2004).

3.7. Suspected implication of Pho1 in granule initiation

Starch phosphorylases are involved in starch metabolism, catalyzing the reversible transfer of a glucose residue from glucose-1-phosphate (G-1-P) to α-1,4-glucan chains. In higher plants, two isoforms exist: the plastidial starch phosphorylase, named Pho1 (L-type), and the cytosolic form Pho2 (H-type) (Albrecht et al., 2001; Brisson et al., 1989; Sonnewald et al., 1995). These enzymes contribute to both starch biosynthesis and degradation (Flores-Castellanos & Fettke, 2023; Hwang et al., 2010; Y. Lu et al., 2006; Satoh et al., 2008). In potato, two isoforms of Pho1 have been identified. Pho1a corresponds to the isoform primarily localized in amyloplasts, while Pho1b is mainly found in chloroplasts. In contrast, Pho2a and Pho2b are both cytosolic (Albrecht et al., 2001; Brisson et al., 1989; Nakano et al., 1989; Sonnewald et al., 1995; Van Harsselaar et al., 2017).

The precise role of Pho1 in starch granule initiation remains debated. In Arabidopsis, loss of PHS1 (Pho1) alone has minor effects on starch metabolism and does not alter starch granule initiation (Malinova et al., 2014). However, in *phs1* mutants lacking either MEX1, a

maltose exporter, or DPE2, the number of starch granules per chloroplast is significantly reduced. The most severe phenotype is observed in *dpe2 phs1* double mutants, which contain only a single granule per chloroplast, whereas *mex1 phs1* mutants generally have two or three (Mérida & Fettke, 2021). Furthermore, the activity and mRNA expression of both PHS1 and PHS2 are increased in Arabidopsis *ss4* mutants, suggesting a compensatory mechanism (Roldán et al., 2007). Additionally, it has been suggested that PHS1 and PHS2 contribute to abiotic stress tolerance (Zeeman et al., 2004). Since *ss4* mutants suffer from starch starvation, it has been proposed that the increased expression of PHS1 and PHS2 may be a response to this deficiency (Roldán et al., 2007).

In wheat endosperm, PHS1 (Pho1) interacts with BGC1, a homolog of *Arabidopsis* PTST2, which is involved in B-type starch granule initiation (Kamble et al., 2023). Wheat mutants deficient in PHS1 exhibit less but larger B-type granules, without affecting A-type granules or starch content. These results suggest that PHS1 is crucial for B-type granule initiation, indicating distinct mechanisms for the two types of granules in wheat endosperm.

In potato, PHS1 has been shown to bind short glucans, including maltose (DP2), particularly in the presence of high concentrations of glucose-1-phosphate (Sonnewald et al., 1995). Mutants lacking Pho1a, the isoform expressed in tubers, produced an increased number of rounded starch granules and exhibit a reduced apparent amylose content (S. Sharma et al., 2023). Furthermore, Fettke et al. (2010) demonstrated that exogenous glucose 1-phosphate is efficiently taken up by potato tuber parenchyma cells and directly incorporated into starch granules. Their data revealed that this pathway involves plastidial phosphorylase (Pho1) directly transferring glucosyl units from G1P to starch granules, bypassing the classical ADP-glucose-dependent pathway. This evidence supports the hypothesis of a second elongation pathway for starch biosynthesis in potato, likely involving phosphorylases.

Similarly, in rice endosperm, mutants lacking PHS1 (Pho1), the main phosphorylase activity, leads to abnormal starch biosynthesis, characterized by an accumulation of small granules and a modification of amylopectin structure (Satoh et al., 2008). Interestingly, this phenotype is temperature-sensitive: at 20°C, the defects are more pronounced, whereas at 30°C, the effects are mild, possibly due to the action on an unidentified compensatory factor referred to as the “factor X”.

Altogether, these results suggest that PHS1 may contribute to the regulation of starch granule initiation in different species, although its precise role likely varies depending on the tissue, species, and environmental conditions. Further research will be necessary to clarify whether PHS1 participates directly in granule initiation, acts as a modulator of glucan availability, or functions within a larger regulatory complex.

4. ESV1 and LESV: two recently identified proteins influencing starch metabolism

EARLY STARVATION 1 (ESV1) and LIKE EARLY STARVATION 1 (LESV) were first identified in Arabidopsis thaliana and have recently been recognized as key players in starch metabolism in this species (Feike et al., 2016; C. Liu et al., 2023). Both proteins are involved in starch-related processes, with LESV being one of the most abundant starch-bound proteins in potato tuber (Figure 13). Despite multiple studies on *Arabidopsis thaliana*, the precise role of these proteins remains unclear.

4.1. ESV1 and LESV structure

The LESV protein in *Arabidopsis thaliana* has a molecular weight of 66 kDa and consists of 578 amino acids, whereas its homolog in potato is slightly smaller, with a molecular weight of 63 kDa and 554 amino acids. The ESV1 protein has a molecular weight of 49 kDa in Arabidopsis and potato, and comprises 426 and 432 amino acids, respectively. Arabidopsis has a molecular weight of 49 kDa and comprises 426 amino acids, while in potato, it has a slightly increased molecular weight of 49 kDa with 432 amino acids.

Interestingly, no known catalytic domain was identified in these two proteins (Feike et al., 2016). However, ESV1 contains a specific motif composed of a proline-rich domain in its C-terminal region (11 proline residues between amino acids 397 and 425) (Figure 10). LESV and ESV1 share a strongly conserved C-terminal domain of approximately 240 amino acids (Feike et al., 2016; C. Liu et al., 2023). This region forms an anti-parallel β-sheet that contains acidic and aromatic amino acid residues, particularly tryptophan, that align on both sides of the sheet (Figure 10). Interestingly, these alignments are 70 Å long and are spaced by approximately 14 Å, a configuration that could correspond to the size of the amylopectin double helices (Buléon et al., 1998). Due to its specific amino acid composition, this region was hypothesized to be involved in the binding of long glucans (Feike et al., 2016), an hypothesis that has since been experimentally confirmed. Electromobility shift assay (EMSA) experiments revealed that both LESV and ESV1 interact with amylopectin, but not amylose, via their C-terminal domain (Osman et al., 2024). This affinity increases with the amount of substrate, suggesting a highly specific interaction (Figure 11). Additionally, LESV was shown to be involved in helping amylopectin phase transition from amorphous to crystallin state (C. Liu et al., 2023).

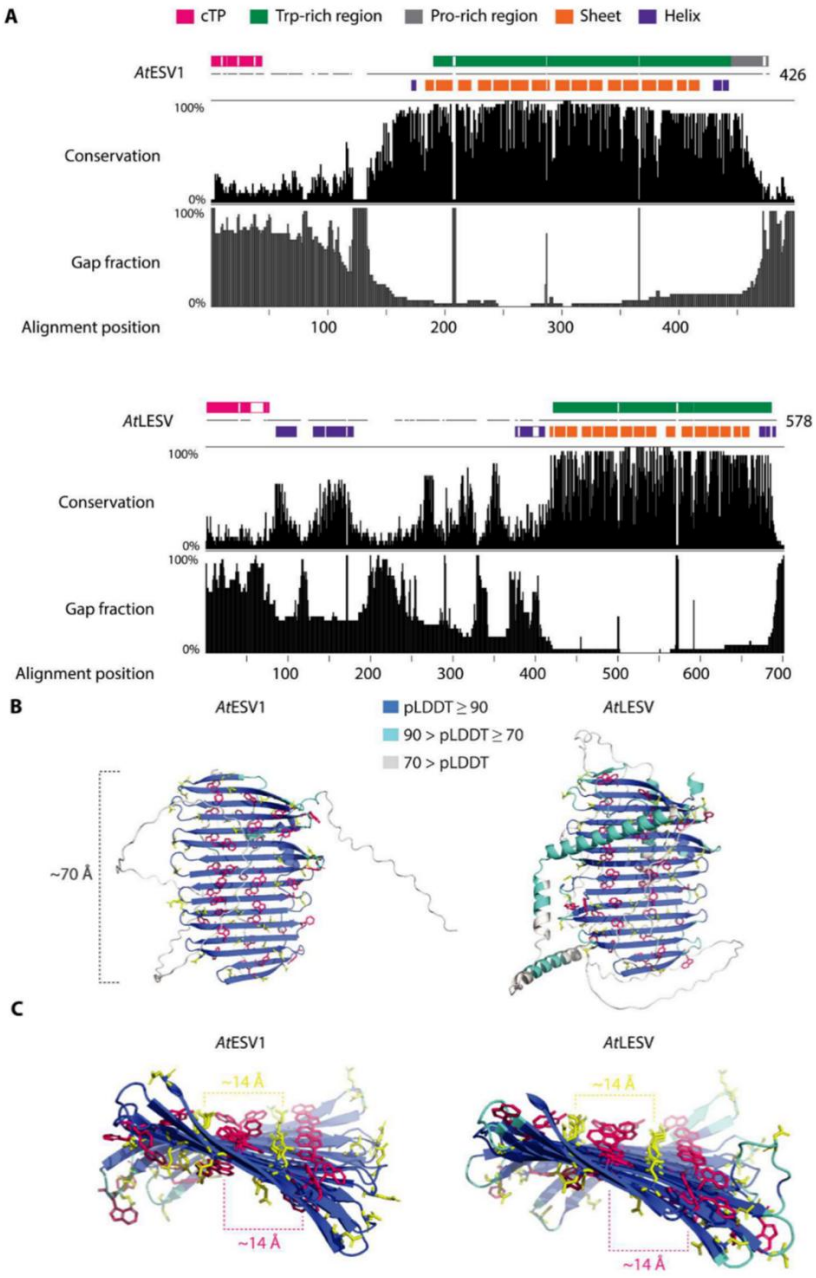

Figure 10 : Structures and conservation of ESV1 and LESV proteins. (A) Conservation of homologous ESV1 and LESV protein sequences. Gap frequencies are based on ≥25 orthologous ESV1 and LESV sequences from (Feike et al., 2016). Indicated in colored boxes above the Arabidopsis sequence are the chloroplast transit peptide (cTP), Trp-rich region, and Pro-rich region (ESV1 only) of the respective proteins. Colored boxes below represent the AlphaFold secondary structure predictions [see (B)]. Note that the alignment position does not correspond to the Arabidopsis protein residue numbering because of gaps. (B) AlphaFold predictions of ESV1 and LESV. Cartoon representations of the full-length proteins; the side chains of aromatic (Trp, Tyr, and Phe) and acidic residues (Asp and Glu) are shown in pink and yellow, respectively, and the protein backbone is colored according to confidence of the model (pLDDT value; see color key). (C) Isolated β sheet plane regions of ESV1 and LESV, reoriented to reveal the view along the length of the planes (C. Liu et al., 2023).

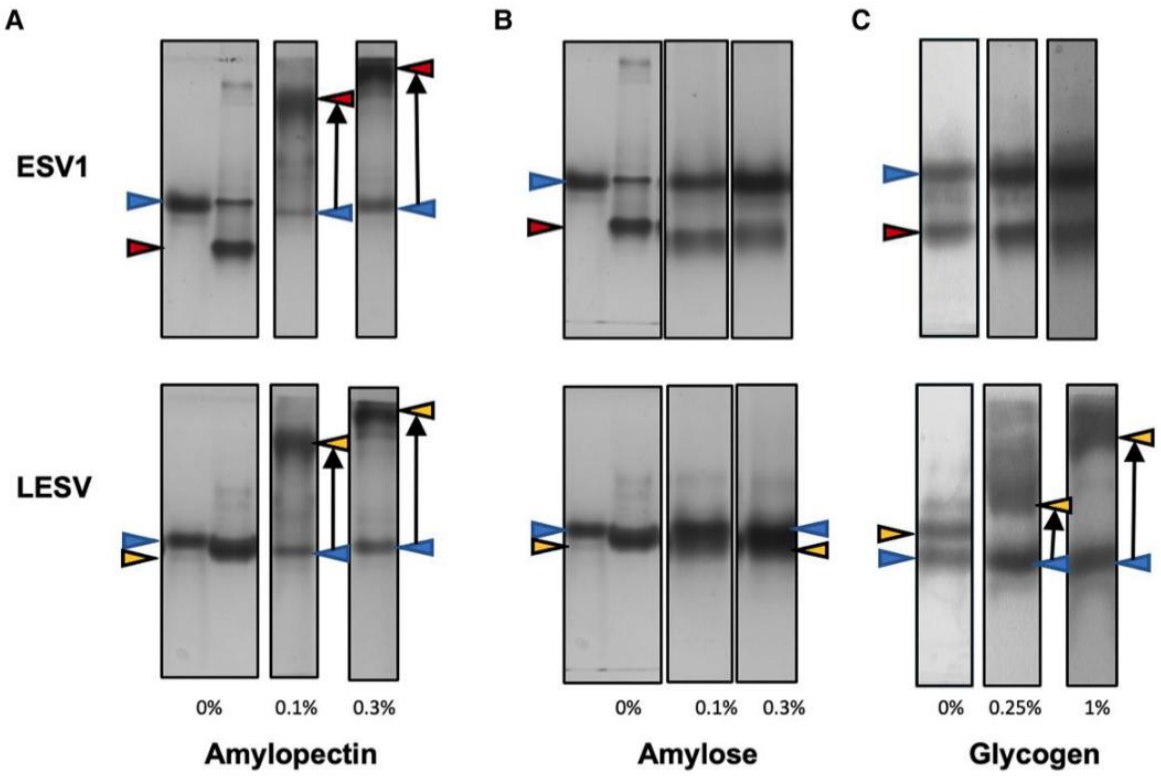

Figure 11 : Electromobility shift assays (EMSA) gels analyzing the interaction between ESV1 or LESV and starch glucans. A) Interaction with amylopectin, B) interaction with amylose, and C) interaction with glycogen. Blue, red, and yellow arrows indicate the bands corresponding to the reference protein, ESV1 and LESV, respectively. The migration shift is indicated by a black arrow (Osman et al., 2024).

Although both proteins bind to the same substrate, their functions diverge, a topic that will be further detailed in the following sections. These functional differences may be attributed to variations in their N-terminal regions. While ESV1 and LESV contain a chloroplast transit peptide (cTP), their N-termini regions exhibit significant differences (Figure 10). In particular, the N-terminal region of LESV is longer (304 bp) than that of ESV1 (130 bp). This difference suggests that the N-terminal region could play a role in modulating glucan binding or facilitating protein-protein interactions, as observed in rice (Yan et al., 2024). Furthermore, synchrotron radiation circular dichroism (SR-CD) experiments demonstrated that when LESV interacts with amylopectin during starch biosynthesis, its N-terminal region undergoes conformational changes (Osman et al., 2024). This finding suggests that this region is also involved in the specific recognition of amylopectin. Finally, LESV N-terminal region also contain aromatic amino acids that are predicted to be either in alpha-helical structure or to be unstructured (C. Liu et al., 2023). The role of this particular region needs to be further investigated.

4.2. ESV1 and LESV localization

The plastidial localization of ESV1 and LESV, predicted by the presence of the chloroplast transit peptide (cTP), was experimentally confirmed by expressing the C-terminal YFP fusion constructs of the two proteins in *Nicotiana sylvestris* leaves (Feike et al., 2016). In wild-type plants, YFP fluorescence was detected within the chloroplasts, specifically associated with distinct points that likely correspond to starch granules (Figure 12A). To further validate this hypothesis, the same experiment was performed in the *pgm* mutant, which lacks phosphoglucomutase and is consequently unable to produce starch granules. In this mutant, YFP localization appeared diffuse, confirming that the punctate signals observed in wild-type plants were indeed starch granules (Figure 12A).

To further support the binding of ESV1 and LESV to starch granules, soluble and insoluble leaf fractions were separated (Feike et al., 2016). Both proteins were detected in both fractions; however, they were predominantly soluble at the end of the night when starch amount is minimal and largely insoluble at the end of the day when this concentration is maximal (Figure 12B). Additionally, proteins extracted from starch granules confirmed the presence of ESV1 and LESV, revealing that these proteins are among the most abundant granule-bound proteins in the leaves (Figure 12C). Furthermore, the transient expression of LESV and ESV1 in *Nicotiana benthamiana* leaves demonstrated that the tryptophan-rich domain alone is sufficient to mediate granule localization, highlighting the critical role of this region in starch granule binding (C. Liu et al., 2023).

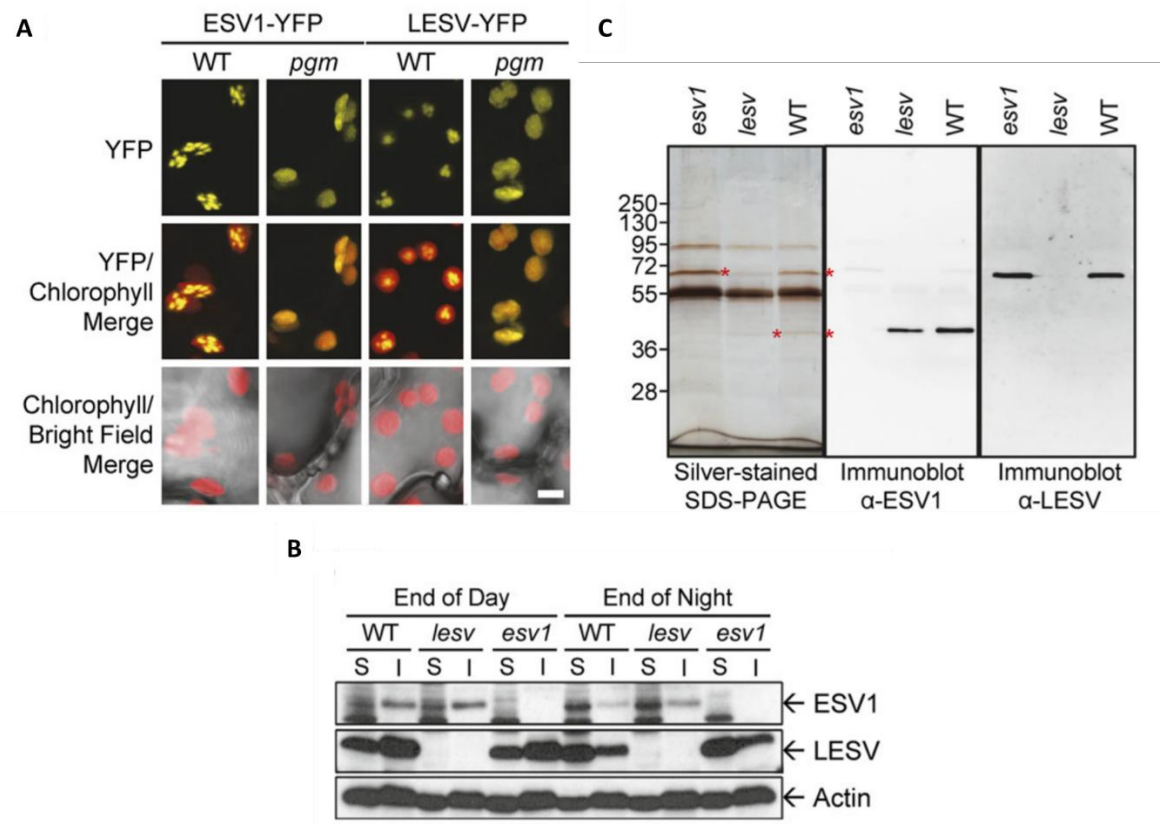

Figure 12 : Location of ESV1 and LESV proteins. (A) Transient expression, in N. sylvestris, of ESV1-YFP and LESV-YFP in leaves of wild-type (WT) and *pgm* mutant (deficient in phosphoglucomutase). For each genotype expressing constructs, top, middle, and bottom panels show the YFP *fluorescence*, the merged chlorophyll and YFP fluorescence, and the chlorophyll fluorescence on a bright-field image for the same leaf area. All panels are at the same magnification. Bar (bottom right) = 5 mm. (B) Immunoblots with antisera against ESV1 (upper panel) or LESV (middle panel) of extracts of wild-type, *esv1*, and *lesv* Arabidopsis leaves. Crude extracts were separated into soluble (S) and insoluble (I; containing starch) fractions by centrifugation. Each lane contains material from the same fresh weight of leaf (1.35 mg). The lower panel shows, as a loading control, immunoblots of identical gels with an antiserum against plant actin. (C) Gel (left) and immunoblots of starch granule-bound proteins from wild-type (Col-0), *lesv*, and *esv1* mutants. Each lane on the left panel contained proteins extracted from 1.3 mg purified starch. Each lane on the middle and right panels contained proteins extracted from 0.3 mg purified starch. Numbers indicate the positions of molecular mass markers (values in kilodaltons). The ESV1 antiserum cross-reacts slightly with LESV (middle panel). On the gel, red asterisks are to the right of LESV bands (upper asterisks) and ESV bands (lower asterisks) (Adapted from Feike et al., 2016).

In the perspective to identify new potential target genes involved in starch metabolism in potato, an analysis of the potato tuber starch granule proteome was performed in our lab a few years ago (Helle et al., 2018). This study was based on the hypothesis that proteins embedded into the starch granule are likely to play a role in its metabolism. Indeed, the presence of proteins with well-established roles in the starch granule metabolism was confirmed, such as synthases, branching enzymes, debranching enzymes and others (Figure 13). A particularly interesting aspect of this work was the detection of ESV1 and LESV in potato

tuber starch granules—proteins previously characterized in Arabidopsis but never studied in the context of storage starch, with LESV standing out as one of the most abundant granule-bound proteins (Helle et al, 2018) (Figure 13). Although these proteins have never been characterized in potato, these data suggest a potentially significant role, particularly for LESV, in potato tuber starch metabolism.

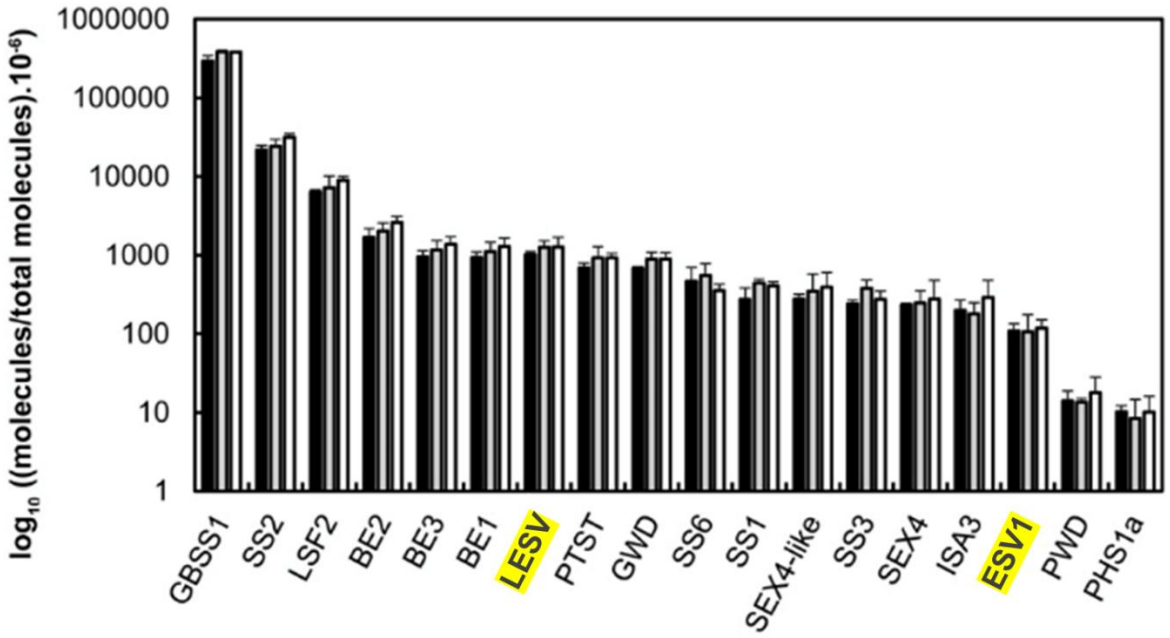

Figure 13 : **Label free quantification of proteins following SDS- or thermolysin- treatment of potato tuber starch granules**. Proteins were isolated from starch prior to nano LC-MS/MS shotgun analysis of the trypsin digests. The amount of each starch metabolic protein was estimated with the use of the MaxQuant software and the number of observed molecules/total number of predicted molecules was plotted on a log-10 scale. Black bars: non-treated starch, gray bars: SDS-treatment, open bars: thermolysin-treatment (Helle et al., 2018).

4.3. ESV1 and LESV conservation in plant kingdom

LESV and ESV1 were first identified in *Arabidopsis thaliana* and potato (Feike et al., 2016; Helle et al., 2018). They are largely conserved in the plant kingdom. Both proteins were found in land plants such as maize and rice and green algae (Feike et al., 2016) (Figure 14). However, they are absent from prokaryotes, red algae and other eukaryotic life forms. This high level of evolutionary conservation suggests that both proteins have an important role that are specific to the Viridiplantae.

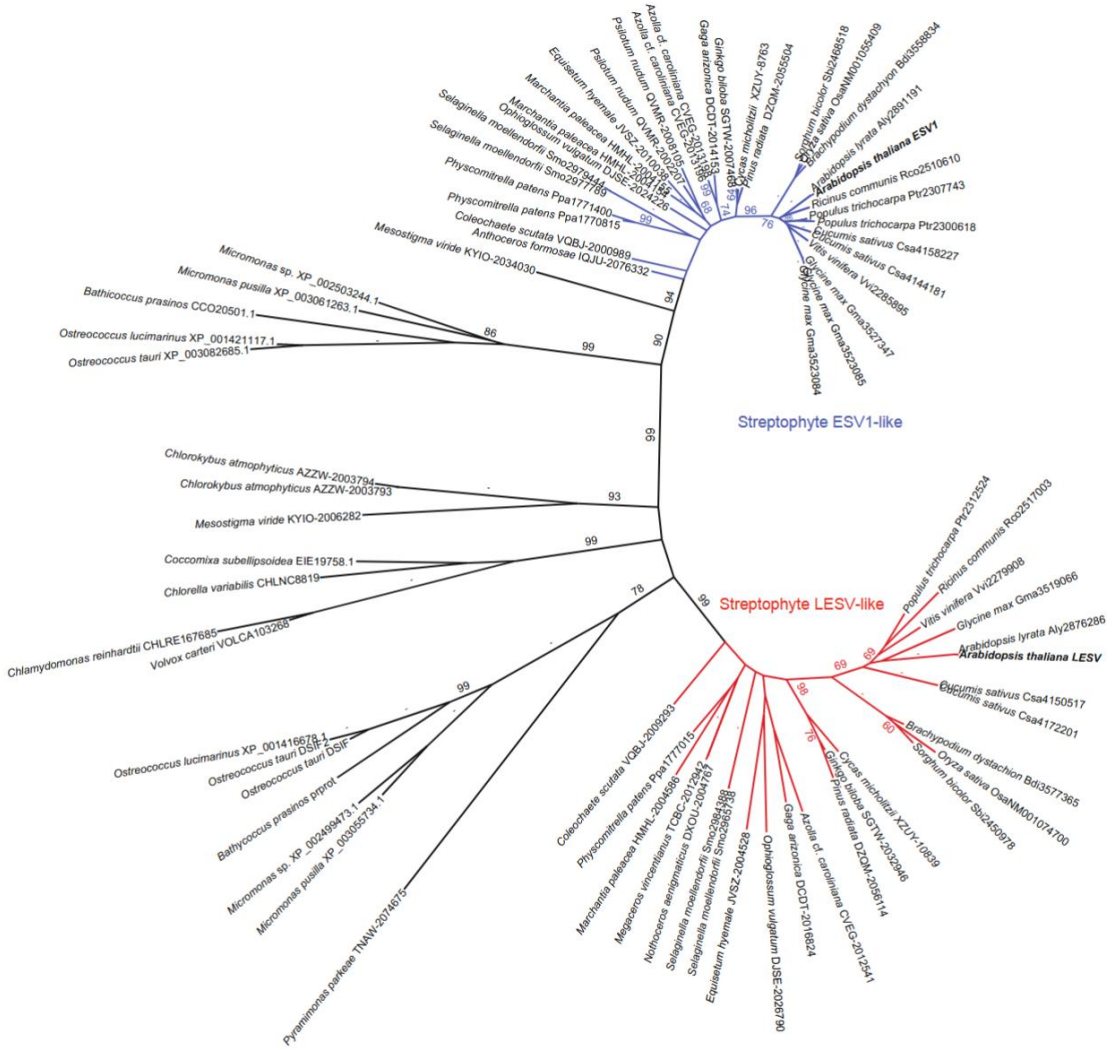

Figure 14 : Conservation of ESV1 and LESV proteins in land plants and algae. Maximum likelihood phylogenetic tree of ESV1 and LESV proteins from a MAFFT alignment. ESV1 sequences are shown in blue, and LESV sequences are shown in red. Bootstrap values that are >50 are shown over the branches. (Feike et al., 2016)

4.4. ESV1 and LESV deficient and overexpressing plants

Although little was known about ESV1 when it was discovered in potato, several studies have since investigated their role in other species. For instance, ESV1 play a crucial role in regulating transitory starch degradation in *Arabidopsis thaliana* leaves (Feike et al., 2016).

A forward genetic screen allowed the identification of a mutant defective in the control of carbon availability at night (Feike et al., 2016). This mutant, presenting a starvation phenotype before the end of the night, was named *esv1* for *early starvation 1* (Figure 15A). *esv1* has a mutation in the *Atg42430* gene. Two *esv1* mutant lines obtained from either the forward

genetic screen (*esv1-1)* or T-DNA insertion in the *Atg42430* gene (*esv1-2*) were used to study the effect of the mutation on plant growth. Following the identification of *esv1* mutant deficient in the regulation of carbon availability, a BLAST search has allowed the identification of a second protein, sharing 38% of identity with ESV1, which was named LIKE EARLY STARVATION 1 (LESV).

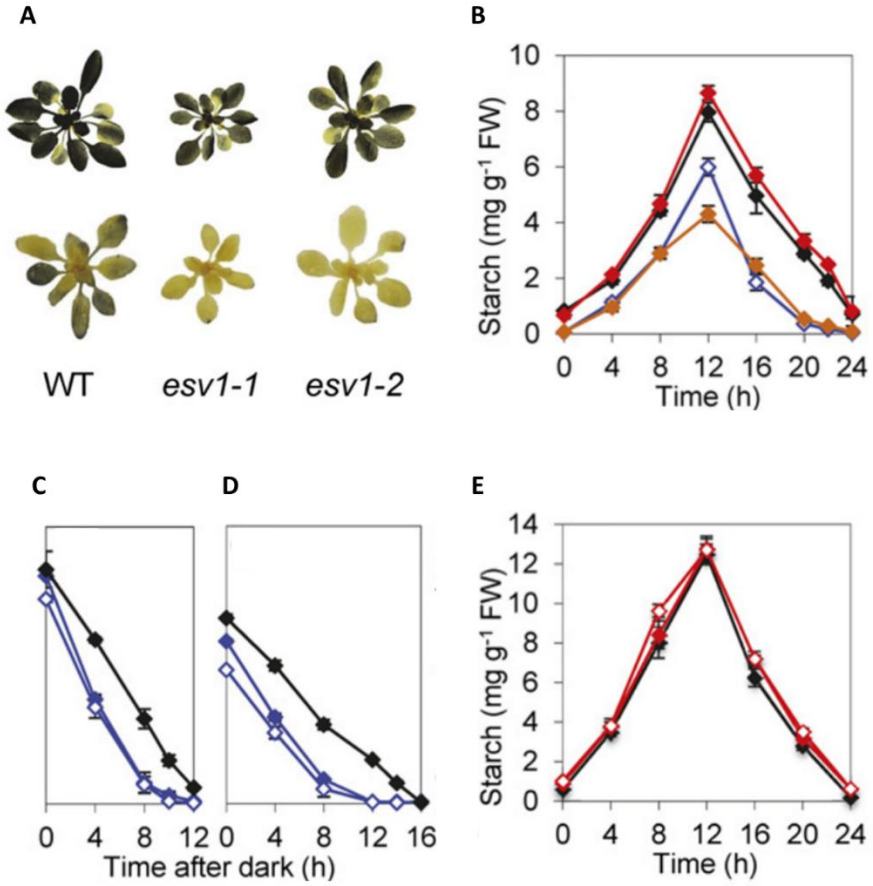

Figure 15 : Starch turnover in leaves of *esv1* mutants (A) Iodine staining of rosettes at the end of the day (top) and 2 hours before the end of a 12-h night (bottom). Left, control plant (Col-0). Middle, the *esv1-1* mutant derived from the forward genetic screen. Right, *esv1-2*, a T-DNA insertion mutant for At1g42430 (B) Starch contents over the day-night cycle in wild-type rosettes (black) and rosettes of *esv1-2* (blue), *lesv-1* (red), and *esv1-2 lesv-1* (orange). Plants were 3 weeks old. Values are means ± SE of measurements made on six rosettes. (C) Starch contents during a normal, 12-h night in wild-type rosettes (black) and rosettes of *esv1-1* (blue, closed symbols) and *esv1-2* (blue, open symbols) mutants. Plants were 3 weeks old and from a different batch from those in (B). Values are means ± SE of measurements on five rosettes. (D) Starch contents during a 16-h night starting 8 h after dawn, in wild-type rosettes (black) and rosettes of *esv1-1* (blue, closed symbols) and *esv1-2* (blue, open symbols) mutants. Plants were 3 weeks old. Values are means ± SE of measurements on five rosettes. Starch contents over the day-night cycle in wild-type rosettes (black) and rosettes of lesv-1 (red, closed symbols) and lesv-2 (red, open symbols) mutants. Plants were 3 weeks old and from a different batch from those in (B). Values are means ± SE of measurements on five rosettes (Adapted from Feike et al, 2016).

esv1 mutants exhibit an abnormal turnover of starch level during day/night cycling. In addition to a lower net starch accumulation rate than wild-type plants during the day (Figure 15B), the *esv1* mutants could not adjust the rate of starch degradation to the length of the night (Feike et al., 2016). Indeed, starch reserves were exhausted approximately 2 hours before the end of the night (12 hours), or 4 hours in the case of a short day (8 hours) and a prolonged night (16 hours) (Figure 15C and D). Additionally, *esv1* mutants accumulate higher levels of maltose during the day than the wild-type plants, but less during the night (Feike et al., 2016). Since high maltose levels are indicative of starch degradation (Weise et al., 2004), these results suggest that *esv1* accumulate less starch than wild-type plants, as starch degrades both during the day and at night in the mutant. Moreover, *esv1* mutant plants were significantly smaller than wild-type plants, likely as an indirect consequence of impaired starch mobilization, leading to premature starch depletion before the end of the night (Feike et al., 2016).

Unlike *esv1*, *lesv* mutants exhibited a normal starch level during the diel cycle (Feike et al., 2016; C. Liu et al., 2023). Moreover, *esv1 lesv* double mutant showed similar starch content than *esv1* single mutant (Figure 15B) (Feike et al., 2016). However, it was found that the absence of phenotype in *lesv* is conditional. In standard conditions (12h day/12h night), most of the granules in *lesv* single mutant displayed a wild type phenotype at the end of the day (Figure 16B) (C. Liu et al., 2023). Only 5% of the chloroplasts exhibited a different phenotype, composed of small granules with an irregular surfaces and surrounded by small particles. However, when *lesv* mutant was completely destarched after a single prolonged night (16h), a significant change in its phenotype was observed at the end of the next day. Starch content was strongly decreased (Figure 16C) and the granule morphology was severely altered, with 58% of the chloroplasts exhibiting a mix of aberrant granules and small soluble particles, and 38% only small particles (Figure 16D). This suggests that LESV may be required when initiation of new starch granule occurs.

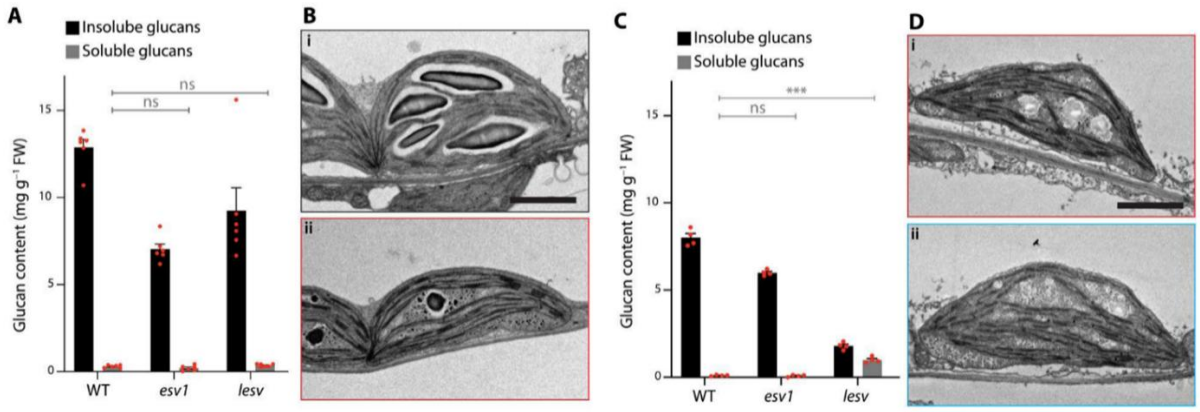

Figure 16 : The *lesv* single mutant has a conditional mutant phenotype. (A) Glucan quantification of plants grown in 12-hour light/12-hour dark cycles, harvested after a 12-hour day. FW, fresh weight. Values are means ± SE (n = 6). Statistical comparisons were performed using two-way ANOVA with Dunnett's multiple comparisons test; see data S3 (A and B). Only comparisons to the wild type for soluble glucans are shown. WT, wild type. (B) TEMs of selected lesv chloroplast sections, obtained from plants grown and sampled as in (A). Most *lesv* plastids appear wild-type like (i), but a few contain unusual glucans (ii). Scale bar, 2 µm. (C) Glucan quantification of plants grown as in (A), subjected to a single prolonged night (16 hours), and harvested after an 8-hour day. Values are means ± SE (n = 4). Statistical comparisons were performed as in (A). Only comparisons to the wild type for soluble glucans are shown. ***P ≤ 0.001. (D) TEMs of lesv plants grown and harvested as in (C). Most chloroplast sections contain either a mixture of starch and phytoglycogen (i) or phytoglycogen-like inclusions only (ii). Scale bar, 2 µm. (Adapted from Liu et al, 2023).

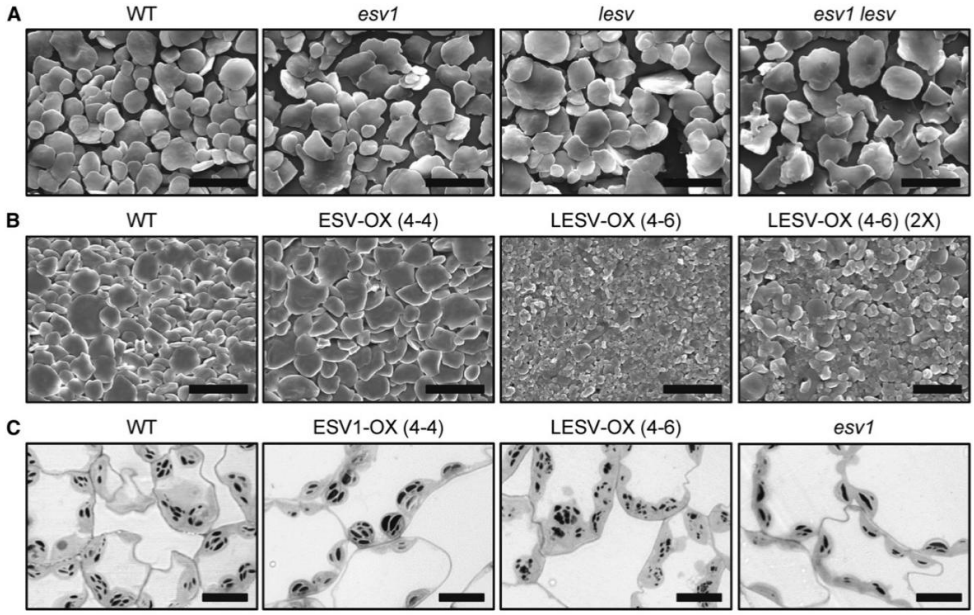

Figure 17 : Starch Granule Morphology in *esv1* and *lesv* mutants and overexpressing plants. For starch extraction, rosettes were 4 weeks old and were harvested at the end of the day. For microscopy, young leaves were harvested from 3-week-old rosettes in the second half of the light period. (A) Scanning electron micrographs of purified starch granules from leaves of wild-type (Col), *esv1, lesv,* and *esv1 lesv* double mutants. Bars = 2 mm. (B) Scanning electron micrographs of purified starch granules from leaves of wild-type (Col) and transgenic lines overexpressing ESV1 or LESV (OX lines). Bars = 2 mm apart from the image of LESV OX starch, where the bar = 1 mm. (C) Light micrographs of leaf sections stained with toluidine blue. Bars = 10 mm (Feike et al, 2016).

Additionally, alteration of ESV1 and LESV levels also affects starch granule morphology and number. Granules from *esv1* and *lesv* mutants present a discoid shape, like those of wild-type leaves, but exhibit irregular outlines (Figure 17A). ESV1-overexpressing plants exhibited larger starch granules than wild-type plants (Figure 17C), along with elevated starch content throughout the day-night cycle (Feike et al., 2016; C. Liu et al., 2023). In contrast, LESV-overexpressing plants showed an increased number of granules per chloroplast, which tended to be smaller than those in WT plants (Feike et al., 2016). These plants also displayed a premature starvation phenotype before the end of the night (Feike et al., 2016; C. Liu et al., 2023).

4.5. ESV1 and LESV expression promote insoluble glucan accumulation

To investigate the roles of ESV1 and LESV in starch biosynthesis, both proteins were expressed in two different lines of engineered *Saccharomyces cerevisiae* (C. Liu et al., 2023). Line 28 expresses only SS1 to SS4, BE2 and BE3 and produces a high amount of soluble glucan (phytoglycogen), while line 29, expressing the same proteins with the addition of ISA1 and ISA2, produces starch-like insoluble glucans in addition to phytoglycogen (Figure 18). LESV and ESV1 were expressed individually or both together in these lines. In line 28 expressing ESV1 (line 559), a small amount of insoluble glucan was found. This effect was exacerbated in line 28 expressing LESV (line 562), and when both proteins were expressed simultaneously (line 563). A similar pattern was obtained when expressing ESV1, LESV or both proteins simultaneously in lines 29, which already accumulates insoluble glucans, with the amount of insoluble glucans exceeding soluble glucans.

The insoluble glucans particles formed in the different engineered yeasts were observed using Scanning Electron Microscopy (SEM) (Figure 19). No insoluble starch-like particle could be purified for SEM in line 28. However, in the lines with the same background expressing ESV1 (559), LESV (562) or both proteins (563), small aggregated particles were observed. This effect was reinforced in the lines with ISA1/ISA2 background (line 29) expressing ESV1 (569), LESV (572) or both (573), where aggregates of larger particles with smooth surfaces were observed.

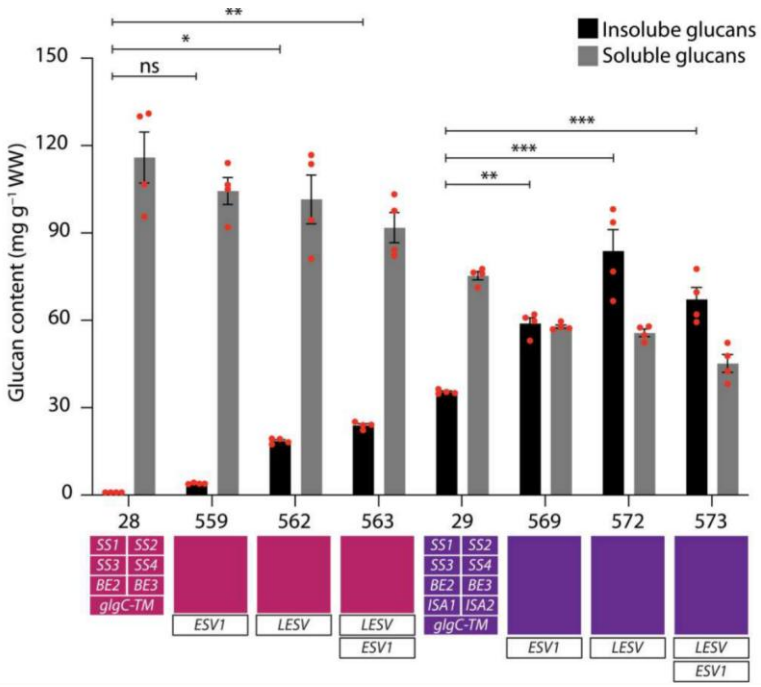

Figure 18 : Quantification of insoluble and soluble glucans from yeast strains expressing ESV1, LESV, or both proteins in the 28 and 29 genetic backgrounds (expression sets indicated above the strain number). Yeasts were grown in liquid culture for 5.75 hours under inducing conditions. Values are means ± SE (n = 4); independent replicate cultures arose from different precultures. WW, wet weight. Statistical comparisons were performed using two-way analysis of variance (ANOVA) with Dunnett's multiple comparisons test. Note that only comparisons for insoluble glucans to the respective parental strain are indicated in the graph. *P ≤ 0.05, **P ≤ 0.01, and ***P ≤ 0.001. ns, not significant (C. Liu et al., 2023).

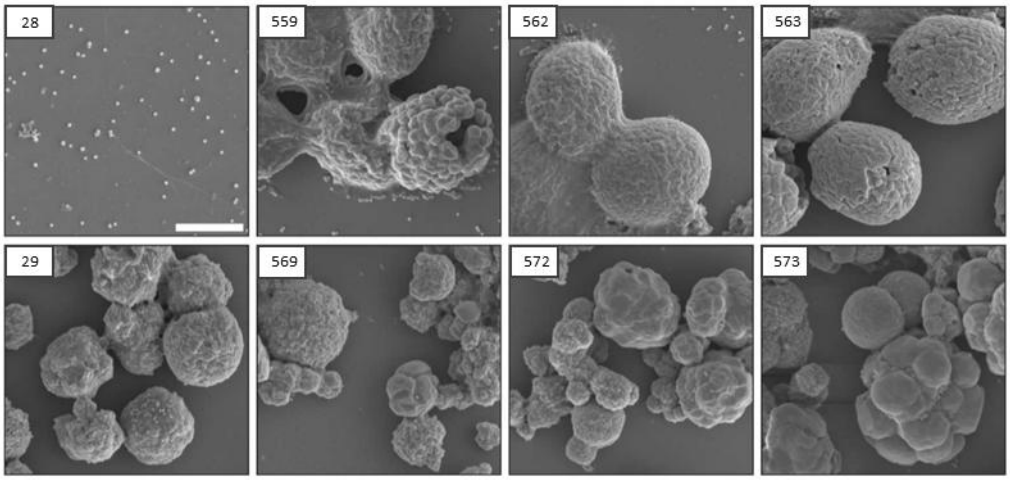

Figure 19 : Scanning electron microscopy images of insoluble glucans purified from yeast strains expressing ESV1 and LESV. Glucans were extracted from yeast lines expressing *SS1*, *SS2*, *SS3*, *SS4*, *BE2*, *BE3*, and *glgC-TM* (line 28), either alone or in combination with *ESV1* (line 559), *LESV* (line 562), or both proteins (line 563). Additional lines also expressed *ISA1* and *ISA2* (line 29) and were similarly transformed with *ESV1* (line 569), *LESV* (line 572), or both proteins (line 573). Scale bar, 2 µm (adapted from C. Liu et al., 2023).

Overall, the presence of ESV1 in engineered yeast promote the synthesis of insoluble glucans. This effect was more pronounced upon LESV expression, and more importantly when both proteins were expressed.

To further understand the impact of ESV1 and LESV on starch metabolism, both proteins were overexpressed in an Arabidopsis *isa1isa2* background, which accumulates soluble phytoglycogen due to the absence of isoamylase activity (Figure 20) (Feike et al., 2016). Overexpression of either protein led to increased starch accumulation compared to the mutant background, but with distinct effects. *isa1isa2ESV1-OX* plants maintained high phytoglycogen levels and retained starch at the end of the night, indicating that ESV1 inhibits starch degradation without impacting phytoglycogen synthesis. In contrast, *isa1isa2LESV-OX* plants showed reduced phytoglycogen levels and complete starch degradation overnight, resembling the phenotype of the *isa1isa2* mutant on this precise point, suggesting that LESV promotes the formation of insoluble glucans at the expense of phytoglycogen, without altering starch turnover.

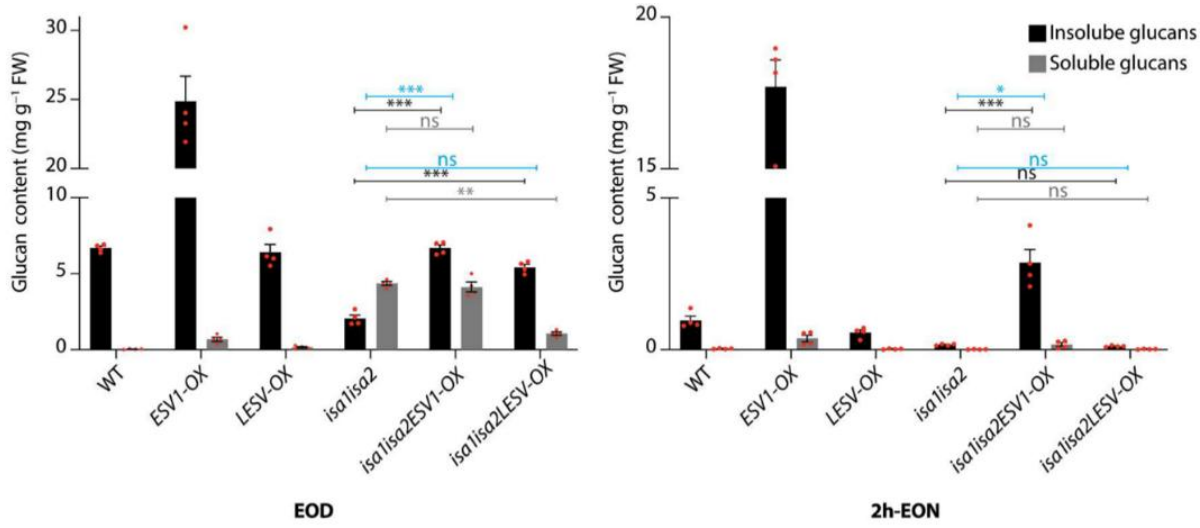

Figure 20 : Glucan accumulation and turnover in plants overexpressing ESV1 and LESV in the *isa1isa2* background. Glucan quantification of plants harvested at the end of the day (EOD) and 2h before the end of the night (2h-EON). Values are means ± SE (n = 4 biological replicates). Statistical comparisons were performed using two-way ANOVAs with Dunnett's multiple comparisons test. Comparisons of total summed glucans are indicated in blue, those of soluble glucans (phytoglycogen) in gray, and those of insoluble glucans (starch) in black. *P ≤ 0.05, **P ≤ 0.01, and ***P ≤ 0.001 (Feike et al, 2016).

The effect of LESV and ESV1 alteration in *isa1isa2* background was also investigated by producing *isa1isa2esv1* and *isa1isa2lesv* triple mutants (C. Liu et al., 2023). The triple mutants exhibited less glucan compared to their parental lines, especially in the *isa1isa2esv1* triple mutants (Figure 21). Two hours before the end of the night, almost all insoluble glucans were degraded in the mutants with an *isa1isa2* background, indicating that these lines prematurely used their glucan reserves.

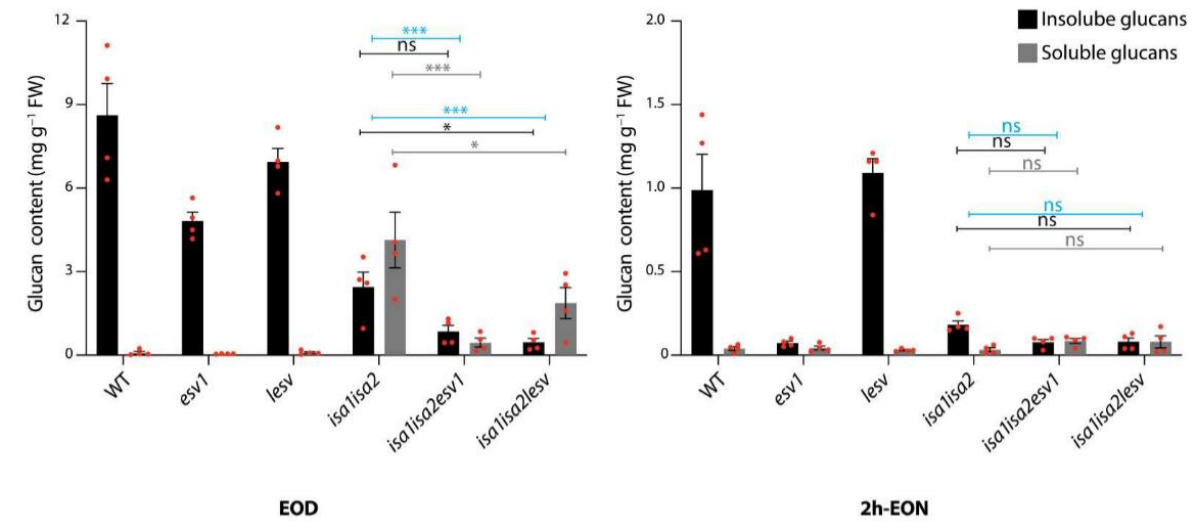

Figure 21 : Glucan content of *isa1isa2, esv1, lesv*, and triple mutants. Glucan quantification in plants, harvested at the EOD and 2h-EON. Values are means ± SE (n = 4 biological replicates). Statistical comparisons were performed using two-way ANOVA with Dunnett's multiple comparisons test. Comparisons of total summed glucan contents are indicated in blue, soluble glucans (phytoglycogen) in gray, and insoluble glucans (starch) in black. For clarity, only selected comparisons are shown. *P ≤ 0.05 and ***P ≤ 0.001 (C. Liu et al., 2023).

4.6. LESV and ESV1 promote and stabilize amylopectin phase transition

As previously detailed, LESV and ESV1 alter glucan accumulation in a *isa1isa2* background (C. Liu et al., 2023). Small angle X-ray scattering (SAXS) was used to investigate whether the presence of these proteins influence the crystal structure of insoluble glucans. Starches extracted from the different mutant combinations show no differences in lamellar repeats (approximately 10 nm). However, the same analysis on engineered yeast expressing only SS1 to SS4, BE2 and BE3 (line 28) or with the addition of ISA1 and ISA2 (line 29) exhibited a SAXS profile with a 13.1 nm repeat. When LESV and/or ESV1 were also expressed in these lines, a shorter repeat of 10.6 to 10.8 nm, closer to wild-type starch pattern, was observed.

Overall, it has been proposed that LESV and ESV1 may be involved in promoting and stabilizing the phase transition of amylopectin. This model is based on several arguments. First, in the engineered yeast experiment (C. Liu et al., 2023), LESV was able to increase the conversion of the soluble glucans fraction to the insoluble state. The same pattern was observed in isoamylase-deficient plants overexpressing LESV. The additional loss of LESV in *isa1isa2* background further decreased the amount of insoluble glucans. Finally, while no particular phenotype was observed in standard conditions (Feike et al., 2016), the *lesv* mutant exposed to an extended night produced aberrant starch granule, with a strong increase of soluble glucan (C. Liu et al., 2023). LESV is believed to help in promoting the phase transition of amylopectin, arranging glucan double helices into a compact ordered tertiary structure (Figure 22). The β-sheet domain of LESV, capable of binding to amylopectin through its aromatic and acidic amino acid residues (Osman et al., 2024), would serve as an initial template to align the glucan double helices. These double helices could then contribute to the alignment of other double helices, propagating the phase transition in a wave-like manner, resulting in the formation of a crystalline lamella. This model would explain the presence of LESV embedded in the starch granule, as demonstrated in Arabidopsis and potato (Feike et al., 2016; Helle et al., 2018).

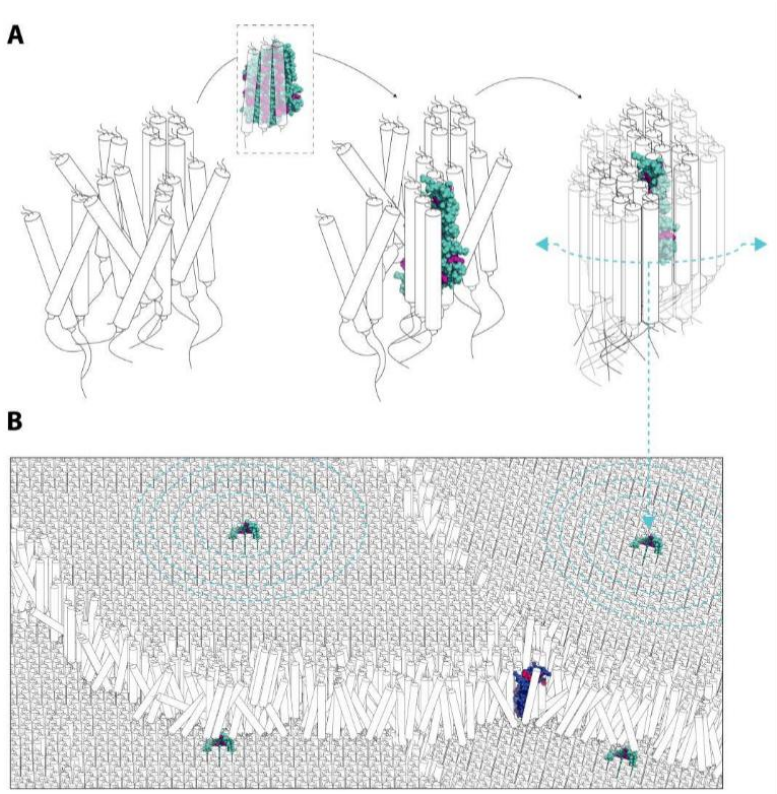

Figure 22 : Model of the proposed ESV1 and LESV functions. (A) LESV interacts with glucans that have adopted a helical secondary structure via its Trp-rich domain and possibly aided by its N-terminal domain (not shown) and thereby facilitates their arrangement into compact, ordered tertiary structures. Once seeded, regular glucan arrangements can self-propagate and spread. (B) Regions of ordered glucan helices, seeded by LESV, form adjacent blocks of crystalline lamellae. ESV1 binds to and stabilizes exposed helices at the margins of these regions, restricting access to hydrolytic activities. In both (A) and (B), ESV1 and LESV proteins are represented as simplified versions of their predicted AlphaFold structures (only Trp-rich region is shown; aromatic residues are highlighted by color; pLDDT values are disregarded) (C. Liu et al., 2023).

The proposed role of ESV1 is different. This protein is thought to stabilize the amylopectin structure after its formation (C. Liu et al., 2023). The β-sheet domain would allow ESV1 to maintain the amylopectin structure and protect it from hydrolytic activities by binding to several amylopectin molecules on each side of this β-sheet. Once again, several arguments support this model. First, the effect of ESV1 in the promotion of phase transition from soluble to insoluble glucans is less significant than that of LESV. Second, in the engineered yeast strain experiments, the overexpression of ESV1 led to starch accumulation, but, unlike LESV, had no impact of soluble glucan content. The increase of insoluble glucans is thought to be due to a reduced degradation at night, as presented in ESV1 overexpressing plants (Feike et al., 2016).

4.7. LESV is involved in ISA1 targeting to starch in rice

A recent study based on a forward genetic screen in rice allowed the identification of a mutant defective in starch accumulation (Yan et al., 2024). This mutant produced a floury endosperm filled with loose starch granules and a hollow core, in contrast to the translucent endosperm of the wild-type plant (Figure 23A and B). This mutant was subsequently named *floury endosperm 9* (*flo9*), and is caused by the loss of OsLESV, a protein homolog to Arabidopsis and potato LESV. Quantification in *flo9* showed that, compared to wild-type plants, starch and amylopectin contents were reduced, while the water-soluble-glucans (WSG) were increased (Figure 23C). This increase in WSG in consistent with the model proposed in *Arabidopsis thaliana*, suggesting that LESV influence the amylopectin phase transition of (C. Liu et al., 2023). The analysis of amylopectin chain length distribution revealed a strong increase of short chains (between DP6 and DP14), while a decrease in the amount of intermediate chains was observed (Figure 23D). These results suggest that the loss of OsLESV affects amylopectin synthesis in rice.

The *flo9* mutant partially phenocopied rice *isa1* mutant (Nakagami et al., 2017; Nakamura et al., 1997). It was subsequently suggested that OsLESV, the protein responsible for *flo9* phenotype, might regulate starch biosynthesis in rice by associating with ISA1 (Yan et al., 2024), a starch debranching enzyme involved in amylopectin synthesis (Fujita et al., 2003; Nakamura et al., 1996). This hypothesis was demonstrated in several points. First, rice ISA1 is unable to spontaneously bind to starch while OsLESV directly binds to starch by its C-terminal tryptophan-rich region similarly to Arabidopsis LESV (Fujita et al., 2003; C. Liu et al., 2023; Nakamura et al., 1996; Yan et al., 2024). Second, yeast two hybrid (Y2H) and co-immunoprecipitation assays demonstrated the interaction between OsLESV and ISA1 via its N-terminal region (Yan et al., 2024). Third, OsLESV has been shown to also interacts with FLO6, a protein homolog to Arabidopsis PTST2, which is already known to associate with ISA1 (Peng et al., 2014; Yan et al., 2024). The presence of LESV or FLO6 significantly improved FLO6 or LESV interaction with ISA1 (Yan et al., 2024). The loss of either OsLESV or FLO6 completely altered ISA1 targeting to starch. The authors proposed that OsLESV, in association with FLO6, forms a non-enzymatic module responsible for the binding of ISA1 to starch granules in rice endosperm, and then indirectly regulate starch biosynthesis and endosperm development (Yan et al., 2024).

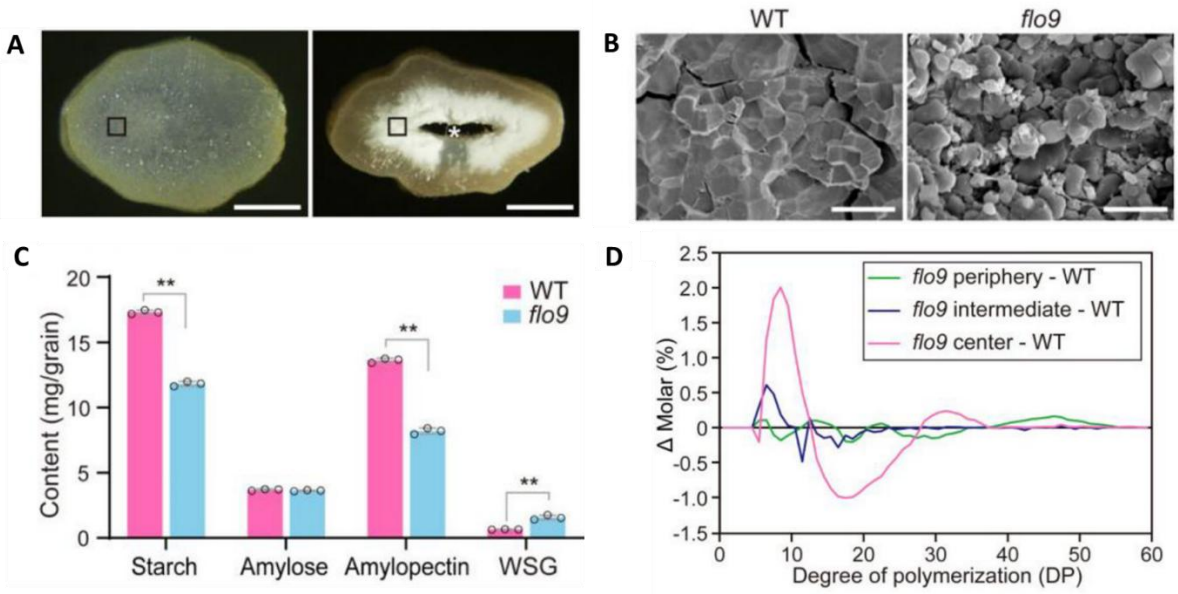

Figure 23 : Phenotypic characterization of the *flo9* mutant. A) Transverse sections of the representative WT and *flo9* mature grains. Bars = 1 mm. Asterisk indicates the hollow core. B) Comparison of SGs observed via scanning electron microscope in magnified regions of WT and *flo9* indicated by black squares in A). Bars = 20 µm. C) Determination of total starch, amylose, amylopectin, and WSG contents of WT and *flo9* mature grains. Values are means ± SD. **P < 0.01 by Student's t-test (n = 3). D) Differences in CLD patterns of total glucans between WT and *flo9*. Note that rice powder collected from the periphery, intermediate, and center of grains was separately used to determine the glucan CLD (Yan et al., 2024).

4.8. LESV and ESV1 influence in vitro activities of enzymes involved in starch metabolism

Both LESV and ESV1 were found to influence the *in vitro* activities of enzymes involved in starch metabolism. First, ESV1 was found to influence the phosphorylation activity of starch-related dikinases (GWD and PWD), key enzymes required for starch degradation (Malinova, Mahto, et al., 2018). Specifically, *in vitro* experiments revealed that the activity of PWD – that phosphorylates glucose residues at C3 position - is increased when incubated in presence of ESV1. In contrast, the *in vitro* activity of GWD – that phosphorylates glucose residues at position C6 (crucial for PWD activity) – decreased in presence of ESV1. Similar effects as ESV1 on GWD and PWD activities were observed with LESV (Singh et al., 2022). Furthermore, the activities of BAM (β-amylase) and ISA (isoamylase), two enzymes related to starch degradation, were increased when incubated with ESV1 or LESV. Likewise, enzymes related to biosynthesis such as SSI (starch synthase 1) and SSIII (starch synthase 3) also showed altered activities when incubated with either LESV or ESV1 (Singh et al., 2022). Consequently,

LESV and ESV1 appear to play a role in influencing starch biosynthesis and degradation enzymes. It was proposed that these proteins might be involved in regulating the activity of starch metabolism enzymes by binding to the granule surfaces (Singh et al., 2022). This hypothesis was supported by two arguments. First, an increase in the total release of glucans by isoamylase was observed when starch was pre-incubated with LESV and ESV1. Second, when incubated with ESV1 or LESV, a stronger release of glucans from the crystalline maltodextrins was observed. Thus, the binding of both proteins to the crystalline glucan structure results in a transition of the glucans on the surface from an insoluble state to a watersoluble state, without affecting the chain length distribution of the glucans. This suggests that when LESV and ESV1 bind to the granule surface, the glucans undergo a conformational change that promotes access to starch metabolism enzymes (Figure 24).

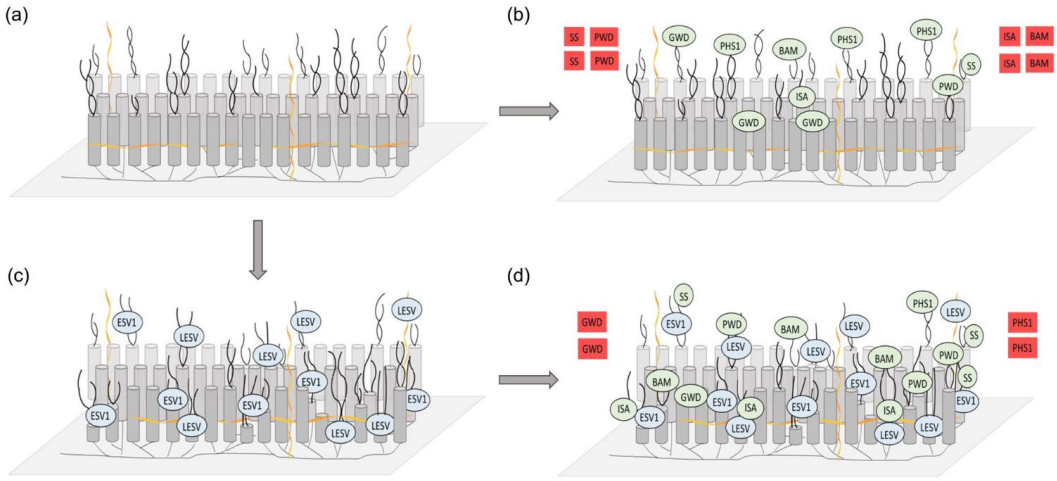

Figure 24 : Impact of ESV1 and LESV on starch granule surface properties. (a) Starch granules are highly organized: neighboring glucan chains of the amylopectin form crystalline structures, signified by cylinders. Some solubilized chains of different length can be found on the surface that are not in the crystalline network. (b) a-Glucan, water dikinase (GWD) binds to the crystalline regions and PHS1 (a-glucan phosphorylase 1) binds to the longer solubilized chains on the surface. Both enzymes have extensive substrate access, whereas starch synthases (SS), phosphoglucan, water dikinase (PWD), and hydrolases such as ISA (isoamylase) and BAM (b-amylase) have only limited substrate accessibility. Green ovals indicate that the enzymes are active and bound to the starch granule surface, whereas red rectangles indicate that they are presently unbound in the stroma. (c) (d) When the proteins ESV1 and LESV bind to the starch granules, the surface structure changes, and thus the substrate availability of the enzymes also changes. The binding opens the double helical chains and reduces the crystallinity, so that GWD has fewer substrate binding sites and fewer long chains for PHS1 are available. However, the reduction in crystallinity leads to an increase in the action of PWD, BAM and ISA. In addition, multiple short chains are available for SS, which also increases their action (Singh et al., 2022).

4.9. ESV1 is involved in the gravitropism perception

ESV1 has been found to be involved in gravitropic responses in *Arabidopsis thaliana* and rice. Mutants lacking ESV1 in these plants exhibit a lack of starch granules in root columella and reduced root gravitropism (Song et al., 2021). This feature has also been observed in other starch mutants, such as *pgm*1, *sex1*, or *ss4,* respectively lacking phosphoglucomutase, GWD and SS4 (Caspar et al., 1991; Crumpton-Taylor et al., 2013; Vitha et al., 2007). Thus, the loss of gravitropism in roots of *esv1* mutants is likely to be a consequence of reduced formation of granules in the root cap, rather than a direct implication of ESV1 in the gravitropic response of these plants.

Overall, it appears that ESV1-like proteins might be involved in multiple physiological role in starch biosynthesis, depending on plant species, organs and growth conditions (Yan et al., 2024). Two models were proposed in *Arabidopsis thaliana*, one suggesting a modulation of glucan structure at the surface of starch granules by ESV1 and LESV, influencing the activity of starch metabolic enzymes, the other one proposing a role of both proteins in promoting phase transition of amylopectin and stabilizing the structure (C. Liu et al., 2023; Singh et al., 2022). However, investigations of the role of LESV in rice suggested that the protein indirectly influence starch biosynthesis by targeting ISA1 to the starch granule in the endosperm (Yan et al., 2024). Although these models are different, depending on plant species and organs, they are not mutually exclusive and might co-exist. However, further studies are necessary to investigate the role of ESV1 and LESV across species and organs, and investigate the possibility of co-existence of multiple physiological roles.

Chapter 4. Problematic and objectives of this work

This work builds upon previous studies, including the analysis of the starch tuber proteome conducted in our laboratory (Helle et al., 2018). Additionally, the resequencing of *Solanum tuberosum* cultivar (cv.) Désirée and the identification of Single Nucleotide Polymorphisms (SNPs) in this cultivar, as described by (Sevestre et al., 2020), form essential foundations for this study.

Given the established roles of ESV1 and LESV in *Arabidopsis thaliana*, particularly in the regulation of transitory starch metabolism, and more recently, the implication of LESV in compound granule formation in rice endosperm, we hypothesized that these proteins might also be involved in the control of starch metabolism in potato tubers. LESV, in particular, is highly abundant in potato starch granules (Helle et al, 2020), which reinforced our hypothesis.

However, despite their conserved domains, the roles of ESV1 and LESV may differ not only between transitory and storage starch metabolism, but also across plant species, as observed for many other enzyme families involved in starch biosynthesis. These potential differences underscore the need for species- and organ-specific investigations.

Unraveling the role of LESV and ESV1 in potato tuber is essential to a better understanding of storage starch metabolism. The main objective of my thesis is to characterize the phenotype of mutants with inactivated LESV and ESV1, providing valuable information on the roles of these proteins in storage starch metabolism. In this study, LESV and ESV1 were inactivated by CRISPR/Cas9 approach. Several independent KO lines were selected and analyzed for plant growth and development, tuber starch granule morphology, starch structure, physicochemical properties, tuber starch granule proteome analysis and protein-protein interactions.

Altogether, this study shed new light on the role of these non-catalytic proteins, in storage starch metabolism and reveals potentially distinct regulatory mechanisms operating between species and between transitory and storage starch metabolisms.

MATERIAL AND METHODS

Plant Material and Growth Conditions

The potato cultivar used in this study is *Solanum tuberosum* cv. Désirée. The genome of this cultivar has been sequenced by our laboratory, and a polymorphism map was generated at the genome scale (Sevestre et al., 2020).

For *in vitro culture, p*lants were grown on MS (Murashig and Skoog) medium including vitamins (Duchefa), supplemented with 2% sucrose and 0.8% plant agar (Duchefa) in a growth cabinet under a 16 h light (80 µmol.m^{-2}.s^{-1}) : 8 h dark photoperiod, 22°C day : 20°C night. Plants were maintained and propagated *in vitro* by cuttings every six weeks.

For tuber production, three-weeks old *in vitro* plants were cultured in three liters pots in commercial soil. They were placed in a growth cabinet under a 16 h light (80 µmol.m^{-2}.s^{-1}):8 h dark photoperiod, 22°C day : 20°C night, for approximatively 12 weeks. After 4 weeks of culture, approximatively 5 cm of soil was added at the basis of the stem. Plants were watered twice a week for 11 weeks and tubers were harvested one week after the last watering, during plant senescence. Pictures of plants were taken every week. The background was removed on the plant and tubers pictures using the image editing tool removebg (https://www.remove.bg/).

Potato flours from *ss5* knock-out mutant lines were provided by David Seung's group from John Innes Centre in Norwich. *ss5* knockout mutant lines were produced by the Simplot company that grew the mutants, harvested, lyophilized and grounded the tubers to produce potato flour.

Selection of Targets and Plasmids Constructs

Target sites adjacent to NGG protospacer adjacent motifs (PAM) were identified for *LESV* using Geneious software and CRISPOR online tool (http://crispor.tefor.net/) (Concordet & Haeussler, 2018). Single guide RNA (sgRNA) was selected according to predicted specificity, efficiency, out-of-frame scores, and Single Nucleotide Polymorphism (SNP) map (Sevestre et al., 2020). The vector used for mutagenesis is pDIRECT_22A (Addgene, plasmid #91133) (Annex 1). It contains a kanamycin resistance gene. Plasmid vectors were constructed according to (Čermák et al., 2017). Briefly, oligonucleotides containing the sgRNA sequence

were phosphorylated using a T4 polynucleotide kinase (Thermo Fisher Scientific) and hybridized using a T4 DNA ligase buffer (Thermo Fisher Scientific), creating a double strand DNA fragment with sticky ends complementary to AarI restriction site (for oligonucleotide sequences, see Table S1). This fragment was introduced in the pDIRECT_22A vector (Annex 1) digested by AarI (Thermo Fisher Scientific) using a Golden Gate reaction. Plasmid construct was then multiplied by being produced in a chemically competent *Escherichia coli* TOP10 strain (genotype: FmcrA Δ(mrr-hsdRMS-mcrBC) Φ80lacZΔM15 ΔlacX74 recA1 araD139 Δ(ara-leu) 7697 galU galK rpsL (Str^R) endA1 nupG λ-) (Invitrogen) and purified using the NucleoSpin Plasmid Kit of Macherey-Nagel.

Agrobacterium-mediated transformation

Agroinfection of potato was performed as described in (Sevestre et al., 2020). Briefly, *A. tumefaciens* strain GV3101, was transformed with 1 µg of the plasmid construct containing the sgRNA prior to selection on solid LB petri dishes containing 50 $mg.L^{-1}$ of kanamycin as a selection agent. Potato explants of 3-4 mm in length from stems and petioles were prepared from three to four-week-old plants cultivated *in vitro*. They were placed on Petri dishes containing MS including vitamins (Duchefa) supplemented by 2% sucrose, 0.8% plant agar (Duchefa) and 1 $mg.L^{-1}$ of indole-3-acetic acid (IAA), gibberellic acid (GA_3) and zeatin-riboside (ZR) (Sigma Aldrich) for 48 h. Explants were then dipped into the *A. tumefaciens* culture with a DO_{600} adjusted to 0.2 using MS medium supplemented by 2% sucrose for 30 min with a slow mixing. Explants were then replaced on the same Petri dish for 48 h at 25°C in the dark. After removal of residual bacteria, explants were placed on Petri dishes containing MS medium including vitamins with 2% sucrose, 0.8% plant agar supplemented by 1 $mg.L^{-1}$ of IAA, GA_3 and ZR, 500 $mg.L^{-1}$ of timentin and cefotaxime (Duchefa) and 50 $mg.L^{-1}$ of kanamycin for two weeks to allow the development of calli. They were then placed on Petri dishes containing the same medium with an IAA concentration reduced to 0.1 $mg.L^{-1}$ to allow the differentiation of the callus in stems. Those stems were taken and placed in tubes containing MS including vitamins with 2% sucrose and 0.8% plant agar and 50 $mg.L^{-1}$ of kanamycin to allow the development of roots.

Characterization of Induced Mutations

DNA was extracted from leaves of three-week-old regenerated plants to assess the mutation caused by *Agrobacterium*-mediated transformation following the method by (Porebski et al., 1997). The presence of the Cas9 gene was checked by PCR using specific primers (Table S1) with GoTaq® G2 Flexi DNA Polymerase (Promega). Primers specific to the targeted sequence were used to assess the Cas9-induced mutations (Table S1) and PCR products were analyzed by Sanger sequencing through subcontracting (Eurofins Genomics). Genotype was determined by analyzing the sequencing results using the ICE analysis tool by Synthego (https://ice.synthego.com/). K.O. mutants were selected according to R^2 and K.O. scores.

Starch Extraction

Three independent cultures were made, and the starch extracted from the tubers of these three replicates was used for the following experiments. After a washing step with tap water, tubers (100-120 g) were crushed on ice with deionized water using a Polytron homogenizer. Starch was filtered through a nylon net with a 100 µm mesh size (Sefar). Two to three centrifugation steps were performed at 4,000 g and 4°C using deionized water until water appears clean. The supernatant obtained from the first centrifugation step was collected, boiled at 100°C for 10 min and then stored at -20°C for subsequent measurements of sugar and water-soluble polysaccharides content. Cellular debris were removed from starch through a centrifugation step at 4,000 g and 4°C for 45 min in a Percoll density gradient (Cytiva). The starch suspensions were then stored in 20% ethanol at 4°C for further analysis.

When potato flour was obtained from Simplot company (*ss5* mutants and corresponding wild-type lines), starch was purified by the following method. A 6% (w/v) suspension of potato flour in 0.5 M sodium chloride was vortexed thoroughly. The suspension was then filtered through a 100 µm cell strainer (VWR) and washed with deionized water. After centrifugation at 2000 × g for 10 minutes, the pellet was resuspended in a 90% (v/v) Percoll solution buffered with 50 mM Tris-HCl (pH 8) to remove residual cell wall debris. The starch pellet was subsequently washed three times with 2% (w/v) SDS and resuspended in

acetone. Following centrifugation at maximum speed, excess acetone was removed, and the pellet was left to evaporate overnight under a fume hood.

Starch, glucose and water-soluble polysaccharides content

To assay the starch content, starch suspensions were submitted to *in vitro* digestion with amyloglucosidase (AGS) from *Aspergillus niger* (Megazyme) for 30 min at 58°C. Subsequently, the starch content was measured using the Enzytec™ Starch kit according to the manufacturer's specifications. The content of the soluble extracts was also analyzed using the same kit, both before and after digestion with AGS, to measure the glucose and water-soluble polysaccharides contents, respectively.

A second technique was used to measure sucrose, glucose and fructose in soluble extracts using capillary electrophoresis. Briefly, soluble extracts prepared as described in "Tuber production and starch extraction" were analyzed prior to injection in a SCIEX PA 800 Plus Pharmaceutical Analysis System equipped with a silicon capillary column (inner diameter: 50 µm; outer diameter: 360 µm; length: 60 cm). The capillary was rinsed and coated with NaOH 80 mM, Na_2HPO_4 55 mM prior to injection of the sample 4 s at 0.5 psi. The migration was performed at 16 kV during 1 h at 15 °C. The detection was made with a 270 nm deuterium lamp, and a UV detector. The detection window was located 10 cm above the outlet of the capillary column.

Color evaluation after frying

After harvest, the tubers were immediately used for frying tests or placed in a well-ventilated and temperature-controlled room at 4°C, in the dark for three weeks. 4–6 slices of 1.5 mm of each tuber were fried in commercial sunflower oil at 190 °C until no more bubbles emerged (approximately 3 min). To evaluate the color intensity of potato tuber slices after frying, we used ImageJ software with the RGB Measure plugin. Fried tuber slices were photographed under lighting conditions. Each tuber slice was manually selected in ImageJ using the freehand selection. The RGB Measure plugin was then used to extract the average blue channel intensity for each slice, corresponding to the yellow-brown color, with values

ranging from 0 (black) to 255 (white). Lower blue intensity values corresponded to darker browning after frying. Measurements were recorded for wild-type controls and mutant lines.

Granulomorphometry

Two different devices were used to measure the granule diameter. With the first one, starch granule size and shape were determined using a Flow-Cell FC200S+ granulomorphometer (Occhio). A filter was applied to exclude particles with a diameter smaller than 4 µm because of the camera resolution limits and a roundness inferior to 0.5 to exclude cellular debris. An average of 3,000 granules after filtration was analyzed for each sample. For determination of size and shape, the ISO area diameter and ellipsoid roundness parameters were retained. Ellipsoid roundness was determined by measuring the ratio between the average radius of peripheral circles and the radius of the maximal circle included in the outlined particle (this ratio ranges from 0 to 1, with 1 corresponding to a perfect circle).

With the second one, starch granule diameter was analyzed using the Coulter counter. Purified starch granules were analyzed on the Multisizer 4e Coulter counter (Beckman Coulter), fitted with a 100 µm aperture. A minimum of 100 000 particles were analyzed per sample.

Scanning electron microscopy

Purified starch granules were glued on an aluminum support with carbon double-sided tape and observed at 1 kV accelerating voltage with a Zeiss Merlin VP Scanning Electron Microscope.

Assay of Phosphorylated Glucose Residues in Starch

The quantification of phosphorylated glucose residues was made according to (Verbeke et al., 2016). Briefly, 1 mg of starch was hydrolyzed in 100 µL of 2 M trifluoroacetic acid (TFA) at 95°C for 80 min. 20 µL of the hydrolysate was added to 200 µL of ultrapure water and dried at room temperature in a speed-vac. After the addition of 200 µL of ultrapure water,

a new drying step was performed. The samples were labeled using 2 µL of cyanoborohydride in tetrahydrofuran (THF) and 2 µL of 200 mM 8-aminopyrene-1,3,6-trisulfonic acid (APTS) in 15% acetic acid and incubated at 42°C overnight. 96 µL of ultrapure water was added and 15 µL of this dilution was re-diluted in 185 µL of ultrapure water prior to injection in a SCIEX PA 800 Plus Pharmaceutical Analysis System equipped with a laser induced fluorescence detector (Verbeke et al., 2016).

Label-free quantitative proteomics

Briefly, 15 µg of proteins from starch were digested with eFASP (enhanced Filter Aided Sample Preparation) and the analysis of peptides was performed on nanoLC Q-Exactive plus (Thermo Scientific) as previously described (Helle et al., 2018, 2019). Proteins were quantified with MaxQuant software 2.0.3.0 with custom *solanum tuberosum* database from Potato Genome Sequencing ConsortiumPublic Data Release (52,570 sequences). The restriction method was Trypsin/P and allowed up to two missing cleavages; the minimum length of the peptide was set to six amino acid residues; the mass error tolerance of the primary precursor ion of the first search and the main search was set to 20 ppm and 5 ppm, respectively. The mass error tolerance of the secondary fragment ion was 0.02 Da. Cysteine alkylation was set as a fixed modification, variable modification was methionine oxidation, protein N-terminal acetylation, deamidation (NQ). The proteomics datasets have been deposited to the ProteomeXchange Consortium via the PRIDE partner repository (Perez-Riverol et al., 2019) (https://www.ebi.ac.uk/pride/).

Optical and Scanning Electron Microscopy

Transversal tuber slices of an approximate thickness of 1 mm were cut with a kitchen slicer and placed on a microscope slide and observed using an upright A1R Nikon confocal microscope (Nikon Instruments Europe B.V) with a Plan Apo ×60 Oil (NA = 1.4) objective, using bright field illumination. Purified starch granules were observed under transmitted light microscopy using a Leica AF6000 LX microscope (Leica Microsystems SAS) with a Plan Apo x100 Oil (NA=1.4) objective with Differential Interference Contrast. The birefringence of purified starch granules was assessed under polarized light using a Nikon Eclipse TE2000-E

microscope (Nikon Instruments Europe B.V) with a Plan Apo x60 Oil (NA=1.4) objective after being sonicated four times at 60 % during 10 sec using a sonifier cell disruptor B-30 (Branson).

Wide-angle X-ray scattering

X-ray diffraction was used to identify the type of crystalline structure and to quantify the crystalline/amorphous structure ratio in the starch samples. Before analysis, starch water content was stabilized in a desiccator containing a saturated NaCl solution with a relative humidity of 75% for a week at room temperature. Fifty milligrams of sample were sealed in a copper ring between two adhesive tape sheets to prevent any change in water content during analysis. Two-dimensional diffraction diagrams were recorded using a Bruker D8 X-ray diffractometer (Karlsruhe, Germany) equipped with a GADDS detector. The X-ray radiation, Cu K□1 (□ = 0.15406 nm), produced in a sealed tube at 40 kV and 40 mA, was selected and parallelized using crossed Göbel mirrors and 3 collimated to produce a 500 □m beam diameter. Data were monitored by a GADDS 2D detector for 10 min and normalized.

Small-angle X-ray scattering (SAXS)

SAXS measurements were performed on a Xeuss 2.0 apparatus (Xenocs) equipped with point collimation (beam size: 300×300 µm2) and a micro source using a Cu-Kα radiation (λ =1.54 Å). The sample to detector distance was calibrated using silver behenate as a standard and was around 150 cm for the measurements. Through view 2D diffraction patterns were recorded on a Pilatus 200k detector (Dectris). From the 2D patterns integrated intensity profiles were computed using a Foxtrot® software. The lamellar repeat distance, designated as d, representing the alternative crystalline and amorphous lamellae, was calculated by the Bragg equation, $d = 2\pi/qmax$.

Maximum Wavelength of Starch/Iodine Complex

Two milligrams of starch were solubilized in 100% dimethylsulfoxide (DMSO) by heating 15 min at 100°C. After cooling down, they were diluted 100 times and 80 µL of the dilution was added to 20µL of iodine solution (I2 0.2% [w/v] and KI 2% [w/v]) and the

absorbance was read between 500 and 700 nm using a SPECTROstar Nano spectrometer (BMG LABTECH's), to determine the wavelength at the maximum of absorbance of the starch/iodine complex.

Determination of Amylose Content

Two different methods were used to measure amylose content. In the first one, starch was fractionated using exclusion size chromatography to separate amylose and amylopectin molecules. 1.5 mg of starch was first gelatinized in 200 µL of dimethylsulfoxide (DMSO) by heating 15 min at 100°C, and precipitated in 800 µL of 100% ethanol to remove lipids. After 10 min of centrifugation at 10,000 g and 4°C, starch was then resolubilized in 300 µL of 10 mM sodium hydroxide. It was loaded on a column (0.5 cm x 65 cm), containing Sepharose CL-2B resin (Cytiva) equilibrated with 10mM sodium hydroxide. The flow rate was equilibrated at 12 mL.h-1. Fractions of 300 µL were collected. 80 µL of each fraction were mixed with 20 µL of iodine solution (I2 0.2% [w/v] and KI 2% [w/v]) and analyzed by spectrophotometry between 500 and 700 nm. The fractions containing either amylose or amylopectin were pooled and the amount of each glucan was measured using the EnzytecTM Starch kit.

In the second one, 0.05% of starch [w/v] was added to 5.4 mM iodine and 90% DMSO and mixed overnight on a blood rotator at 20 rpm. The mix was then diluted by 10 and the absorbance was read after 30 min at 600 nm using Cecil CE 2041. The amylose/amylopectin ratio was determined compared to a commercial potato amylose (Sigma A0512) standard curve.

Chain Length Distribution

The starch chain length distribution was measured according to (Helle et al., 2018). Briefly, two milligrams of starch were gelatinized in 250 µL of ultrapure water by heating at 100°C with regular stirring. It was then debranched at 42°C overnight with 20 U of isoamylase and 1 U of pullulanase (Sigma). The samples were then desalted on Alltech Carbograph columns and freeze-dried. Dried samples were labeled using 2 µL of cyanoborohydride in tetrahydrofuran (THF) and 2 µL of 200 mM 8-aminopyrene-1,3,6-trisulfonic acid (APTS) in 15% acetic acid and incubated at 42°C overnight. 46µL of ultrapure water was added and the

samples were diluted 50 times with ultrapure water. They were then analyzed in a SCIEX PA 800 Plus Pharmaceutical Analysis System equipped with a laser induced fluorescence detector according to (Fermont et al., 2022).

In vitro enzymatic hydrolysis of starch

The enzymatic degradation of *lesv* starch was assayed by measuring the production of reducing glucose using 3,5-dinitrosalicylic acid (DNS). The enzyme used to hydrolyze starch is the porcine pancreatic α-amylase (PPA) (Megazyme). 128 U/mL of PPA was suspended in a 20 mM phosphate, 0.02 % sodium azide, 2 mM NaCl, 0.25 mM CaCl2 pH 7.0 buffer. 1 mL of the enzyme suspension was added to 10 mg of starch in a 1.5 mL tube. The mixture was incubated at 37°C in a thermomixer and stirred. The estimation of hydrolyzed starch was performed by taking 15 µL aliquots after 0, 20, 60, 360, 1440, 1800 and 2880 min and mixing it with a DNS solution, according to (5). After heating 10 min at 37°C, the absorbance was read at 540 nm in a spectrophotometer. Standard curves of glucose were realized (0, 1, 2, 3, 4 and 5 g.L-1). A negative control containing no PPA was realized for each sample and subtracted to the measures.

Pasting properties

Pasting properties of starch were analyzed using a Rapid Visco-Analyzer (RVA type 4, Newport Scientific Pty) connected to Thermocline Software. Starch suspension containing 14% of starch (w/v) was equilibrated at 50 °C for 1 min, heated to 95 °C for 3.5 min and held at temperature for 2.5 min. It was then cooled to 20°C (-8°C/min), and held at 20°C for 2 min. A constant stirring with a 160-rpm speed was applied to the rotation paddle.

Differential Scanning Calorimetry

Starch was stabilized in a desiccator containing a saturated NaBr solution with a relative humidity of 57% for two weeks at room temperature, to reach equilibrated water content before subsequent analysis. The thermal characteristics of the starch were measured using a Differential Scanning Calorimeter (DSC) Q1000 apparatus (TA Instruments). 40 µL of

ultrapure water was added to 10 mg of starch in a stainless-steel sealed pan. The scan was performed from 10 to 120°C at a rate of 3°C/min. The onset temperature (*To*), peak temperature (*Tp*), conclusion temperature (*Tc*) and transition enthalpy (*ΔH*) were measured using TA Instruments Universal Analysis software.

Filter fractionation of starch granules

Granules were separated according to (Helle et al., 2019). Briefly, granules were separated in two fractions, using nylon filter with a mesh width of 11 µm. The granules above 11 µm were designated as "large granules" (LG) and the ones below 11 µm were called "small granules" (SG).

Protein-protein interaction assays

Untargeted approach: immunoprecipitation on tubers and mass spectrometry

Proteins were extracted from frozen wild-type and *lesv* potato tubers as described in (Kamble et al., 2023) with some modifications. Briefly, tubers were crushed in ice-cold extraction medium (50 mM Tris-HCl, pH 8; 1 mM DTT; 1% [v/v] Triton X-100, 150 mM NaCl, and 1 tablet of Roche Complete Protease Inhibitor cocktail for 50 mL) at a rate of 2 mL of medium for 1 g of tuber. Insoluble material was removed by centrifugation at full speed for 5 min at 4 °C, and proteins were collected in the supernatant. µMACS™ protein A microbeads were added to soluble protein extracts, diluted serum anti-LESV from *Arabidopsis thaliana* (1:100, produced in rabbit) and incubated for 1 h at 4 °C. The beads were captured with a µColumn on a magnetic stand (Miltenyi Biotec), washed 5 times with extraction medium, before eluting the bound proteins with hot (85°C) elution medium (50 mM Tris-HCl, pH 8, 2 mM DTT and 2% [w/v] SDS). Proteins were precipitated and digested as described in (Kamble et al., 2023). Peptides were analyzed by nano-LC-MS/MS.

Targeted approach: transient expression of proteins in *Nicotiana benthamiana* and immunoprecipitation

The coding sequences of LESV and ISA1 were ordered as a gBlocks DNA fragment flanked by attB Gateway recombination sites. These coding sequences were cloned into the Gateway entry vector, pDONR221 (Annex 2), using the BP Clonase II enzyme kit (Thermo Scientific). The coding sequences in pDONR221 were recombined into either pB7YWG2 (C-terminal YFP fusion) (Annex 3) or pJCV52 (C-terminal HA-tag fusions) (Annex 4) using the LR Clonase II enzyme kit (Thermo Scientific). The sequences of all vectors were confirmed using Sanger technic (performed by Azenta) before use. *Nicotiana benthamiana* leaves were transformed by infiltrating *Agrobacterium tumefaciens* (GV3101 strain) cultures previously transformed with the constructs, and pairwise immunoprecipitations on leaf soluble extracts using anti GFP/YFP or anti-HA microbeads (Miltenyi Biotech) were carried out after 3 days as previously described in (Kamble et al., 2023) with some modifications. Briefly, four leaf discs (1 cm of diameter) were crushed in 1.3 mL of ice-cold extraction medium (50 mM Tris-HCl, pH 8; 1 mM DTT; 1% [v/v] Triton X-100, 150 mM NaCl, and 1 tablet of Roche Complete Protease Inhibitor cocktail for 50 mL). Insoluble material was removed by centrifugation at full speed for 5 min at 4 °C, and proteins were collected in the supernatant. µMACS™ magnetic microbeads conjugated to anti-YFP/GFP or anti-HA were added to soluble leaf extracts to precipitate the bait protein and incubated for 1 h at 4 °C. The beads were captured with a µColumn on a magnetic stand (Miltenyi Biotec), washed 3 times with extraction buffer, before eluting the bound proteins with hot elution medium (50 mM Tris-HCl, pH 8, 2 mM and 2% [w/v] SDS). The presence of the bait (LESV) and the prey (ISA1) proteins was detected using antibodies against YFP or HA-tag.

Yeast-two hybrid assays

The coding sequences of *LESV* and *ISA1* genes previously cloned into pDONR221 plasmid (see the previous section) were subsequently recombined into the destination vectors pGADT7 (containing the activation domain) (Annex 5) or pGBKT7 (containing the DNA-binding domain) (Annex 6) via LR Clonase II-mediated recombination (Thermo Scientific). Various plasmid combinations (see results section) were co-transformed into *Saccharomyces cerevisiae* strain AH109 (MATa, trp1-901, leu2-3, 112, ura3-52, his3-200, gal4Δ, gal80Δ,

LYS2::GAL1UAS-GAL1TATA-HIS3, MEL1 GAL2UAS- GAL2TATA-ADE2, URA3::MEL1UAS-MEL1TATA-lacZ). Transformed yeast cells were selected on Double Dropout medium (DDO, SD/-Leu-Trp) (Takara) to confirm the presence of both plasmids and screened for protein-protein interactions on Quadruple Dropout medium (QDO, SD/-Leu-Trp-Ade-His) (Takara), where growth indicates a positive interaction.

Preparation of Leaf Sections for Microscopy Observation

Transitory starch granules were observed *in vivo* within leaf plastids. Plants were grown in soil in 3-liter pots inside a growth chamber under a 16-hour light cycle (90 $\mu mol \cdot m^{-2} \cdot s^{-1}$) at 22°C, followed by 8 hours of darkness at 20°C. Young leaves were harvested from one-month-old plants at the end of the light phase. Leaf sections (~0.5 × 0.5 cm) were fixed in a buffer containing 1X PBS, pH 7.3, 4% sucrose, and 4% paraformaldehyde. Samples were then placed under vacuum for several hours. After rinsing with deionized water, the leaf sections were mounted on microscope slides for preliminary observations using a Zeiss LSM 780 confocal laser scanning microscope.

RESULTS

The results presented in this section originate from the experimental work I carried out during my PhD, and focus on the functional characterization of ESV1 and LESV in potato. This work builds upon and significantly extends the data included in the article *"LIKE EARLY STARVATION is involved in the regulation of starch initiation in potato (Solanum tuberosum cv. Désirée) tubers."* (available on BioXRiv, https://doi.org/10.1101/2025.06.23.661224). I personally generated all the data shown here, except for the initial generation of the *lesv* and *esv1* mutants performed by M. Berti, mass spectrometry analyses performed by F. Bray, scanning electron microscopy (SEM) images produced in collaboration with N. Barois (UAR 2014), and X-ray diffraction analyses conducted in collaboration with H. Hulin from BIA Unit at INRAE in Nantes and G. Stoclet from UMR 8207 – UMET at the University of Lille.

1. Production of *lesv* and *esv1* mutants

This first section focuses on the generation of *lesv* and *esv1* knockout mutants. Targeted mutagenesis in potato presents challenges due to the complexity of the tetraploid genome. To overcome this, we used the CRISPR/Cas9 genome editing approach, which offers the ability to target all four alleles simultaneously with high efficiency and specificity.

Although the mutagenesis experiments were conducted by Mara Berti, a brief overview of the method is included here to provide essential context for the mutation validation work that I carried out.

1.1. Targeted mutagenesis of *LESV* and *ESV1* gene using the CRISPR/Cas9 approach

To ensure the highest specificity and efficiency, multiple bioinformatic tools (Geneious, CRISPR-P, and CRISPOR) were used to design and assess candidate gRNAs targeting all four alleles of *LESV* and *ESV1* as well as the polymorphism map described by Sevestre et al. (2020). The characteristics of the gRNAs are presented in Table 1. The selected gRNAs targeted the third exon in both genes (Figure 25). They were subsequently cloned into the pDIRECT_22A plasmid using a Golden Gate assembly as described by Čermák et al. (2017) (Annex 1). This vector carries a kanamycin resistance gene. The resulting construct was

introduced into potato plants via *Agrobacterium tumefaciens*-mediated nuclear genome transformation.

Table 1 : Characteristics of the guide RNAs (gRNAs) targeting *LESV* and *ESV1*. gRNAs were designed using the CRISPOR online tool (https://crispor.gi.ucsc.edu/) based on the Solanum tuberosum reference genome (NCBI GCF_000226075.1, SolTub_3.0). The MIT specificity score (0–100) reflects the uniqueness of a guide sequence in the genome (Hsu et al., 2013); higher scores indicate fewer predicted off-target effects. The CFD specificity score, based on a more accurate off-target model, correlates better with actual cleavage events (Doench et al., 2016). Efficiency was predicted using the Doench 2016 model (also known as the Fusi score, range: 0–100), suitable for gRNAs expressed under a U6 promoter (Doench et al., 2016; Fusi et al., 2015). The higher the efficiency score, the more likely is cleavage at this position. The "Outcome" prediction estimates the most likely sequence resulting from DNA repair after Cas9 cleavage. The frameshift score (0–100) predicts the likelihood that indels will result in a frameshift mutation (W. Chen et al., 2019). Off-target counts are indicated for alignments with 0 to 4 mismatches (e.g., 0–0–0–0–9 means 9 predicted off-targets with 4 mismatches). Only potential off-targets adjacent to canonical PAM sequences (NGG, NAG, or NGA) were considered.

gRNA sequence + **PAM** and position in the gene	Specificity score		Predicted efficiency, Doench' 16 score	Outcome, frameshift score	Off-targets for 0-1-2-3-4 mismatches
	MIT	CFD			
gRNA for *LESV* GGAGTGGCATGAGAAATGGT**GGG** Strand: forward, exon: 3	91	94	72	69	0-0-0-5-36 With 1 off-target with 4 mismatches present in an exon
gRNA for *ESV1* GCAGTGATGGTACCTTAGAA**TGG** Strand: forward, exon 3	99	99	53	78	0-0-0-0-9 With 2 off-targets with 4 mismatches present in an exon

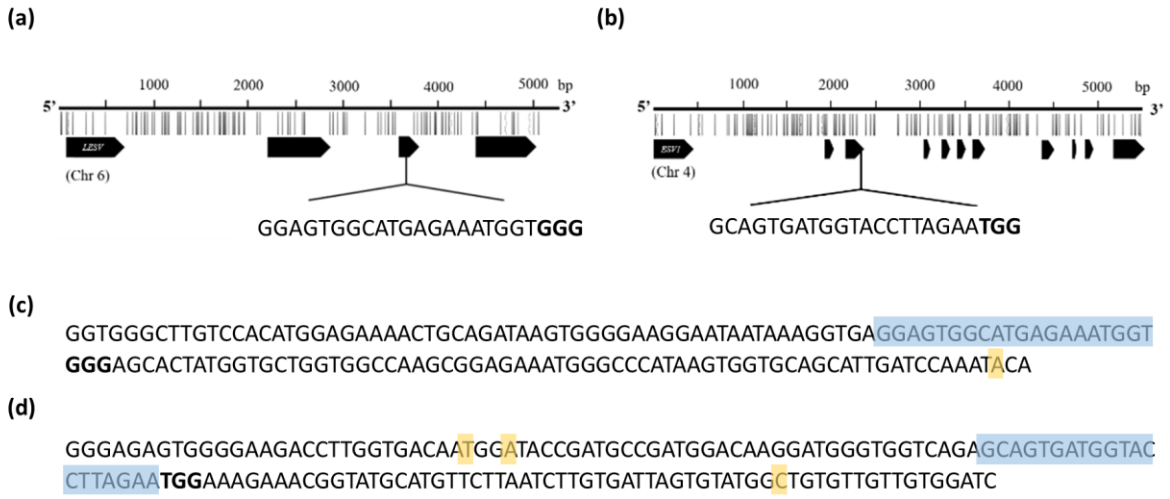

Figure 25 : Targeted mutagenesis of the LESV and ESV1 genes using CRISPR/Cas9 system. (a, b) Respective target site of the guide RNA (gRNA) within the LESV and ESV1 genes. Black arrows represent exons, the Protospacer Adjacent Motif (PAM) is marked in bold. Vertical lines above exons are single nucleotide polymorphisms (transversions or transitions), broken lines are insertions. Chr: chromosome. (c, d) 150 bp window of *LESV* and *ESV1* sequences around the gRNAs. gRNAs are highlighted in blue, transitions are highlighted in yellow. PAM is marked in bold.

1.2. Mutation verification by genotyping

To confirm the success of the transformation, the presence of the Cas9 gene in the genome was verified by PCR amplification using specific primers (Annex 9 and Figure 26)

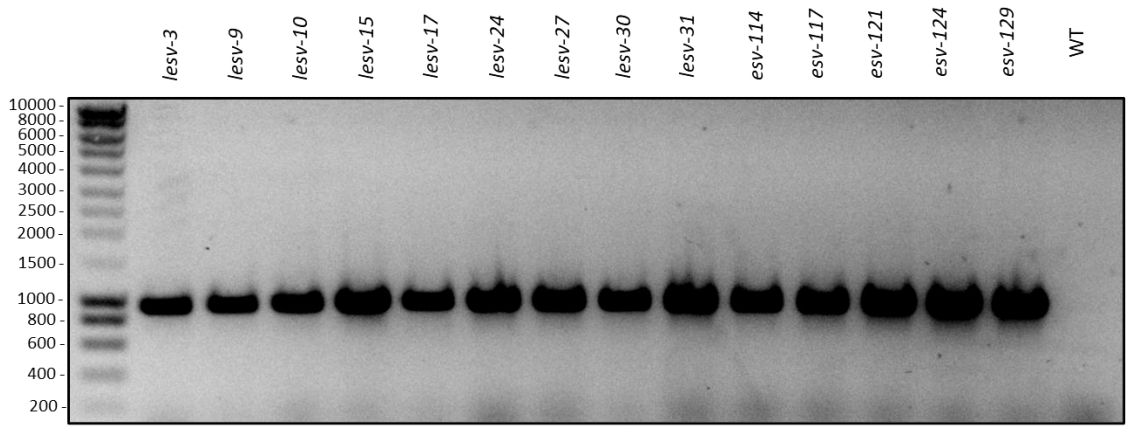

Figure 26 : PCR amplification of a 959 bp region of the *CAS9* gene in mutants. The first lane corresponds to the SmartLadder MW1700-10 (Eurogentec) molecular weight standard, in bp. The last lane is a negative control, from a wild type (WT) plant.

Genotyping of the regenerated kanamycin resistant plants was performed by sequencing the targeted regions of *LESV* and *ESV1* after PCR amplification using the primers listed in Annex 9. The PCR reaction amplifies the four alleles at the same time, therefore, sequencing the PCR products results in overlapping signals corresponding to the sequence of these four alleles. The chromatograms were then analyzed with the ICE analysis tool (https://ice.synthego.com/#/) (Annex 10 and Annex 11) that separates the overlapping signals. The number of edited alleles was inferred from the predicted sequences and their relative proportions, assuming that one allele corresponds to approximately 25% of the signal. Among 35 and 31 transformants confirmed to carry the *CAS9* gene, 28 and 21 exhibited at least one edited allele for *LESV* and ESV1 respectively. From these, nine independent full knock-out lines were selected for *LESV* and five for *ESV1* (Table 2). This corresponded to 32.2% and 23.8% of the total transformants. In all selected lines, the four alleles carried frameshift mutations.

Except granule morphology that was examined in all generated lines, subsequent analyses were conducted on three *lesv* (*lesv*-10, *lesv*-15 and *lesv*-24) and two *esv1* (*esv1*-121 and *esv1*-129) lines, randomly selected among the knockout lines that displayed a KO score above 90% (Table 2)The absence of the corresponding proteins in mutant starches was confirmed by label-free quantitative proteomics following starch gelatinization and protein isolation (Figure 27) and Western Blot analysis (Annex 12).

Once the mutants had been successfully generated and their genotypic profiles validated, we proceeded to investigate their development and carbohydrate metabolism at plant level.

Table 2 : Genotyping results of targeted mutagenesis in *LESV* and *ESV1* genes. Nine *lesv* mutants (a) and five *esv1* mutants (b) were identified as shift mutants using the ICE Synthego algorithm. In the sequences, red letters highlight the gRNA and the PAM motif is marked in bold. The "deletion" column specifies the number of deleted bases (in parentheses) in the inferred sequences, with their relative proportions in the edited population noted in red. The KO (knock-out) score is the proportion of deletions that led to a frameshift, the R2 value indicates how well the proposed deletions fit the Sanger sequence data of the edited sample. Differences between the percentages in the "deletions" column and the KO score are attributed to weak signals (~5% of the edited population, not represented here), potentially coming from PCR amplification or sequencing errors, or misinterpretation by the Synthego algorithm.

(a)

line	sequence	deletions	KO score (%)	R^2
WT	GGGAAGGAATAATAAAGGTGAGGAGTGGCATGAGAAATGGT**GGG**AGCACTATGGTGCTGGTGGC	(0) 100%	/	/
lesv-3	GGGAAGGAATAATAAAGGTGAGGAGTGGCATGAG - - - - GGT**GGG**AGCACTATGGTGCTGGTGGC GGGAAGGAATAATAAAGGTGAGGAGTGGCATGAGAA--GGT**GGG**AGCACTATGGTGCTGGTGGC	(-4) 55% (-2) 34%	89	0.97
lesv-9	GGGAAGGAATAATAAAGGTGAGGAGTGGCATGAGAA - - GGT**GGG**AGCACTATGGTGCTGGTGGC	(-2) 81%	84	0.87
lesv-10	GGGAAGGAATAATAAAGGTGAGGAGTGGCATGAGA - - TGGT**GGG**AGCACTATGGTGCTGGTGGC GGGAAGGAATAATAAAGGTGAGGAGTGGCATGA - - - - - - - - - - **G**AGCACTATGGTGCTGGTGGC	(-2) 70% (-10) 27%	97	0.97
lesv-15	GGGAAGGAATAATAAAGGTGAGGAGTGGCATGAGAAA - GGT**GGG**AGCACTATGGTGCTGGTGGC GGGAAGGAATAATAAAGGTGAGGAGTGGCATGA - - - - - - - - - - **G**AGCACTATGGTGCTGGTGGC	(-1) 47% (-10) 39%	94	0.94
lesv-17	GGGAAGGAATAATAAAGGTGAGGAGTGGCATGAGAA - - GGT**GGG**AGCACTATGGTGCTGGTGGC GGGAAGGAATAATAAAGGTGAGGAGTGGCATGAGAAA - GGT**GGG**AGCACTATGGTGCTGGTGGC GGGAAGGAATAATAAAGGTGAGGAGTGGCATGA - - - - - GGT**GGG**AGCACTATGGTGCTGGTGGC	(-2) 34% (-1) 22% (-5) 19%	80	0.96
lesv-24	GGGAAGGAATAATAAAGGTGAGGAGTGGCATGAGAA - - GGT**GGG**AGCACTATGGTGCTGGTGGC	(-2) 92%	98	0.98
lesv-27	GGGAAGGAATAATAAAGGTGAGGAGTGGCATGAGAA - - GGT**GGG**AGCACTATGGTGCTGGTGGC	(-2) 94%	74	0.95
lesv-30	GGGAAGGAATAATAAAGGTGAGGAGTGGCATGAGAAA - GGT**GGG**AGCACTATGGTGCTGGTGGC GGGAAGGAATAATAAAGGTGAGGAGTGGCATGAGAA - - GGT**GGG**AGCACTATGGTGCTGGTGGC GGGAAGGAATAATAAAGGTGAGGAGTGGCATGAG - - - - GGT**GGG**AGCACTATGGTGCTGGTGGC	(-1) 35% (-2) 29% (-4) 27%	92	0.95
lesv-31	GGGAAGGAATAATAAAGGTGAGGAGTGGCATGAGAA - - GGT**GGG**AGCACTATGGTGCTGGTGGC	(-2) 77%	81	0.81

(b)

line	sequence	deletions	KO score (%)	R^2
WT	GACAAGGATGGGTGGTCAGAGCAGTGATGGTACCTTAGAA**TGG**AAAGAAACGGTATGCATGTT	(0) 100%	/	/
esv1-114	GACAAGGATGGGTGGTCAGAGCAGTGATGGTAC- - - - GAA**TGG**AAAGAAACGGTATGCATGTT GACAAGGATGGGTGGTCAGAGCAGTGATGGTACCTT - - AA**TGG**AAAGAAACGGTATGCATGTT GACAAGGATGGGTGGTCAGAGCAGTGATGGTACCT - - GAA**TGG**AAAGAAACGGTATGCATGTT	(-4) 44% (-2) 32% (-2) 13%	89	0.95
esv1-117	GACAAGGATGGGTGGTCAGAGCAGTGATGGTA - - - - - GAA**TGG**AAAGAAACGGTATGCATGTT	(-5) 99%	99	0.99
esv1-121	GACAAGGATGGGTGGTCAGAGCAGTGATGGTA - - - - - GAA**TGG**AAAGAAACGGTATGCATGTT GACAAGGATGGGTGGTCAGAGCAGTGATGGTACCTT - - AA**TGG**AAAGAAACGGTATGCATGTT GACAAGGATGGGTGGTCAGAGCAGTGATGGTACCT - - GAA**TGG**AAAGAAACGGTATGCATGTT	(-5) 60% (-2) 19% (-2) 17%	96	0.96
esv1-124	GACAAGGATGGGTGGTCAGAGCAGTGATGGTACCT - - - - - **TGG**AAAGAAACGGTATGCATGTT GACAAGGATGGGTGGTCAGAGCAGTGATGGTACCTTA - - - - - **G**AAAGAAACGGTATGCATGTT	(-5) 74% (-5) 14%	91	0.92
esv1-129	GACAAGGATGGGTGGTCAGAGCAGTGATGGT - - - - - - - - A**TGG**AAAGAAACGGTATGCATGTT GACAAGGATGGGTGGTCAGAGCAGTGATGGTAC - - - - GAA**TGG**AAAGAAACGGTATGCATGTT GACAAGGATGGGTGGTCAGAGCAGTGATG - - - - - - - - GAA**TGG**AAAGAAACGGTATGCATGTT	(-8) 44% (-4) 30% (-8) 17%	91	0.92

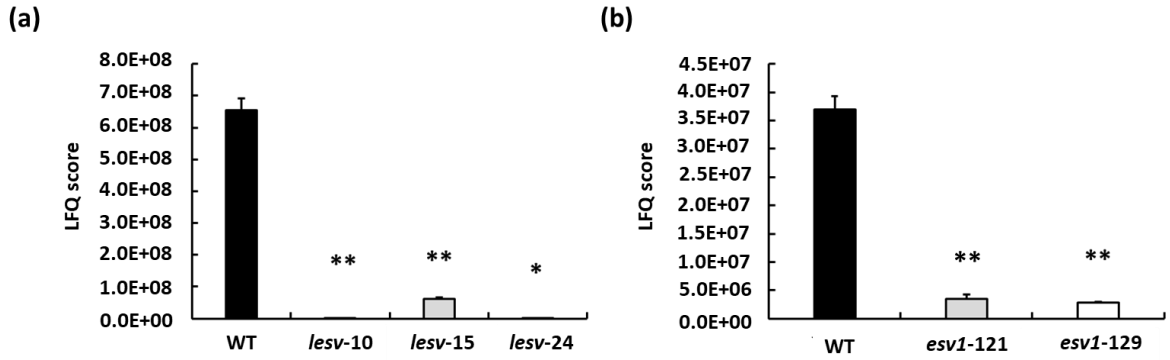

Figure 27 : Label free quantification of proteins. Proteins were isolated from starch prior to nanoLC-MS/MS analysis. The amount of each protein was estimated with the use of the MaxQuant software and the Label-Free Quantification (LFQ) intensities were used to compare samples. (a) LFQ score of LESV protein in wild-type (WT) and *lesv* mutants. (b) LFQ score of ESV1 in WT and *esv1* mutants. For (a) and (b), values are mean (+/-SE) of three experimental replicates (n = 3) except for WT that is mean of three biological replicates and three experimental replicates (n=9). Statistical analysis was made using Mann-Whitney tests, comparing the mean of the mutant line to the wild type. (* = $p \leq 0,05$; ** = $p \leq 0,01$).

2. Characterization of mutants at the plant level

Mutant plants were cultivated in soil for three months under a 16 h light / 8 h dark photoperiod (light intensity: 80 $\mu mol \cdot m^{-2} \cdot s^{-1}$), at 22°C during the light phase and 20°C during the dark phase. Various developmental and metabolic parameters were evaluated.

2.1. Impact of mutations on plant development

The inactivation of *LESV* and *ESV1* did not result in any major changes in plant development. Stem height, overall appearance, and tuber morphology appeared similar to those of wild-type plants (Figure 28a-f). Moreover, both tuber yield and number of tubers per plant were unaffected by the mutations (Figure 28g and h).

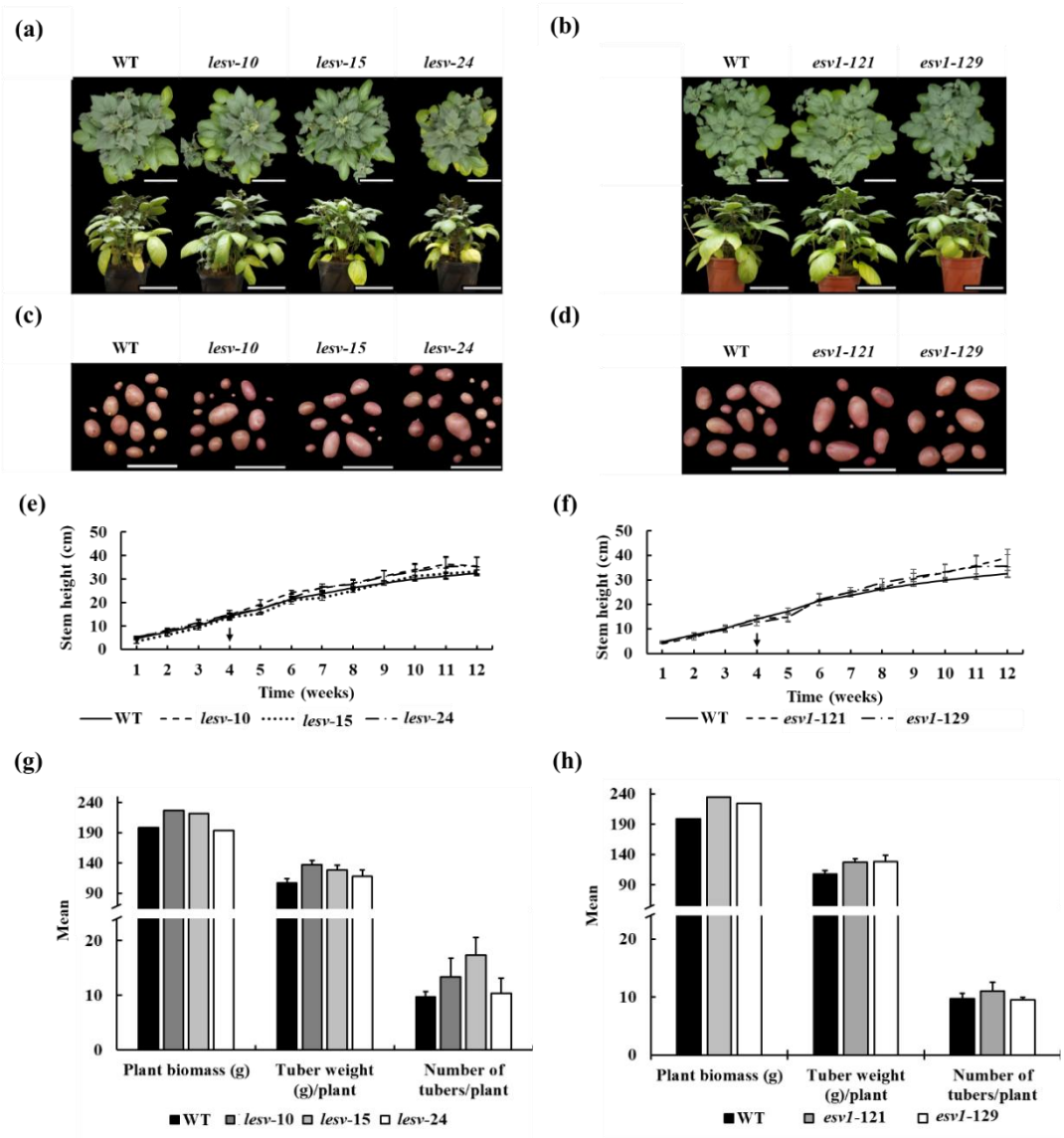

Figure 28 : Potato growth and development. (a, b) Pictures of two-month-old wild type (WT) and mutant plants grown on soil in a growth cabinet with 16 h light/8 h dark photoperiod (80 µmol.m-2.s^{-1}). (c, d) Tubers harvested from three-month-old WT or *lesv* and *esv1* mutant plants. (e, f) Stem size of WT and mutant plants over 12 weeks of culture. The black arrow indicates the moment when additional soil was added to the base of the stem. For WT, values are the mean (+/- SE) of three independent biological replicates from three independent cultures (n=9). For mutant lines, values are the mean (+/- SE) of three independent cultures (n=3). (g, h) Plant biomass, tuber weight per plant, and tuber number per plant of three-month-old plants. Except for plant biomass that was measured in a unique culture, values are mean (+/- SE) of three independent cultures. Statistical analysis was made using Mann-Whitney tests, comparing the mutant line to the wild type (* = $p \leq 0,05$; ** = $p \leq 0,01$; *** = $p \leq 0,005$). Scale bar in (a) and (b) = 15 cm, and in (c) and (d) = 10 cm. The background was removed on the plants tubers pictures (a-d) using the image editing tool removebg (https://www.remove.bg/).

2.2. Carbohydrate content in mutant lines

Beyond developmental traits, we assessed carbohydrate accumulation in the mutant lines in comparison to wild-type plants. Starch, glucose, and water-soluble polysaccharide

(WSP) contents were quantified. No significant differences were detected for starch, glucose and WSP levels (Figure 29).

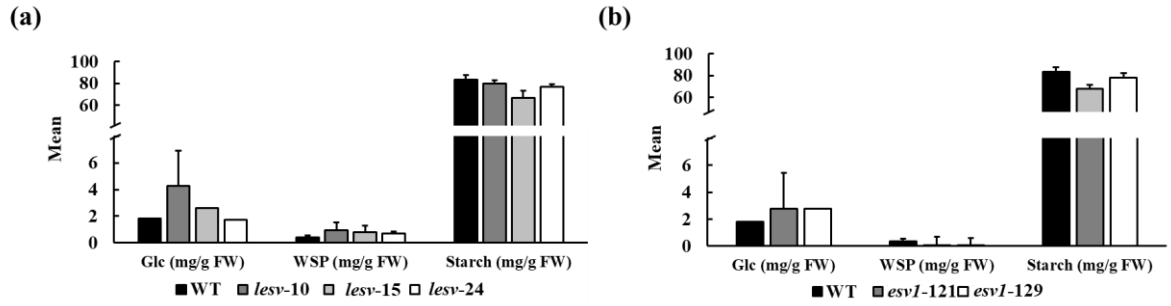

Figure 29 : Carbohydrate quantification of wild-type and *lesv* (a) and *esv1* (b) mutants. Glucose (Glc), water-soluble polysaccharides (WSPs) and starch contents in tubers expressed in $mg.g^{-1}$ of fresh weight (FW). For WT, values are mean (+/- SE) of three biological replicates from three independent cultures and three experimental replicates for each culture (n=27). For each mutant line, values are mean (+/- SE) of three independent cultures and three experimental replicates for each culture (n=9). Statistical analysis was made using Mann-Whitney tests, comparing the mutant line to the wild type (* = $p \leq 0,05$; ** = $p \leq 0,01$; *** = $p \leq 0,005$).

2.3. Impact of mutations on cold-induced sweetening

Cold-induced sweetening (CIS) is a physiological response specific to storage organs such as potato tubers, in which starch degradation is triggered during cold storage (typically below 8 °C), leading to the accumulation of reducing sugars such as glucose and fructose. This breakdown is driven by the coordinated action of several hydrolytic enzymes, including amylases, invertases, and other glucan-degrading enzymes. While this process helps protect the tuber from cold damage, it poses a major concern for the food industry. The accumulation of reducing sugars promotes browning reactions during high-temperature processing (e.g., frying) via the Maillard reaction and leads to the formation of acrylamide, a potentially carcinogenic compound. Understanding the molecular mechanisms underlying CIS is therefore crucial for improving the industrial quality and safety of potato-derived products.

Our laboratory focuses the mechanisms governing CIS in potato. In this context, and given that *ESV1* and *LESV* were initially described in *Arabidopsis thaliana* as regulators of starch degradation in leaves (Feike et al., 2016; C. Liu et al., 2023) (Feike et al., 2016; Liu et al., 2023), we sought to investigate whether their inactivation in potato tubers might alter the CIS response. This question was further justified by the possibility that these proteins might

have conserved functions in starch degradation across species, or, conversely, might play distinct roles in storage versus transitory starch metabolism.

To evaluate the impact of LESV and ESV1 on CIS, fresh tubers from wild-type and mutant lines were harvested and either processed directly or stored for three weeks at 4 °C before being sliced and fried for 3 minutes at 190 °C (Figure 30a-d). The resulting coloration was quantified by measuring the average blue intensity in the fried slices. Only minor differences were observed between wild-type and mutant lines after cold storage and no modification of color was associated with an increase in sugar content (Figure 30e). Indeed, no significant differences in sugar levels were detected between wild-type and mutant lines, either before or after cold storage. These results suggest that neither LESV or are involved in the regulation of CIS or in starch degradation during cold-storage in potato tubers. This contrasts with findings in *Arabidopsis,* where they were proposed to modulate starch degradation in leaves, and implies that their role may not be conserved in storage starch metabolism. Alternatively, a potential functional redundancy between these two proteins in tubers cannot be excluded and might mask individual contributions to starch degradation.

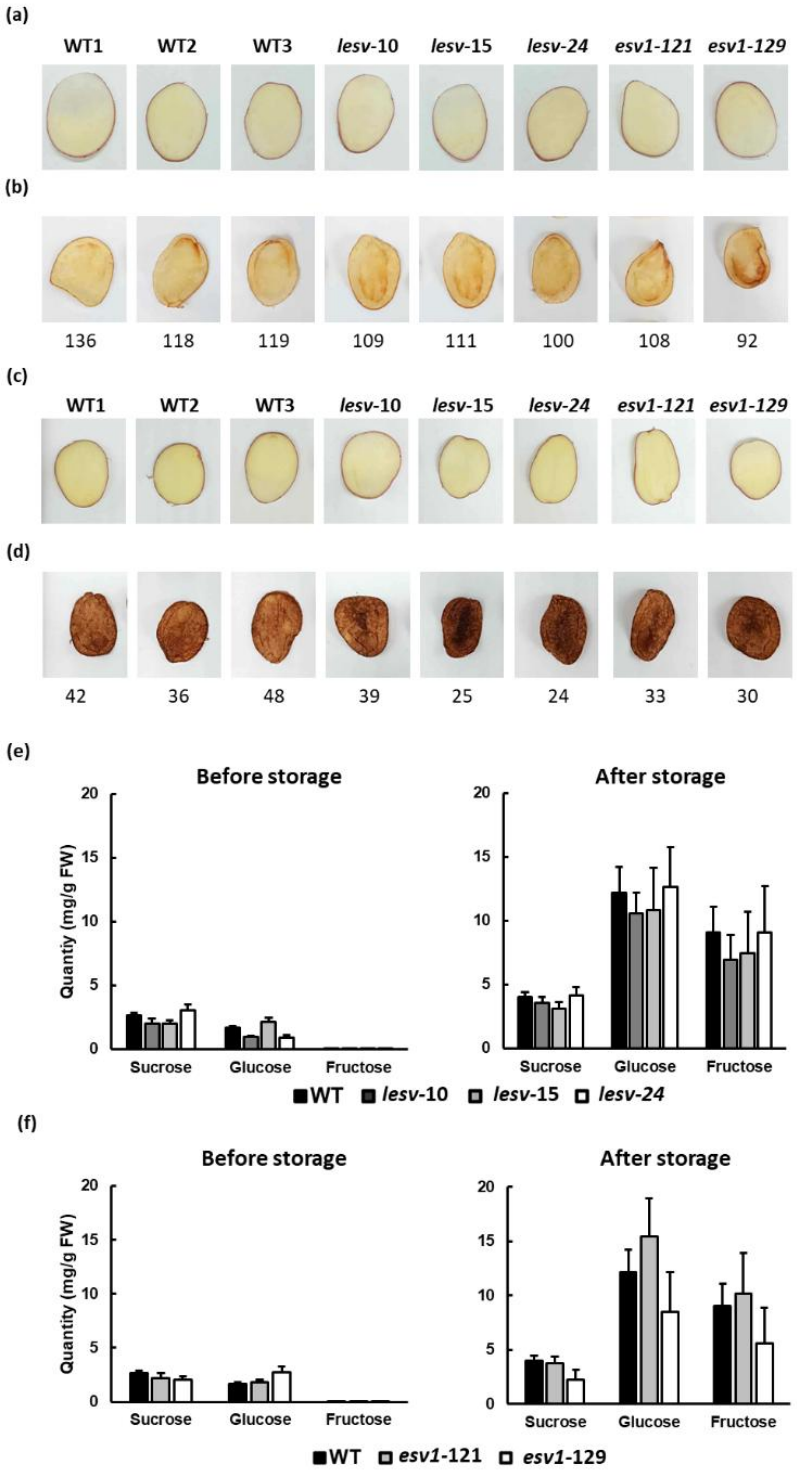

Figure 30 : Coloration of fried potato tuber slices and sugar content in wild-type and *lesv* and *esv1* mutant lines. (a and c) Raw tuber slices before (a) and after (c) storage 3 weeks at 4°C. (b and d) Same tuber slices as (a) and (c) after frying 3 min at 190°C. Color intensity, indicated above images, was quantified using the blue channel from the RGB color space in ImageJ. A lower blue intensity value indicates darker browning. (e,f) The bar graph represents the sucrose, glucose, and fructose content measured by capillary electrophoresis in wild-type, *lesv* and *esv1* tubers. For wild-type, values are mean (±SE) of three biological replicates and two experimental replicates (n=6). For *lesv* and *esv1* lines, values are mean (±SE) of two biological replicates and two experimental replicates (n=4).

3. Influence of *LESV* and *ESV1* inactivation on starch granule morphology and structure

Since LESV and ESV1 were found tightly bound to the starch granule, it has been suggested that these proteins play a role in starch metabolism (Helle et al., 2018). We therefore focused our attention on the characterization of starch granules in the mutant lines.

3.1. Starch granule morphology is drastically affected in *lesv* mutants

Starch granule morphology, specifically their diameter and roundness, was analyzed using a granulomorphometer. A striking reduction of granule diameter was observed in *lesv* knockout mutant lines compared to WT plants, while no modification was observed in *esv1* mutants (Figure 31). On average, *lesv* lines exhibited a two-fold reduction in granule diameter. Notably, 50% of granules had a diameter between 4 µm and 5 µm, compared to 13% in WT plants (Figure 31a). This phenotype was consistently observed across all nine independent *lesv* K.O. mutants. Additionally, granule roundness was strongly reduced in the *lesv* mutants, with an average roundness of 0.83 compared to 0.87 in WT (Figure 31c). Roundness is quantified on a scale from 0 to 1, where a value of 1 corresponds to a perfect circle and values closer to 0 indicate more irregular or angular shapes.

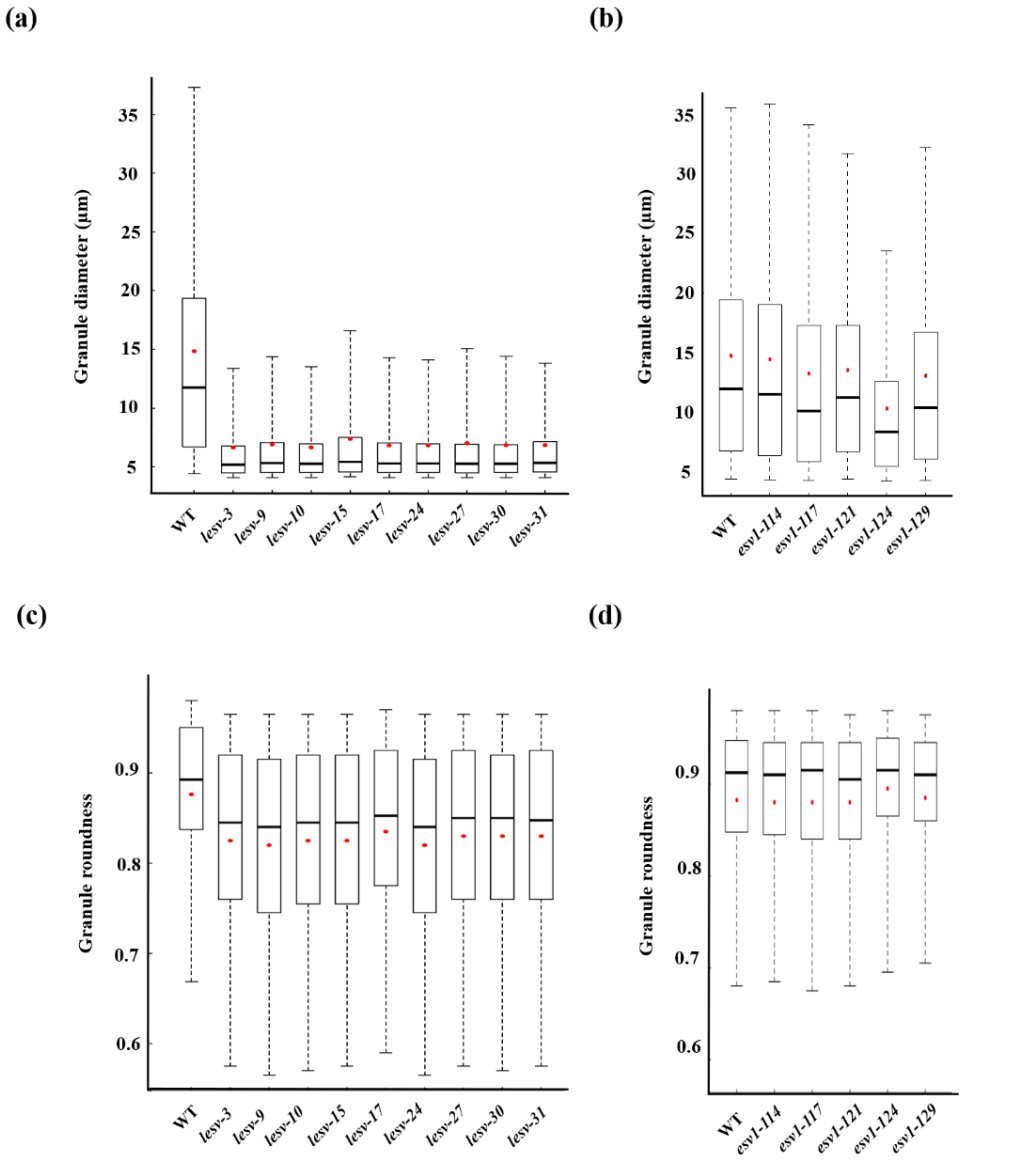

Figure 31: Starch granule granulomorphometry. (a, b) Starch granule diameter. (c, d) Starch granule ellipsoid roundness. For each measurement, the values corresponding to the percentiles P5, P25, P50, P75, and P95 were extracted from the dataset of each experimental replicate. The mean values were then calculated for each percentile across replicates of the same genotype. These averaged percentile values were used to generate the graphs. In the boxplots, the P5 and P95 values represent the extremities of the whiskers, the P25 and P75 values correspond to the bottom and top of the box, and the P50 (median) is shown as a black horizontal line within the box. Red dots represent the mean value for each mutant or wild-type line. For WT, data correspond to the mean of two biological replicates, each with two experimental replicates (n = 4). For mutant lines, data represent the mean of two experimental replicates (n = 2).

To further investigate the size reduction, starch granules - either purified or observed *in situ* - were examined by optical and scanning electron microscopy (Figure 32 and Figure 33). In WT plants, large and regularly shaped granules were predominant. In contrast, *lesv*

mutants displayed a notable accumulation of tiny granules, often coexisting with larger ones within the same cell (Figure 32a).

Microscopy also revealed atypical structures in *lesv* mutants: small granules fused into aggregates, or forming composite structures characterized by deep fissures (Figure 33). Some granules even exhibited flat surfaces with sharp edges, resembling to compound granule. To assess whether these aggregates could be dissociated, purified starch granules were subjected to ultrasonication and SDS washes, followed by observation under Differential Interference Contrast (DIC) microscopy (Figure 32b). Despite these treatments, the aggregates remained intact, suggesting a strong binding between the granules. In contrast, granules from *esv1* mutants remained indistinguishable from wild-type samples in all microscopy observations (Figure 32 and Figure 33).

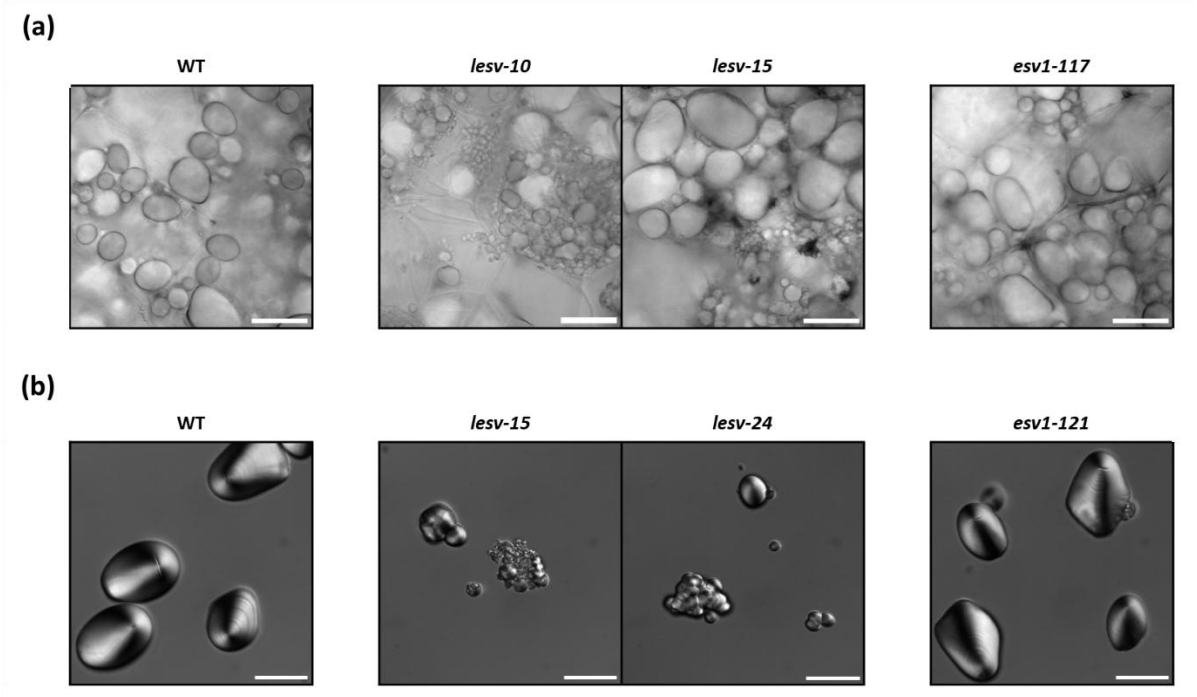

Figure 32: Light microscopy of starch granules. (a) Starch granules observed *in vivo* in a transversal slice of tuber by transmitted light with a confocal microscope. (b) Purified starch granules observed by transmitted light using Differential Interference Contrast microscope. Scale bar in (a) = 50 µm; in (b) = 25 µm.

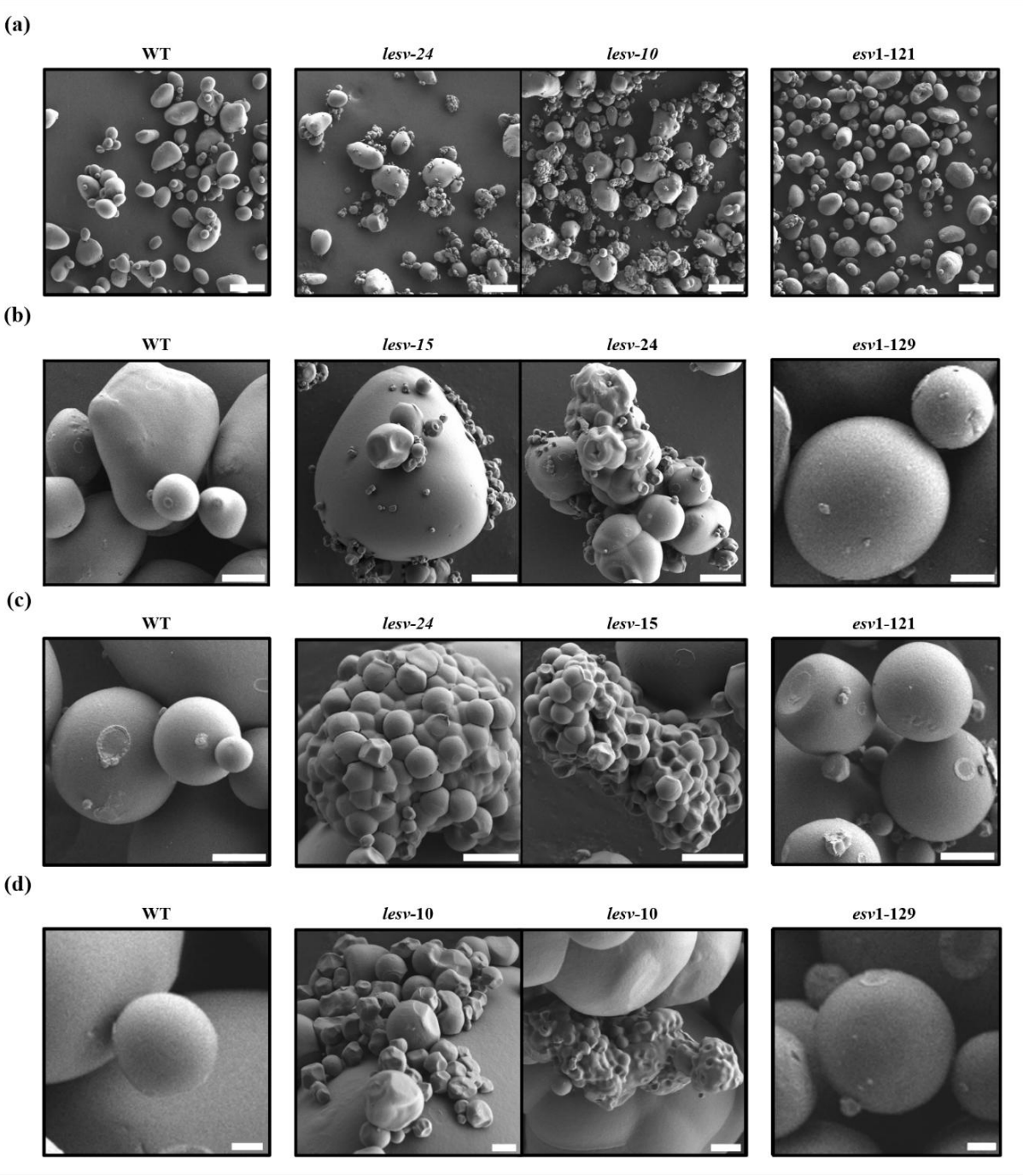

Figure 33: Scanning Electron Microscopy of purified starch granules from wild type (WT), lesv and *esv1* mutants tubers. Starch samples were glued on an aluminum support with carbon double-sided tape and observed at 1 kV accelerating voltage with a Scanning Electron Microscope. Scale bar in (a) = 50 µm; in (b) = 10 µm; in (c) = 5 µm and in (d) = 2 µm.

We next focused on the structural characteristics of the starch granules, which are crucial for understanding the phenotypic changes observed.

3.2. Starch ultrastructure is unaffected in both *lesv* and *esv1* mutants

Starch composition and ultrastructure were investigated through several techniques (Figure 35 and Figure 36).

Crystallinity was determined by wide angle X-ray scattering (WAXS). WAXS experiments were conducted in collaboration with Hyazann Hulin, and obtained during two research stays at the BIA Unit at INRAE, Nantes, where I collaborated with Dr. Denis Lourdin's team. WAXS experiments revealed that all starch samples (both WT and mutants) exhibited the characteristic B-type structure. The degree of crystallinity was unaltered in all the mutants (Figure 35a and Figure 36a).

The lamellar repeat distance (noted as "d") was measured by Small Angle X-ray Scattering (SAXS) (Figure 35b and Figure 36b). SAXS experiments were conducted in collaboration with Gregory Stoclet from UMR 8207 – UMET at the University of Lille. Results showed consistent d-value ranging between 7.2 and 7.4 for all starch samples. Radial orientation of starch glucan was confirmed by polarized light microscopy of starch suspensions (Figure 34). The characteristic Maltese cross pattern was easily observed in WT, *esv1* and the largest granules from *lesv* mutants. However, it was more challenging to detect the Maltese cross in the aggregates of tiny granules in *lesv*, although it remained visible, confirming the preservation of crystalline structure in these granules.

Furthermore, amylose content (Figure 35c and Figure 36c) and the maximum wavelength of starch/iodine complex (Figure 35c and Figure 36c) were not significantly altered in the mutants compared to the WT. Additionally, the amylopectin chain length distribution (CLD) was measured, revealing no significant differences between the mutants and the WT (Figure 35e and f and Figure 36e and f).

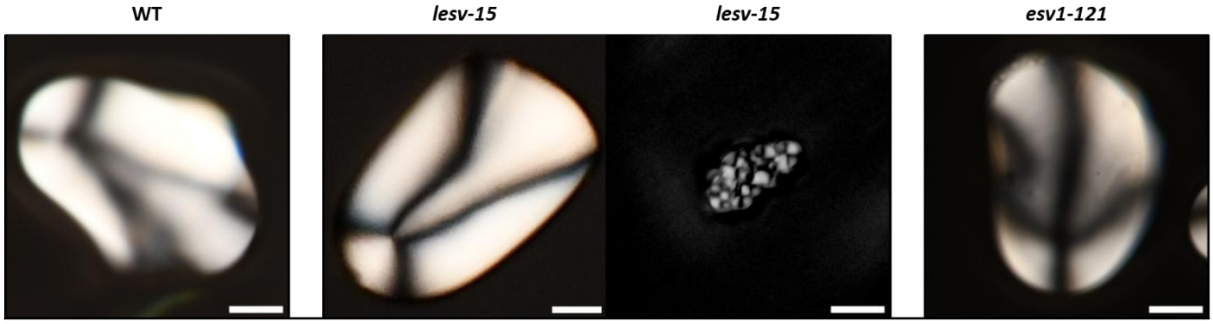

Figure 34 : Purified starch granules observed under polarized light. Scale bar = 10µm.

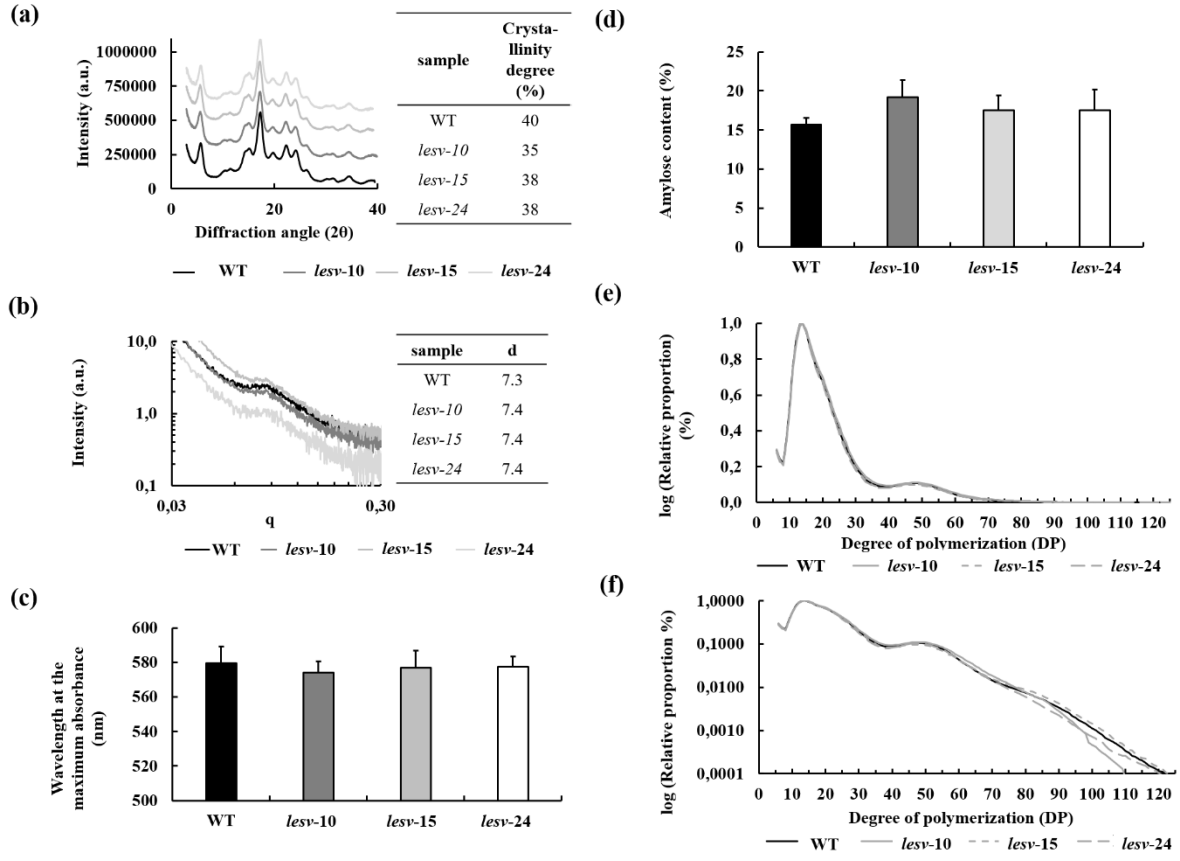

Figure 35: Molecular structure of *lesv* starches. (a) Crystalline-type determined by Wide Angle X-ray Scattering (WAXS). (b) Size of the lamellar repeat distance "d", analyzed by Small Angle X-ray Scattering (SAXS). (c) Wavelength of the maximum absorbance of the iodine-starch complex of wild type (WT) and *lesv*. (d) Amylose content of WT and *lesv.* (e, f) Comparison of the chain length distribution (CLD) profiles of WT and *lesv* starch. Values were normalized according to the highest peak. For (a), (c) and (d), values are mean of three independent cultures. For (e) and (f) values are the mean (+/-SE) of three independent cultures and two experimental replicates. Statistical analysis was made using Mann-Whitney tests, comparing the mutant line to the wild type.

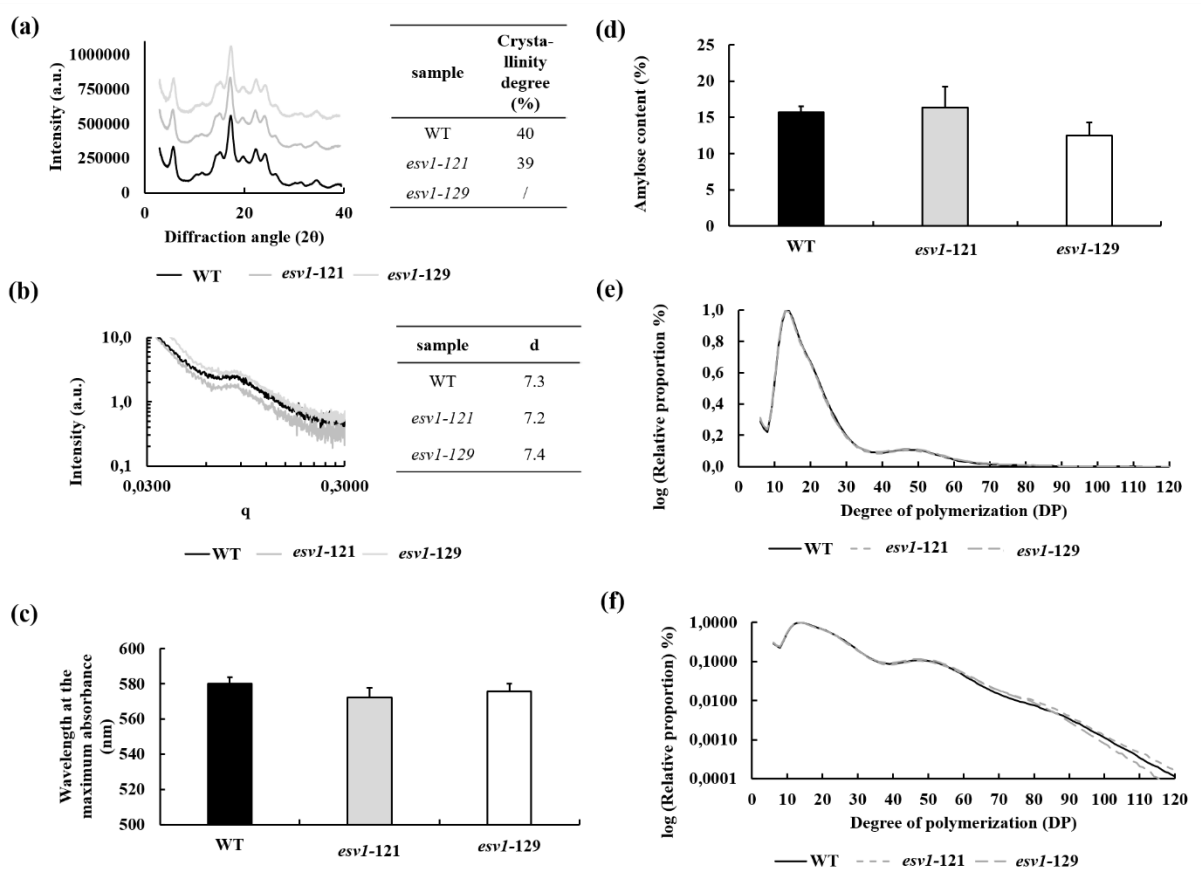

Figure 36: Molecular structure of *esv1* starches. (a) Crystalline-type determined by Wide Angle X-ray Scattering (WAXS). / indicates missing data. (b) Size of the lamellar repeat distance "d", analyzed by Small Angle X-ray Scattering (SAXS). (c) Wavelength of the maximum absorbance of the iodine-starch complex of wild type (WT) and *esv1*. (d) Amylose content of WT and *esv1.* (e, f) Comparison of the chain length distribution (CLD) profiles of WT and *esv1* starch. Values were normalized according to the highest peak. For (a), (c) and (d), values are mean of three independent cultures. For (e) and (f) values are the mean (+/-SE) of three independent cultures and two experimental replicates. Statistical analysis was made using Mann-Whitney tests, comparing the mutant line to the wild type.

3.3. *lesv* and *esv1* mutations affect starch phosphate content

To investigate the impact of *lesv* and *esv1* mutations on starch phosphorylation, the content of covalently bound phosphoesters was quantified using fluorescence-assisted capillary electrophoresis following acid hydrolysis. Phosphorylation of starch occurs on the C6 and C3 positions of certain glucose residues within the glucan chains. A significant increase in total phosphate content was observed in *lesv* mutants, ranging from 19% to 28% compared to wild-type (Figure 37a). This increase was mainly due to higher levels of phosphorylation at the C6 position, while C3 phosphorylation remained unchanged. This finding is consistent with previous observations by Helle et al. (2019), who reported a similar pattern of increased

C6-phosphorylation in starch granules smaller than 10 µm in diameter. As previously shown, *lesv* mutant lines produce smaller starch granules on average, and it has been well established that small starch granules tend to contain more phosphate groups than larger ones. The observed enrichment in C6-phosphorylation in *lesv* mutants is therefore in line with these prior findings. In contrast, *esv1* mutant lines showed a slight but consistent reduction in total phosphate content, by approximately 18% to 20%, even if it was only statistically significant for *esv1*-121 (Figure 37b).

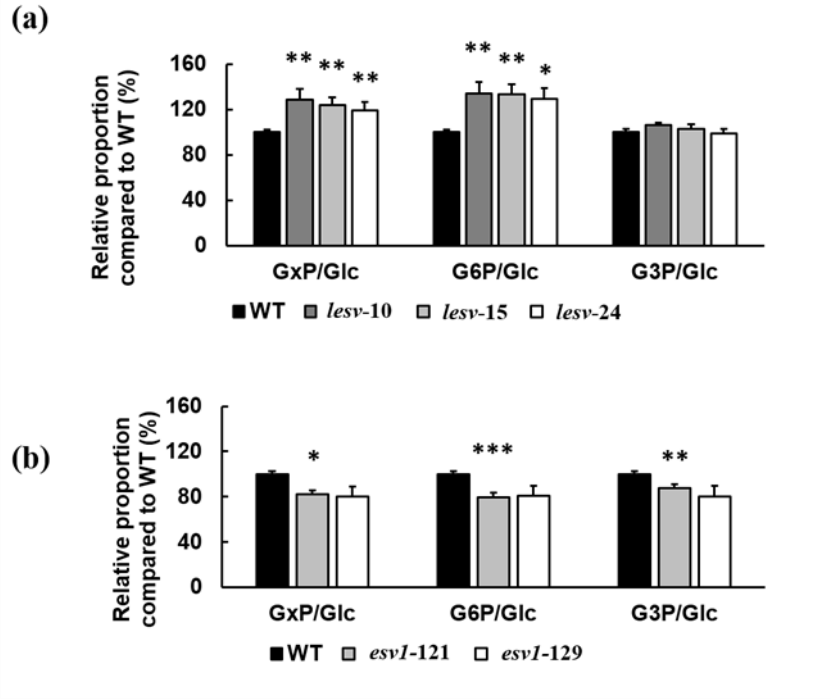

Figure 37: **Assay of phosphoester residues: ratio of total phosphoester residues (GxP) over total glucose residues (GxP/Glc), ratio of O-6-phosphoesters (G6P/Glc) and ratio of O-3-phosphoesters (G3P/Glc) over total glucose residues**. Data for *lesv* (a) and *esv1* (b) mutants were normalized according to the WT ratio (arbitrarily spotted at 100%). For WT, values are mean (+/- SE) of three biological replicates from three independent cultures and two experimental replicates for each culture (n=18). For each mutant lines, values are mean (+/- SE) of three independent cultures and two experimental replicates for each culture (n=6). Statistical analysis was made using Mann-Whitney tests, comparing the mutant line to the wild type (* = $p \leq 0{,}05$; ** = $p \leq 0{,}01$; *** = $p \leq 0{,}005$).

Overall, these morphological and structural analyses provided valuable insights into the starch granules alterations in the mutants. To further investigate these changes, we next focused on the physicochemical properties of starch.

4. Physicochemical properties of starch

The results presented in this section were obtained during two research stays at the BIA Unit at INRAE, Nantes, where I collaborated with Dr. Denis Lourdin's group.

4.1. α-amylolysis of starch granules

The hydrolysis rate of starch was assessed *in vitro* by measuring the production of reducing ends following enzymatic digestion with porcine pancreatic α-amylase (Figure 38). A significantly higher starch degradability was observed in *lesv* mutant lines compared to wild-type (WT) plants: after 48 hours, the average hydrolysis rate of *lesv* starch reached 26%, while WT starch was degraded at a rate of only 17%, corresponding to a 53% increase in starch digestibility. Starch from *esv1* mutants also exhibited enhanced degradability, with hydrolysis rates ranging from 26% to 30% after 48 hours, compared to 21% for the WT, corresponding to a 33% percent increase in starch digestibility. The slight variation in WT values between experiments is likely due to biological variability and differences in experimental conditions, as both assays were conducted independently.

4.2. Pasting properties

Pasting properties of starch were analyzed using a Rapid Visco-Analyzer (RVA) (Figure 39). Due to the large amount of biological material required for each analysis, the experiment could not be repeated, preventing statistical analysis. However, peak viscosity in *lesv* mutants was found to increase by 11% to 34% compared to WT starch, along with a higher pasting temperature. These results suggest that *lesv* mutants exhibit a stronger gelatinization capacity compared to the WT, and that the absence of LESV might contribute to increased thermal stability of starch, requiring a higher temperature for gelatinization. In contrast, *esv1* mutants showed an 11% to 21% decrease in peak viscosity, with no other parameters showing significant changes. This alteration may indicate a reduced gelatinization profile compared to WT.

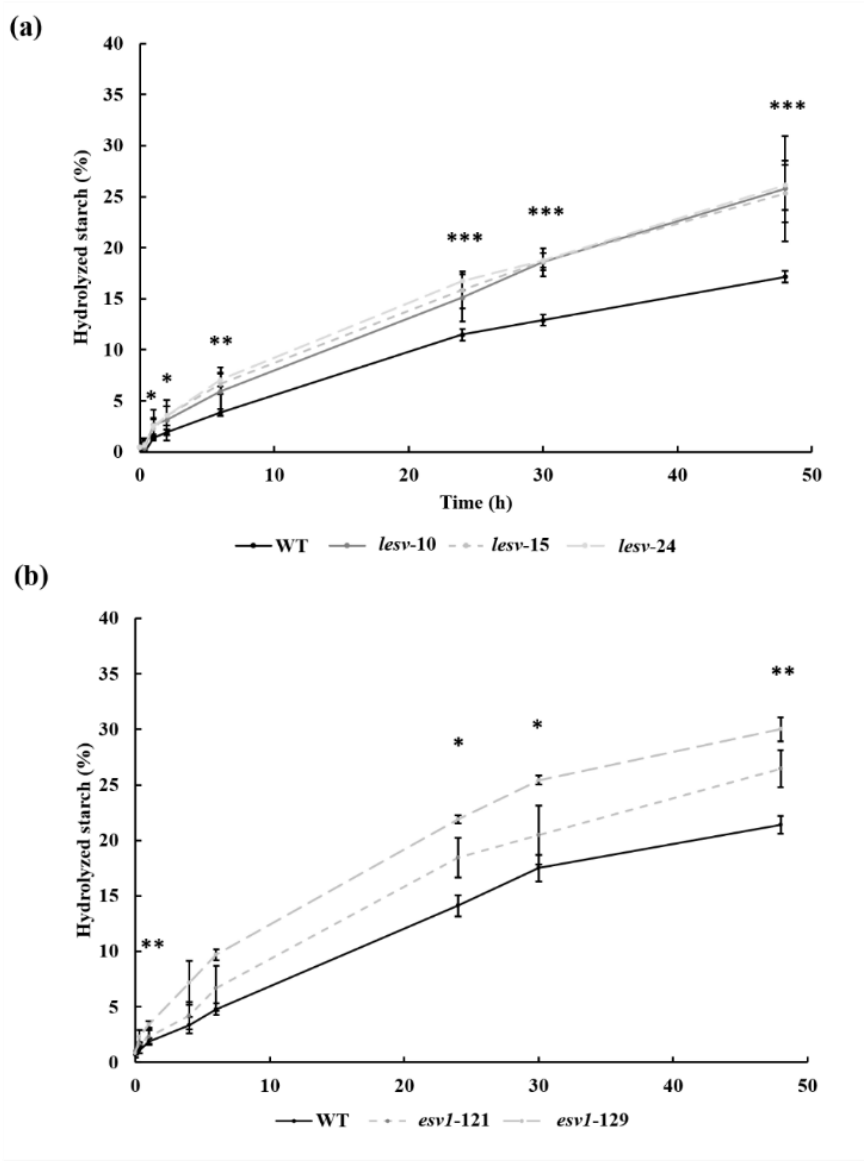

Figure 38 : Enzymatic hydrolysis of starch by porcine pancreatic α-amylase (PPA). A suspension of 128U/mL of PPA was added to ten milligrams of starch and incubated for 48h (x axis) at 37°C. The % of hydrolyzed starch is plotted on the y-axis. For each line, starch was extracted from tubers of three independent cultures, each biological sample being submitted to three independent assays. Values are then mean (SE) of these nine measures. Statistical analysis was made using Mann-Whitney tests, comparing the three mutant lines to the wild type (n=8-9; * = $p \leq 0,05$; ** = $p \leq 0,01$; *** = $p \leq 0,005$).

a)

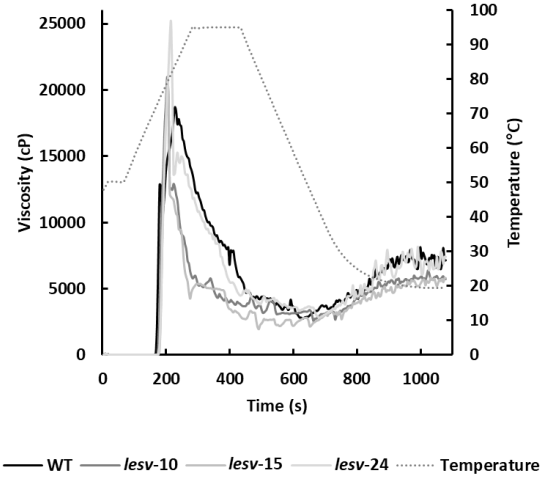

b)

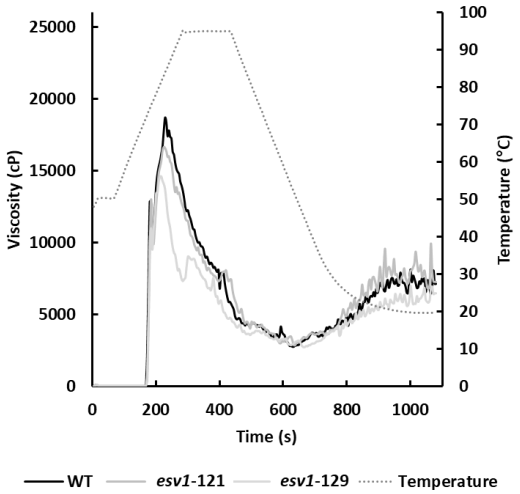

c)

	Peak viscosity (cP)	Viscosity at the beginning of cooling (cP)	Final viscosity (cP)	Peak time (min)	Pasting temperature (°C)
WT	18703	2745	7136	3.8	71.9
lesv-10	21001	2573	5758	3.4	73.5
lesv-15	20752	1972	5825	3.4	73.6
lesv-24	25080	2801	7396	3.6	73.7
esv1-121	16643	2832	7245	3.7	72.8
esv1-129	14600	2715	6465	3.6	71.8

Figure 39 : Pasting properties of starch analyzed using a Rapid Visco-Analyzer (RVA). (a, b) Viscosity profiles over time for *lesv*, and *esv1* mutants respectively. (c) Summary table of pasting parameters. Values correspond to a single measurement.

4.3. Differential Scanning Calorimetry

To complement the analysis performed by the Rapid Visco-Analyzer, Differential Scanning Calorimeter was used. Differential Scanning Calorimetry (DSC) is a technique used to analyze the thermal properties of a sample, such as transition temperatures and enthalpy changes during these transitions. The onset temperature (*To*), peak temperature (*Tp*), conclusion temperature (*Tc*) and transition enthalpy (*ΔH*) of WT and mutant starches were measured (Table 3a). The *lesv*-24 exhibited a lower onset and peak temperature, but a slightly higher enthalpy, suggesting subtle structural changes in starch that allow it gelatinize earlier but require slightly more energy. These differences were not statistically significant because of the variability observed between the biological replicates, but were consistently observed in all the analyses (Table 3b to d). *esv1*-121 showed similar characteristics to WT although it displayed a slightly broader gelatinization range.

Table 3 : Differential Scanning Calorimetry (DSC) transition parameters of starch. To: onset temperature; Tp: peak temperature; Tc: conclusion temperature, R: gelatinization range (Tc – To); ΔH: enthalpy of gelatinization. (a) Mean values (+/- SE) of three independent biological replicates (presented in b, c and d) each with two experimental replicates (n=6). (b, c and d) Individual biological replicates. Values are mean (+/- SE) of two experimental replicates (n=2).

(a)

	To (°C)	**Tp (°C)**	**Tc (°C)**	**R (°C)**	**ΔH (J/g)**
WT	62.38 ± 1.52	66.54 ± 2.16	71.91 ± 2.41	9.53 ± 0.90	14.94 ± 0.66
lesv-24	60.30 ± 1.40	65.05 ± 1.65	71.00 ± 1.94	10.17 ± 0.78	15.68 ± 0.97
esv1-121	61.65 ± 0.73	66.40 ± 2.02	72.23 ± 3.16	10.58 ± 2.44	15.04 ± 0.53

(b)

	To (°C)	**Tp (°C)**	**Tc (°C)**	**R (°C)**	**ΔH (J/g)**
WT	60.92 ± 0.14	64.54 ± 0.18	69.53 ± 0.16	8.61 ± 0.02	15.69 ± 0.01
lesv-24	59.88 ± 0.04	63.74 ± 0.02	69.05 ± 0.24	9.18 ± 0.28	16.43 ± 1.21
esv1-121	60.81 ± 0.02	64.38 ± 0.14	68.87 ± 0.65	8.07 ± 0.63	15.21 ± 0.71

(c)

	To (°C)	**Tp (°C)**	**Tc (°C)**	**R (°C)**	**ΔH (J/g)**
WT	62.00 ± 0.12	65.87 ± 0.08	71.39 ± 0.33	9.40 ± 0.21	14.77 ± 0.24
lesv-24	59.99 ± 0.12	64.25 ± 0.11	70.62 ± 0.23	10.64 ± 0.11	14.82 ± 0.36
esv1-121	61.72 ± 0.04	65.99 ± 0.15	71.95 ± 0.12	10.23 ± 0.08	15.35 ± 0.35

(d)

	To (°C)	**Tp (°C)**	**Tc (°C)**	**R (°C)**	**ΔH (J/g)**
WT	64.24 ± 0.39	69.22 ± 0.17	74.82 ± 0.38	10.59 ± 0.01	14.38 ± 0.59
lesv-24	62.63 ± 0.23	67.16 ± 0.16	73.32 ± 0.3	10.69 ± 0.07	15.80 ± 0.67
esv1-121	62.44 ± 0.01	68.83 ± 0.23	75.89 ± 0.26	13.45 ± 0.28	14.57 ± 0.34

While the physicochemical properties of starch have been characterized, it is important to understand the underlying proteomic changes that may contribute to the observed morphological alterations, particularly in *lesv* mutants. Since many of the proteins involved in starch granule biosynthesis are tightly associated with or trapped within the granules (Helle et al., 2018), analysis of the starch granule proteome can provide some clues on the modifications of protein abundance, complex formation, or granule targeting that may occur in the absence of LESV or ESV1. We therefore shifted our focus to proteomic analyses of the starch granules.

5. Proteomics and protein interactions

5.1. Starch granule proteome

Proteomics analyses were conducted in collaboration with Fabrice Bray from UAR 3290 - MSAP at the University of Lille. The proteomic analysis of starch-bound proteins was carried out following enzymatic digestion using eFASP and peptide analysis by nanoLC-Q Exactive Plus. Protein identification and quantification were performed with MaxQuant software using a custom *Solanum tuberosum* database. The data analysis allowed the identification of a wide range of starch-associated proteins, with overall limited differences in protein abundance between the different genotypes (Figure 40).



Figure 40 : Label free quantification of proteins. Proteins were isolated from starch prior to nanoLC-MS/MS analysis. The amount of each protein was estimated with the use of the MaxQuant software and the Label-Free Quantification (LFQ) intensities were used to compare samples. (a) LFQ score of proteins in WT and lesv mutants. Values are mean (+/-SE) of three experimental replicates (b) LFQ score of proteins in WT and esv1 mutants. Values are mean (+/-SE) of three experimental replicates.

However, specific and significant variations were detected in the abundance of a few key proteins in the starch granule proteome. In *lesv* mutants, as expected, the LESV protein was strongly reduced. The remaining signal, nearly 1000 times lower than in the wild type, may likely correspond to truncated protein fragments, as the detected peptides map upstream of the CRISPR-targeted sequence. This residual presence is therefore not indicative of a functional protein. Western blot analysis further confirmed the complete absence of full-length LESV protein in these lines (Annex 12). Interestingly, *lesv* mutants also exhibited a significant increase in SS5 abundance, which may reflect a compensatory mechanism or an adjustment of starch biosynthesis in response to the loss of LESV.
In *esv1* mutants, the ESV1 protein was also found at lower levels, consistent with its expected absence due to gene inactivation.

These results highlight specific proteomic alterations in the mutants, while the overall starch-associated protein profile remains largely unchanged.

The proteomic analysis revealed a marked and specific increase in SS5 abundance in *lesv* mutants. This observation raises the possibility of compensatory or alternative pathways being activated in response to LESV deficiency. The potential role of SS5 in the *lesv* phenotype will therefore be further examined in Section 6.4.

5.2. Protein-protein interactions studies

The results presented in this section were obtained during and following a research stay at the John Innes Centre, where I collaborated with Dr. David Seung's team.

The alterations observed in *lesv* mutants suggest that LESV plays a key role in starch granule initiation and growth. The phenotype observed in *lesv* mutants closely resembles that of the antisense lines *Stisa1* and *Stisa2*, in which a strong reduction in granule size and the presence of aggregates were also noticed (Bustos et al., 2004). Since the interaction between OsLESV and ISA1 has been demonstrated in rice (Yan et al., 2024), we hypothesized that these proteins might also interact in potato.

5.2.1. Untargeted approach: immunoprecipitation from tubers and mass spectrometry

An exploratory approach was used to identify potential LESV interactors without prior assumptions. Soluble proteins were extracted from wild-type and *lesv* mutant potato tubers, with the latter serving as a negative control. Immunoprecipitation was performed using protein A microbeads coupled with anti-LESV serum to retain LESV and its associated proteins. After elution, the samples were digested and analyzed by nano-LC-MS/MS.

Three experimental conditions were applied:

(A) Immunoprecipitation of proteins extracted from wild-type tubers. The objective here was to specifically retain LESV and identify co-precipitated proteins.

(B) Immunoprecipitation of proteins extracted from *lesv* mutant tubers (negative control). This control was used to ensure the specificity of the antibody for LESV. In the absence of

LESV protein in the *lesv* mutant, no proteins should be immunoprecipitated, confirming that the antibody does not cross-react with other proteins.

(C) Precipitation of proteins extracted from wild-type tubers without antibody (control for non-specific precipitation). This condition was used to assess background precipitation.

Nano-LC-MS/MS analysis confirmed the success of the immunoprecipitation based on spectral abundance ratios. Specifically, the A/C ratio for the anti-LESV antibody was 920, indicating that the antibody was found at 920 times higher abundance in sample A (immunoprecipitation from WT extract using anti-LESV) compared to sample C (same extract incubated with beads only, without antibody). This high ratio confirms that the antibody was effectively retained in condition A and not nonspecifically present in condition C.

The A/B ratio for the antibody was 1.5, indicating a similar level of antibody detection in samples A (WT) and B (*lesv* mutant). This is expected, as the antibody was added in equal amounts in both conditions. Therefore, this ratio confirms that the signal corresponds to the antibody itself and not to proteins differentially present in the extracts.

In contrast, LESV detection itself remained very low across all samples. The A/B ratio for LESV was only 2.9, indicating only a weak enrichment in WT compared to *lesv*, and the A/C ratio was 0.9 suggesting no clear enrichment compared to the beads-only control. These values suggest that LESV was not efficiently retained in condition A.

This contrasts with previous Western blot analyses, which successfully detected LESV in WT starch granules but not in *lesv* mutants (Annex 12), further supporting the specificity of the antibody. Given these findings, we questioned whether LESV might be present in the soluble phase, even prior to immunoprecipitation. To address this, proteins were separately extracted from the soluble and insoluble (starch-containing) fractions of wild-type tubers by heating at 180°C for 15 minutes. The resulting fractions were analyzed by SDS-PAGE followed by immunoblotting using the same anti-LESV antibody.

LESV was detected exclusively in the insoluble phase (Figure 41). In the soluble fraction, a strong band around 48 kDa was observed. Initially, we considered the possibility that this band might correspond to ESV1, a protein with high sequence similarity to LESV. However, ESV1 was not identified in any of the three conditions analyzed by mass spectrometry, and it is known to be localized in the starch granule (Helle et al., 2018), yet it

was not detected in the insoluble fraction of the Western blot. These observations strongly suggest that the 48 kDa band is unlikely to be ESV1. Regarding the protein detected at this molecular weight in the MS results, we could not confidently determine its identity.

These results confirmed that LESV is absent from the soluble phase of potato tubers. The immunoprecipitation approach requires non-denatured proteins to preserve protein-protein interactions. However, extracting and analyzing proteins from starch granules requires a 10-minute treatment at 100°C in an SDS/β-mercaptoethanol solution, which denatures proteins and prevents the detection of interactions. Consequently, this method cannot be used to identify LESV interactors.

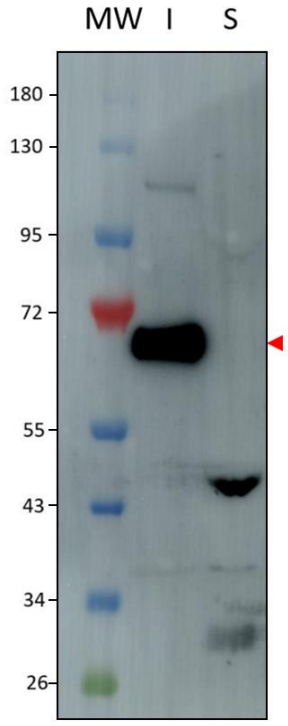

Figure 41 : Immunoblot analysis of LESV protein in the soluble and insoluble fractions of potato tubers. Proteins were extracted separately from the soluble phase (S) and the insoluble phase (I) of wild-type tubers and the resulting fractions were analyzed by SDS-PAGE followed by immunoblotting. LESV protein was detected using a polyclonal serum raised against *Arabidopsis* LESV (rabbit, 1:100). Detection was performed via chemiluminescence using a horseradish peroxidase (HRP)-conjugated anti-rabbit secondary antibody. LESV protein (63 kDa) was designated by the red arrow. The first lane corresponds to the molecular weight standard (in kDa).

In contrast to the previous untargeted proteomics approach, we next implemented two targeted strategies to specifically test a potential interaction between LESV and ISA1.

5.2.2. Transient expression of LESV and ISA1 proteins for pairwise immunoprecipitation

The first strategy involved transient co-expression of LESV and ISA1 in *Nicotiana benthamiana* leaves via agroinfiltration, followed by immunoprecipitation. LESV was fused to either a YFP or HA tag at its C-terminus, while ISA1 was tagged with HA or YFP, respectively, for reciprocal co-immunoprecipitation experiments. After protein extraction from infiltrated leaves, immunoprecipitation was performed using beads coupled with anti-YFP or anti-HA antibodies, and detection was carried out by Western blot using anti-tag antibodies.

Unfortunately, we were unable to achieve co-expression of both proteins simultaneously (Figure 42). When LESV-YFP was used as the bait protein and ISA-HA as the prey, a single band was detected in both the input and anti-YFP immunoprecipitation (IP) fractions (Figure 42a). However, the expected molecular weight of LESV-YFP is approximately 92 kDa, while the observed band migrated higher in the gel, suggesting it may not correspond to LESV-YFP, despite being precipitated in the anti-YFP IP. Moreover, no ISA1-HA signal was observed in either fraction, indicating a failure to express the prey protein.

A similar pattern was observed in the reverse configuration, where LESV-HA was used as bait and ISA-YFP as prey (Figure 42b). LESV-HA was not detected in the anti-HA IP fractions, suggesting that immunoprecipitation was unsuccessful. ISA1-YFP again failed to express in the leaf tissue.

Given these expression issues in *Nicotiana benthamiana*, we turned to an alternative approach, yeast two-hybrid (Y2H), to further explore the potential interaction between LESV and ISA1.

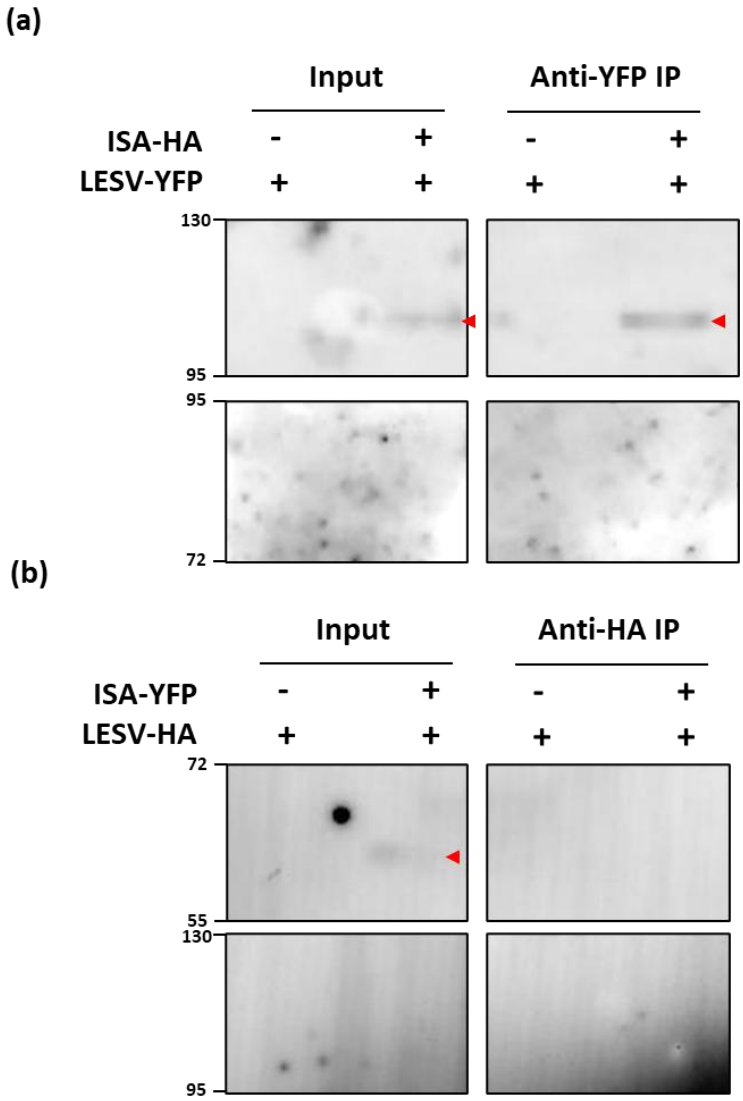

Figure 42 : Immunoprecipitation assay of LESV and ISA1 expressed in *Nicotiana benthamiana* leaves. (a) Pairwise immunoprecipitations using LESV-YFP as bait protein, against ISA1-HA prey protein. Immunoprecipitations were conducted with anti-YFP beads. The presence of the bait and prey proteins in the input and immunoprecipitates were detected using immunoblots with HA (top) and YFP (down) antibodies. Visible bands are designated by the red arrows. (b) Pairwise immunoprecipitations using LESV-HA as bait protein, against ISA1-YFP prey protein. Immunoprecipitations were conducted with anti-HA beads. The presence of the bait and prey proteins in the Input and immunoprecipitates were detected using immunoblots with YFP (top) and HA (down) antibodies. A visible band is designated by the red arrow.

5.2.3. Yeast two hybrid assay

Yeast two-hybrid assay (Y2H) was used as a second strategy to test for a potential interaction between LESV and ISA1. The principle of the yeast two-hybrid assay is explained in Figure 43. The full-length coding sequences of LESV and ISA1 were cloned into pGADT7 (activation domain, AD) or pGBKT7 (DNA-binding domain, BD) vectors (Annex 5 and Annex 6). These constructs were transformed in pairs into the AH109 yeast strain.

To ensure rigorous validation, multiple combinations and appropriate controls were tested:

- Empty vector controls: pGADT7 + pGBKT7 (no interaction expected)
- Single construct controls: pGADT7-ISA1 + empty pGBKT7 and pGADT7 + pGBKT7-LESV (to test for autoactivation)
- Test combinations:
    - pGADT7-LESV + pGBKT7-ISA1
    - pGADT7-ISA1 + pGBKT7-LESV
    - pGADT7-LESV + pGBKT7-LESV
    - pGADT7-ISA1 + pGBKT7-ISA1

Yeast cells were first selected on Double Dropout (DDO: -Leu -Trp) medium to confirm the presence of both plasmids (Figure 43b). Protein-protein interactions were then assessed on Quadruple Dropout (QDO: -Leu -Trp -His -Ade) medium. In this system, an interaction between the two proteins of interest brings together the GAL4 activation and binding domains, thereby activating reporter genes that allow yeast growth on QDO medium (Figure 43c). Typically, growth appears after 4 to 5 days if a true interaction occurs.

When ISA1 was cloned in pGADT7 (AD) and LESV in pGBKT7 (BD), we observed robust yeast growth on QDO medium after only two days, not only in the test condition (pGAD7-ISA1/pGBKT7-LESV) but also in the negative control (empty pGADT7/pGBKT7-LESV). This premature and non-specific growth suggests that LESV exhibits autoactivation when fused to the DNA-binding domain in pGBKT7 (Figure 44 and Annex 13). In other words, LESV alone, without a partner fused to the activation domain, is able to activate reporter gene expression, as explained in Figure 43c. This likely reflects a structural feature of LESV allowing it to function as a transcriptional activator when bound to DNA. As a result, any combination

involving pGBKT7-LESV cannot be reliably interpreted, including pAD-ISA1/pDB-LESV and pAD-LESV/pDB-LESV.

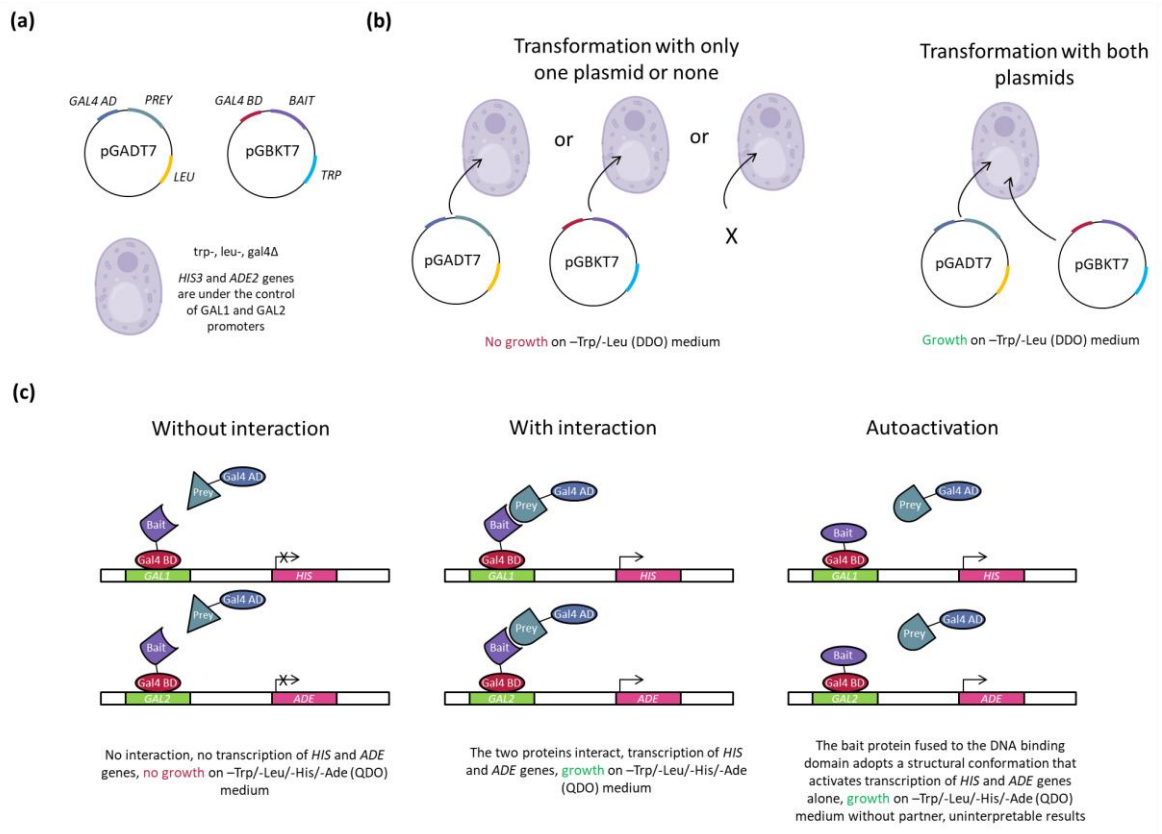

Figure 43 : Principle of the yeast two-hybrid assay. (a) Plasmid constructs and genotype of AH109 yeast strain. Genes encoding proteins of interest (bait and prey) are cloned into pGBKT7 (carrying the *TRP1* selection marker and expressing the bait protein fused to the GAL4 DNA-binding domain, GAL4-BD) and pGADT7 (carrying the *LEU2* marker and expressing the prey protein fused to the GAL4 activation domain, GAL4-AD), respectively. The AH109 strain (MATa, trp1-901, leu2-3,112, ura3-52, his3-200, gal4Δ, gal80Δ, LYS2::GAL1UAS-GAL1TATA-HIS3, MEL1::GAL2UAS-GAL2TATA-ADE2, URA3::MEL1UAS-MEL1TATA-lacZ) carries deletions in several auxotrophic markers and reporter genes (*HIS3*, *ADE2*) under the control of GAL1 or GAL2 promoters, which are only activated when GAL4-AD and GAL4-BD are brought into proximity by protein-protein interaction. (b) Selection on -Leu/-Trp (DDO) medium. Only yeast that have successfully taken up both plasmids can grow on this medium, confirming co-transformation. These yeasts are used for further selection on QDO medium. (c) Selection on -Leu/-Trp/-His/-Ade (QDO) medium. When the two proteins interact, GAL4-AD and GAL4-BD are brought together, activating the transcription of *HIS3* and *ADE2* through GAL1 and GAL2 promoters, allowing yeast growth. In absence of interaction, these genes are not expressed and yeasts fail to grow. In some cases, the bait protein can autonomously activate transcription without a prey partner (autoactivation), which leads to yeast growth even without interaction and renders such combinations uninterpretable. TRP, LEU, HIS, ADE: selection or reporter genes. GAL1, GAL2: inducible promoters. GAL4-BD: DNA-binding domain. GAL4-AD: transcription activation domain.

In contrast, when LESV was cloned in pGADT7 (AD) and ISA1 in pGBKT7 (BD), a clear and specific growth on QDO medium was observed after 4–5 days, in two independent

replicates (Figure 44 and Annex 13). In this configuration, no growth was observed in the corresponding negative controls, confirming the absence of autoactivation in either construct. These results demonstrate a physical interaction between LESV and ISA1.

Additionally, yeast growth on QDO medium confirmed a physical interaction between ISA1 and itself, indicating that ISA1 can form homodimers.

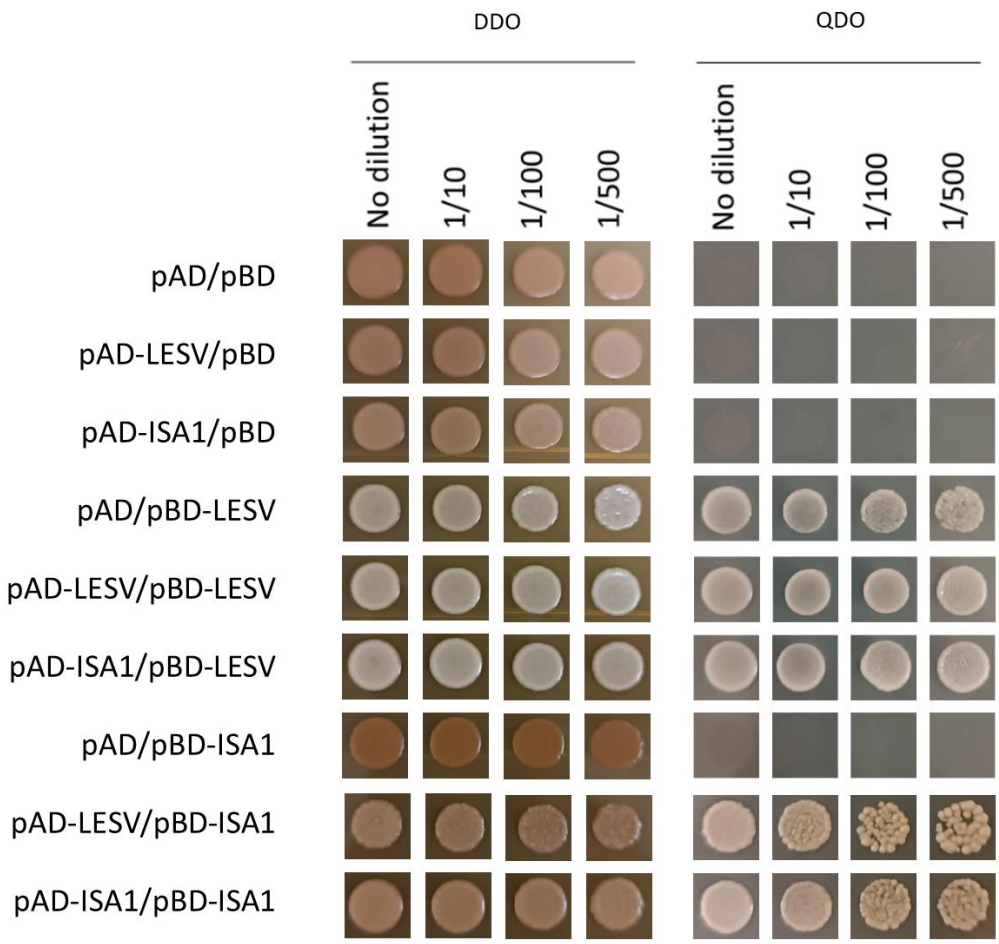

Figure 44 : Yeast two hybrid assay showing LESV and ISA1 physical interaction. Picture was taken after 5 days of growth. AD: activation domain (contained in pGADT7 vector); BD: DNA-binding domain (contained in pGBKT7 vector); DDO (Double Dropout Medium): control medium (SD/-Trp-Leu); QDO (Quadruple Dropout Medium): selective medium (SD/-Trp-Leu-His-Ade).

Having identified key proteomic features and protein-protein interactions in the starch granules, we next explored complementary analyses to gain further insights into the phenotype of the *lesv* mutants, particularly their granule behavior in different tissues and developmental stages.

6. Complementary analyses to further explore the *lesv* and *esv1* phenotype

6.1. Granule size-based separation and fraction characterization

We investigated whether the increased phosphoester content observed in *lesv* mutants was a direct consequence of LESV absence or a secondary effect associated with the reduced granule diameter. Indeed, previous studies have shown that small potato starch granules exhibit higher phosphoester content (Helle et al., 2019). Additionally, structural differences in small granules could be masked by the presence of larger granules. Indeed, while small granules (<11 µm) account for 86–90% of the total granule number in *lesv* mutants, they represent only 16–25% of the total starch granule volume (Table 4).

Table 4 : Proportion of small granules (SG) (<11 µm) in total starch granules volume and number.

	Proportion of SG in total starch granules volume (%)	Proportion of SG in total starch granules number (%)
WT	**6,5**	**7,8**
***lesv*-10**	**25.2**	**90.9**
lesv-15	**16.2**	**86.2**

To further investigate this question, starch from wild-type and *lesv* mutants was fractionated based on granule size, using a nylon mesh with 11 µm pore width. Granules larger than 11 µm were designated as “large granules” (LG), while those smaller than 11 µm were classified as “small granules” (SG).

Granule diameter of each fraction was measured using a Flow-Cell FC200S+ granulomorphometer. A filter was applied to exclude particles smaller than 4 µm

(corresponding to the limit of the camera resolution) and those with a roundness below 0.5 (likely cellular debris). The ISO area diameter parameter was used as the standard parameter. Before fractionation (NF), the mean diameter of *lesv* granules was approximatively three times smaller than in WT (Figure 45). Within LG fraction, the mean diameter appears to be slightly higher in WT than *lesv*-10 and *lesv*-15. Likewise, the mean diameter of the WT-SG fraction is almost twice as high as those in *lesv* mutants. These results suggest a different size distribution between WT and *lesv*, although the filter most likely leads to underestimation of SGs.

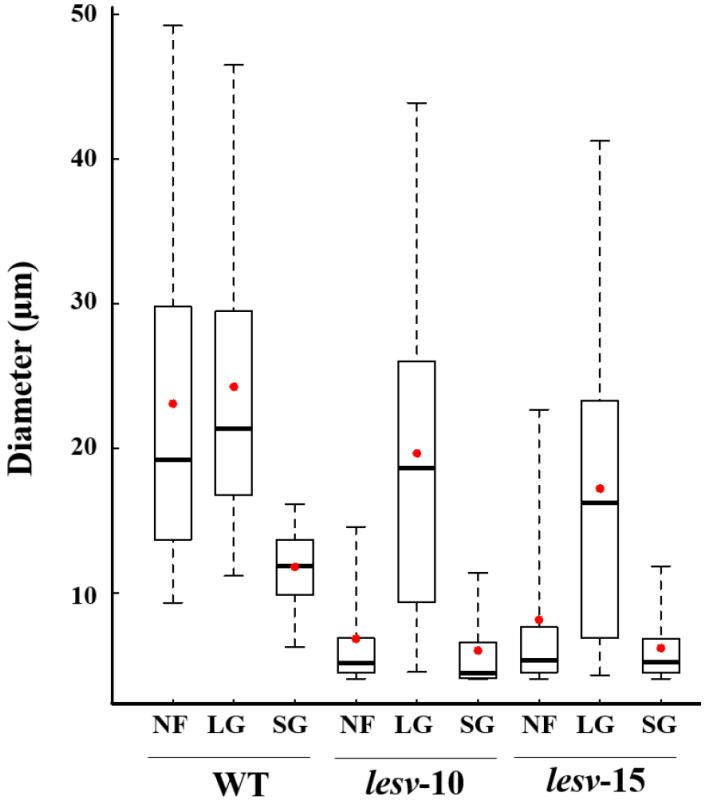

Figure 45 : Granulomorphometry of fractionated starch based on granule size. Red dots represent the mean diameter values for each fraction. NF : not fractionated; LG : large granules (> 11 µm); SG : small granules (< 11 µm). Each line corresponds to a single experimental replicate of starch extracted from tubers of a single culture (n=1). A minimum of 3,000 granules was analyzed for each sample.

Phosphorylated glucose residues were then quantified in each fraction. In unfractionated samples, *lesv* mutants showed a 30% increase in the ratio of phosphoester residues over total glucose residues ratio (GxP/Glc) (Figure 46a). This difference became more

pronounced in the SG fractions, reaching nearly 70%, while it was only around 20% in LG fractions. Since these increases are not uniform across equivalent size fractions, this suggests that the elevated phosphoester content in *lesv* mutants primarily results from reduced granule size, rather than a direct effect of the LESV mutation itself. This interpretation is consistent with previous work by Helle et al. (2019), who reported a higher frequency of phosphate groups in smaller starch granules.

To further investigate this phenomenon, we performed a more detailed analysis, to discriminate between the two main types of phosphoesters in starch: glucose-6-phosphate - G6P) and glucose-3-phosphate (G3P). The results showed that the increase in total phosphoester content observed in *lesv* mutants was predominantly due to a rise in G6P residues (Figure 46b), rather than in G3P levels (Figure 46c). This differential enrichment was particularly evident in the SG fractions, where the G6P content was markedly higher than in the corresponding wild-type granules. These findings are supported by the work of Helle et al. (2019), who also reported a significant increase in G6P levels in smaller granules.

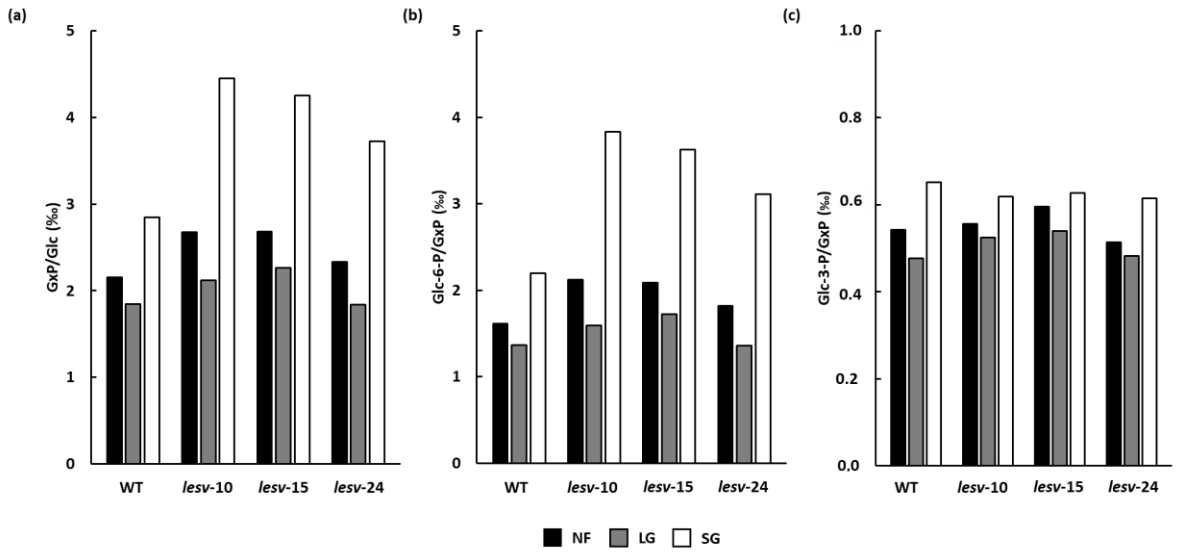

Figure 46 : Starch phosphorylation profile in size-fractionated granules from *lesv* mutants. Relative content of covalently bound phosphate esters in starch, expressed as the ratio of (a) total phosphoester residues (GxP), (b) C6-bound phosphate esters (G6P), and (c) C3-bound phosphate esters (G3P), over total glucose residues (Glc) in each size fraction. Starch was analyzed either without fractionation (NF) or after separation into larges granules (LG; > 11 µm) and small granules (SG; < 11 µm). Data correspond to a single biological replicate, with one technical replicate per fraction (n=1).

6.2. Granule morphological evolution along tuber development

As the evolution of starch granule morphology has never been studied along tuber development, we investigated whether the starch granule aggregates present in mature tubers of *lesv* mutant plants and observed by SEM (Figure 33) originated from anarchic initiation events during the early stage of tuber development or were the results of late (and partially aborted) fusions between pre-existing granules. Indeed, one hypothesis is that, in tuber, large starch granules form via the coalescence of smaller ones, as shown in *Arabidopsis thaliana* (Bürgy et al., 2021). This process could be disrupted in *lesv,* giving rise to aggregates of partially fused granules. Alternatively, the small granules observed in *lesv* mutants could arise from partial degradation of large granules.

To test these hypotheses, we monitored the granule morphology of starch granules at different stages of tuber development in WT and *lesv-10* plants. Seven plants of each genotype were grown in a growth chamber and tubers were harvested weekly starting from week 6 (Figure 47). Tubers from one wild-type and one mutant plant were harvested weekly (from week 6 to 11), and starch was extracted from granulomorphometer analysis and microscopic observation.

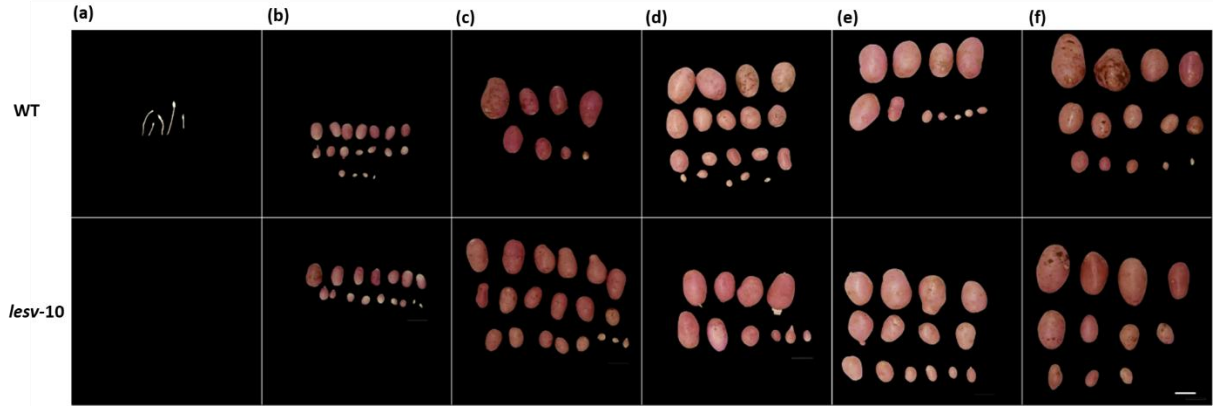

Figure 47 : Tubers harvested at different stage of WT and *lesv-10* plants development. Tubers of (a) 6 weeks, (b) 7 weeks, (c) 8 weeks, (d) 9 weeks, (e) 10 weeks and (f) 11 weeks. Scale bar = 2 cm. The background was removed on the tubers pictures using the image editing tool removebg (https://www.remove.bg/).

Granule diameter was determined using a Flow-Cell FC200S+ granulomorphometer (Occhio). In WT, granule diameter increased over time. In contrast, granule size in *lesv* mutants remained nearly constant or even slightly decreased during tuber growth (Figure 48).

Therefore, the size difference between WT and *lesv* granules became increasingly pronounced as the plants grew. These results suggest that the granule morphology between WT and *lesv* plants is already different in the early stages of tuber development. The hypothesis that the aggregated small granules in *lesv* result from the degradation of larger granules over the plant development can therefore be rejected.

However, light microscopy of purified granules revealed no aggregates in WT tubers, whereas such aggregates were already visible in *lesv* mutants from the 7th week (Figure 49). Therefore, although we cannot confirm that aggregation of small granules is a normal stage of granule initiation, this hypothesis cannot be completely excluded either.

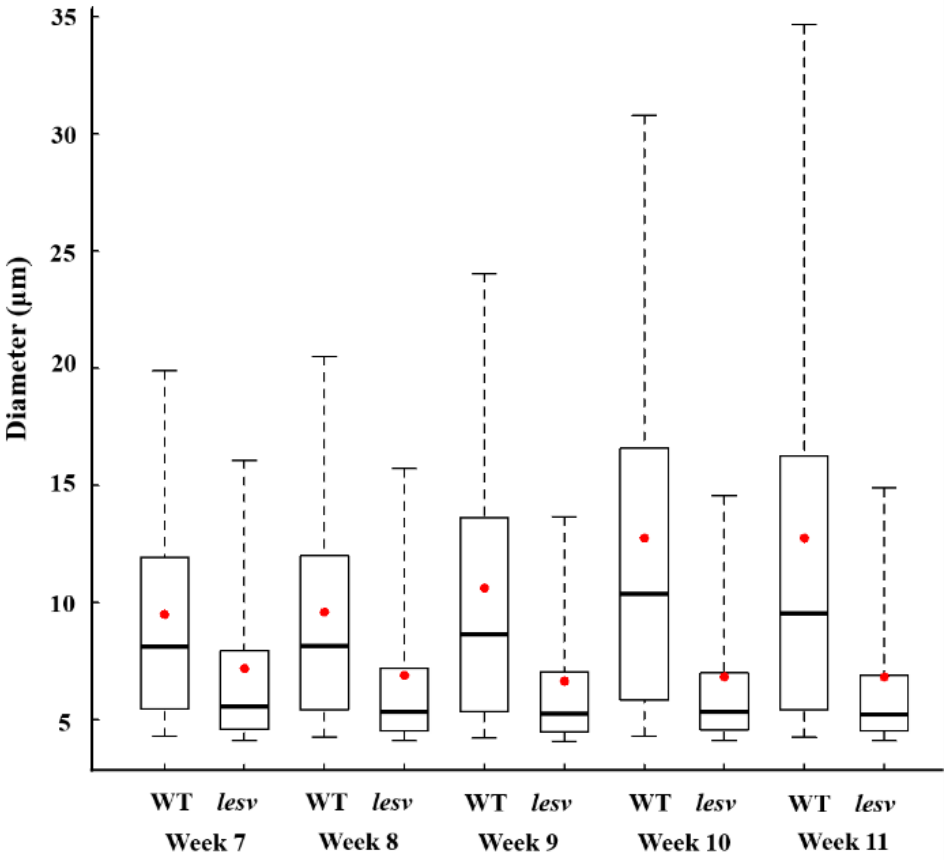

Figure 48 : Boxplot of starch granule granulometry along tuber growth. The red dots represent the mean diameter values for each plant. WT : wild type plant, *lesv*: *lesv*-10 mutant plant, Week X: Age of the plant at tubers harvest. For each sample, n=1.

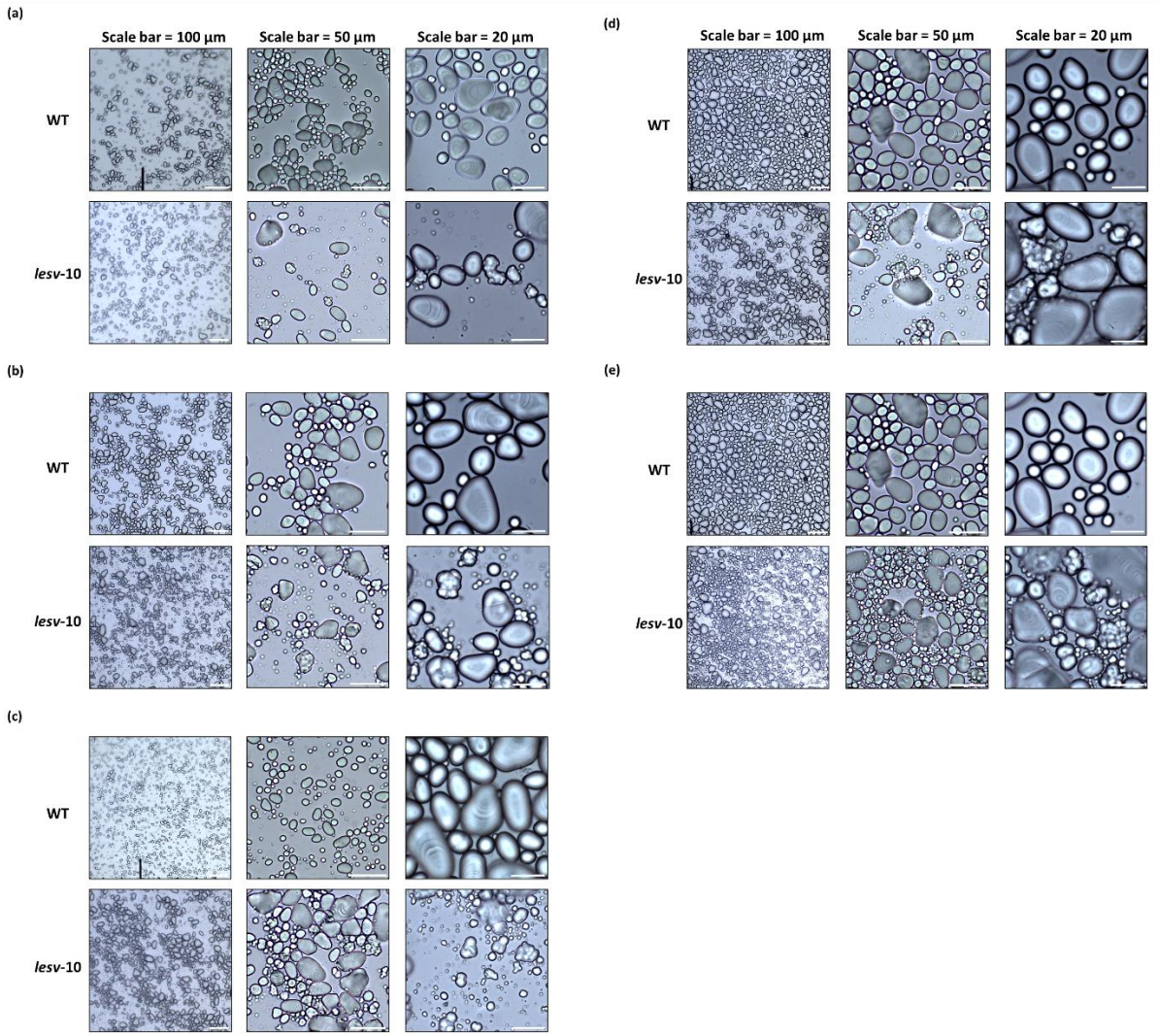

Figure 49 : Light microscopy images of purified starch granules extracted from tubers harvested after (a) seven, (b) eight, (c) nine, (d) ten, (e) eleven weeks of culture.

6.3. Starch granules in *lesv* and *esv1* leaves

After analyzing the phenotype of tubers and storage starch, we turned our attention to leaves and their transitory starch in order to determine whether *LESV* and *ESV1* play a similar role in different plant organs. This also provided an opportunity to investigate whether the functions previously described for these proteins in *Arabidopsis thaliana* leaves, where they are involved in the regulation of transitory starch metabolism, are conserved in potato, a species in which both transient and storage starch are synthesized in distinct plastids. By comparing the effects of *LESV* and *ESV1* in these two contexts, we aimed to gain further

insight into the organ-specific functions and potential divergence of these proteins across species.

Transitory starch granules were observed *in vivo* within the plastids of leaves harvested at the end of the day using confocal microscopy. Initial observations revealed a reduction in the number of granules per plastid in *lesv* (Figure 50). On average, 3 to 5 granules per chloroplast were observed in WT, while approximatively 1 to 2 granules were noted in *lesv* mutants. Moreover, the granules in *lesv* appeared larger.

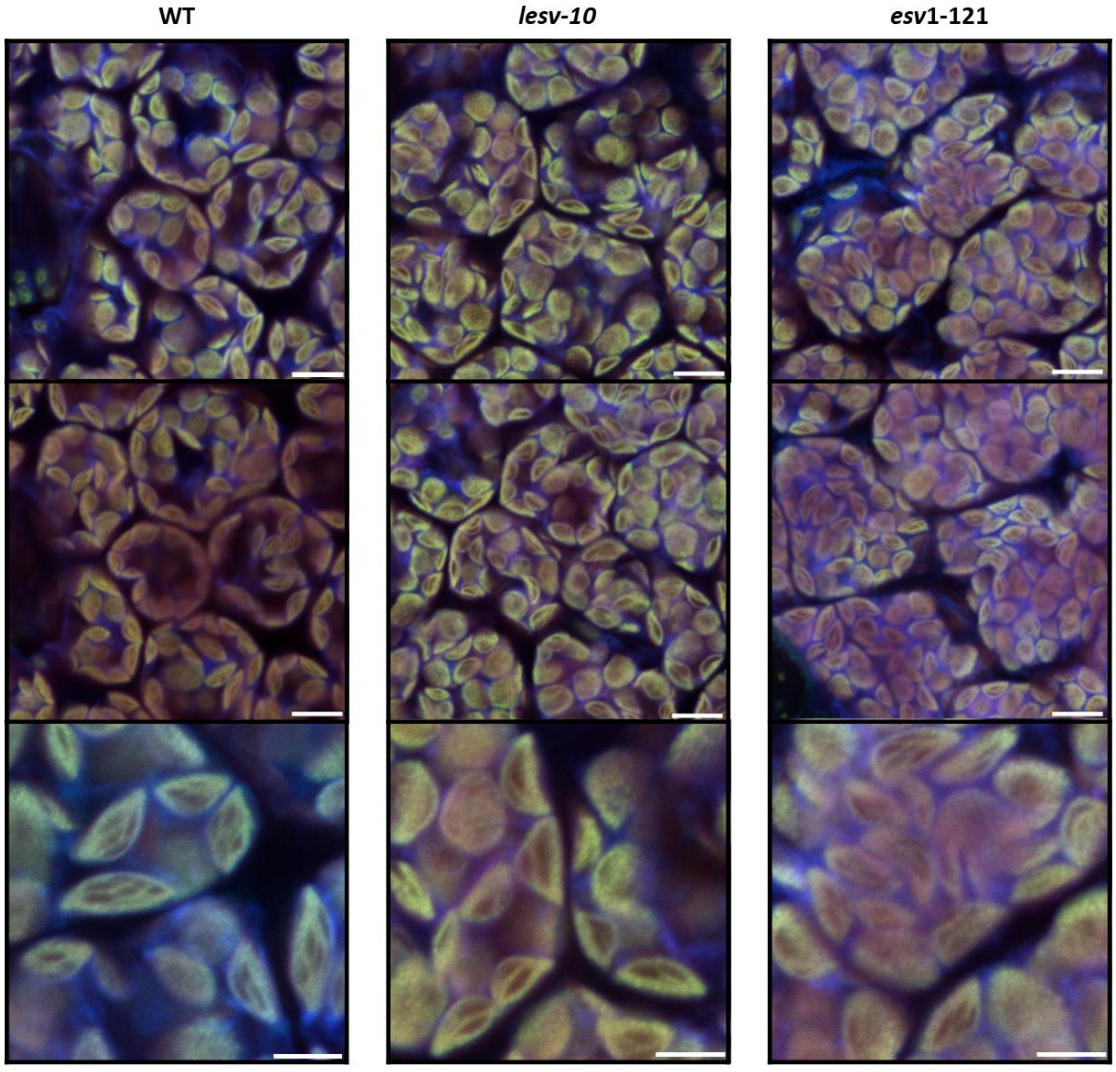

Figure 50 : Confocal microscopy images of leaf starch in wild-type (WT) and mutant plants. Leaves were collected at the end of the day from one-month-old soil-grown plants, and fixed sections were imaged using a Zeiss LSM 780 laser scanning confocal microscope. Cells appear in blue, chloroplasts in yellow, and starch granules in black. Enlarged views of selected regions are shown in the bottom row to highlight starch granules. Scale bars = 10 µm (upper and middle panels) and 5 µm (lower panel with zoomed-in images). These observations are preliminary data; further analyses and statistical evaluation will be required.

To further investigate granule morphology, purified starch granules were observed using scanning electron microscopy (Figure 51). Although some impurities were present in the samples, likely due to the starch extraction method, the morphology of starch granules from *lesv, esv1* and wild-type plants appeared very similar.

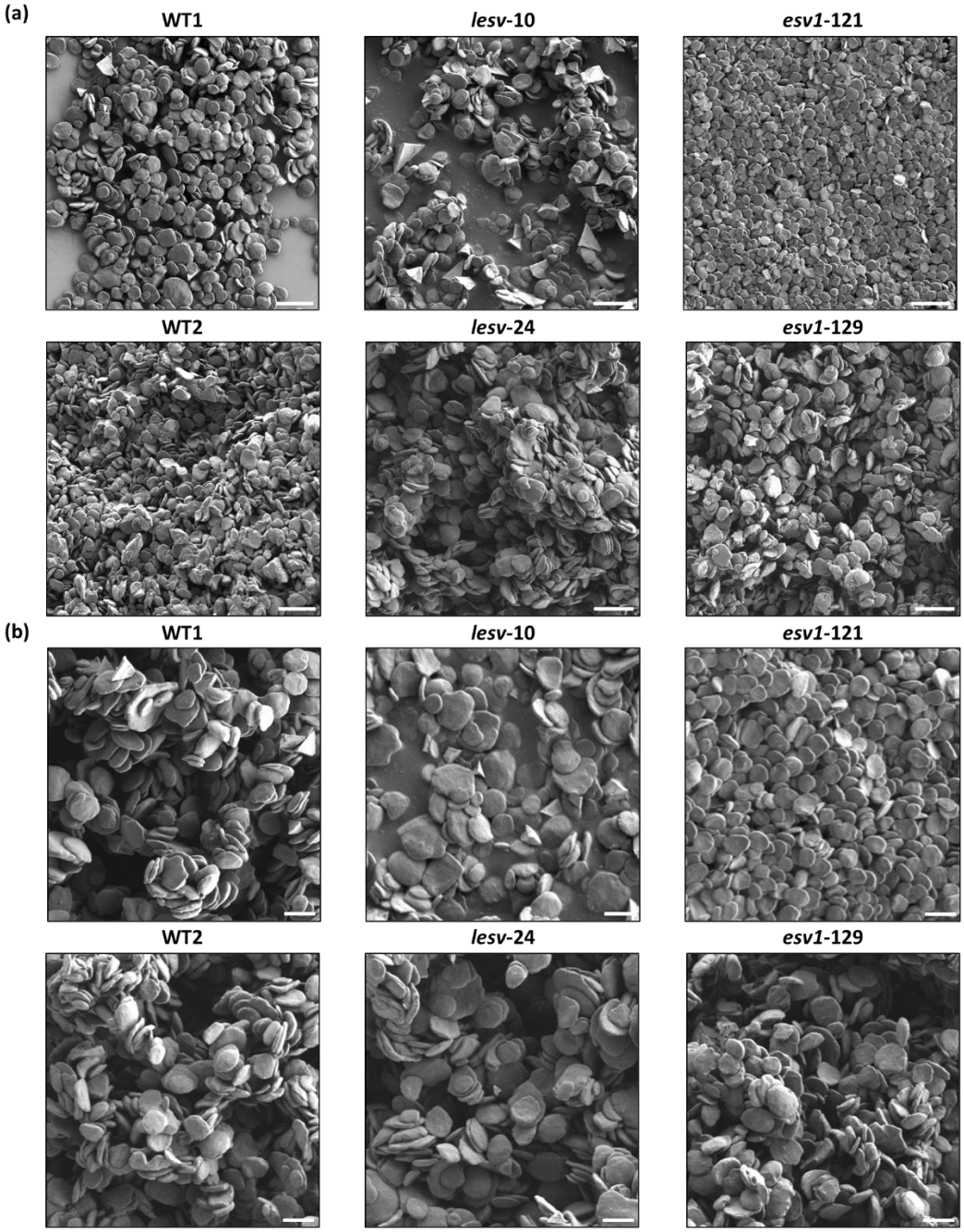

Figure 51 : Scanning Electron Microscopy of purified starch granules from wild type (WT), lesv and *esv1* mutants leaves. Starch samples were glued on an aluminum support with carbon double-sided tape and observed at 1 kV accelerating voltage with a Scanning Electron Microscope. Scale bar in (a) = 10 µm, in (b) = 5 µm. These observations are preliminary data; further analyses and statistical evaluation will be required.

These preliminary observations require further confirmation through quantitative analysis to determine whether the differences in granule number and morphology are statistically significant. Nevertheless, the starch phenotype observed in leaves appears markedly different from that in tubers, suggesting that the protein may play distinct roles in transient versus storage starch metabolism.

6.4. Characterization of *ss5* knock-out mutants

In *lesv* mutants, a significant increase in SS5 abundance was observed in the granule proteome compared to wild-type plants. SS5 is known to participate in the regulation of granule initiation in the leaves of *Arabidopsis thaliana* (Abt et al., 2020). Given that the *lesv* phenotype, characterized by a strong accumulation of small granules, could be linked to altered granule initiation, we hypothesized a possible relationship between LESV and SS5. To explore this further, we analyzed the tuber starch phenotype in *SS5* knock-out mutants.

The *ss5* knockout mutants were provided by Dr. David Seung's group at the John Innes Centre in Norwich and were originally developed by the Simplot company. The data presented in this section were obtained during and after a research stay at the John Innes Centre, where I collaborated with Dr. David Seung's team.

After starch purification from potato flour, the granule diameter was measured using a Multisizer 4e Coulter counter (Beckman Coulter). This device allows the analysis of the granule size distribution within the total starch granules population either by granule number or volume (Figure 52). No particular difference was observed when comparing the *ss5* mutants to the wild-type control lines.

To further confirm the absence of change in granule morphology, starch granules were observed using SEM. Purified starch granules were glued onto SEM stubs. All stubs were sputter coated with gold and observed using Zeiss Gemini 300 SEM instrument. The general aspect of purified granules was very similar between *ss5* and wild-type control lines (Figure 53). However, a minor fraction of *ss5* mutants exhibited a cracked aspect. This may be due to the extraction method, but no such granule was observed in wild-type plants.

Although no notable modifications of granule morphology were observed, the structure of the granules was further analyzed in *ss5* mutants. The amylose/amylopectin ratio was measured by dissolving starch in iodine/DMSO. The amylose content was determined

compared to a potato amylose standard curve. No modification of the amylose content was observed in *ss5* mutant lines compared to control lines (Figure 54).

These complementary analyses, particularly the temporal monitoring of granule morphology during tuber development and the comparative analysis between starch in leaves and tubers, provided additional insight into the specific role of LESV in starch granule metabolism. While the *ss5* mutant showed no apparent phenotype, except the cracked aspect of a few number of granules, the *lesv* mutants exhibited strikingly different granule morphologies depending on the tissue, suggesting that LESV may contribute to distinct functions in transient starch, in leaves, versus storage starch in tubers. Altogether, the phenotypic characterization of these non-catalytic mutants builds a comprehensive framework for interpreting their specific contributions to starch granule biogenesis, which will be discussed in the next section.

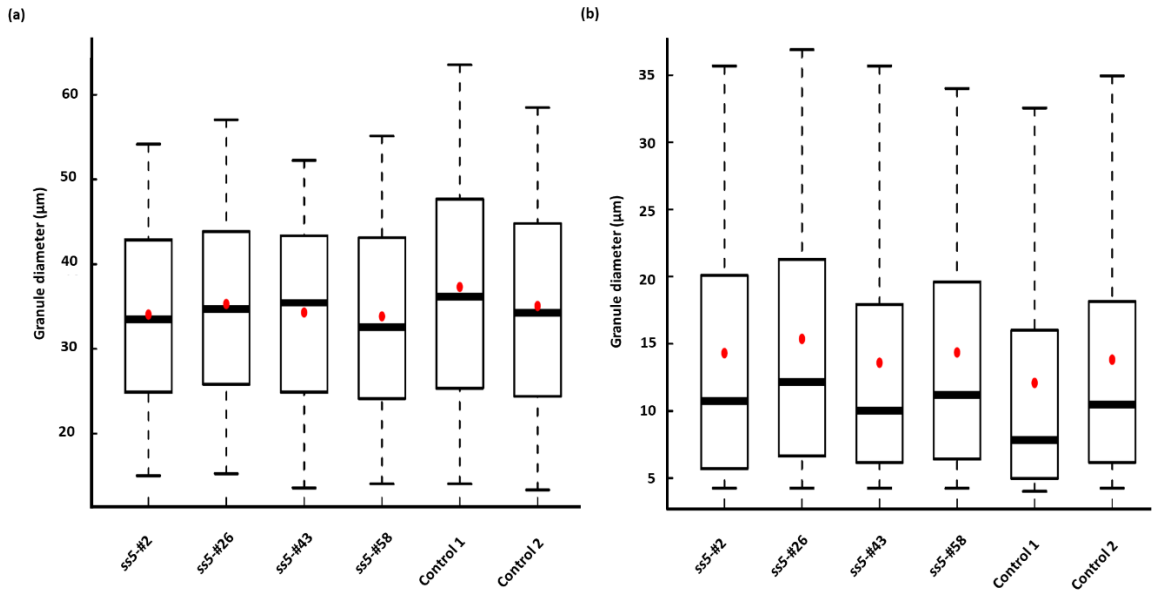

Figure 52 : Starch granule diameter in *ss5* mutants. (a) Starch granule diameter distribution and boxplot represented by starch granules volume. (b) Starch granule diameter distribution and boxplot represented by starch granules number. For each measurement, the values corresponding to the percentiles P5, P25, P50, P75, and P95 were extracted from the dataset of each biological replicate. The mean values were then calculated for each percentile across replicates of the same genotype. These averaged percentile values were used to generate the graphs. In the boxplots, the P5 and P95 values represent the extremities of the whiskers, the P25 and P75 values correspond to the bottom and top of the box, and the P50 (median) is shown as a black horizontal line within the box. Red dots represent the mean value for each mutant or wild-type line. Starch granule diameters were measured over a range of 4 to 100 µm in 0.24 µm intervals, yielding approximately 400 data points per measurement. Data represent the mean of three biological replicates (n=3). Control 1: untransformed wild-type; Control 2: wild-type plant that has been through transformation but has no edits

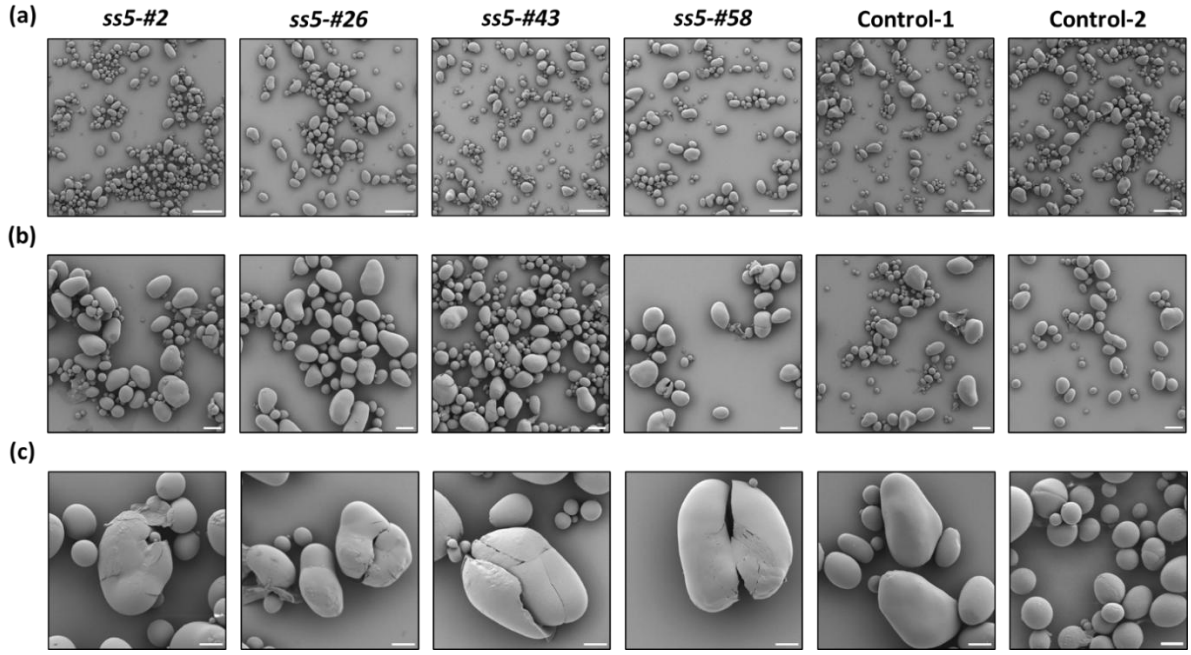

Figure 53 : Scanning Electron Microscopy of purified starch granules from *ss5* mutants and wild-type controls. Starch samples were mounted onto SEM stubs and were sputter-coated with gold before observation at an acceleration voltage of 3 kV using a Zeiss Gemini 300 SEM instrument. *ss5-#:* knock-out mutants; control 1: untransformed wild-type; control 2: wild-type plant that has been through transformation but has no edits. Scale bar = 100 µm (a); 30 µm (b); 10 µm (c). Panel (c) highlights cracked granules occasionally observed in *ss5* lines. Although such granules are rare, particular attention was paid to them in this panel to better visualize their unusual morphology.

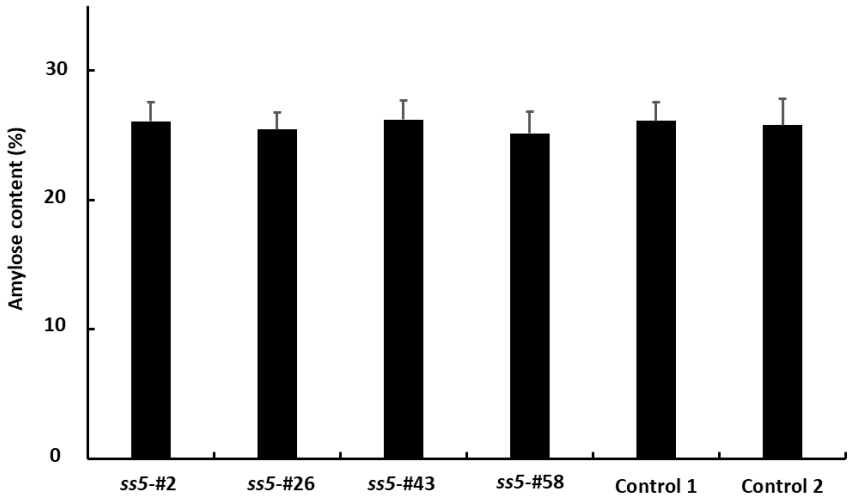

Figure 54 : Amylose content of *ss5* mutants and control lines. For each values, data are mean (+/- SE) of three biological replicates with three experimental replicates each (n=9).

DISCUSSION AND PERSPECTIVES

The aim of this work was to investigate the function of the non-catalytic proteins LESV and ESV1 in potato tuber storage starch metabolism. To this end, knock-out (KO) mutants were generated by targeted genomic edition using the CRISPR/Cas9 approach. Nine and five independent KO lines were selected for *LESV* and *ESV1* respectively. Three *lesv* and two *esv1* mutant lines were phenotyped in depth, providing a solid basis for dissecting the functional contribution of each gene. The results converge toward a central conclusion: LESV is crucial for regulating starch granule initiation in potato tuber, whereas ESV1 appears largely dispensable under the tested conditions. Below, we discuss the implications of each key result and outline future research directions.

lesv mutation alters the regulation of starch initiation in potato tuber

After selecting several KO lines for LESV and ESV1, we initially observed that the main agronomic traits, including plant growth, tuber production and starch yield per plant, were not significantly affected by the mutations (Figure 28). However, the *lesv* mutation induced important alterations in starch granule morphology characterized by a notable reduction in both granule diameter and roundness, as revealed by granulomorphometry (Figure 31). Additionally, small granules aggregates were observed using microscopy (Figure 32 and Figure 33). It is important to note that these morphological changes are likely underestimated, as seen in SEM (Figure 33). Indeed, the technical limitation of the granulomorphometer, related to the camera's resolution, leads to the exclusion from the analysis of particles smaller than 4 µm. Moreover, any possible cellular debris still present in the analyzed sample is also excluded by applying a filter that removed particles with an ellipsoid roundness below 0.5. These limitations result in the exclusion of nearly 85% of the detected particles in *lesv* starch samples. In addition, the presence of granules aggregates compromises the accurate determination of the granule size distribution in *lesv* mutants.

Nevertheless, these observations align with previous findings in *Arabidopsis thaliana*, where transitory starch granule morphology was altered by either downregulation or overexpression of the LESV protein (Feike et al., 2016). Interestingly, in *A. thaliana*, the reduction in granule diameter was only observed in LESV-overexpressing plants, suggesting potential differences in how LESV regulates transitory or storage starch metabolism.

Recent studies in rice (*Oryza sativa*) further demonstrated that LESV (FLO9) directly binds starch through its C-terminal tryptophan-rich region (Yan et al., 2024), a mechanism similar to that described for *Arabidopsis* LESV (C. Liu et al., 2023). In the same study, LESV was shown to interact with Floury Endosperm 6 (FLO6), homolog to Arabidopsis PTST2 (Seung et al., 2017), and with ISA1, a starch debranching enzyme that cannot bind starch independently and requires protein partners for proper localization (Fujita et al., 2003; Nakamura et al., 1996). The loss of LESV function impaired ISA1 targeting to starch (Yan et al., 2024). The authors proposed that LESV acts as a non-enzymatic regulator that promotes amylopectin synthesis in rice endosperm through its interaction with ISA1.

In potato, a striking phenotype was observed in *lesv* mutants, where amyloplasts were filled with tiny, morphologically altered starch granules (Figure 32), a feature that mirrors the one observed in rice *flo9* mutants lacking LESV (Yan et al., 2024). This striking phenotype was also reported in potato plants with downregulated expression of *ISA1* and *ISA2* through antisense RNA approach (Bustos et al., 2004). This prompted the authors to suggest that isoamylases are involved in the control of starch initiation in potato tuber by preventing or limiting the formation of glucans serving as primers for the formation of new starch granules.

Building on this, we hypothesized that LESV interacts with ISA1 in potato. This interaction was confirmed using yeast two-hybrid assays (Figure 44). We propose that, similar to rice, LESV associates with ISA1 in potato tubers to regulate its substrate specificity and/or localization. ISA1 appears to have a dual function in starch granule formation. When associated with LESV, ISA1 may contribute to the initiation of granule formation, possibly by modulating the structure of pre-amylopectin or pre-crystalline glucans to enable further elongation or organization. Independently of LESV, ISA1 is known to be involved in the trimming of branched glucans during amylopectin maturation, thereby contributing to the formation of semi-crystalline structures and proper starch granule architecture synthesis (S. Ball et al., 1996; Bustos et al., 2004; Myers et al., 2000). This dual role (initiation in association with LESV and structuration during amylopectin crystallization) may reflect a dynamic functional shift depending on the developmental stage and protein complex context. The hypothesis of the implication of LESV/ISA1 complex in granule initiation is supported by three lines of evidence.

First, in *A. thaliana*, pre-incubation of ISA1 with LESV was shown to enhance ISA1 activity, particularly its ability to remove DP9-10 glucans from amylopectin (Singh et al., 2022). This suggests that LESV modulates ISA1 function.

Second, *isa1* and *isa2* antisense potato lines exhibit a phenotype highly similar to our *lesv* mutants, characterized by the clusters of small starch granules (Bustos et al., 2004) (Figure 33). This supports the idea that LESV, ISA1 and ISA2 participate in a common process, possibly related to starch granule organization or maturation. Apart from their implication in granule initiation, ISA1 and ISA2 form a functional debranching complex that is essential for proper amylopectin structuring synthesis (S. Ball et al., 1996; Bustos et al., 2004; Myers et al., 2000), with ISA1 capable of self-interaction, as shown in maize (Facon et al., 2013; Q. Lin et al., 2013), and confirmed in this study (Figure 44). ISA1 and ISA2 interact to form an amylopectin debranching complex essential for proper starch granule structuring. In absence of LESV, this complex may be mislocalized or destabilized, leading to impaired amylopectin organization and accumulation of smaller granules that aggregate.

Intriguingly, LESV was detected exclusively bound to starch granule and not in the soluble fraction of plastids (Figure 41), while ISA1 was not detected bound to the granule (Figure 40) (Helle et al., 2018). While this limitation constrained the initial approach, the findings remain valuable, as they provide new insights into LESV localization. Moreover, this suggests that the LESV-ISA1 interaction, confirmed in this study (Figure 44) is likely transient. This discovery strengthens the hypothesis that LESV facilitates ISA1 targeting to starch, as seen in rice (Yan et al, 2024), since ISA1 alone cannot directly bind to starch. In this context, conventional colocalization assays may not be sensitive enough to capture this transient interaction. More advanced interaction assays might be required in the future to better resolve this dynamic mechanism.

Interestingly, despite the loss of LESV function, *lesv* mutants did not exhibit significant accumulation of water-soluble polysaccharides (WSPs) (Figure 29). This is in contrast to some *isa* antisense lines, where the disruption of ISA activity leads to WSP accumulation due to impaired glucan trimming during amylopectin synthesis (S. Ball et al., 1996; Bustos et al., 2004; Myers et al., 2000). This absence of WSP accumulation in *lesv* mutants suggests that ISA1 may retain some functional activity in the absence of LESV, at least enough to prevent the release of soluble glucans into the plastid. However, if LESV is required to properly localize

or stabilize ISA1 at the starch granule surface, its absence might cause ISA1 to function less efficiently or inappropriately.

If ISA1, in absence of LESV, fails to remove newly synthesized glucans that compete with starch granule formation, we would expect an increased number of small granules in amyloplasts. Light microscopy observations supported this (Figure 32), and scanning electron microscopy (SEM) of purified *lesv* starch samples revealed tightly fused small granules within aggregates (Figure 33). Attempts to separate these granules using SDS or ultrasonication were unsuccessful, suggesting strong binding between them. This aligns with the hypothesis that multiple small granules coexist within a single amyloplast.

Third, no distinct phenotype was observed in *esv1* mutants compared to wild-type plants. LESV and ESV1 share notable sequence similarity, about 34% of overall identity and 50% similarity in potato, and up to 52% identity and 67% similarity within the conserved tryptophan-rich C-terminal region (127 amino acids), which forms an antiparallel β-sheet domain responsible for starch binding (C. Liu et al., 2023; Osman et al., 2024) (Figure 55a and b). However, LESV possesses an N-terminal overhang, that is absent in ESV1 (Figure 55a). In *Arabidopsis thaliana*, this region undergoes conformational changes upon amylopectin binding (Osman et al., 2024). In rice, truncation studies demonstrated that LESV interacts with ISA1 via this N-terminal region (Yan et al., 2024).

In this context, the strong phenotype observed in *lesv* mutants, in contrast to the lack of phenotype in *esv1,* supports the hypothesis that the N-terminal extension of LESV plays an important role in starch granule initiation. However, whether this domain is strictly required for interaction with ISA1, and whether such interaction occurs in potato between ISA1 and ESV1, remains to be experimentally tested. It is possible that ESV1, despite lacking the N-terminal domain, could still interact with ISA1 through alternative mechanisms or contribute to other stages of starch granule biosynthesis, such as structural stabilization or phase transition.

The similarity in the C-terminal region between LESV and ESV1 raises the possibility of functional redundancy in potato, at least in part, especially if the two proteins act at different steps of granule formation. In this scenario, LESV may be involved in regulating the number of soluble starch granule precursors via its N-terminal interaction with ISA1, while both LESV

and ESV1 could contribute to glucan organization through their C-terminal domain. This dual mode of action could explain the lack of phenotype in *esv1* mutants if LESV is sufficient to compensate for ESV1 absence. Conversely, the inability of ESV1 to compensate for LESV loss might reflect the importance of LESV N-terminal region in granule initiation.

We propose a model to explain the role of LESV and ESV1 in potato (Figure 55c). In wild-type plants, LESV interacts through its N-terminal domain with ISA1/ISA2 complex to regulate the number of soluble starch granule precursors, similar to what was described in rice by Yan et al. (2024). On the other hand, LESV and ESV1 interacts with glucans via their C-terminal domain to promote and stabilize phase transition, respectively, as proposed by C. Liu et al. (2023), leading to the formation of a single starch granule in mature amyloplast. Inactivation of ESV1 does not impact the number and structure of starch granules due to compensation by LESV. Inactivation of LESV deregulates the control of starch initiation and the promotion of phase transition is performed by ESV1. The abnormal high number of starch granule initiations leads to smaller starch granules and to granules aggregates.

To further explore this model, yeast-two-hybrid or co-immunoprecipitation assays could determine whether ESV1 interacts with ISA1. Recombinant versions of LESV and ESV1 with or without the LESV N-terminal domain could further clarify the role of this region in the interaction with ISA1. Further investigations, including the generation and analysis of *lesv esv1* double mutants could provide insight into potential redundancy or cooperation between the two proteins. Finally, untargeted co-immunoprecipitation approach could help determine ESV1 potential partners.

Furthermore, the *lesv* mutation caused notable changes in starch granule morphology at early developmental stages (Figure 48), reinforcing the idea that LESV plays a key role in the early stages of starch metabolism, likely at granule initiation. It would be interesting to measure *LESV* expression throughout tuber development and to determine if LESV in mandatory only at the earlier stage of starch synthesis or for granule initiation and throughout granule growth. One of our hypothesis was that small aggregates observed in *lesv* mutants represent a normal early step in granule initiation, but these granules should then fuse over time to form larger granules, as observed in *Arabidopsis* leaves (Bürgy et al., 2021; Crumpton-Taylor et al., 2012). In absence of LESV, this fusion of small granules would not be complete, leading to the formation of tiny granules aggregated to each other. In this hypothesis, LESV

could be directly involved in the coalescence of the small granules. While our developmental observations were not sufficient to fully test this hypothesis, silencing LESV in wild-type plants after tuber development could help determine whether only the initiation step is impaired in absence of LESV, or whether this protein is essential for other mechanisms such as the coalescence or the growth of starch granules.

Finally, granules arising from fused, multiple initiations have been previously observed in potato following the mutations of branching enzymes (Tuncel et al., 2019). Indeed, the presence of a huge numbers of tiny granules was observed, as well as “nodular granules” with multiple hila, which highlights a loss of control over the granule initiation process in mutants lines lacking SBE2. The authors proposed that inadequate glucan branching disrupts mechanisms that normally limit the number of initiations. Strikingly, this phenotype resembles that of both lesv and *Stisa1* mutants (Figure 33) (Bustos et al., 2004), raising the possibility that SBE2, LESV, and ISA1 are components of a same mechanism that tightly regulates starch granule initiation. Interaction studies between LESV and SBE2, and ISA1 and SBE2 could help to further understand the mechanisms underlying granule initiation in potato.

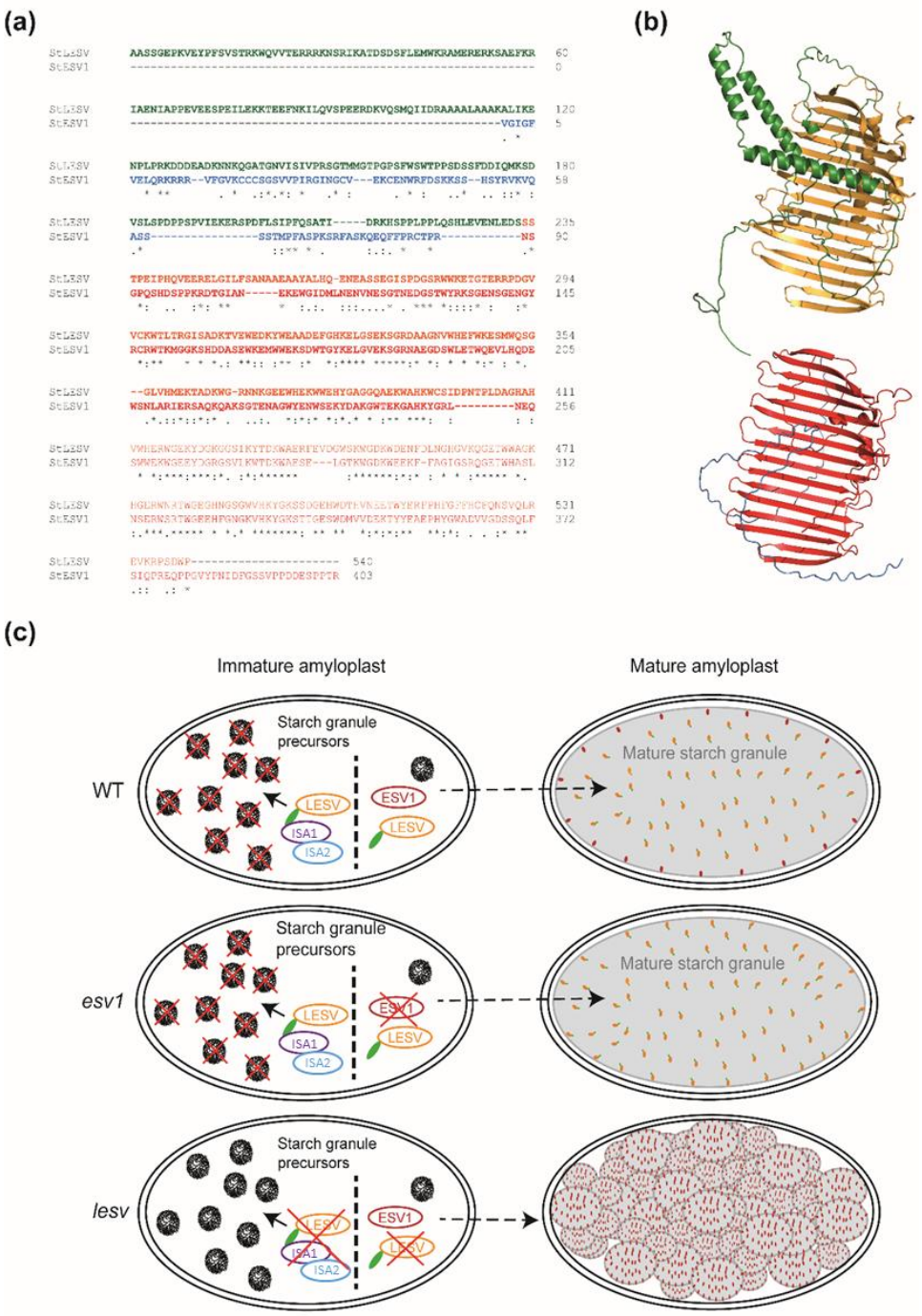

Figure 55 : Proposed model for the functions of LESV and ESV1 in amyloplasts. (a). LESV and ESV1 protein sequences were retrieved from the potato genome sequence database and processed with Localizer software for transit peptide removal prior to alignment using Clustal omega. Orange and red lettering: conserved C-terminal domains. Green and blue lettering: highly divergent N-terminal regions of LESV and ESV1, respectively. (b). Protein models were generated with Colabfold software using Alphafold 2 and MMseqs2. The color code is the same as in (a). (c). Proposed model for LESV and ESV1 functions in potato amyloplasts. In wild-type plants, LESV interacts through its N-terminal domain with ISA1/ISA2 complex to regulate the number of soluble starch granule precursors, similar to what was described in rice by Yan et al. (2024). On the other hand, LESV and ESV1 interacts with glucans via their C-terminal domain to promote and stabilize phase transition, respectively, as proposed by C. Liu et al. (2023), leading to the formation of a single starch granule in mature amyloplast. Inactivation of ESV1 does not impact starch granules due to compensation by LESV. Inactivation of LESV deregulates the control of starch initiation and the promotion of phase transition is performed by ESV1. The abnormal high number of starch granule initiations leads smaller starch granules and to granules aggregates.

Divergence in the control of starch granule initiation across organs and species

Starch plays a central role in plant physiology, serving as a major energy reservoir. It allows energy storage over both short and long period, within the leaves for daily metabolic needs, and in storage organs such as seeds and tubers for later use, particularly sprouting. The initiation of starch granules is a key process because it determines the number, shape and size of the granules, and therefore directly impacts starch functionality. This process has been the subject of numerous studies in recent years. Significant advances have been made in our understanding of granule initiation in the leaf chloroplasts of the model plant *Arabidopsis thaliana* (Figure 56a)

The chloroplasts of the wild-type Arabidopsis plants typically contain five to seven granules, depending on the chloroplast volume (Crumpton-Taylor et al., 2012). In these leaves, starch granule initiation is tightly regulated by a network of interacting proteins. The starch synthase SS4 plays a central role in granule initiation, working in concert with PTST2, PTST3, PII1/MRC, MFP1 and SS5. First, MFP1 contributes to granule initiation by regulating the spatial localization of the initiation complex (M. Sharma et al., 2024). Then, PTST2 binds maltooligosaccharides and facilitates their delivery to SS4 (Seung et al., 2017, 2018; Watson-Lazowski et al., 2022). PTST3 may act redundantly or synergistically with PTST2, although its precise role remains less clearly defined. After that, SS4 elongates glucans, and its loss can be partially compensated by SS3 (Roldán et al., 2007; Szydlowski et al., 2009). PII1/MRC functions as a regulatory factor of SS4 activity (Seung et al., 2018; Vandromme et al., 2019, 2023) and SS5, a non-catalytic starch synthase-like protein, appears to influence granule number through scaffolding or regulatory functions of SS4 (Abt et al., 2020). Several interactions among these proteins have been experimentally confirmed, supporting the existence of a multimeric protein complex involved in granule initiation (Figure 8 and Figure 56a). However, it remains unclear whether all these interactions occur simultaneously within a single stable complex, or represent dynamic associations that vary depending on developmental stage or cellular context.

However, while the initiation process in Arabidopsis leaves is becoming relatively well understood, this model is not universal across plant species and organs. Starch granule initiation exhibits a multi-level regulation.

First, regulation differs between species. When comparing granule initiation across species, striking diversity in the process and associated protein networks becomes apparent (Figure 56). In Arabidopsis, 5 to 7 granules form per chloroplast. In contrast, rice (*Oryza sativa*) amyloplasts typically form compound granules consisting of multiple individual starch granules separated by septa, believed to originate from the inner envelope of the amyloplast. These physical barriers are thought to prevent granule fusion and allow multiple initiation events to persist independently (Kawagoe, 2013; Yun & Kawagoe, 2010). Initiation of compound granules in rice (*Oryza sativa*) is less well understood (Figure 56b). A functional analog of PTST2, FLO6, has been shown to interact with LESV to recruit ISA1 to starch granules (Yan et al., 2024). This complex appears to be required for proper granule initiation, as mutants deficient in either LESV or FLO6 accumulate unusually high numbers of tiny granules within amyloplasts (Peng et al., 2014; Yan et al., 2024). This raises the possibility that in potato, LESV may similarly interact with PTST2b (the isoform presents in tuber) to coordinate the recruitment or the localization of the ISA1/ISA2 complex.

Rice also expresses two isoforms of SS4 (SS4a and SS4b) during endosperm development (Ohdan et al., 2005). While SS4b loss leads to only mild effects in the starch granule formation (Toyosawa et al., 2016), the presence of SS4a may partially mask the impact of SS4b loss. Indeed, rice lines lacking SS4a expression exhibit severe developmental defects, including reduced plant growth and unfilled grains although the causes of this phenotype is unclear (Jung et al., 2018). It was also suggested that PHS1 (Pho1), the major plastidial phosphorylase in rice endosperm also contributes to starch granule initiation. Satoh et al. (2008) reported that loss of PHS1 alters granule number and amylopectin structure, with more pronounced effects under low-temperature conditions, highlighting a temperature-dependent control of initiation involving PHS1.

Second, regulation can differ within the same species. In potato, the starch initiation process differs significantly between tubers and leaves (Figure 56c). Wild-type tuber amyloplasts usually harbor a single large ovoid granule (Kram et al., 1993), while chloroplasts contain several granules, like Arabidopsis. In potato tuber of wild-type plants, LESV protein is

highly expressed and localizes to starch granules (Figure 40) (Helle et al., 2018). Our results indicated that LESV plays a major role in controlling granule initiation in tubers, as evidenced by the significant reduction in granule diameter in *lesv* mutants and the accumulation of aggregated small granules within a single amyloplast (Figure 31Figure 32Figure 33). Moreover, we demonstrated that LESV interacts with ISA1, a protein previously known to be involved in granule initiation (Bustos et al., 2004). We proposed that LESV modulates the number of soluble starch granule precursors by interacting with ISA1, as presented in Figure 55.

It is also worth noting that the starch phenotype of *lesv* mutants is organ-specific. In tubers, granule accumulation is remarkable, whereas in leaves, chloroplasts seem to display less granules, slightly larger than in wild-type plants, although replicates and statistical analyses are needed to confirm these modifications (Figure 50, Figure 51). This organ-specificity suggests that the role of LESV is context-dependent, possibly replaced or compensated by other proteins in photosynthetic tissues. Such differences between leaves and tubers, may reflect divergent regulatory pathways adapted to the distinct metabolic needs and plastid types involved in transient versus storage starch synthesis.

Additionally, the abundance of starch bound SS5 in strongly increased in absence of LESV. This suggests that this protein, that was recently confirmed to participate in granule initiation in potato tubers (Hu et al., 2025), as previously shown in Arabidopsis (Abt et al., 2020), may be part of the same regulatory network. *ss5* mutants display a reduction in granule diameter in tubers, the presence of supernumerary granules in amyloplasts, and a decrease in gelatinization temperatures as revealed by DSC analysis. A reduction in granule number was also reported in chloroplasts. If these traits are reminiscent of those observed in *lesv* mutants, *ss5* mutants also exhibit a decrease in overall starch content and an increased amylose/amylopectin ratio, which were not detected in *lesv* lines. This suggests that while SS5 may be involved in granule initiation, in a mechanism that may imply LESV, it is also involved in distinct regulatory pathways influencing starch quantity and composition.

Moreover, the plastidial phosphorylase PHS1 (Pho1a), which has been implicated in granule initiation in cereals, may also contribute to this process in tubers. Potato mutants lacking Pho1a exhibit an increased number of rounded starch granules and a reduction in apparent amylose content (S. Sharma et al., 2023). These phenotypes suggest that Pho1a

could be involved in regulating the number or spatial organization of initiation events. Moreover, the ability of phosphorylases to incorporate glucose into starch from glucose-1-phosphate (Fettke et al., 2010) supports the hypothesis that a secondary elongation pathway could contribute to early glucan priming, possibly linked to granule initiation control.

Although homologs of proteins involved in granule initiation in Arabidopsis are also expressed in potato leaves, suggesting at least a partially conserved mechanism for transient starch granule initiation across species, their expression is markedly lower in potato tubers, with the exception of SS5 (Hochmuth et al., 2024). This differential expression highlights a substantial divergence in the composition of the starch initiation machinery between photosynthetic organs.

Third, regulation may even vary within the same organ. The complexity increases further in wheat, where granule initiation varies temporally in the endosperm (Figure 56d). In wild-type wheat (*Triticum aestivum*), a single large A-type granule initiates around 4 days post-anthesis, during early grain development, through action of SS4 and BGC1 (Chia et al., 2020; Hawkins et al., 2021). After 15 to 20 days post anthesis, B-type granules are formed around the A-type, within structures named stromules, through coordinated action of PHS1 and BGC1 that interact together (Chia et al., 2020; Kamble et al., 2023). Potato mutants lacking Pho1a (the isoform present in tuber) exhibit an increased number of rounded starch granules with a reduced apparent amylose content (S. Sharma et al., 2023). Altogether, these findings suggest a potential role for Pho1a in regulating the starch granule initiation in potato, though further research is needed to fully elucidate its function. MRC (PII1) was also found involved in granule initiation in wheat, where it regulates the timing of starch granule initiation by repressing the early formation of B-type granules, highlighting a case of function diversification among granule initiation proteins (J. Chen et al., 2024).

Consistently, phenotypic outcomes of starch initiation defects differ significantly depending on the context. This highlights an evolutionary divergence in starch initiation mechanisms between species and organs. To better understand LESV function in potato tuber starch initiation, it would be valuable to identify its interaction partners. While a potential interaction with PTST2b is plausible, a comprehensive screen including other known or suspected players in initiation control, such as SS5, PHS1, SBE2, PII1/MRC and MFP would provide a better understanding of the LESV regulatory network in potato.

Finally, it is worth to note that, despite the important differences between storage and transitory starch metabolisms in a same plant, and the physiological differences between species, the data presented here and the proposed model suggesting that LESV and ESV1 directly promote and stabilize glucan phase transition (C. Liu et al., 2023) are not mutually exclusive. Although no major alteration in starch ultrastructure was measured in potato *lesv* or *esv1* mutants, the absence of the corresponding proteins could induce subtle changes not detectable with the current methods. The analysis of the double mutant could provide deeper insights into the role of these proteins in amylopectin phase transition.

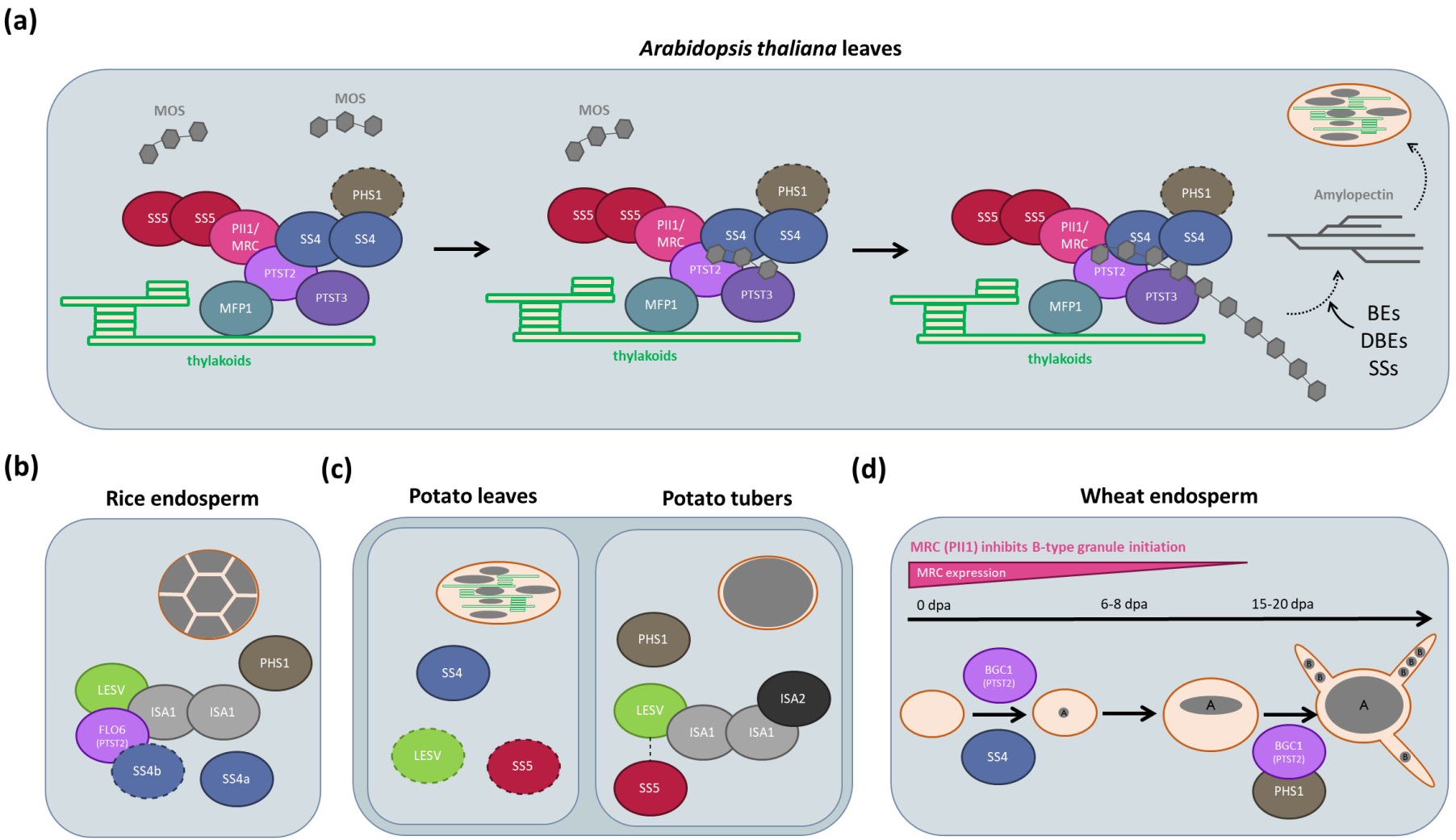

Figure 56 : Regulation of starch granule initiation across plant species and tissues. (a) In *Arabidopsis thaliana* leaves, the initiation of transitory starch granules is mediated by a multiprotein complex anchored to the thylakoid membrane via MFP1 (MAR1-Binding Filament Protein 1). PTST2 (Protein Targeting to Starch 2), together with PTST3, binds and transfers maltooligosaccharides (MOS) to SS4 (Starch Synthase 4), which elongates them. The resulting glucans are then processed by branching enzymes (BEs),

debranching enzymes (DBEs), and other starch synthases (SSs) to form amylopectin and initiate starch granule formation. Typically, five to seven starch granules are formed per chloroplast. PII1/MRC (Protein Involved in Initiation 1/Myosin-Related Chloroplast protein) regulates SS4 activity and interacts with SS5, which may act as a scaffold or regulatory subunit. SS4 also interacts with PHS1, although its precise function remains unclear. In the absence of SS4, SS3 can partially compensate. However, this model is not universal, and starch initiation is tightly regulated at multiple levels. (b) A first level of regulation is observed between species. In rice (*Oryza sativa*), amyloplasts in the endosperm form compound granules. This process involves a distinct set of proteins, including, SS4 and PHS1, as well as FLO6 (a PTST2 homolog) and LESV, which recruit ISA1 to starch granules. (c) A second level of regulation occurs within the same species, as shown in *Solanum tuberosum*. While initiation in potato leaves remains poorly studied, proteins such as LESV, SS4 (unpublished data, personal communication from Dr. Nicolas Szydlowski), and SS5 (Hu et al., 2025) appear to participate in granule initiation, suggesting slight divergence from the *Arabidopsis* model. In contrast, tuber amyloplasts typically contain a single large starch granule. Our study demonstrates that LESV plays a key role in granule initiation in tubers by interacting with ISA1 to regulate the number of initiation events. This function has not been described in any other species. We also observed a potential regulatory link between LESV and SS5, represented by dashed lines (indicating a functional relationship, not necessarily a physical interaction). (d) A third level of regulation is observed within a single organ, as in wheat (*Triticum aestivum*) endosperm. A-type granules are initiated early after anthesis through the combined action of SS4 and BGC1 (a PTST2 homolog). The repression of B-type granule formation is maintained until approximately 15 days post-anthesis by MRC (PII1), after which BGC1 and PHS1, which physically interact, allow the initiation of multiple B-type granules within stromules. In the diagram, proteins with suspected but unconfirmed roles in granule initiation are outlined with dashed borders. Starch granules are shown in grey.

SS5 quantity is strongly increased in granules of *lesv* mutants

One of the most striking observations in *lesv* mutants is the strong and consistent increase of SS5 abundance within starch granules, as detected by mass spectrometry (Figure 40). In contrast, SS5 was weakly present in only one of the three wild-type samples analyzed.

While our tetraploid ss5 mutants did not exhibit any significant phenotypic alteration compared to the wild type (Figure 52,Figure 53 and Figure 54), a very recent study using dihaploid lines reported alterations in starch granule initiation upon SS5 disruption (Hu et al., 2025). These included a reduced granule size, increased number of starch granules per amyloplast (often forming compound granules), lower gelatinization temperatures and changes in amylose/amylopectin ratio. Interestingly, some of these traits are reminiscent of those observed in our *lesv* mutants, suggesting a possible overlap in the molecular mechanisms involving SS5 and LESV, or a reciprocal regulation.

However, the phenotypes are not entirely redundant: *ss5* dihaploid mutants also display a reduction in total starch content and an altered amylose/amylopectin ratio (Hu et al., 2025), which are not observed in *lesv* lines (Figure 29Figure 35). This suggests that while SS5 may contribute to granule initiation in a manner similar to LESV, it may also influence distinct metabolic or regulatory processes affecting starch quantity and structure. This is supported by the fact that, in *Arabidopsis thaliana*, SS5 interacts with PII1/MRC to control granule initiation, but this protein is not expressed in potato tubers (Abt et al., 2020; Hochmuth et al., 2024). This implies that SS5 may interact with unknown partners or participate in an alternative initiation mechanism specific to potato.

A key factor that may explain the observed phenotypic divergence is ploidy level. In tetraploid potatoes, the presence of four allelic copies allows for stronger buffering of genetic perturbations through gene redundancy or dosage compensation. Even in the case of complete gene knockout, the overall network regulating starch biosynthesis may remain sufficiently robust to mask the effect of SS5 loss. SS5 role could be compensated in our tetraploid variety by other enzymes or factors involved in granule initiation (e.g. LESV). On the contrary, the dihaploid potatoes are more sensitive to perturbation and thus may reveal a role for a protein that remains hidden in a tetraploid context. It is plausible that the

dihaploid line used by Hu et al. lacks such compensatory capacity, leading to a clearer phenotype.

We observed that SS5 is strongly enriched in starch granules of *lesv* mutants, whereas it is barely detectable in wild-type granules (Figure 40). This suggests a compensatory upregulation of SS5 in the absence of LESV, potentially as a feedback response to the disruption of the initiation complex. We could hypothesize that this compensatory mechanism might partially mask the effects of LESV loss, though this response might not fully restore granule initiation. *lesv* phenotype could be more severe in the absence of SS5. Thus, generating and analyzing *lesv/ss5* double mutant could be particularly helpful to evaluate whether the accumulation of SS5 in *lesv* backgrounds limits the extent of the phenotype. Moreover, quantifying SS5 transcript and protein levels in both wild-type and *lesv* mutant backgrounds would help clarify whether the increase in SS5 abundance is transcriptional or post-transcriptional. Protein-protein interaction assays (e.g., Co-IP, BiFC, yeast two-hybrid) could determine if SS5 physically interacts with LESV. Moreover, analyzing SS5 localization using GFP could reveal whether SS5 is targeted to starch granules in the presence or absence of LESV.

Altogether, these observations highlight that the role of SS5 in starch granule initiation is likely context-dependent, based on ploidy level and potential feedback regulation within the initiation complex. The contradictory findings between tetraploid and dihaploid studies should thus not be viewed as mutually exclusive. In summary, these results suggest that SS5 role may be partially redundant or conditionally required. Nevertheless, its altered abundance in *lesv* lines remains intriguing, suggesting a possible indirect interaction or regulatory feedback loop between LESV and proteins of the initiation complex. To further investigate this, interaction assays and transcriptomic analyses could shed light on shared regulatory pathways.

lesv mutation alters starch phosphorylation and functional properties

The *lesv* mutation leads to a notable increase in starch phosphate content, particularly in C-6-phosphoester residues. This observation is consistent with two previously reported findings. First, small starch granules in potato tubers have been shown to naturally exhibit

elevated phosphate levels, mainly due to a higher proportion of C-6-bound phosphate groups (Helle et al., 2019). Second, LESV in *Arabidopsis thaliana* was recently identified as a regulator of starch-related dikinase activity, which plays a key role in starch degradation (Singh et al., 2022). *In vitro* assays revealed that LESV enhances the activity of PWD (phosphoglucan water dikinase), which phosphorylates glucose at the C3 position, while attenuating the activity of GWD (glucan water dikinase), responsible for C6 phosphorylation and essential for PWD function. The increased C-6-phosphorylation observed in *lesv* mutants may thus result from the loss of this negative regulation on GWD, leading to excessive C6 phosphorylation and potentially altering granule architecture and enzyme accessibility.

Starch extracted from *lesv* mutants exhibited a significantly higher hydrolysis rate—up to 53% faster than that of the wild type (Figure 38). This enhanced digestibility is likely an effect of the reduced granule size, which provides a greater surface-to-volume ratio facilitating enzyme access and activity. Indeed, this result is consistent with previous reports on the increased enzyme susceptibility of small granules due the higher amount of enzyme adsorption sites for a given starch weight (Dhital et al., 2010; Naguleswaran et al., 2012; Noda et al., 2005).

Interestingly, such modifications may hold considerable promise for industrial applications. The production of starch with faster enzymatic degradation kinetics could reduce processing time and enzyme costs in the production of glucose syrups or bioethanol. Furthermore, small starch granules have unique physical and chemical properties that make them attractive for a variety of uses, including as fat replacers, carriers for bioactive compounds, binders in paper or textile industries, and components in biodegradable packaging (Kim et al., 2015). While natural small granules from sources like quinoa, rice, amaranth and taro are typically used, producing small granules from potato could allow a higher yield production.

Beyond functional aspects, altered phosphorylation in *lesv* mutants may influence the organization of starch granules at the ultrastructural level. It has been proposed that phosphate content in developing tubers modulates the activity of starch biosynthetic enzymes and thereby impacts granule morphology (Xu et al., 2017). In potato starch, blocklet size varies radially within granules—larger blocklets at the periphery and smaller ones at the core (Gallant et al., 1992, 1997). These structures are thought to contribute to digestion

resistance, with larger blocklets conferring greater resilience to enzymatic attack. Whether the changes observed in *lesv* starch influence blocklet size or arrangement remains to be investigated, but this could offer further insights into the link between starch microstructure and degradability.

Finally, pasting profiles of *lesv* and *esv1* mutants also reflect alterations in starch properties. *lesv* starch tend to display higher peak viscosities and reduced gelatinization temperatures, suggesting a modified internal structure that affects swelling and gelation behavior (Figure 39 and Table 3). In contrast, *esv1* starch shows reduced viscosity parameters (Figure 39), indicating potential defects in granule integrity or amylopectin architecture that we did not detect with the available methods. These differences highlight the distinct contributions of LESV and ESV1 to starch properties and open the way for modulating starch functional parameters through targeted genetic modifications.

esv1 mutants have a wild-type phenotype

In contrast to *lesv*, *esv1* mutants displayed no clear phenotype under our conditions. Granule morphology, size, structure, and plant growth were comparable to wild-type. This is somewhat surprising, given that ESV1 is structurally related to LESV and plays a role in starch accumulation in other plant models.

As previously discussed, the absence of a visible phenotype in potato tubers of *esv1* mutants could be related to the lack of the N-terminal extension in ESV1, a domain that is present in LESV. Although this N-terminal extension is also absent in Arabidopsis ESV1, and Arabidopsis *esv1* mutants do show an altered phenotype in leaves, the role of ESV1 in storage starch has never been investigated and may differ from that in transitory starch metabolism. Therefore, the lack of phenotype in potato tubers could reflect a functional divergence of ESV1 depending on the organ. Nonetheless, several other hypotheses could account for this absence of phenotype.

A first hypothesis concerns the existence of a functional redundancy between ESV1 and LESV (or other proteins) which could limit the phenotype of the *esv1* mutation. As LESV and ESV1 share a high similarity, we can hypothesize that the absence of ESV1 alone is not

sufficient to observe an alteration of granule features. Moreover, the potato genome harbors a gene encoding a protein highly similar to ESV1, here referred to as ESV2, which shares approximately 75% sequence identity. This high degree of similarity raises the possibility of functional redundancy between ESV1 and ESV2. In this scenario, the loss of one protein might be compensated by the presence of the other, thereby limiting any potential phenotypic effect in the single mutants. Additionally, no gene encoding a protein similar to ESV2 was identified in Arabidopsis genome, which could explain the phenotype observed in simple *esv1* mutant. It is noteworthy, however, that ESV2 was not detected by mass spectrometry in potato tuber starch granules, unlike ESV1, which was clearly identified. This absence might suggest a differential expression profile, a distinct subcellular localization, or a lower protein abundance in granule-associated fractions, challenging the hypothesis of complete functional redundancy and raising questions about the specific role of ESV2 in starch metabolism. To further explore this hypothesis, it would be informative to generate an *esv2* single mutant, as well as an *esv1 esv2* double mutant. The observation of a phenotype in either of these genetic backgrounds would support the idea of a functional overlap between the two proteins. Furthermore, the precise role of ESV2 remains unknown, and its expression pattern, subcellular localization, or protein–protein interactions could differ from those of ESV1 despite their sequence similarity.

Secondly, ESV1 may act only under specific environmental or metabolic conditions not encountered during our experiments (e.g. stress, circadian regulation). Modification of the growth conditions, including stress assays, would help clarify ESV1 functional contribution in starch granule in potato. It is also plausible that ESV1 is important for starch metabolism in leaves, but not in tubers.

In addition to loss-of-function approaches, overexpressing ESV1 in a wild-type background could help clarify whether increased ESV1 dosage can modulate granule phenotypes. These complementary strategies would provide valuable insight into the extent of functional divergence or redundancy among the EARLY STARVATION proteins in potato, and help better understand their roles in starch granule biosynthesis.

Overall, the present study contributes to improve our understanding of starch metabolism, highlighting the essential role of LESV in starch granule initiation in potato tubers. Our results support the hypothesis that LESV is involved in the control of granule initiation and growth, probably through its interaction with ISA1/ISA2 complex. The presence of granule aggregates in *lesv* mutants, combined with the absence of structural differences in separated granule fractions, points to a defect in granule initiation. Tissue-specific differences between tubers and leaves, and between potato and Arabidopsis, suggest that LESV role could be modulated by plastid type, metabolic context, or interacting partners. Future work should focus on determining the precise molecular interactions of LESV. Protein interaction assays, and *in silico* modeling could provide valuable insights. It would also be relevant to explore whether manipulating LESV expression could modulate granule number or size, thus offering potential biotechnological applications for starch yield or quality improvement. In conclusion, LESV appears to be a key component of starch granule initiation in storage tissues. Elucidating its mode of action and identifying all of its interactors would not only clarify the mechanism controlling the initiation of starch granules but would also open up new perspectives for crop improvement and industrial starch production.

ANNEX PROJECT 1: PRODUCTION OF HERITABLE TRANSGENE FREE GENE EDITED PLANTS

1. Introduction

The use of Agrobacterium-mediated transformation to produce transgenic potato mutants has yielded significant results so far. However, the prospect of efficiently and rapidly producing transgene-free plants is a major challenge. This is why I aimed to address this issue in the potato model.

A recent publication by Yang et al., (2023) introduces an innovative technique for producing transgene-free gene-edited plants through grafting. The main advantage of this approach is the production of a transgene-free plant, without the time consuming and complex processes typically associated with traditional transformation methods.

Researchers designed fusions of the CRISPR-Cas9 system with tRNA-like sequence (TLS) motifs, facilitating the transport of Cas9 and guide RNA (gRNA) transcripts from transgenic rootstocks to grafted wild-type shoots. A TLS refers to an RNA sequence that shares structural and functional similarities with transfer RNA (tRNA) but is not a canonical tRNA. These sequences serve as signals for the long-distance movement of RNA molecules within plants. By integrating TLS into the CRISPR/Cas9 system, researchers have enabled the transport of gene-editing components from transgenic rootstocks to non-transgenic scions (the grafted shoots).

In this approach, a transgenic rootstock expressing the CRISPR/Cas9 system fused with TLS is grafted with a wild-type (non-transgenic) scion. The TLS allows the movement of the CRISPR/Cas9 RNAs from the rootstock into the scion, where they induce targeted genetic modifications without integrating any transgene into the plant genome. This mobility is mediated through the phloem, one of the two main vascular tissues in plants, alongside the xylem. While the xylem primarily conducts water and minerals from the roots to the aerial parts of the plant, the phloem distributes sugars and signaling molecules, including RNA and proteins from sources (leaves) to sink (roots and storage organs).

Recent findings by Zhang et al. (2016) have demonstrated that specific RNA motifs, such as TLS are sufficient to mediate this RNA mobility across graft junctions via the phloem. These TLSs mimic endogenous structural features found in transfer RNAs and are recognized by the transport machinery of the plant. Once transported into distant tissues, these mobile mRNAs can not only reach their target cells, but also be translated into functional proteins. This suggests that, in the grafting-based editing system, CRISPR/Cas9 mRNAs delivered from

the rootstock are able to enter cells of the scion, be imported into the nucleus and mediate precise genome editing.

Importantly, these edits are inheritable, meaning that the genetic modifications can be transmitted to the next generation without any integration of transgenic material. In this system, the rootstock is genetically modified and contains the transgenes required for expressing the CRISPR/Cas9 complex and the guide RNAs fused to TLS. These ribonucleoprotein complexes are synthesized in the root cells and, thanks to the TLS motifs described earlier, they are transported into the non-transgenic scion, which serves as the grafted shoot. Once in the scion, the CRISPR/Cas9 complex enters the cells and performs targeted genome editing, without integrating any foreign DNA into the plant genome. If the genome editing occurs in the reproductive organs of the scion, the resulting progeny will inherit the desired edits, while remaining free of any transgene.

In the study of Yang et al. (2023), the authors demonstrated the inactivation of the NITRATE REDUCTASE1 (NIA1) gene in Arabidopsis using this method. The edited plants exhibited the expected phenotypes, proving the functional mobility and effectiveness of the Cas9-TLS and gRNA-TLS constructs.

This method offers a significant advantage by producing gene-edited plants without the integration of foreign DNA, thereby addressing regulatory and public concerns associated with transgenic organisms. It has been successfully demonstrated in species such as *Arabidopsis thaliana* and *Brassica rapa*, highlighting its potential applicability across various plant species.

This study could significantly facilitate the development of gene-edited crops, constituting a promising alternative to conventional transformation techniques, with potential applications for agricultural biotechnology and plant breeding. The integration of TLS into genome editing strategies represents a promising advancement in plant biotechnology, enabling precise genetic modifications while preserving a transgene-free status in the resulting plants.

Considering the potential industrial applications of potato plants with low levels of LESV expression for example, we aim to develop this technique in potato to facilitate gene editing of this species. Furthermore, since he absence of phenotype observed in *esv1* mutants may be compensated by the presence of LESV, the production of *lesv/esv1* double mutants could provide valuable insights about the respective function of these proteins. Producing

such double mutant might be more efficient through grafting rather than low-efficiency multiplexing approaches. This technique could allow a simpler and faster production of mutants that combine multiple mutations by generating a collection of simple mutants that could be used for grafting.

To adapt the transgene-free gene editing strategy developed in *Arabidopsis thaliana* to potato, several key modifications must be implemented. In *Arabidopsis*, the genetically modified rootstock (lower part of the graft) expresses the CRISPR/Cas9 and guide RNAs (gRNAs), which are transported via the xylem into the wild-type scion (upper part of the graft) to edit the reproductive tissues and generate transgene-free seeds. In contrast, potato is vegetatively propagated via tubers, not seeds. Therefore, the strategy must be inverted: the scion will be transgenic, expressing CRISPR/Cas9 fused with tRNA-like sequence (TLS) motifs and the corresponding gRNA-TLS, while the rootstock will be wild-type. The goal is to achieve shoot-to-root movement of the CRISPR/Cas9 ribonucleoprotein complex, via the phloem, allowing genome editing to occur in the rootstock, and more specifically, in the developing tubers, thereby producing transgene-free edited potatoes (Figure 57).

To demonstrate the feasibility of this adapted approach in potato, we will perform proof-of-concept experiments by targeting the *GBSS* gene. *GBSS* encodes the granule-bound starch synthase responsible for amylose synthesis. Inactivation of *GBSS* results in amylose-free starch composed only of amylopectin, which can be easily detected using a simple iodine staining assay: while normal starch gives a blue color with iodine, amylose-free starch produces a red-brown color, enabling a fast and easy phenotypic screening (Okagaki & Wessler, 1988; Tsai, 1974; Zhao et al., 2023).

To achieve this, CRISPR-Cas9/TLS constructs will be modified for use in potato (Figure 57). The experimental pipeline will consist of generating transgenic potato scions through traditional *Agrobacterium*-mediated transformation, introducing the Cas9-TLS and gRNA-TLS constructs. These scions will then be grafted onto wild-type rootstocks. The resulting tubers, potentially edited and transgene-free, will be harvested and regrown in soil. Screening for the loss of *GBSS* function will be conducted via iodine staining on tuber slices, allowing us to rapidly identify edited lines.

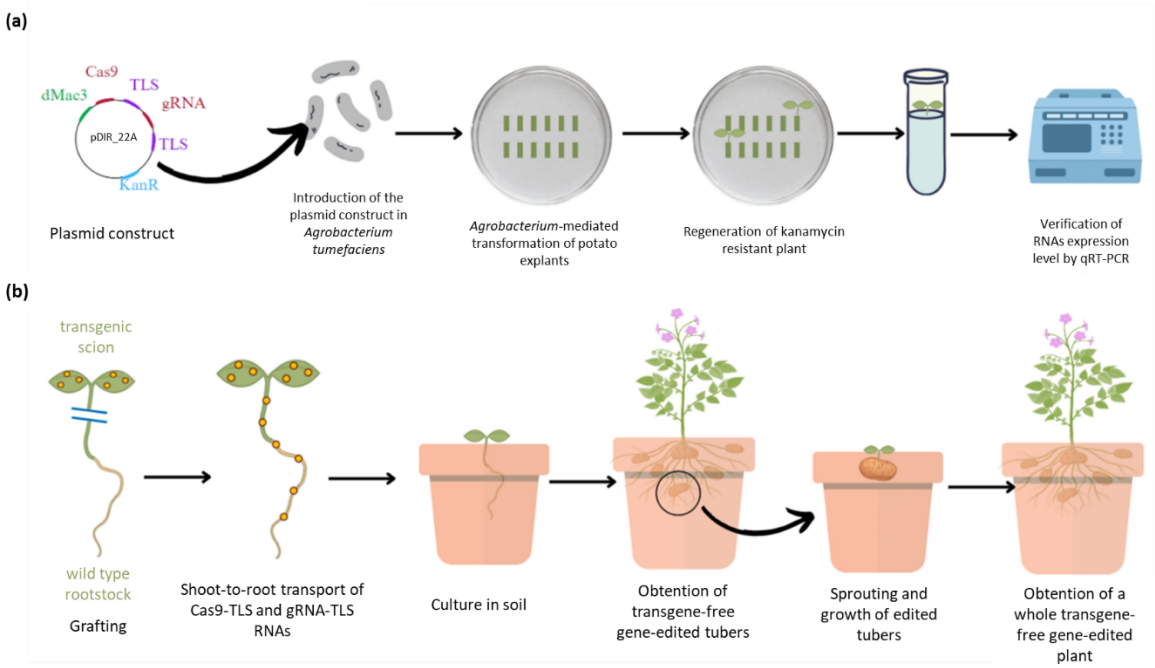

Figure 57 : Workflow of the production of transgene-free gene-edited plants through grafting. (a) Production of the transgenic scion. (b) Production of transgene free gene edited plants though grafting of the transgenic scion on the wild-type rootstock. Cas9-TLS and gRNA-TLS RNAs are represented by the yellow dots.

2. Material and methods

Plasmid construct

To produce transgene-free gene-edited potato plants, the well-established pDIRECT_22A plasmid (Annex 1) for *Agrobacterium*-mediated transformation was used. Modifications were made to the pDIRECT_22A plasmid. The dMac3 sequence was introduced to enhance Cas9 expression in potato, as outlined by (Kusano et al., 2023). This 158 bp sequence, part of the 5'-UTR of OsMac3 mRNA, was positioned upstream of the Cas9 coding sequence and acted as a translation enhancer, significantly multiplying the transformant production rate by three. The original SV40 NLS sequence, essential for nuclear localization, was moved upstream of the Cas9 gene to avoid potential interference with the RNA mobility or the nuclear localization signal due to the presence of both the TLS sequence and SV40 NLS at the end of the Cas9 gene. SfbI and SalI restriction enzymes were used to digest pDIRECt_22A and insert the first fragment (insert 1) containing SV40 NLS and dMac3 sequences. Additionally, a second modification was made to insert the second fragment (insert 2) containing the 74 bp $tRNA^{Met}$ (TLS1) sequence from Yang et al. (2023) downstream

of the Cas9 gene and the gRNA scaffold (Figure 58 and Annex 7), using PmeI and KflI restriction enzymes. Insert 1 and insert 2 were synthesized by the Genscript company. The complete vector map is provided in Annex 8.

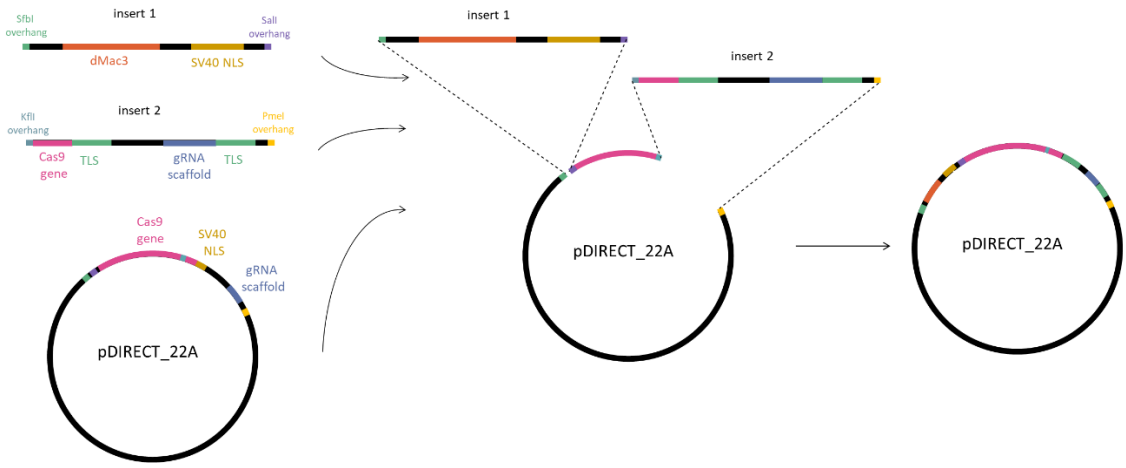

Figure 58 : Plasmid construction for graft-mobile editing system.

Design of the gRNAs targeting *GBSS*

Target specific gRNAs for the GBSS gene were designed using Geneious software and the online tools CRISPR-P (http://crispr.hzau.edu.cn/CRISPR2/) and CRISPOR (http://crispor.tefor.net/). Selection criteria included predicted specificity, efficiency, out-of-frame scores, and absence of SNPs (Sevestre et al., 2020). The RNA folding predictions for the gRNA/gRNA scaffold/TLS were evaluated using the RNAfold webserver (http://rna.tbi.univie.ac.at/), ensuring conformity with the structures described by Yang et al. (2023). These selected gRNAs were subsequently introduced into the plasmid construct following the protocol by Čermák et al. (2017).

Agrobacterium-mediated transformation, regeneration of the plants and assessment of the presence of the *Cas9* gene in these plants were performed as described earlier (page 90).

Grafting procedure

Grafting was performed on two-weeks-old mutant and wild type potato plants. Prior to grafting, plants were grown vertically for 14 days in square Petri dishes containing solid Murashige and Skoog (MS) medium supplemented with vitamins (Duchefa), 2% sucrose, and 0.8% agar. Growth conditions were set to a 16 h light / 8 h dark photoperiod at 22 °C during the day (light intensity: 90 µmol m^{-2} s^{-1}) and 20 °C at night.

For grafting, a clean transverse cut was made 5 mm below a node on the mutant scion and 5 mm above a node the wild-type rootstock, keeping the wild-type roots in contact with the MS medium. The two cut surfaces were carefully aligned, and the grafting junction was stabilized using a 0.5 cm-long silicon (split lengthwise) with an internal diameter of 1.02 mm and an external diameter of 2.16 mm (ref: 60-411-44, VWR).

Following grafting, the plants were maintained vertically on MS plates for approximately 4-6 days, to allow the graft union formation. After this period, the silicon tubes were gently removed, and the successfully grafted plants were transferred to soil and grown in a glasshouse for three months (April to July 2025), under controlled temperature (maximum 25°C) and without specific light conditions.

3. Results

3.1. Design of the gRNAs

Target-specific gRNAs for the GBSS gene were designed using Geneious software and the online tools CRISPR-P and CRISPOR. Selection criteria included predicted specificity scores, cleavage efficiency, out-of-frame scores, and absence of SNPs in the target sequence, resulting in the selection of six candidate gRNAs (Table 5).

To ensure the compatibility of each gRNA with the graft-transmissible editing system described by Yang et al. (2023), RNA secondary structure predictions were performed using the RNAfold webserver. The goal was to replicate as closely as possible the structure of the chimeric RNA molecule described in that study, composed of three elements: the gRNA target, the gRNA scaffold, and a TLS.

Table 5 : guide RNAs (gRNAs) targeting GBSS selected for grafted-mobile editing system. The CFD specificity score, based on a more accurate off-target model, correlates better with actual cleavage events (Doench et al., 2016). Efficiency was predicted using the Doench 2016 model (also known as the Fusi score, range: 0–100), suitable for gRNAs expressed under a U6 promoter (Doench et al., 2016; Fusi et al., 2015). The higher the efficiency score, the more likely is cleavage at this position. The RNA folding predictions for the gRNA/gRNA scaffold/TLS were evaluated using the RNAfold webserver (http://rna.tbi.univie.ac.at/), ensuring conformity with the structures described by Yang et al. (2023) (Annex 14).

gRNA	Sequence	Doench efficiency score	CFD specificity score	Folding prediction of gRNA/gRNA scaffold/TLS RNA
1	AAGTCAATGTACCAGTCCAG	0.69	0.95	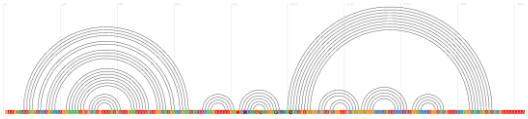
2	TTGTCATTACCCGATGTCCG	0.63	0.99	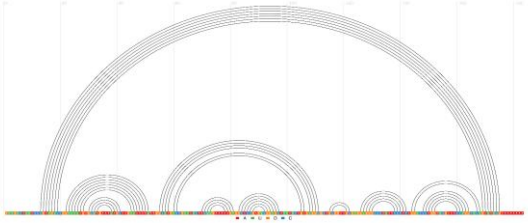
3	CCTTGTCACAGATAGGACTC	0.63	0.99	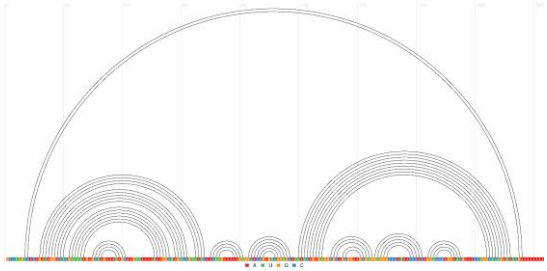
4	CCTGAGTCCTATCTGTGACA	0.61	0.98	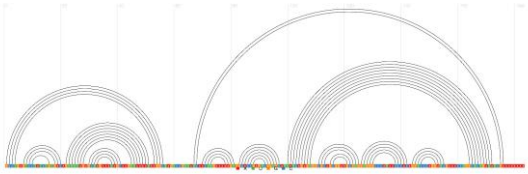
5	AGAACTGAGACCAAGAGACC	0.57	0.98	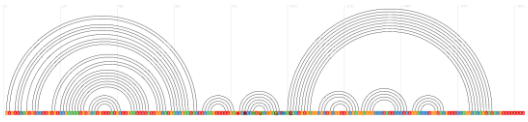
6	ATTTGGTGTCTAGTGAAGTT	0.44	0.84	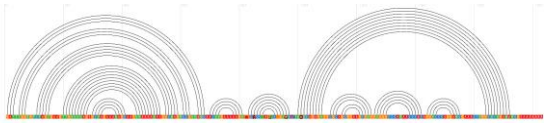

Correct folding was defined based on two key criteria. First, the gRNA target and scaffold regions must form the expected CRISPR-associated hairpin structure, which is

essential for Cas9 recognition and cleavage activity. Improper folding or long unstructured regions within this segment may impair the functionality of the editing complex (Nishimasu et al., 2014). Second, the TLS region must independently fold into a cloverleaf structure mimicking a tRNA. This conformation is essential for ensuring long-distance mobility of the RNA in planta, as demonstrated by Yang et al. (2023).

The presence of unintended interactions (base pairing) between the TLS and the gRNA portion would compromise either the editing function or the mobility of the transcript. Therefore, gRNAs predicted to form stable secondary structures involving the TLS and gRNA segments were excluded. This analysis allowed us to identify gRNA1 and gRNA5 as optimal candidates, which displayed proper and independent folding of both the gRNA and TLS regions, and correct activity and specificity scores.

These gRNAs were subsequently cloned into the final constructs using the Golden Gate assembly protocol described by Čermák et al. (2017).

3.2. Production of the transgenic scion

Transgenic potato lines were generated via *Agrobacterium tumefaciens*-mediated transformation of the nuclear genome. Approximately 600 explants per gRNA (gRNA1 and gRNA5) were co-cultivated with *Agrobacterium*, leading to the regeneration of 40 and 33 plantlets for gRNA1 and gRNA5 respectively. The presence of the *CAS9* gene was assessed by PCR using specific primers (Annex 9). Out of the 15 tested lines, 10 were confirmed to contain the *CAS9* transgene, validating successful transformation and genomic integration (Figure 59).

For grafting experiments, transgenic lines were selected randomly from the confirmed transformants. Specifically, lines #6, #25, # 26, #33, #38 were chosen for gRNA1, and lines #18, #27, #32 for gRNA5.

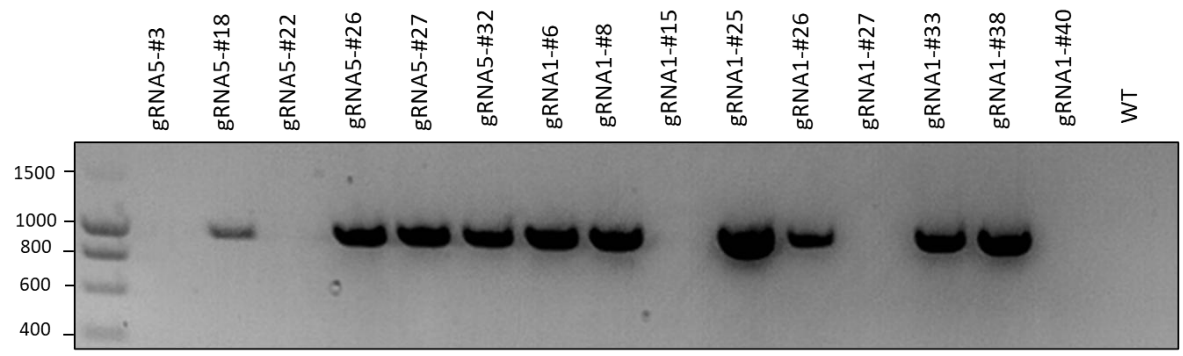

Figure 59 : PCR amplification of a 959 bp region of the *CAS9* gene in mutants. The first lane corresponds to the SmartLadder MW1700-10 (Eurogentec) molecular weight standard, in bp. The last lane is a negative control, from a wild type (WT) plant.

3.3. Grafting of transgenic scions on wild-type rootstocks

The selected transgenic lines, along with wild-type controls, were grown vertically on square Petri dishes containing MS medium for two weeks, to promote root development (Figure 60a). For each selected transgenic line, six grafts were performed by attaching a transgenic scion onto a wild-type rootstock (Figure 60b). Grafts between two wild-type plants served as controls.

A clean transverse cut was made and the graft junction was secured using a longitudinally split silicon tube. The grafted plants were cultured vertically on MS medium for 4-6 days to allow healing (Figure 60c). Once healed, the silicon tubes were removed and the grafted plants were transferred to soil and grown in a controlled growth chamber for 10 days (Figure 60d). This point marked the beginning of the 3-month cultivation period.

Among the 54 grafting attempts carried out with the selected transgenic scions and wild-type rootstocks, only 18 grafts healed and were successfully transferred to soil, with two corresponding to control grafts of wild-type scions onto wild-type rootstocks.. This relatively low success rate highlights the technical difficulty of potato grafting under in vitro conditions and the sensitivity of young shoots during the graft healing process.

After this initial acclimatation phase, plants were transferred to a glasshouse (Figure 60e) and repotted after 10 days (Figure 60f). They were maintained under these glasshouse conditions for the remainder of the cultivation period. Figure 60g was taken after two months of growth illustrates the overall health and development of the plants.

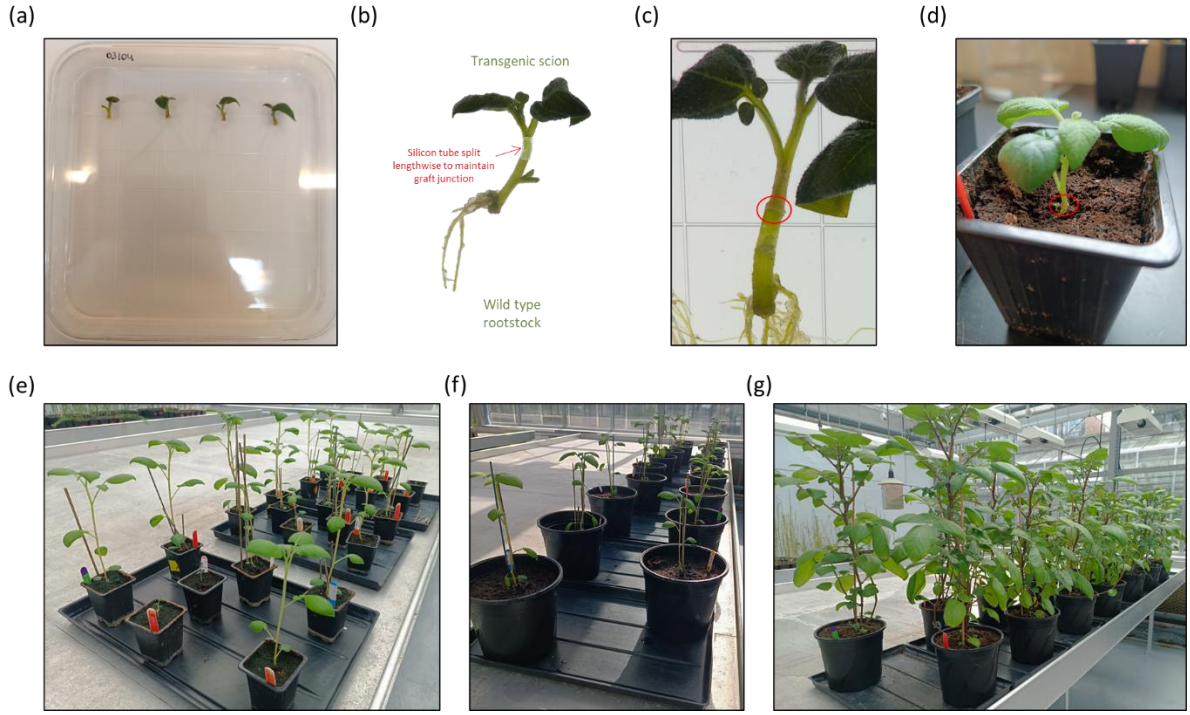

Figure 60 : Workflow of grafting and cultivation of transgenic scions. (a) Transgenic and wild-type potato plants grown vertically on MS medium for root development. (b) Grafting of transgenic scions onto wild-type rootstocks secured with silicone tubes. (c) Grafted plants after the healing phase. (d) Transfer of grafted plants to soil and acclimatization in growth chamber for 10 days. (e) Transfer of acclimated plants to greenhouse. (f) Repotting of plants after 10 days in the greenhouse. (g) Evolution of grafted plants after two months of greenhouse cultivation. In (c) and (d), the red circle designates the graft junction.

These cultures are still ongoing at the time of writing. The objective is to carry the plants to full tuber development, harvest the tubers, and let them sprout. Tubers will be cut into multiple pieces: some will be tested for mutations in the GBSS gene via iodine staining of starch in tuber slices (detecting a shift from blue to reddish staining in amylose-free starch), while others will be planted in soil to regenerate new plants, potentially mutated yet transgene-free lines.

4. Discussion

In this approach, a transgenic scion expressing the CRISPR/Cas9 system fused with TLS motifs was grafted onto a wild-type (non-transgenic) rootstock, with the aim of directing CRISPR/Cas9 RNA molecules into the root system. The long-distance transport mediated by the TLS motifs is expected to enable editing events within the rootstock, and more specifically

in the developing tubers. Importantly, this strategy allows the generation of transgene-free gene-edited tubers, bypassing the stable integration of foreign DNA and responding to both regulatory constraints and public concerns regarding GMOs.

The culture is still ongoing and the results are not known yet. Monitoring RNA mobility directly will help confirm that the gRNA/Cas9 complex reaches the rootstock. qRT-PCR targeting Cas9 transcripts in the root tissues could provide useful insight

The experimental application of this method in potato has faced several technical challenges. Out of all the grafting attempts, only 18 grafted plants could be successfully transferred to soil, highlighting the low efficiency of the grafting process in these conditions. Among them, two corresponded to control grafts between wild-type scions and wild-type rootstocks. Several improvements can be considered to enhance the efficiency of this technique. First, inconsistent stem diameters between scion and rootstock often prevented proper alignment and stable graft junctions. The heterogenous growth of plants made it difficult to match diameters precisely. Increasing the number of plants grown for each line would increase the probability of finding compatible pairs. Second, a lack of contact at the graft site was sometimes observed, possibly due to a slight delay between cutting and alignment, causing partial desiccation of the graft surface. Even when using a microscope, movement or misalignment could occur after grafting. Future attempts could benefit from performing cuts in a humid environment and immediately securing contact with tighter mechanical support. Moreover, vertical positioning of the Petri dishes post-grafting may have contributed to graft failure, as gravity and minor disturbances during manipulation led to graft separation. Horizontal positioning or slightly embedding the base of the graft junction in soft agar may help prevent movement. Third, maintaining sterility during grafting proved to be particularly difficult, and contamination on the MS medium was frequently observed, potentially weakening or stressing the grafted plants. Reinforced aseptic techniques could be considered to reduce this risk. Finally, post-graft handling also appeared critical: several grafts began healing successfully but broke during the transition to soil due to insufficient mechanical support. Allowing a longer healing phase before transfer and keeping the silicon tube may help.

From a strategic standpoint, even if this method does not yet lead to the recovery of full knock-out mutants, its primary objective remains the generation of genetically edited,

transgene-free plants. In this context, detecting even partial or mosaic edits is informative. If no knockout mutations are observed in the resulting tubers, this does not invalidate the method: the primary objective is to demonstrate that CRISPR-induced editing is possible without integrating foreign DNA. Even a slight change in iodine staining (from dark blue to reddish-brown) would indicate a modification in amylose content and provide strong evidence of gene editing at the *GBSS* locus. These preliminary observations would be followed by genotyping to confirm the presence of targeted mutations. Further improvements could include the design of new gRNAs. gRNA1 and gRNA5 were selected based on predicted folding and scoring parameters, but their actual efficiency in planta remains to be demonstrated. Additional gRNAs targeting different exons or with improved activity scores could increase the chances of success. Finally, further optimization of TLS fusion constructs or delivery conditions may also enhance long-distance transport and editing efficiency. Alternative promoters, such as tissue-specific or stronger constitutive promoters, may enhance Cas9 expression in the scion and improve RNA mobility.

In summary, although the system requires optimization, it represents a very promising strategy for producing transgene-free edited plants, particularly relevant for clonally propagated crops like potato. Ongoing greenhouse cultivation of grafted plants aims to recover tubers for testing. These will be allowed to sprout and be sectioned, enabling both iodine staining and molecular genotyping. If successful, the germinated segments will be propagated to establish entirely transgene-free edited lines, thereby validating this editing strategy.

ANNEX PROJECT 2 : ENZYMATIC CHARACTERIZATION OF SS6

1. Introduction

Starch-synthases (SSs) are glycosyltransferases responsible for the elongation of starch glucans (D'Hulst et al., 2015). These enzymes catalyze the transfer of a glucosyl unit onto an elongating glucan using ADP-glucose (ADP-Glc) as a donor substrate and releasing ADP (D'Hulst et al., 2015). Six isoforms of SSs have been characterized. SS1, SS2 and SS3 elongate amylopectin chains while GBSS synthesizes amylose glucans (Rongine De Fekete et al., 1960; Szydlowski et al., 2011b; X. Zhang et al., 2008). On the other hand, SS4 and SS5 participate to starch initiation in an intricate mechanism requiring protein-protein interactions and that have not been fully elucidated (Abt et al., 2020; Crumpton-Taylor et al., 2013; Roldán et al., 2007). Although starch metabolism is not completely understood, this polymer is widely used by industries in food and non-food applications (S. Jobling, 2004). Mutants for SS genes accumulate modified starches with rheological properties of interest. A well-known example is "waxy" starch produced by *gbss*– mutants (Tsai, 1974). This starch is devoid of amylose, gelatinize easily and is used as a texturizing agent in food products (Ellis et al., 1998).

Recently, an additional isoform named Starch Synthase 6 (SS6) was identified in potato (Helle et al., 2018). This protein, absent from *Arabidopsis thaliana* and cereals, has never been characterized (Figure 61). SS6 sequence is highly similar to known starch synthases but phylogenetic analyses demonstrate that it constitutes a distinct class from those previously identified (Helle et al., 2018) (Figure 61). The presence of this new class of starch synthases has been detected in potato starch granule by mass spectrometry (Helle et al., 2018). The SS6 class belongs to the group B starch synthases, similar to SS3-5, and most closely resembles SS4 (Leterrier et al., 2008) (**Figure 62**). Additionally, the SS6 sequence contains the highly conserved K-X-G-G-L and X-X-G-G-L motifs, suggesting a role in the elongation of α-1,4-linked starch polysaccharides. Interestingly, SS6 differs from SS4 by the absence of the long N-terminal extension, but both proteins share the catalytic glucosyltransferase domain (**Figure 62**). SS6 belongs to the group B of starch synthases, similar to SS3-5 (Leterrier et al., 2008) (**Figure 62**), that are known to be involved in granule initiation in Arabidopsis thaliana (only in absence of SS4 for SS3) (Abt et al., 2020; Roldán et al., 2007; Szydlowski et al., 2009). Then, we hypothesized that SS6 may be one the actors involved in granule initiation in potato tuber.



Figure 61 : Cladogram of the proteins most closely related to *Solanum tuberosum* SS6 across major plant groups. The most similar sequences to *Solanum tuberosum* SS6 were retrieved using BLASTP with the StSS6 protein sequence as a query. The cladogram was constructed using the neighbor-joining method in Geneious software. Some groups were colored to facilitate interpretation of the figure (Sevestre, 2020)

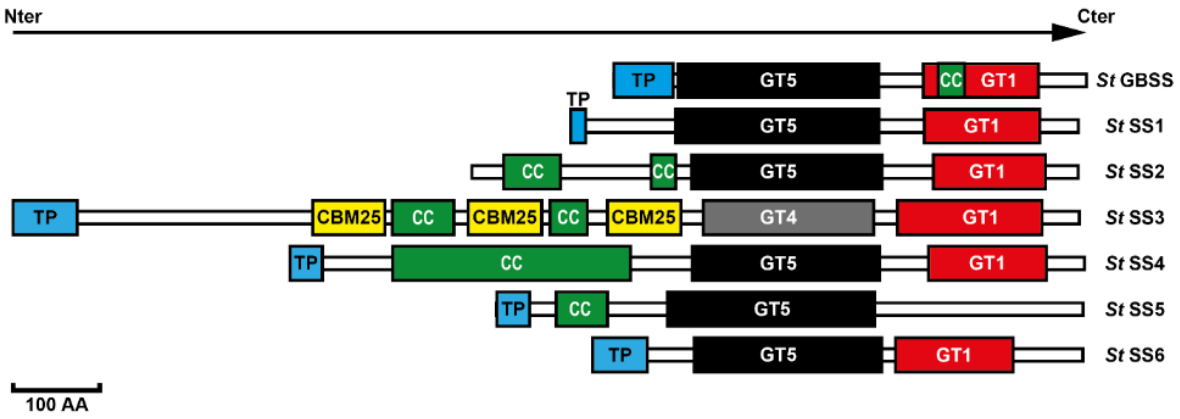

Figure 62 : Domain structure of Starch Synthases (SSs) from potato. Different structural domains are highlighted. Black and red boxes represent glycosyl-transferase domain (GT1, GT4 and GT5). Yellow boxes represent Carbohydrate Binding Domain (CBM). Green boxes represent coiled-coil (CC) regions, involved in protein-protein interaction. Blue boxes represent transit peptide signal. *St*: *Solanum tuberosum*, GBSS : Granule Bound Starch Synthase, SS : soluble Starch Synthase, AA : amino acids. (Helle et al., (2018)).

This secondary project is based on the previous work of François Sevestre, who characterized the phenotype of *ss6* potato knockout mutants and initiated the production of recombinant SS6 protein. In the present study, my objective was to produce the recombinant SS6 protein and investigate its enzymatic properties. To achieve this, we first developed a method for assessing starch synthase activity using capillary electrophoresis. This approach provides a precise and sensitive means of characterizing the enzymatic function of SS6, offering new insights into its role in starch biosynthesis. Further understanding the role of SS6 isoform is the main objective of the present study.

2. A capillary electrophoresis method for determining starch-synthase activities

2.1. Introduction

Characterization of starch synthase activities has long relied on the incorporation of radioactive glucose using ^{14}C-labeled ADP-Glc as a substrate (Delvallé et al., 2005). While sensitive, this method involves the use of expensive radioactive materials and requires strict safety protocols, limiting its accessibility. Other approaches have been developed, based on the quantification of released ADP. For example, luminescence assay using luciferase allowed

to quantify ADP following its conversion in ATP by pyruvate kinase and the subsequent use of the luciferin-luciferase system (Ching, 1982). Although effective, this approach requires multiple enzymatic steps and costly reagents. More recently, SS4 Raynaud et al., (2016) used high-performance liquid chromatography (HPLC) with photodiode array detection to assess the activity of Arabidopsis SS4, offering improved precision but requiring specialized equipment and approximately five times more ADP-Glc than our method.

In this context, we developed a capillary electrophoresis method to measure ADP production during starch synthase activity assays. This approach offers a simple, precise, and cost-effective alternative that does not require radioactive substrates or enzymatic amplification steps. In addition, capillary electrophoresis provides high resolution and allows direct quantification of reaction products. Capillary electrophoresis offers high resolution and allows the direct quantification of ADP, while requiring lower substrate quantities than previously described methods. Additionally, it enables more precise monitoring of reaction specificity and potentially allows characterization of the size distribution of synthesized glucans, making it a powerful tool for studying starch synthase activity with both sensitivity and efficiency.

2.2. Methods

A PA800 plus apparatus (Sciex separations, Les Ulis, France) equipped with a photodiode array detector (PAD) and set on normal polarity was used for this study. Separation was performed in a 50 µm internal diameter., 375 µm outer diameter bare fused silica capillary of 60.2 cm in length. Injection was carried out at 0.5 psi during 10 sec prior to separation at 30 kV in 100 mM borate buffer pH 8.5. Each run was preceded by 3 rinses at 20 psi (0.1 N NaOH; ultrapure water; capillary performance run buffer A) during 1, 1 and 1.5 min, respectively, in forward pressure mode.

1.5 mM solutions of ADP and ADP-G standards (Sigma-Aldrich, Saint-Quentin-Fallavier, France) were prepared in a routine SS enzymatic activity mix incubation buffer (50mM glycylglycine sodium hydroxide buffer, pH 9.0, 100mM ammonium sulfate, 5mM magnesium chloride, 0.25g.L-1 bovine serum albumin, 5mM 2-mercaptoethanol) prior to hydrodynamic injection. Absorbance scans (between 190 nm and 300 nm) were recorded during 15 min with

a data rate of 4 Hz (Figure 63). ADP was detected at about 7.2 min (Figure 63a to c) while ADP-Glc was observed at 6.5 min (Figure 63d to f). Both compounds showed similar absorbance spectra with one peak at a maximum absorbance of 215 nm and a second peak at about 260 nm (Figure 63a, b, d and e).

In order to evaluate detection linearity, serial dilutions of the ADP solution were performed in the SS activity incubation buffer. 1.5, 0.75, 0.38, 0.19 and 0.01 mM ADP standard solutions were then injected and peak areas were determined on the absorbance max plot with 32 karats software (Figure 64). In the range of 0.01 to 1.5 mM, peak areas followed a linear model (Figure 64b) and the latter detection range was used in the rest of study.

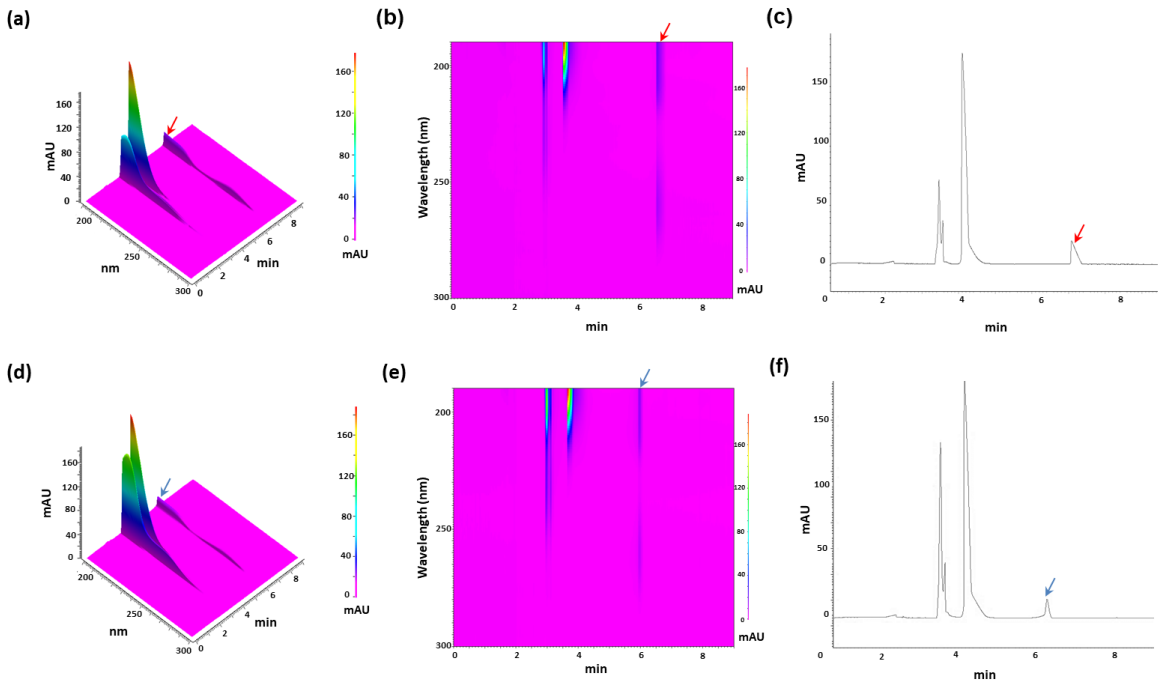

Figure 63 : Electrophoretic profiles of ADP and ADP-glucose standards. 1.5 mM solutions of ADP (a, b and c) or ADP-Glc (d, e and f) were injected at 0.5 psi during 10 sec prior to electrophoretic run at 30 kV during 9 min in 100 mM borate buffer, pH 8.5. 3D- (a and d) and 2D-plots (b and e) were drawn with 32 karats software and show the absorbance spectra (in milliabsorbance units, mAU) in the 190 - 300 nm range over time. (c) and (f) correspond to the max plot spectra. In (a) to (c), the red arrow designates ADP peak, at approximately 7.2 min. In (d) to (f), the blue arrow designates ADP-Glc peak, at approximately 6.5 min.

We were prompt to apply this method for determining starch synthase activities. Since no SS is commercially available, we investigated the activity associated to potato starch granules as this was already described by (Ching, 1982). Some SSs are associated with starch

granules and GBSS activity can be observed by directly incubating starch granules with ADP-Glc.

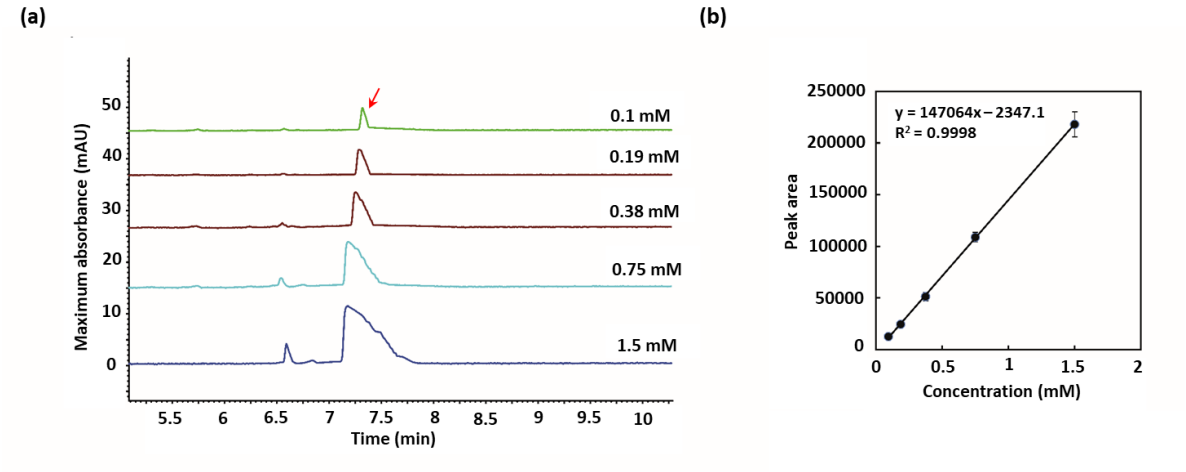

Figure 64 : Linearity of ADP detection. (a) Electrophoretic profiles of ADP standards at different concentrations. A 1.5 mM solution of ADP in SS activity incubation buffer was submitted to serial dilutions prior to CE analysis. (b) Peak areas in (a), at 7.3 min were plotted versus ADP concentration in mM. Error bars represent the standard deviation of three experimental replicates.

Starch granules were isolated from commercial potato tubers according to (Helle et al., 2018) and resuspended in SS activity incubation buffer containing 1 mM ADP-G. Enzyme activity was then followed by measuring released ADP during 60 min at 30 °C (Figure 65). After incubation for the indicated amount of time, starch samples were heated at 100 °C for 15 min prior to centrifugation at 14680 g during 15 min. The supernatant was directly used for capillary electrophoresis analysis as described above. The concentration of released ADP was determined with the use of the equation in Figure 64b. The reaction rate was estimated at 0.08 nmol.min^{-1} which is in accordance with previous descriptions (Figure 65b) (Ahmed et al., 2015; Ching, 1982; Fulton et al., 2002).

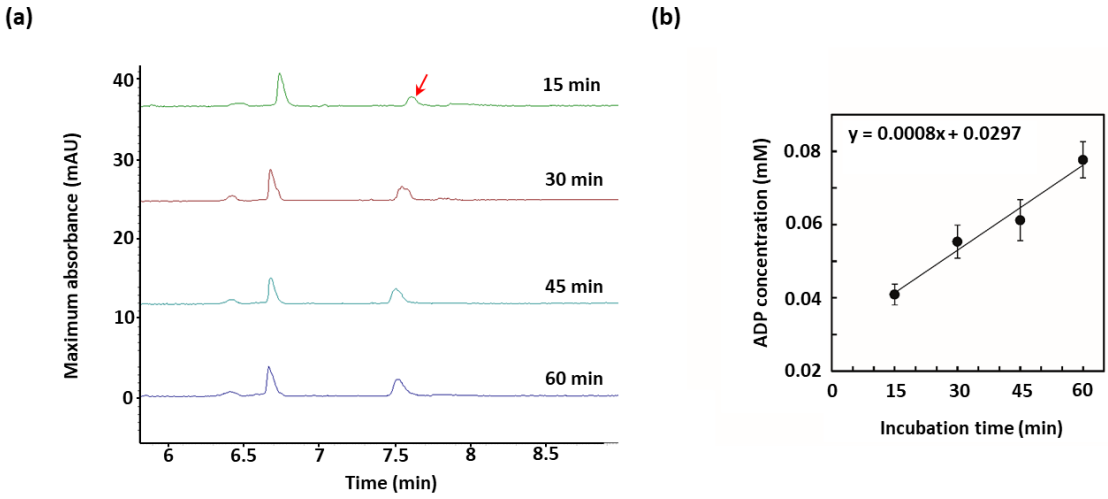

Figure 65 : GBSS activity assay. (a) Electrophoretic profiles of 5 mg of starch granules purified from potato tubers, incubated with 100 µL of SS activity incubation buffer (50 mM glycylglycine sodium hydroxide buffer, pH 9.0, 100 mM ammonium sulfate, 5 mM magnesium chloride, 0.25 $g.L^{-1}$ bovine serum albumin, 5 mM 2-mercaptoethanol) during 15, 30, 45 or 60 min, prior to CE analysis. (b) Released ADP was quantified using peak areas of the max plot spectra in (a), at 7.6 min, and the equation in Figure 64b. Error bars represent the standard deviation of three experimental replicates.

3. Production, purification and enzymatic characterization of SS6 protein

This subchapter describes the production, purification and enzymatic characterization of the recombinant SS6 protein carried out using the method we developed and which is described in the previous paragraph.

3.1. Material and methods

Bacterial material

SS6 recombinant protein was produced in *Escherichia coli* BL21-AI strain (genotype: F^- *ompT* *hsdS*$_B$ (r_B^- m_B^-) *gal* *dcm* *ara*B::T7RNAP-*tet*A). This strain was chosen for its low expression of the protein in the absence of induction factors. These factors include L-arabinose, which enables the expression of T7 RNA polymerase and isopropyl ß-D-1

thiogalactopyranoside (IPTG), which induces protein expression, that is under the dependance of the lacI promoter, via T7 RNA polymerase.

Production of SS6 recombinant protein

An aliquot of chemically competent *E.coli* BL21-AI was transformed with pET28-a(+)-SS6 (Annex 15). This plasmid allows the fusion of a His-TAG to the C-ter of our protein of interest allowing its purification. After selection of the transformed bacteria on LB plates containing kanamycin (50 $mg.mL^{-1}$), a 300 mL culture was launched and grown at 37°C until OD_{600} reaches 0.6. A sample was collected as a pre-induction control. Protein expression was induced by adding 0.1 mM of L-arabinose and 0.2 % of IPTG, respectively. The incubation temperature was immediately reduced to 20 °C for overnight growth.

The culture was placed on ice for 15 min before centrifugation at 4,000 g for 15 min at 4 °C. The supernatant is discarded, and the pellet is resuspended in 1 mL of lysis buffer (phosphate buffer, 30 mM imidazole, Roche Complete Protease Inhibitor cocktail). Cell lysis is performed using sonication 8 times at 60% during 30 sec. The lysate was centrifuged at 4000 g for 30 min at 4°C. Insoluble and soluble fractions were collected.

Purification of SS6 recombinant protein

The soluble protein extract containing SS6 protein was placed in a 10 mL plastic column with 2mL nickel-NTA (nitrilotriacetic acid) chelate microbeads (Ni-NTA HisPur™; Thermo Scientific™) and gently mixed for 1 hour at 4 °C. Then, the column was set vertically to allow sedimentation, and excess liquid, corresponding to unbound fraction, was removed. The resin was washed to eliminate non-polyhistidine-tagged proteins by rinsing four times with 25 mL of phosphate buffer containing 60 mM imidazole. The wash fractions were collected. 2.5 mL of phosphate buffer containing 500 mM imidazole was then added four times through the column to elute the recombinant protein and collected. After SDS-PAGE analysis, the fraction containing the pure recombinant protein was dialyzed using a membrane with a cutoff of 6-8 kD (Spectrum™) overnight in phosphate buffer 1X. The protein was then frozen in liquid nitrogen with the addition of 5% glycerol and stored at −80 °C for later use.

SDS-PAGE and native gel

An SDS-PAGE was performed to allow the separation of denatured proteins according to their molecular mass. The polyacrylamide concentrations were 5% in stacking (125 mM Tris-HCl pH 6.8 and 0.5% SDS) and 8% in running (375 mM Tris-HCl pH 8.8 and 0.1% SDS) gels, respectively. Protein samples were dissolved in a denaturing buffer containing 0.375 M Tris, 2 mM DTT, 1.4 M SDS, 2% glycerol (v/v), and 0.02% bromophenol blue (w/v). Low and high-molecular weight (LMW and HMW, respectively) protein markers were used for gel calibration. Electrophoresis was carried out at 75 V per gel in a migration buffer composed of 25 mM Tris, 192 mM glycine and 0.1% SDS [w/v]. After migration, the gel was stained using InstantBlue® Coomassie (Sigma-Aldrich) for 15 min.

A native gel was performed to observe starch synthases activities under non-denaturing conditions. The gel is similar to the previously described one, with exception of the following modifications. The separating gel contained 10% acrylamide, and 0.3% glycogen as a substrate. Migration occurs under a constant voltage of 75 V per gel for 2 hours and 30 minutes at 4 °C in a migration buffer identical to the previous one, but without SDS. After migration and rinsing with water, the gel is incubated overnight at room temperature in an incubation buffer (50 mM glycylglycine sodium hydroxide buffer, pH 9.0, 100 mM ammonium sulfate, 5 mM magnesium chloride, 0.25 g.L-1 bovine serum albumin, 5 mM 2-mercaptoethanol, 1 mM ADP-Glc). Finally, starch synthase activity is detected by incubating the gel for 30 min in a Lugol solution (0.1% I2, 1% KI).

Enzymatic characterization - General Conditions

All analyses were performed using the method developed in this study, as detailed in Section 2.2 (page 183). Briefly, experiments were carried out a PA800 Plus apparatus (Sciex Separations, Les Ulis, France) equipped with a photodiode array detector (PAD) and set to normal polarity. Separation was carried out in a 50 µm internal diameter, 375 µm outer diameter bare fused silica capillary of 60.2 cm in length. Injection was conducted at 0.5 psi for 10 seconds prior to separation at 30 kV in 100 mM borate buffer at pH 8.5. Each run was

preceded by three rinses at 20 psi (0.1 N NaOH, ultrapure water, and Capillary Performance Run Buffer A) for 1, 1, and 1.5 minutes, respectively, using forward pressure mode.

The incubation buffer consisted of 50 mM glycylglycine sodium hydroxide buffer, pH 9.0, 100 mM ammonium sulfate, 5 mM magnesium chloride, 0.25 $g.L^{-1}$ bovine serum albumin, and 5 mM 2-mercaptoethanol, 1 mM ADP-Glc.

A single batch of purified recombinant SS6 (63 $\mu g.mL^{-1}$) was used for this study. For each sample, reaction was stopped by boiling the tubes at 100°C for 15min. After a centrifugation step at 14680 rpm for 15 min, the supernatant was directly put in microvials for analysis.

ADP Standard Curve

Serial dilutions of the ADP standard (Sigma-Aldrich) were prepared in the incubation buffer (lacking ADP-Glc) at concentrations of 1.5, 0.75, 0.38, 0.19, and 0.1 mM. These solutions were injected, and peak areas were determined using 32 Karat software.

Kinetic Analysis of SS6 with Glycogen

Different tubes containing recombinant SS6 were incubated with glycogen at different incubation period (0, 5, 10, 15, 30, 45, 60, 90 min) to determine the linear phase of the reaction. Each reaction contained 5 µL of enzyme, 45 µL of incubation buffer, and 10 $g.L^{-1}$ oyster glycogen.

Optimal pH Determination

SS6 was incubated in different incubation buffers with varying pH values (pH 6, 7, 8, 9 and 10). Each reaction contained 5 µL of enzyme, 45 µL of incubation buffer, and 10 $g.L^{-1}$ oyster glycogen. Incubations were performed at 30°C for 45 minutes.

Optimal Temperature Determination

SS6 was incubated at different temperatures (20, 25, 30, 35, 40°C) to determine the optimal reaction conditions. Reactions contained 5 µL of enzyme, 45 µL of incubation buffer, and 10 $g.L^{-1}$ oyster glycogen, and incubations were performed for 20 minutes.

Determination of SS6 affinity for ADP-Glc

The affinity of SS6 for ADP-Glc was determined by incubating the enzyme with varying ADP-Glc concentrations (0, 0.1, 0.25, 0.5, 1, 2, 3, 5 mM). Each reaction contained 5 µL of enzyme, 45 µL of incubation buffer with different ADP-Glc concentrations, and 10 $g.L^{-1}$ oyster glycogen. Incubations were carried out at 30°C for 60 minutes.

Substrate Preference of SS6

SS6 was incubated with different substrates (DP1 to DP7) to determine its substrate preference. Each reaction contained 5 µL of enzyme, 45 µL of incubation buffer, and 10 mM of the respective substrate. Incubations were performed at 30°C for 15 minutes.

Reaction Products on Amylopectin

SS6 was incubated with amylopectin, and the chain length distribution (CLD) of reaction products was analyzed. Each reaction contained 5 µL of enzyme (63 µg/mL), 45 µL of incubation buffer, and 10 mM amylopectin. Incubations were performed at 30°C for 30 minutes, and CLD analysis was conducted as previously described. Briefly, after incubation with SS6, amylopectin was gelatinized by heating at 100°C with regular stirring. It was then debranched at 42°C overnight with 20 U of isoamylase and 1 U of pullulanase (Sigma). The samples were then desalted on Alltech Carbograph columns and freeze-dried. Dried samples were labeled using 2 µL of cyanoborohydride in tetrahydrofuran (THF) and 2 µL of 200 mM 8-aminopyrene-1,3,6-trisulfonic acid (APTS) in 15% acetic acid and incubated at 42°C overnight. 46µL of ultrapure water was added and the samples were diluted 50 times with ultrapure water. They were then analyzed in a SCIEX PA 800 Plus Pharmaceutical Analysis System equipped with a laser induced fluorescence detector according to (Fermont et al., 2022).

3.2. Results

3.2.1. Production of the SS6-His-TAG recombinant protein

Purification of recombinant SS6 was assessed using Ni-NTA resin (Figure 54). In the SDS-PAGE analysis (Figure 54a), non-bound proteins were efficiently eliminated in the flow-through and wash fractions. A distinct band corresponding to the expected size of SS6-His (66 kDa) is observed in elution fractions 1 and 2 (EF1 and EF2), with a stronger signal in EF2. This band remains visible after dialysis (dEF2).

In the native gel assessing starch synthase activity (Figure 54b), strong enzymatic activity was detected in the soluble extract before purification (fraction SE). A portion of this activity was lost in the first wash fraction (W1), suggesting the removal of some non-specifically bound proteins. The majority of enzymatic activity was recovered in the elution fraction EF2, and although slightly diminished, remained clearly detectable after dialysis in the dEF2 fraction. Despite this loss, dEF2 was retained for subsequent enzymatic characterization of SS6.

An intense band with high affinity for glycogen was detected near the top of the gel after dialysis and was identified by mass spectrometry as *Escherichia coli* glycogen synthase. However, in the non-dialyzed sample, this band was very faint, making it unlikely that the enzymatic activity observed after dialysis could be primarily attributed to glycogen synthase from *E.coli*. Moreover, mass spectrometry analysis of the dEF2 fraction revealed that SS6 was approximately 10,000 times more abundant than glycogen synthase. These results confirm that the activity detected in our assays originates predominantly from SS6 and not from residual *E. coli* glycogen synthase.

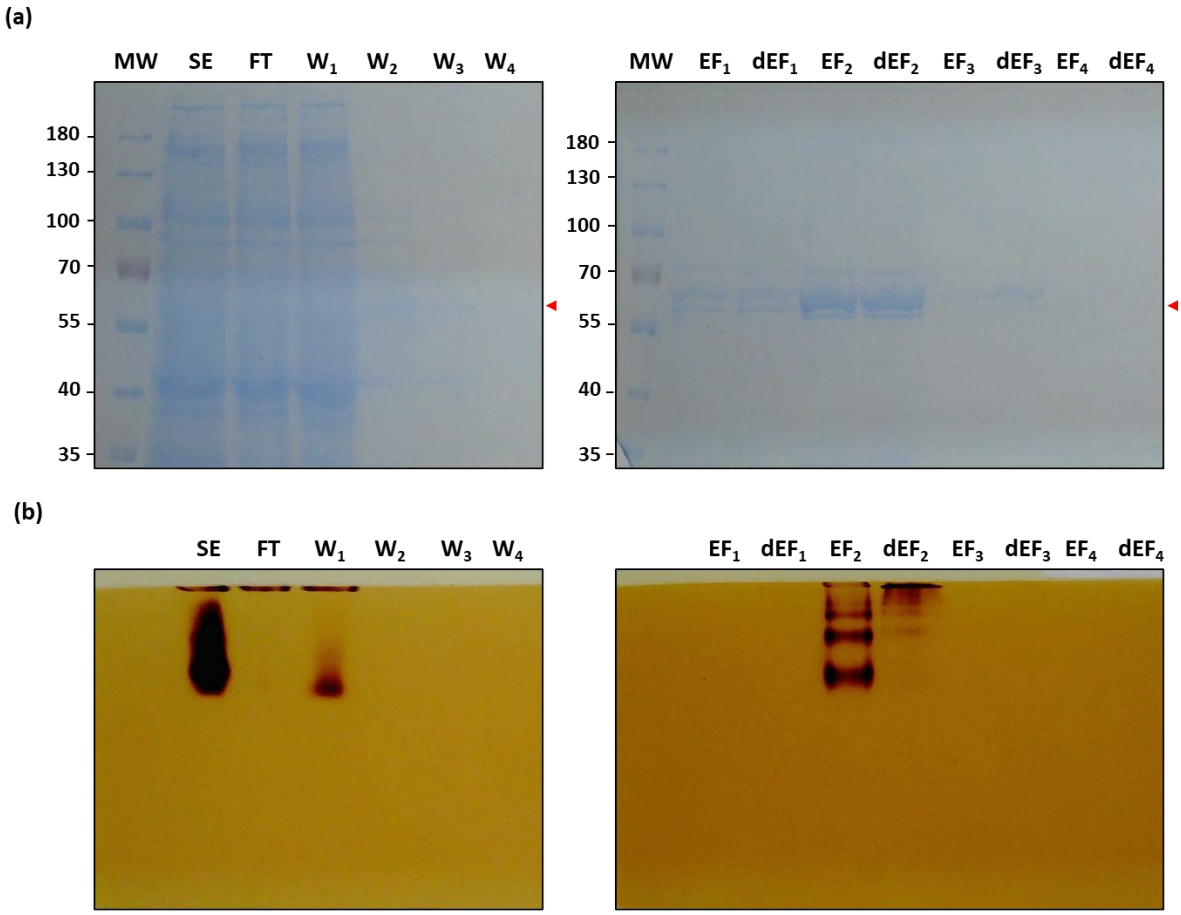

Figure 66 : Purification of recombinant SS6 using Ni-NTA resin. (a) SDS-PAGE analysis of purification fractions. The expected band size for SS6-His is 66 kDa, indicated by red arrows. (b) Native gel showing starch synthase activity in purification fractions. MW, molecular weight marker (kDa); SE, soluble extract (before purification); FT, flow-through; W1–W4, wash fractions 1–4; EF1–EF4, elution fractions; dEF1–dEF4, dialyzed elution fractions EF1–EF4.

3.2.2. Enzymatic characterization of SS6 recombinant protein

The ADP standard curve used in this study is presented in Figure 64. The kinetic analysis of SS6 with glycogen showed a linear reaction phase even after 90 minutes, indicating prolonged enzyme activity under the tested conditions with a linear trend presenting a R^2 value of 0.9882, confirming the reliability of ADP quantification (Figure 67a).

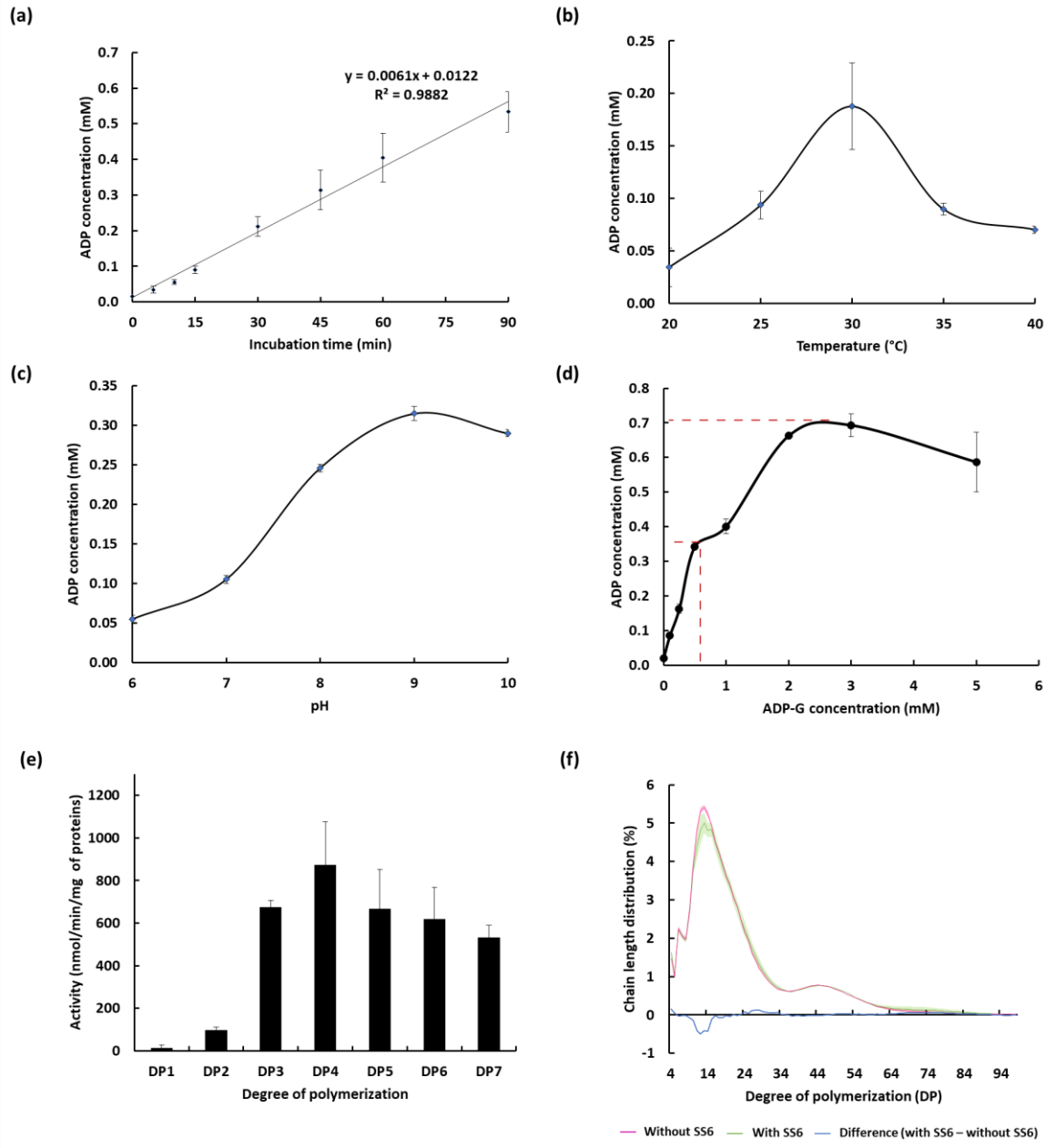

Figure 67 : Enzymatic characterization of recombinant SS6. (a) Kinetics of SS6 with glycogen. (b) Optimal temperature. (c) Optimal pH. (d) Determination of Km for ADP-Glc. Red dotted lines indicate the values used for Km determination with the upper line representing Vmax and the lower line representing Vmax/2. (e) Substrate preference among maltooligosaccharides (DP1-7). (f) Chain length distribution of reaction products of amylopectin incubated with (green) or without (pink) SS6. The blue line represents the difference between the chain length distributions of amylopectin incubated without SS6 and with SS6. The shaded areas around the green and pink curves represent the uncertainty, calculated as the standard error (SE). For (a) to (f), values represent the mean ± SE of three experimental replicates (n = 3).

The optimal pH for SS6 activity was determined to be 9.0, while the optimal temperature was found to be 30°C (Figure 67b and c). The affinity of SS6 for ADP-Glc,

represented by its Km value, was calculated in the presence of glycogen (Figure 67). The Vmax value is reached for an ADP concentration of 0.7mM. The Km value is found at Vmax/2 = 0.7/2 = 0.35. The ADP-Glc concentration is 0.5mM, representing the Km. Substrate preference assays revealed that SS6 exhibited the highest activity in the presence of DP4, suggesting a preference for this substrate over others (Figure 67e). The analysis of reaction products on amylopectin revealed slight changes in the chain length distribution, with a small decrease in medium chains (DP 10–15) and a slight increase in longer chains (DP 27–37) (Figure 67f). However, these changes are minimal, with the increase accounting for only 0.5 percentage points, indicating that SS6 does not significantly alter the amylopectin structure under the tested conditions.

4. Discussion

In this study, we developed a capillary electrophoresis-based method to measure starch synthase activity, offering a fast and accurate alternative to conventional assays. This method allows for a 150-fold detection range without the need for complex sample preparation. Additionally, the automated injection system enables medium-throughput analysis, improving efficiency. Finally, it eliminates the use of radiolabeled compounds, reducing costs and improving safety.

The enzymatic characterization of SS6 revealed key functional properties, including its optimal pH, temperature, substrate preference, and affinity for ADP-Glc. The reaction kinetics with glycogen showed sustained enzymatic activity, suggesting a role in prolonged glucan synthesis or modification. The enzyme displayed optimal activity at pH 9.0 and 30°C, aligning with the alkaline conditions observed for starch synthase activity. This is consistent with earlier findings from Ponstein et al. (1990), who reported that potato starch synthases exhibited maximal activity within a pH range of 8.8 to 9.1.

The calculated Km value of 0.5 mM for ADP-Glc suggests a moderate substrate affinity, seven-times lower than SS2 affinity for ADP-Glc in presence of amylopectin for example (Km = 0.07) (Edwards et al., 1999), but equivalent or even higher than the affinity of SS4 for ADP-Glc in presence of amylopectin (0.47) or glycogen (0.96) (Szydlowski et al., 2009). Furthermore, SS6 displayed a strong preference for DP4 maltooligosaccharides, implying a possible role in initiating glucan chain elongation rather than extending long-chain

polysaccharides. This is also suggested by its similarity with SS4, a protein known to be involved in granule initiation (Roldan et al, 2007, Helle et al, 2018).

Interestingly, SS6 had only a minor impact on amylopectin chain length distribution. A slight decrease in medium-length chains (DP 10–15) was accompanied by a modest increase in longer chains (DP 27–37), but these changes were minimal (only 0.5 percentage points). This limited effect suggests that SS6 is not a major determinant of amylopectin structure and may require additional cofactors or interact with other enzymes to exert a more significant effect on starch architecture.

Instead, our results open the possibility that this protein might be involved in starch granule initiation rather than elongation. This hypothesis is supported by several observations. First, the phylogenetic analysis shows that SS6 is more closely related to SS4 and SS5, two starch synthases known to participate in granule initiation (Abt et al., 2020; Hu et al., 2025; Roldán et al., 2007), than to SS1 and SS2, which are directly involved in amylopectin chain elongation. Second, the enzymatic characterization performed in this study reveals that SS6 preferentially acts on short glucan chains, particularly DP4 (Figure 67e). a similar specificity has been reported for SS4, further supporting the idea of a shared functional profile. Third, SS6 displays very limited activity on amylopectin, a feature that once again mirrors SS4 (Roldán et al., 2007) and contrasting with elongating enzymes.

Altogether, these findings suggest that SS6 may play a minor role in amylopectin biosynthesis, but could contribute to early steps of granule formation in potato tuber. This hypothesis remains to be fully tested, but it provides a direction for future research. Notably, *ss6* mutant lines were produced during the PhD work of F. Sevestre (2020), and their detailed phenotypic characterization should provide crucial insights into SS6 function in starch metabolism.

Overall, these findings contribute to a deeper understanding of SS6 function within starch biosynthesis. Understanding starch metabolism is essential for biotechnological applications, including crop improvement strategies to enhance the nutritional, industrial, and functional properties of starch.

Literature

Abel, G. J. W., Springer, F., Willmitzer, L., & Kossmann, J. (1996). Cloning and functional analysis of a cDNA encoding a novel 139 kDa starch synthase from potato (Solanum tuberosum L.). *The Plant Journal*, *10*(6), 981-991. https://doi.org/10.1046/j.1365-313X.1996.10060981.x

Abt, M. R., Pfister, B., Sharma, M., Eicke, S., Bürgy, L., Neale, I., Seung, D., & Zeeman, S. C. (2020). STARCH SYNTHASE5, a Noncanonical Starch Synthase-Like Protein, Promotes Starch Granule Initiation in Arabidopsis. *The Plant Cell*, *32*(8), 2543-2565. https://doi.org/10.1105/tpc.19.00946

Adamson, J. G., Zhou, N. E., & Hodges, R. S. (1993). Structure, function and application of the coiled-coil protein folding motif. *Current Opinion in Biotechnology*, *4*(4), 428-437. https://doi.org/10.1016/0958-1669(93)90008-K

Adewale, P., Yancheshmeh, M. S., & Lam, E. (2022). Starch modification for non-food, industrial applications : Market intelligence and critical review. *Carbohydrate Polymers*, *291*, 119590. https://doi.org/10.1016/j.carbpol.2022.119590

Ahmed, Z., Tetlow, I. J., Ahmed, R., Morell, M. K., & Emes, M. J. (2015). Protein-protein interactions among enzymes of starch biosynthesis in high-amylose barley genotypes reveal differential roles of heteromeric enzyme complexes in the synthesis of A and B granules. *Plant Science: An International Journal of Experimental Plant Biology*, *233*, 95-106. https://doi.org/10.1016/j.plantsci.2014.12.016

Albrecht, T., Koch, A., Lode, A., Greve, B., Schneider-Mergener, J., & Steup, M. (2001). Plastidic (Pho1-type) phosphorylase isoforms in potato (Solanum tuberosum L.) plants : Expression analysis and immunochemical characterization. *Planta*, *213*(4), 602-613. https://doi.org/10.1007/s004250100525

Apriyanto, A., Compart, J., & Fettke, J. (2022). A review of starch, a unique biopolymer – Structure, metabolism and in planta modifications. *Plant Science*, *318*, 111223. https://doi.org/10.1016/j.plantsci.2022.111223

Bahaji, A., Li, J., Ovecka, M., Ezquer, I., Muñoz, F. J., Baroja-Fernández, E., Romero, J. M., Almagro, G., Montero, M., Hidalgo, M., Sesma, M. T., & Pozueta-Romero, J. (2011). Arabidopsis thaliana Mutants Lacking ADP-Glucose Pyrophosphorylase Accumulate Starch and Wild-type ADP-Glucose Content : Further Evidence for the Occurrence of Important Sources, other than ADP-Glucose Pyrophosphorylase, of ADP-Glucose Linked to Leaf Starch Biosynthesis. *Plant and Cell Physiology*, *52*(7), 1162-1176. https://doi.org/10.1093/pcp/pcr067

Ball, S. G., & Morell, M. K. (2003). FROM BACTERIAL GLYCOGEN TO STARCH : Understanding the Biogenesis of the Plant Starch Granule. *Annual Review of Plant Biology*, *54*(1), 207. https://doi.org/10.1146/annurev.arplant.54.031902.134927

Ball, S. G., Van De Wal, M. H. B. J., & Visser, R. G. F. (1998). Progress in understanding the biosynthesis of amylose. *Trends in Plant Science*, *3*(12), 462-467. https://doi.org/10.1016/S1360-1385(98)01342-9

Ball, S., Guan, H.-P., James, M., Myers, A., Keeling, P., Mouille, G., Buléon, A., Colonna, P., & Preiss, J. (1996). From Glycogen to Amylopectin : A Model for the Biogenesis of the Plant Starch Granule. *Cell*, *86*(3), 349-352. https://doi.org/10.1016/S0092-8674(00)80107-5

Ballicora, M. A., Laughlin, M. J., Fu, Y., Okita, T. W., Barry, G. F., & Preiss, J. (1995). Adenosine 5'-diphosphate-glucose pyrophosphorylase from potato tuber. Significance of the N terminus of the small subunit for catalytic properties and heat stability. *Plant Physiology*, *109*(1), 245-251.

Banks, W., & Greenwood, C. T. (1975). Fractionation of the starch granule, and the fine structures of its components. In *Starch and its components* (Edinburgh University Press., p. 5-112).

Baunsgaard, L., Lütken, H., Mikkelsen, R., Glaring, M. A., Pham, T. T., & Blennow, A. (2005). A novel isoform of glucan, water dikinase phosphorylates pre-phosphorylated α-glucans and is involved in starch degradation in Arabidopsis. *The Plant Journal*, *41*(4), 595-605. https://doi.org/10.1111/j.1365-313X.2004.02322.x

Bertoft, E. (1991). Investigation of the fine structure of alpha-dextrins derived from amylopectin and their relation to the structure of waxy-maize starch. *Carbohydrate Research*, *212*, 229-244. https://doi.org/10.1016/0008-6215(91)84060-R

Bertoft, E. (2015). Fine Structure of Amylopectin. In Y. Nakamura (Éd.), *Starch : Metabolism and Structure* (p. 3-40). Springer Japan. https://doi.org/10.1007/978-4-431-55495-0_1

Biliaderis, C. G., Grant, D. R., & Vose, J. R. (1979). Molecular weights distributions of legumes starches by gel chromatography. *Cereal Chem.*, *56*(5), 475-480.

Blauth, S. L., Kim, K.-N., Klucinec, J., Shannon, J. C., Thompson, D., & Guiltinan, M. (2002). Identification of Mutator insertional mutants of starch-branching enzyme 1 (sbe1) in Zea mays L. *Plant Molecular Biology*, *48*(3), 287-297. https://doi.org/10.1023/A:1013335217744

Blauth, S. L., Yao, Y., Klucinec, J. D., Shannon, J. C., Thompson, D. B., & Guilitinan, M. J. (2001). Identification of Mutator insertional mutants of starch-branching enzyme 2a in corn. *Plant Physiology*, *125*(3), 1396-1405. https://doi.org/10.1104/pp.125.3.1396

Blennow, A., & Engelsen, S. B. (2010). Helix-breaking news : Fighting crystalline starch energy deposits in the cell. *Trends in Plant Science*, *15*(4), 236-240. https://doi.org/10.1016/j.tplants.2010.01.009

Boyer, C. D., & Preiss, J. (1981). Evidence for Independent Genetic Control of the Multiple Forms of Maize Endosperm Branching Enzymes and Starch Synthases 12. *Plant Physiology*, *67*(6), 1141-1145.

Brisson, N., Giroux, H., Zollinger, M., Camirand, A., & Simard, C. (1989). Maturation and subcellular compartmentation of potato starch phosphorylase. *The Plant Cell*, *1*(5), 559-566. https://doi.org/10.1105/tpc.1.5.559

Brummell, D. A., Watson, L. M., Zhou, J., McKenzie, M. J., Hallett, I. C., Simmons, L., Carpenter, M., & Timmerman-Vaughan, G. M. (2015). Overexpression of STARCH BRANCHING ENZYME II increases short-chain branching of amylopectin and alters the

physicochemical properties of starch from potato tuber. *BMC Biotechnology*, *15*, 28. https://doi.org/10.1186/s12896-015-0143-y

Brust, H., Orzechowski, S., Fettke, J., & Steup, M. (2013). Starch Synthesizing Reactions and Paths : In vitro and in vivo Studies. *Journal of Applied Glycoscience*, *60*(1), 3-20. https://doi.org/10.5458/jag.jag.JAG-2012_018

Buléon, A., Colonna, P., Planchot, V., & Ball, S. (1998). Starch granules : Structure and biosynthesis. *International Journal of Biological Macromolecules*, *23*(2), 85-112. https://doi.org/10.1016/S0141-8130(98)00040-3

Bull, S. E., Seung, D., Chanez, C., Mehta, D., Kuon, J.-E., Truernit, E., Hochmuth, A., Zurkirchen, I., Zeeman, S. C., Gruissem, W., & Vanderschuren, H. (2018). Accelerated ex situ breeding of GBSS- and PTST1-edited cassava for modified starch. *Science Advances*, *4*(9), eaat6086. https://doi.org/10.1126/sciadv.aat6086

Bürgy, L., Eicke, S., Kopp, C., Jenny, C., Lu, K. J., Escrig, S., Meibom, A., & Zeeman, S. C. (2021). Coalescence and directed anisotropic growth of starch granule initials in subdomains of Arabidopsis thaliana chloroplasts. *Nature Communications*, *12*(1), 6944. https://doi.org/10.1038/s41467-021-27151-5

Burton, R. A., Bewley, J. D., Smith, A. M., Bhattacharyya, M. K., Tatge, H., Ring, S., Bull, V., Hamilton, W. D. O., & Martin, C. (1995). Starch branching enzymes belonging to distinct enzyme families are differentially expressed during pea embryo development. *The Plant Journal*, *7*(1), 3-15. https://doi.org/10.1046/j.1365-313X.1995.07010003.x

Burton, R. A., Jenner, H., Carrangis, L., Fahy, B., Fincher, G. B., Hylton, C., Laurie, D. A., Parker, M., Waite, D., Van Wegen, S., Verhoeven, T., & Denyer, K. (2002). Starch granule initiation and growth are altered in barley mutants that lack isoamylase activity : Isoamylase mutants of barley. *The Plant Journal*, *31*(1), 97-112. https://doi.org/10.1046/j.1365-313X.2002.01339.x

Bustos, R., Fahy, B., Hylton, C. M., Seale, R., Nebane, N. M., Edwards, A., Martin, C., & Smith, A. M. (2004). Starch granule initiation is controlled by a heteromultimeric isoamylase in potato tubers. *Proceedings of the National Academy of Sciences*, *101*(7), 2215-2220. https://doi.org/10.1073/pnas.0305920101

Campos, H., & Ortiz, O. (Éds.). (2020). *The Potato Crop : Its Agricultural, Nutritional and Social Contribution to Humankind*. Springer International Publishing. https://doi.org/10.1007/978-3-030-28683-5

Cao, H., Imparl-Radosevich, J., Guan, H., Keeling, P. L., James, M. G., & Myers, A. M. (1999). Identification of the Soluble Starch Synthase Activities of Maize Endosperm1. *Plant Physiology*, *120*(1), 205-216. https://doi.org/10.1104/pp.120.1.205

Caspar, T., Lin, T. P., Kakefuda, G., Benbow, L., Preiss, J., & Somerville, C. (1991). Mutants of Arabidopsis with altered regulation of starch degradation. *Plant Physiology*, *95*(4), 1181-1188. https://doi.org/10.1104/pp.95.4.1181

Čermák, T., Curtin, S. J., Gil-Humanes, J., Čegan, R., Kono, T. J. Y., Konečná, E., Belanto, J. J., Starker, C. G., Mathre, J. W., Greenstein, R. L., & Voytas, D. F. (2017). A Multipurpose Toolkit to Enable Advanced Genome Engineering in Plants. *The Plant Cell*, *29*(6), 1196-1217. https://doi.org/10.1105/tpc.16.00922

Chen, H.-M., Chang, S.-C., Wu, C.-C., Cuo, T.-S., Wu, J.-S., & Juang, R.-H. (2002). Regulation of the catalytic behaviour of L-form starch phosphorylase from sweet potato roots by proteolysis. *Physiologia Plantarum*, *114*(4), 506-515. https://doi.org/10.1034/j.1399-3054.2002.1140402.x

Chen, J., Chen, Y., Watson-Lazowski, A., Hawkins, E., Barclay, J. E., Fahy, B., Denley Bowers, R., Corbin, K., Warren, F. J., Blennow, A., Uauy, C., & Seung, D. (2024). Wheat MYOSIN-RESEMBLING CHLOROPLAST PROTEIN controls B-type starch granule initiation timing during endosperm development. *Plant Physiology*, *196*(3), 1980-1996. https://doi.org/10.1093/plphys/kiae429

Chen, W., McKenna, A., Schreiber, J., Haeussler, M., Yin, Y., Agarwal, V., Noble, W. S., & Shendure, J. (2019). Massively parallel profiling and predictive modeling of the outcomes of CRISPR/Cas9-mediated double-strand break repair. *Nucleic Acids Research*, *47*(15), 7989-8003. https://doi.org/10.1093/nar/gkz487

Chia, T., Chirico, M., King, R., Ramirez-Gonzalez, R., Saccomanno, B., Seung, D., Simmonds, J., Trick, M., Uauy, C., Verhoeven, T., & Trafford, K. (2020). A carbohydrate-binding protein, B-GRANULE CONTENT 1, influences starch granule size distribution in a dose-dependent manner in polyploid wheat. *Journal of Experimental Botany*, *71*(1), 105-115. https://doi.org/10.1093/jxb/erz405

Chia, T., Thorneycroft, D., Chapple, A., Messerli, G., Chen, J., Zeeman, S. C., Smith, S. M., & Smith, A. M. (2004). A cytosolic glucosyltransferase is required for conversion of starch to sucrose in Arabidopsis leaves at night. *The Plant Journal: For Cell and Molecular Biology*, *37*(6), 853-863. https://doi.org/10.1111/j.1365-313x.2003.02012.x

Chincinska, I. A., Miklaszewska, M., & Sołtys-Kalina, D. (2023). Recent advances and challenges in potato improvement using CRISPR/Cas genome editing. *Planta*, *257*(1), 25. https://doi.org/10.1007/s00425-022-04054-3

Ching, T. M. (1982). A sensitive and simple assay of starch synthase activity with pyruvate kinase and luciferase. *Analytical Biochemistry*, *122*(1), 139-143. https://doi.org/10.1016/0003-2697(82)90262-7

Coleman, W. K. (1987). Dormancy release in potato tubers : A review. *American Potato Journal*, *64*(2), 57-68. https://doi.org/10.1007/BF02853438

Compart, J., Apriyanto, A., & Fettke, J. (2023). Glucan, water dikinase (GWD) penetrates the starch granule surface and introduces C6 phosphate in the vicinity of branching points. *Carbohydrate Polymers*, *321*, 121321. https://doi.org/10.1016/j.carbpol.2023.121321

Concordet, J.-P., & Haeussler, M. (2018). CRISPOR : Intuitive guide selection for CRISPR/Cas9 genome editing experiments and screens. *Nucleic Acids Research*, *46*(W1), W242-W245. https://doi.org/10.1093/nar/gky354

Craig, J., Lloyd, J. R., Tomlinson, K., Barber, L., Edwards, A., Wang, T. L., Martin, C., Hedley, C. L., & Smith, A. M. (1998). Mutations in the Gene Encoding Starch Synthase II Profoundly Alter Amylopectin Structure in Pea Embryos. *The Plant Cell*, *10*, 413-426.

Critchley, J. H., Zeeman, S. C., Takaha, T., Smith, A. M., & Smith, S. M. (2001). A critical role for disproportionating enzyme in starch breakdown is revealed by a knock-out mutation in Arabidopsis. *The Plant Journal*, *26*(1), 89-100. https://doi.org/10.1046/j.1365-313x.2001.01012.x

Crofts, N., Nakamura, Y., & Fujita, N. (2017). Critical and speculative review of the roles of multi-protein complexes in starch biosynthesis in cereals. *Plant Science*, *262*, 1-8. https://doi.org/10.1016/j.plantsci.2017.05.007

Crumpton-Taylor, M., Grandison, S., Png, K. M. Y., Bushby, A. J., & Smith, A. M. (2012). Control of Starch Granule Numbers in Arabidopsis Chloroplasts. *Plant Physiology*, *158*(2), 905-916. https://doi.org/10.1104/pp.111.186957

Crumpton-Taylor, M., Pike, M., Lu, K., Hylton, C. M., Feil, R., Eicke, S., Lunn, J. E., Zeeman, S. C., & Smith, A. M. (2013). Starch synthase 4 is essential for coordination of starch granule formation with chloroplast division during Arabidopsis leaf expansion. *New Phytologist*, *200*(4), 1064-1075. https://doi.org/10.1111/nph.12455

Dang, P. L., & Boyer, C. D. (1988). Maize leaf and kernel starch synthases and starch branching enzymes. *Phytochemistry*, *27*(5), 1255-1259. https://doi.org/10.1016/0031-9422(88)80174-2

Delatte, T., Trevisan, M., Parker, M. L., & Zeeman, S. C. (2005). Arabidopsis mutants *Atisa1* and *Atisa2* have identical phenotypes and lack the same multimeric isoamylase, which influences the branch point distribution of amylopectin during starch synthesis. *The Plant Journal*, *41*(6), 815-830. https://doi.org/10.1111/j.1365-313X.2005.02348.x

del Mar Martínez-Prada, M., Curtin, S. J., & Gutiérrez-González, J. J. (2021). Potato improvement through genetic engineering. *GM Crops & Food*, *12*(1), 479-496. https://doi.org/10.1080/21645698.2021.1993688

Delvallé, D., Dumez, S., Wattebled, F., Roldán, I., Planchot, V., Berbezy, P., Colonna, P., Vyas, D., Chatterjee, M., Ball, S., Mérida, Á., & D'Hulst, C. (2005). Soluble starch synthase I : A major determinant for the synthesis of amylopectin in Arabidopsis thaliana leaves: SSI mutant of Arabidopsis. *The Plant Journal*, *43*(3), 398-412. https://doi.org/10.1111/j.1365-313X.2005.02462.x

Denyer, K., Waite, D., Edwards, A., Martin, C., & Smith, A. M. (1999). Interaction with amylopectin influences the ability of granule-bound starch synthase I to elongate malto-oligosaccharides. *Biochemical Journal*, *342*(Pt 3), 647-653.

Denyer, K., Waite, D., Motawia, S., Møller, B. L., & Smith, A. M. (1999). Granule-bound starch synthase I in isolated starch granules elongates malto-oligosaccharides processively. *Biochemical Journal*, *340*(Pt 1), 183-191.

Deschamps, P., Haferkamp, I., d'Hulst, C., Neuhaus, H. E., & Ball, S. G. (2008). The relocation of starch metabolism to chloroplasts : When, why and how. *Trends in Plant Science*, *13*(11), 574-582. https://doi.org/10.1016/j.tplants.2008.08.009

Dhital, S., Shrestha, A. K., & Gidley, M. J. (2010). Relationship between granule size and in vitro digestibility of maize and potato starches. *Carbohydrate Polymers*, *82*(2), 480-488. https://doi.org/10.1016/j.carbpol.2010.05.018

D'Hulst, C., Wattebled, F., & Szydlowski, N. (2015). Starch Biosynthesis in Leaves and Its Regulation. In Y. Nakamura (Éd.), *Starch Metabolism and Structure* (p. 211-237). Springer Japan. https://doi.org/10.1007/978-4-431-55495-0_6

Dinges, J. R., Colleoni, C., James, M. G., & Myers, A. M. (2003). Mutational analysis of the pullulanase-type debranching enzyme of maize indicates multiple functions in starch metabolism. *The Plant Cell*, *15*(3), 666-680. https://doi.org/10.1105/tpc.007575

Dinges, J. R., Colleoni, C., Myers, A. M., & James, M. G. (2001). Molecular structure of three mutations at the maize sugary1 locus and their allele-specific phenotypic effects. *Plant Physiology*, *125*(3), 1406-1418. https://doi.org/10.1104/pp.125.3.1406

Doench, J. G., Fusi, N., Sullender, M., Hegde, M., Vaimberg, E. W., Donovan, K. F., Smith, I., Tothova, Z., Wilen, C., Orchard, R., Virgin, H. W., Listgarten, J., & Root, D. E. (2016). Optimized sgRNA design to maximize activity and minimize off-target effects of CRISPR-Cas9. *Nature Biotechnology*, *34*(2), 184-191. https://doi.org/10.1038/nbt.3437

Dry, I., Smith, A., Edwards, A., Bhattacharyya, M., Dunn, P., & Martin, C. (1992). Characterization of cDNAs encoding two isoforms of granule-bound starch synthase which show differential expression in developing storage organs of pea and potato. *The Plant Journal*, *2*(2), 193-202. https://doi.org/10.1046/j.1365-313X.1992.t01-42-00999.x

Dumez, S., Wattebled, F., Dauvillee, D., Delvalle, D., Planchot, V., Ball, S. G., & D'Hulst, C. (2006). Mutants of Arabidopsis lacking starch branching enzyme II substitute plastidial starch synthesis by cytoplasmic maltose accumulation. *The Plant Cell*, *18*(10), 2694-2709. https://doi.org/10.1105/tpc.105.037671

Edwards, A., Borthakur, A., Bornemann, S., Venail, J., Denyer, K., Waite, D., Fulton, D., Smith, A., & Martin, C. (1999). Specificity of starch synthase isoforms from potato. *European Journal of Biochemistry*, *266*(3), 724-736. https://doi.org/10.1046/j.1432-1327.1999.00861.x

Edwards, A., Marshall, J., Sidebottom, C., Visser, R. G. F., Smith, A. M., & Martin, C. (1995). Biochemical and molecular characterization of a novel starch synthase from potato tubers. *The Plant Journal*, *8*(2), 283-294. https://doi.org/10.1046/j.1365-313X.1995.08020283.x

Ellis, R. P., Cochrane, M. P., Dale, M. F. B., Duffus, C. M., Lynn, A., Morrison, I. M., Prentice, R. D. M., Swanston, J. S., & Tiller, S. A. (1998). Starch production and industrial use. *Journal of the Science of Food and Agriculture*, *77*(3), 289-311. https://doi.org/10.1002/(SICI)1097-0010(199807)77:3<289::AID-JSFA38>3.0.CO;2-D

Facon, M., Lin, Q., Azzaz, A. M., Hennen-Bierwagen, T. A., Myers, A. M., Putaux, J.-L., Roussel, X., D'Hulst, C., & Wattebled, F. (2013). Distinct functional properties of isoamylase-type starch debranching enzymes in monocot and dicot leaves. *Plant Physiology*, *163*(3), 1363-1375. https://doi.org/10.1104/pp.113.225565

Feike, D., Seung, D., Graf, A., Bischof, S., Ellick, T., Coiro, M., Soyk, S., Eicke, S., Mettler-Altmann, T., Lu, K. J., Trick, M., Zeeman, S. C., & Smith, A. M. (2016). The Starch Granule-Associated Protein EARLY STARVATION1 Is Required for the Control of Starch Degradation in *Arabidopsis thaliana* Leaves. *The Plant Cell*, *28*(6), 1472-1489. https://doi.org/10.1105/tpc.16.00011

Fermont, L., Szydlowski, N., & Colleoni, C. (2022). Determination of Glucan Chain Length Distribution of Glycogen Using the Fluorophore-Assisted Carbohydrate

Electrophoresis (FACE) Method. *Journal of Visualized Experiments*, *181*, 63392. https://doi.org/10.3791/63392

Ferreira, S. J., Senning, M., Fischer-Stettler, M., Streb, S., Ast, M., Neuhaus, H. E., Zeeman, S. C., Sonnewald, S., & Sonnewald, U. (2017). Simultaneous silencing of isoamylases ISA1, ISA2 and ISA3 by multi-target RNAi in potato tubers leads to decreased starch content and an early sprouting phenotype. *PLOS ONE*, *12*(7), e0181444. https://doi.org/10.1371/journal.pone.0181444

Fettke, J., Albrecht, T., Hejazi, M., Mahlow, S., Nakamura, Y., & Steup, M. (2010). Glucose 1-phosphate is efficiently taken up by potato (Solanum tuberosum) tuber parenchyma cells and converted to reserve starch granules. *New Phytologist*, *185*(3), 663-675. https://doi.org/10.1111/j.1469-8137.2009.03126.x

Fisher, D. K., Gao, M., Kim, K. N., Boyer, C. D., & Guiltinan, M. J. (1996). Two closely related cDNAs encoding starch branching enzyme from Arabidopsis thaliana. *Plant Molecular Biology*, *30*(1), 97-108. https://doi.org/10.1007/BF00017805

Flores-Castellanos, J., & Fettke, J. (2023). The Plastidial Glucan Phosphorylase Affects the Maltooligosaccharide Metabolism in Parenchyma Cells of Potato (*Solanum tuberosum* L.) Tuber Discs. *Plant and Cell Physiology*, *64*(4), 422-432. https://doi.org/10.1093/pcp/pcac174

Fontaine, T., D'Hulst, C., Maddelein, M. L., Routier, F., Pépin, T. M., Decq, A., Wieruszeski, J. M., Delrue, B., Van Den Koornhuyse, N., & Bossu, J. P. (1993). Toward an understanding of the biogenesis of the starch granule. Evidence that Chlamydomonas soluble starch synthase II controls the synthesis of intermediate size glucans of amylopectin. *Journal of Biological Chemistry*, *268*(22), 16223-16230. https://doi.org/10.1016/S0021-9258(19)85409-1

Fredriksson, H., Silverio, J., Andersson, R., Eliasson, A.-C., & Åman, P. (1998). The influence of amylose and amylopectin characteristics on gelatinization and retrogradation properties of different starches. *Carbohydrate Polymers*, *35*(3-4), 119-134. https://doi.org/10.1016/S0144-8617(97)00247-6

French, D. (1972). Fine Structure of Starch and its Relationship to the Organization of Starch Granules. *Journal of the Japanese Society of Starch Science*, *19*(1), 8-25. https://doi.org/10.5458/jag1972.19.8

Friedman, M. (2006). Potato Glycoalkaloids and Metabolites : Roles in the Plant and in the Diet. *Journal of Agricultural and Food Chemistry*, *54*(23), 8655-8681. https://doi.org/10.1021/jf061471t

Fujita, N., Kubo, A., Suh, D.-S., Wong, K.-S., Jane, J.-L., Ozawa, K., Takaiwa, F., Inaba, Y., & Nakamura, Y. (2003). Antisense Inhibition of Isoamylase Alters the Structure of Amylopectin and the Physicochemical Properties of Starch in Rice Endosperm. *Plant and Cell Physiology*, *44*(6), 607-618. https://doi.org/10.1093/pcp/pcg079

Fujita, N., Yoshida, M., Asakura, N., Ohdan, T., Miyao, A., Hirochika, H., & Nakamura, Y. (2006). Function and Characterization of Starch Synthase I Using Mutants in Rice. *Plant Physiology*, *140*(3), 1070-1084. https://doi.org/10.1104/pp.105.071845

Fulton, D. C., Edwards, A., Pilling, E., Robinson, H. L., Fahy, B., Seale, R., Kato, L., Donald, A. M., Geigenberger, P., Martin, C., & Smith, A. M. (2002). Role of Granule-bound Starch

Synthase in Determination of Amylopectin Structure and Starch Granule Morphology in Potato *. *Journal of Biological Chemistry*, *277*(13), 10834-10841. https://doi.org/10.1074/jbc.M111579200

Fulton, D. C., Stettler, M., Mettler, T., Vaughan, C. K., Li, J., Francisco, P., Gil, M., Reinhold, H., Eicke, S., Messerli, G., Dorken, G., Halliday, K., Smith, A. M., Smith, S. M., & Zeeman, S. C. (2008). Beta-AMYLASE4, a noncatalytic protein required for starch breakdown, acts upstream of three active beta-amylases in Arabidopsis chloroplasts. *The Plant Cell*, *20*(4), 1040-1058. https://doi.org/10.1105/tpc.107.056507

Fusi, N., Smith, I., Doench, J., & Listgarten, J. (2015). *In Silico Predictive Modeling of CRISPR/Cas9 guide efficiency* (p. 021568). bioRxiv. https://doi.org/10.1101/021568

Gallant, D. J., Bouchet, B., & Baldwin, P. M. (1997). Microscopy of starch : Evidence of a new level of granule organization. *Carbohydrate Polymers*, *32*(3-4), 177-191. https://doi.org/10.1016/S0144-8617(97)00008-8

Gallant, D. J., Bouchet, B., Buléon, A., & Pérez, S. (1992). Physical characteristics of starch granules and susceptibility to enzymatic degradation. *European Journal of Clinical Nutrition*, *46 Suppl 2*, S3-16.

Gámez-Arjona, F. M., Raynaud, S., Ragel, P., & Mérida, Á. (2014). Starch synthase 4 is located in the thylakoid membrane and interacts with plastoglobule-associated proteins in Arabidopsis. *The Plant Journal*, *80*(2), 305-316. https://doi.org/10.1111/tpj.12633

Gao, M., Fisher, D. K., Kim, K. N., Shannon, J. C., & Guiltinan, M. J. (1996). Evolutionary conservation and expression patterns of maize starch branching enzyme I and IIb genes suggests isoform specialization. *Plant Molecular Biology*, *30*(6), 1223-1232. https://doi.org/10.1007/BF00019554

Gao, M., Fisher, D. K., Kim, K. N., Shannon, J. C., & Guiltinan, M. J. (1997). Independent genetic control of maize starch-branching enzymes IIa and IIb. Isolation and characterization of a Sbe2a cDNA. *Plant Physiology*, *114*(1), 69-78. https://doi.org/10.1104/pp.114.1.69

Gao, M., Wanat, J., Stinard, P. S., James, M. G., & Myers, A. M. (1998). Characterization of dull1, a Maize Gene Coding for a Novel Starch Synthase. *The Plant Cell*, *10*, 399-412.

Gardwood, D. L., Shannon, J. C., & Creech, R. G. (s. d.). Starches of endosperms possessing different alleles at the mylose-extender locus in Zea mays L. *Cereal Chem.*, *53*(3), 355-364.

Geiger, D. R., & Servaites, J. C. (1994). Diurnal Regulation of Photosynthetic Carbon Metabolism in C3 Plants. *Annual Review of Plant Physiology and Plant Molecular Biology*, *45*(1), 235-256. https://doi.org/10.1146/annurev.pp.45.060194.001315

Grimaud, F., Rogniaux, H., James, M. G., Myers, A. M., & Planchot, V. (2008). Proteome and phosphoproteome analysis of starch granule-associated proteins from normal maize and mutants affected in starch biosynthesis. *Journal of Experimental Botany*, *59*(12), 3395-3406. https://doi.org/10.1093/jxb/ern198

Guan, H. P., & Preiss, J. (1993). Differentiation of the Properties of the Branching Isozymes from Maize (Zea mays). *Plant Physiology*, *102*(4), 1269-1273.

Hawkins, E., Chen, J., Watson-Lazowski, A., Ahn-Jarvis, J., Barclay, J. E., Fahy, B., Hartley, M., Warren, F. J., & Seung, D. (2021). STARCH SYNTHASE 4 is required for normal starch granule initiation in amyloplasts of wheat endosperm. *New Phytologist*, *230*(6), 2371-2386. https://doi.org/10.1111/nph.17342

Haworth, W. N., Peat, S., & Bourne, E. J. (1944). Synthesis of Amylopectin. *Nature*, *154*(3903), 236-236. https://doi.org/10.1038/154236a0

Hedman, K. D., & Boyer, C. D. (1982). Gene dosage at the amylose-extender locus of maize : Effects on the levels of starch branching enzymes. *Biochemical Genetics*, *20*(5-6), 483-492. https://doi.org/10.1007/BF00484699

Helle. (2020). *Etude de la stœchiométrie des protéines liées à l'amidon : Vers des programmes novateurs pour la sélection et la production de nouvelles variétés de pommes de terre*.

Helle, S., Bray, F., Putaux, J.-L., Verbeke, J., Flament, S., Rolando, C., D'Hulst, C., & Szydlowski, N. (2019). Intra-Sample Heterogeneity of Potato Starch Reveals Fluctuation of Starch-Binding Proteins According to Granule Morphology. *Plants*, *8*(9), 324. https://doi.org/10.3390/plants8090324

Helle, S., Bray, F., Verbeke, J., Devassine, S., Courseaux, A., Facon, M., Tokarski, C., Rolando, C., & Szydlowski, N. (2018). Proteome Analysis of Potato Starch Reveals the Presence of New Starch Metabolic Proteins as Well as Multiple Protease Inhibitors. *Frontiers in Plant Science*, *9*, 746. https://doi.org/10.3389/fpls.2018.00746

Hirose, T., & Terao, T. (2004). A comprehensive expression analysis of the starch synthase gene family in rice (Oryza sativa L.). *Planta*, *220*(1), 9-16. https://doi.org/10.1007/s00425-004-1314-6

Hizukuri, S. (1986). Polymodal distribution of the chain lengths of amylopectins, and its significance. *Carbohydrate Research*, *147*(2), 342-347. https://doi.org/10.1016/S0008-6215(00)90643-8

Hizukuri, S., Takeda, Y., Yasuda, M., & Suzuki, A. (1981). Multi-branched nature of amylose and the action of debranching enzymes. *Carbohydrate Research*, *94*(2), 205-213. https://doi.org/10.1016/S0008-6215(00)80718-1

Hochmuth, A., Carswell, M., Rowland, A., Scarbrough, D., Esch, L., Kamble, N. U., Habig, J. W., & Seung, D. (2024). Distinct effects of PTST2b and MRC on starch granule morphogenesis in potato tubers. *Plant Biotechnology Journal*, *n/a*(n/a). https://doi.org/10.1111/pbi.14505

Hsieh, C.-F., Liu, W., Whaley, J. K., & Shi, Y.-C. (2019). Structure and functional properties of waxy starches. *Food Hydrocolloids*, *94*, 238-254. https://doi.org/10.1016/j.foodhyd.2019.03.026

Hsu, P. D., Scott, D. A., Weinstein, J. A., Ran, F. A., Konermann, S., Agarwala, V., Li, Y., Fine, E. J., Wu, X., Shalem, O., Cradick, T. J., Marraffini, L. A., Bao, G., & Zhang, F. (2013). DNA targeting specificity of RNA-guided Cas9 nucleases. *Nature Biotechnology*, *31*(9), 827-832. https://doi.org/10.1038/nbt.2647

Hu, S., Song, L., Yi, X., Ni, X., Cui, X., Duan, S., Jiang, R., Lyu, D., Wang, J., Hu, B., & Liu, X. (2025). Potato STARCH SYNTHEASE 5 is critical for simple starch granule initiation in

amyloplasts and tuber development. *The Plant Journal*, *122*(4), e70206. https://doi.org/10.1111/tpj.70206

Hussain, H., Mant, A., Seale, R., Zeeman, S., Hinchliffe, E., Edwards, A., Hylton, C., Bornemann, S., Smith, A. M., Martin, C., & Bustos, R. (2003). Three Isoforms of Isoamylase Contribute Different Catalytic Properties for the Debranching of Potato Glucans[W]. *The Plant Cell*, *15*(1), 133-149. https://doi.org/10.1105/tpc.006635

Hwang, S.-K., Nagai, Y., Kim, D., & Okita, T. W. (2008). Direct Appraisal of the Potato Tuber ADP-glucose Pyrophosphorylase Large Subunit in Enzyme Function by Study of a Novel Mutant Form. *Journal of Biological Chemistry*, *283*(11), 6640-6647. https://doi.org/10.1074/jbc.M707447200

Hwang, S.-K., Nishi, A., Satoh, H., & Okita, T. W. (2010). Rice endosperm-specific plastidial alpha-glucan phosphorylase is important for synthesis of short-chain malto-oligosaccharides. *Archives of Biochemistry and Biophysics*, *495*(1), 82-92. https://doi.org/10.1016/j.abb.2009.12.023

Hwang, S.-K., Singh, S., Cakir, B., Satoh, H., & Okita, T. W. (2016). The plastidial starch phosphorylase from rice endosperm : Catalytic properties at low temperature. *Planta*, *243*(4), 999-1009.

Iglesias, A. A., Barry, G. F., Meyer, C., Bloksberg, L., Nakata, P. A., Greene, T., Laughlin, M. J., Okita, T. W., Kishore, G. M., & Preiss, J. (1993). Expression of the potato tuber ADP-glucose pyrophosphorylase in Escherichia coli. *Journal of Biological Chemistry*, *268*(2), 1081-1086. https://doi.org/10.1016/S0021-9258(18)54044-8

Imberty, A., & Perez, S. (1988). A revisit to the three-dimensional structure of B-type starch. *Biopolymers*, *27*(8), 1205-1221. https://doi.org/10.1002/bip.360270803

James, M. G., Robertson, D. S., & Myers, A., M. (1995). (PDF) Characterization of the Maize Gene sugary1, a Determinant of Starch Composition in Kernels. *The Plant Cell*, *7*(4), 417-429. https://doi.org/10.1105/tpc.7.4.417

Jane, J., Kasemsuwan, T., Leas, S., Zobel, H., & Robyt, J. F. (1994). Anthology of Starch Granule Morphology by Scanning Electron Microscopy. *Starch - Stärke*, *46*(4), 121-129. https://doi.org/10.1002/star.19940460402

Jenkins, P. J., & Donald, A. M. (1995). The influence of amylose on starch granule structure. *International Journal of Biological Macromolecules*, *17*(6), 315-321. https://doi.org/10.1016/0141-8130(96)81838-1

Jeong, S. Y., Rose, A., & Meier, I. (2003). MFP1 is a thylakoid-associated, nucleoid-binding protein with a coiled-coil structure. *Nucleic Acids Research*, *31*(17), 5175-5185. https://doi.org/10.1093/nar/gkg693

Jinek, M., Chylinski, K., Fonfara, I., Hauer, M., Doudna, J. A., & Charpentier, E. (2012). A programmable dual RNA-guided DNA endonuclease in adaptive bacterial immunity. *Science (New York, N.Y.)*, *337*(6096), 816-821. https://doi.org/10.1126/science.1225829

Jobling, S. (2004). Improving starch for food and industrial applications. *Current Opinion in Plant Biology*, *7*(2), 210-218. https://doi.org/10.1016/j.pbi.2003.12.001

Jobling, S. A. ., Schwall, G. P. ., Westcott, R. J. ., Sidebottom, C. M. ., Debet, M., Gidley, M. J. ., Jeffcoat, R., & Safford, R. (1999). A minor form of starch branching enzyme in potato (Solanum tuberosum L.) tubers has a major effect on starch structure : Cloning and characterisation of multiple forms of SBE A. *The Plant Journal*, *18*(2), 163-171. https://doi.org/10.1046/j.1365-313X.1999.00441.x

Jung, Y.-J., Nogoy, F. M., Lee, S.-K., Cho, Y.-G., & Kang, K.-K. (2018). Application of ZFN for Site Directed Mutagenesis of Rice SSIVa Gene. *Biotechnology and Bioprocess Engineering*, *23*(1), 108-115. https://doi.org/10.1007/s12257-017-0420-9

Kamble, N. U., Makhamadjonov, F., Fahy, B., Martins, C., Saalbach, G., & Seung, D. (2023). Initiation of B-type starch granules in wheat endosperm requires the plastidial α-glucan phosphorylase PHS1. *The Plant Cell*, *35*(11), 4091-4110. https://doi.org/10.1093/plcell/koad217

Kasemsuwan, T., & Jane, J. (1994). Location of Amylose in Normal Starch Granules. II. Locations of Phosphodiester Cross-Linking Revealed by Phosphorus-31 Nuclear Magnetic Resonance. *American Association of Cereal Chemists*, *71*, 282-287.

Kasemsuwan, T., & Jane, J.-L. (1996). Quantitative Method for the Survey of Starch Phosphate Derivatives and Starch Phospholipids by 31P Nuclear Magnetic Resonance Spectroscopy'. *Cereal Chem.*, *73*(6), 702-707.

Kawagoe, Y. (2013). The Characteristic Polyhedral, Sharp-edged Shape of Compound-type Starch Granules in Rice Endosperm is Achieved via the Septum-like Structure of the Amyloplast. *Journal of Applied Glycoscience*, *60*(1), 29-36. https://doi.org/10.5458/jag.jag.JAG-2012_013

Kim, H.-Y., Park, S. S., & Lim, S.-T. (2015). Preparation, characterization and utilization of starch nanoparticles. *Colloids and Surfaces B: Biointerfaces*, *126*, 607-620. https://doi.org/10.1016/j.colsurfb.2014.11.011

Kossmann, J., Abel, G. J. W., Springer, F., Lloyd, J. R., & Willmitzer, L. (1999). Cloning and functional analysis of a cDNA encoding a starch synthase from potato (Solanum tuberosum L.) that is predominantly expressed in leaf tissue. *Planta*, *208*(4), 503-511. https://doi.org/10.1007/s004250050587

Kötting, O., Pusch, K., Tiessen, A., Geigenberger, P., Steup, M., & Ritte, G. (2005). Identification of a Novel Enzyme Required for Starch Metabolism in Arabidopsis Leaves. The Phosphoglucan, Water Dikinase. *Plant Physiology*, *137*(1), 242-252. https://doi.org/10.1104/pp.104.055954

Kötting, O., Santelia, D., Edner, C., Eicke, S., Marthaler, T., Gentry, M. S., Comparot-Moss, S., Chen, J., Smith, A. M., Steup, M., Ritte, G., & Zeeman, S. C. (2009). STARCH-EXCESS4 is a laforin-like Phosphoglucan phosphatase required for starch degradation in Arabidopsis thaliana. *The Plant Cell*, *21*(1), 334-346. https://doi.org/10.1105/tpc.108.064360

Kram, A. M., Oostergetel, G. T., & Van Burggen, E. (1993). *Localization of Branching Enzyme in Potato Tuber Cells with the Use of Immunoelectron Microscopy*. *101*(1), 237-243. https://doi.org/10.1104/pp.101.1.237

Kubo, A., Colleoni, C., Dinges, J. R., Lin, Q., Lappe, R. R., Rivenbark, J. G., Meyer, A. J., Ball, S. G., James, M. G., Hennen-Bierwagen, T. A., & Myers, A. M. (2010). Functions of

heteromeric and homomeric isoamylase-type starch-debranching enzymes in developing maize endosperm. *Plant Physiology*, *153*(3), 956-969. https://doi.org/10.1104/pp.110.155259

Kusano, H., Takeuchi, A., & Shimada, H. (2023). Efficiency of potato genome editing : Targeted mutation on the genes involved in starch biosynthesis using the CRISPR/dMac3-Cas9 system. *Plant Biotechnology*, 23.0611a. https://doi.org/10.5511/plantbiotechnology.23.0611a

Leterrier, M., Holappa, L. D., Broglie, K. E., & Beckles, D. M. (2008). Cloning, characterisation and comparative analysis of a starch synthase IV gene in wheat : Functional and evolutionary implications. *BMC Plant Biology*, *8*, 98. https://doi.org/10.1186/1471-2229-8-98

Li, Q., Dong, Y., Gao, Y., Du, S., Li, W., & Yu, X. (2021). Functional Properties and Structural Characteristics of Starch–Fatty Acid Complexes Prepared at High Temperature. *Journal of Agricultural and Food Chemistry*, *69*(32), 9076-9085. https://doi.org/10.1021/acs.jafc.1c00110

Lin, Q., Facon, M., Putaux, J.-L., Dinges, J. R., Wattebled, F., D'Hulst, C., Hennen-Bierwagen, T. A., & Myers, A. M. (2013). Function of isoamylase-type starch debranching enzymes ISA1 and ISA2 in the Zea mays leaf. *The New Phytologist*, *200*(4), 1009-1021. https://doi.org/10.1111/nph.12446

Lin, Y.-C., Chang, S.-C., & Juang, R.-H. (2017). Plastidial α-glucan phosphorylase 1 complexes with disproportionating enzyme 1 in Ipomoea batatas storage roots for elevating malto-oligosaccharide metabolism. *PloS One*, *12*(5), e0177115. https://doi.org/10.1371/journal.pone.0177115

Lindeboom, N., Chang, P. R., & Tyler, R. T. (2004). Analytical, Biochemical and Physicochemical Aspects of Starch Granule Size, with Emphasis on Small Granule Starches : A Review. *Starch - Stärke*, *56*(3-4), 89-99. https://doi.org/10.1002/star.200300218

Liu, C., Pfister, B., Osman, R., Ritter, M., Heutinck, A., Sharma, M., Eicke, S., Fischer-Stettler, M., Seung, D., Bompard, C., Abt, M. R., & Zeeman, S. C. (2023). LIKE EARLY STARVATION 1 and EARLY STARVATION 1 promote and stabilize amylopectin phase transition in starch biosynthesis. *Science Advances*, *9*(21), eadg7448. https://doi.org/10.1126/sciadv.adg7448

Liu, F., Makhmoudova, A., Lee, E. A., Wait, R., Emes, M. J., & Tetlow, I. J. (2009). The amylose extender mutant of maize conditions novel protein-protein interactions between starch biosynthetic enzymes in amyloplasts. *Journal of Experimental Botany*, *60*(15), 4423-4440. https://doi.org/10.1093/jxb/erp297

Liu, H., Yu, G., Wei, B., Wang, Y., Zhang, J., Hu, Y., Liu, Y., Yu, G., Zhang, H., & Huang, Y. (2015). Identification and Phylogenetic Analysis of a Novel Starch Synthase in Maize. *Frontiers in Plant Science*, *6*, 1013. https://doi.org/10.3389/fpls.2015.01013

Liu, Q. (2005). *Understanding Starches and Their Role in Foods*.

Lloyd, J. R., Blennow, A., Burhenne, K., & Kossmann, J. (2004). Repression of a novel isoform of disproportionating enzyme (stDPE2) in potato leads to inhibition of starch degradation in leaves but not tubers stored at low temperature. *Plant Physiology*, *134*(4), 1347-1354. https://doi.org/10.1104/pp.103.038026

Lombard, V., Golaconda Ramulu, H., Drula, E., Coutinho, P. M., & Henrissat, B. (2014). The carbohydrate-active enzymes database (CAZy) in 2013. *Nucleic Acids Research*, *42*(Database issue), D490-495. https://doi.org/10.1093/nar/gkt1178

Lu, K.-J., Pfister, B., Jenny, C., Eicke, S., & Zeeman, S. C. (2018). Distinct Functions of STARCH SYNTHASE 4 Domains in Starch Granule Formation. *Plant Physiology*, *176*(1), 566-581. https://doi.org/10.1104/pp.17.01008

Lu, Y., Steichen, J. M., Yao, J., & Sharkey, T. D. (2006). The Role of Cytosolic α-Glucan Phosphorylase in Maltose Metabolism and the Comparison of Amylomaltase in Arabidopsis and Escherichia coli. *Plant Physiology*, *142*(3), 878-889. https://doi.org/10.1104/pp.106.086850

Mahlow, S., Orzechowski, S., & Fettke, J. (2016). Starch phosphorylation : Insights and perspectives. *Cellular and Molecular Life Sciences: CMLS*, *73*(14), 2753-2764. https://doi.org/10.1007/s00018-016-2248-4

Malinova, I., Mahlow, S., Alseekh, S., Orawetz, T., Fernie, A. R., Baumann, O., Steup, M., & Fettke, J. (2014). Double knockout mutants of Arabidopsis grown under normal conditions reveal that the plastidial phosphorylase isozyme participates in transitory starch metabolism. *Plant Physiology*, *164*(2), 907-921. https://doi.org/10.1104/pp.113.227843

Malinova, I., Mahto, H., Brandt, F., AL-Rawi, S., Qasim, H., Brust, H., Hejazi, M., & Fettke, J. (2018). EARLY STARVATION1 specifically affects the phosphorylation action of starch-related dikinases. *The Plant Journal*, *95*(1), 126-137. https://doi.org/10.1111/tpj.13937

Malinova, I., Qasim, H. M., Brust, H., & Fettke, J. (2018). Parameters of Starch Granule Genesis in Chloroplasts of Arabidopsis thaliana. *Frontiers in Plant Science*, *9*, 761. https://doi.org/10.3389/fpls.2018.00761

Manners, D. J. (1989). Recent developments in our understanding of amylopectin structure. *Carbohydrate Polymers*, *11*(2), 87-112. https://doi.org/10.1016/0144-8617(89)90018-0

Mérida, A., & Fettke, J. (2021). Starch granule initiation in *Arabidopsis thaliana* chloroplasts. *The Plant Journal*, *107*(3), 688-697. https://doi.org/10.1111/tpj.15359

Mikkelsen, R., Baunsgaard, L., & Blennow, A. (2004). Functional characterization of alpha-glucan,water dikinase, the starch phosphorylating enzyme. *The Biochemical Journal*, *377*(Pt 2), 525-532. https://doi.org/10.1042/BJ20030999

Morell, M. K., Kosar-Hashemi, B., Cmiel, M., Samuel, M. S., Chandler, P., Rahman, S., Buleon, A., Batey, I. L., & Li, Z. (2003). Barley sex6 mutants lack starch synthase IIa activity and contain a starch with novel properties. *The Plant Journal*, *34*(2), 173-185. https://doi.org/10.1046/j.1365-313X.2003.01712.x

Morrison, W. R., Milligan, T. P., & Azudin, M. N. (1984). A relationship between the amylose and lipid contents of starches from diploid cereals. *Journal of Cereal Science*, *2*(4), 257-271. https://doi.org/10.1016/S0733-5210(84)80014-4

Myers, A. M., Morell, M. K., James, M. G., & Ball, S. G. (2000). Recent Progress toward Understanding Biosynthesis of the Amylopectin Crystal. *Plant Physiology*, *122*(4), 989-998. https://doi.org/10.1104/pp.122.4.989

Naguleswaran, S., Li, J., Vasanthan, T., Bressler, D., & Hoover, R. (2012). Amylolysis of large and small granules of native triticale, wheat and corn starches using a mixture of α-amylase and glucoamylase. *Carbohydrate Polymers*, *88*(3), 864-874. https://doi.org/10.1016/j.carbpol.2012.01.027

Nakagami, T., Yoshihara, H., Nakamura, T., Utsumi, Y., Sawada, T., Fujita, N., Satoh, H., & Nakamura, Y. (2017). Biochemical analysis of new type mutants of japonica rice that accumulate water-soluble α-glucans in the endosperm but retain full starch debranching enzyme activities. *Starch - Stärke*, *69*(3-4), 1600159. https://doi.org/10.1002/star.201600159

Nakamura, Y. (2002). Towards a Better Understanding of the Metabolic System for Amylopectin Biosynthesis in Plants : Rice Endosperm as a Model Tissue. *Plant and Cell Physiology*, *43*(7), 718-725. https://doi.org/10.1093/pcp/pcf091

Nakamura, Y., Kubo, A., Shimamune, T., Matsuda, T., Harada, K., & Satoh, H. (1997). Correlation between activities of starch debranching enzyme and α-polyglucan structure in endosperms of sugary-1 mutants of rice. *The Plant Journal*, *12*(1), 143-153. https://doi.org/10.1046/j.1365-313X.1997.12010143.x

Nakamura, Y., Ono, M., Sawada, T., Crofts, N., Fujita, N., & Steup, M. (2017). Characterization of the functional interactions of plastidial starch phosphorylase and starch branching enzymes from rice endosperm during reserve starch biosynthesis. *Plant Science: An International Journal of Experimental Plant Biology*, *264*, 83-95. https://doi.org/10.1016/j.plantsci.2017.09.002

Nakamura, Y., Ono, M., Utsumi, C., & Steup, M. (2012). Functional interaction between plastidial starch phosphorylase and starch branching enzymes from rice during the synthesis of branched maltodextrins. *Plant & Cell Physiology*, *53*(5), 869-878. https://doi.org/10.1093/pcp/pcs030

Nakamura, Y., Umemoto, T., Takahata, Y., Komae, K., Amano, E., & Satoh, H. (1996). Changes in structure of starch and enzyme activities affected by *sugary* mutations in developing rice endosperm. Possible role of starch debranching enzyme (R-enzyme) in amylopectin biosynthesis. *Physiologia Plantarum*, *97*(3), 491-498. https://doi.org/10.1111/j.1399-3054.1996.tb00508.x

Nakano, K., Mori, H., & Fukui, T. (1989). Molecular cloning of cDNA encoding potato amyloplast alpha-glucan phosphorylase and the structure of its transit peptide. *Journal of Biochemistry*, *106*(4), 691-695. https://doi.org/10.1093/oxfordjournals.jbchem.a122918

Nelson, O. E., & Tsai, C. Y. (1964). Glucose Transfer from Adenosine Diphosphate-Glucose to Starch in Preparations of Waxy Seeds. *Science*, *145*(3637), 1194-1195.

Niittylä, T., Comparot-Moss, S., Lue, W.-L., Messerli, G., Trevisan, M., Seymour, M. D. J., Gatehouse, J. A., Villadsen, D., Smith, S. M., Chen, J., Zeeman, S. C., & Smith, A. M. (2006). Similar protein phosphatases control starch metabolism in plants and glycogen

metabolism in mammals. *The Journal of Biological Chemistry*, *281*(17), 11815-11818. https://doi.org/10.1074/jbc.M600519200

Nishi, A., Nakamura, Y., Tanaka, N., & Satoh, H. (2001). Biochemical and Genetic Analysis of the Effects of Amylose-Extender Mutation in Rice Endosperm. *Plant Physiology*, *127*(2), 459-472.

Nishimasu, H., Ran, F. A., Hsu, P. D., Konermann, S., Shehata, S. I., Dohmae, N., Ishitani, R., Zhang, F., & Nureki, O. (2014). Crystal Structure of Cas9 in Complex with Guide RNA and Target DNA. *Cell*, *156*(5), 935-949. https://doi.org/10.1016/j.cell.2014.02.001

Noda, T., Takigawa, S., Matsuura-Endo, C., Kim, S.-J., Hashimoto, N., Yamauchi, H., Hanashiro, I., & Takeda, Y. (2005). Physicochemical properties and amylopectin structures of large, small, and extremely small potato starch granules. *Carbohydrate Polymers*, *60*(2), 245-251. https://doi.org/10.1016/j.carbpol.2005.01.015

Nsanzabera, F., Irakoze, E., Manishimwe, A., Mwiseneza, A., Nsengiyumva, J. B., & Nkurikiyimana, F. (2023). Starch Metabolism in Plant and Its Applications in Food Industry. *Advances in Biological Chemistry*, *13*(04), 111-127. https://doi.org/10.4236/abc.2023.134009

Ohdan, T., Francisco, P. B., Jr, Sawada, T., Hirose, T., Terao, T., Satoh, H., & Nakamura, Y. (2005). Expression profiling of genes involved in starch synthesis in sink and source organs of rice. *Journal of Experimental Botany*, *56*(422), 3229-3244. https://doi.org/10.1093/jxb/eri292

Okagaki, R. J., & Wessler, S. R. (1988). Comparison of Non-Mutant and Mutant Waxy Genes in Rice and Maize. *Genetics*, *120*(4), 1137-1143.

Oostergetel, G. T., & Van Bruggen, E. F. J. (1993). The crystalline domains in potato starch granules are arranged in a helical fashion. *Carbohydrate Polymers*, *21*(1), 7-12. https://doi.org/10.1016/0144-8617(93)90110-P

Osman, R., Bossu, M., Dauvillée, D., Spriet, C., Liu, C., Zeeman, S. C., D'Hulst, C., & Bompard, C. (2024). LIKE EARLY STARVATION 1 interacts with amylopectin during starch biosynthesis. *Plant Physiology*, kiae193. https://doi.org/10.1093/plphys/kiae193

Peat, S., Whelan, W. J., & Thomas, G. J. (1956). Evidence of multiple branching in waxy-maize starch. *Journal of the Chemical Society*. https://pubs-rsc-org.ressources-electroniques.univ-lille.fr/en/content/articlepdf/1956/jr/jr9560000044?page=search

Peng, C., Wang, Y., Liu, F., Ren, Y., Zhou, K., Lv, J., Zheng, M., Zhao, S., Zhang, L., Wang, C., Jiang, L., Zhang, X., Guo, X., Bao, Y., & Wan, J. (2014). FLOURY ENDOSPERM6 encodes a CBM48 domain-containing protein involved in compound granule formation and starch synthesis in rice endosperm. *The Plant Journal*, *77*(6), 917-930. https://doi.org/10.1111/tpj.12444

Pérez, S., & Bertoft, E. (2010). The molecular structures of starch components and their contribution to the architecture of starch granules : A comprehensive review. *Starch - Stärke*, *62*(8), 389-420. https://doi.org/10.1002/star.201000013

Perez-Riverol, Y., Csordas, A., Bai, J., Bernal-Llinares, M., Hewapathirana, S., Kundu, D. J., Inuganti, A., Griss, J., Mayer, G., Eisenacher, M., Pérez, E., Uszkoreit, J., Pfeuffer, J., Sachsenberg, T., Yılmaz, Ş., Tiwary, S., Cox, J., Audain, E., Walzer, M., … Vizcaíno, J. A.

(2019). The PRIDE database and related tools and resources in 2019 : Improving support for quantification data. *Nucleic Acids Research*, *47*(D1), D442-D450. https://doi.org/10.1093/nar/gky1106

Pfister, B., & Zeeman, S. C. (2016). Formation of starch in plant cells. *Cellular and Molecular Life Sciences: CMLS*, *73*(14), 2781-2807. https://doi.org/10.1007/s00018-016-2250-x

Ponstein, A. S., Vos-Scheperkeuter, G. H., Jacobsen, E., Feenstra, W. J., & Witholt, B. (1990). Selective Measurement of Starch Synthesizing Enzymes in Permeabilized Potato Tuber Slices 1. *Plant Physiology*, *92*(1), 234-241. https://doi.org/10.1104/pp.92.1.234

Porebski, S., Bailey, L. G., & Baum, B. R. (1997). Modification of a CTAB DNA extraction protocol for plants containing high polysaccharide and polyphenol components. *Plant Molecular Biology Reporter*, *15*(1), 8-15. https://doi.org/10.1007/BF02772108

Ragel, P., Streb, S., Feil, R., Sahrawy, M., Annunziata, M. G., Lunn, J. E., Zeeman, S., & Mérida, Á. (2013). Loss of starch granule initiation has a deleterious effect on the growth of arabidopsis plants due to an accumulation of ADP-glucose. *Plant Physiology*, *163*(1), 75-85. https://doi.org/10.1104/pp.113.223420

Raynaud, S., Ragel, P., Rojas, T., & Mérida, Á. (2016). The N-terminal Part of Arabidopsis thaliana Starch Synthase 4 Determines the Localization and Activity of the Enzyme. *The Journal of Biological Chemistry*, *291*(20), 10759-10771. https://doi.org/10.1074/jbc.M115.698332

Reader, J. (2008). *Propitious esculent : The potato in world history* (William Heinemann). The Random House Group.

Regina, A., Bird, A., Topping, D., Bowden, S., Freeman, J., Barsby, T., Kosar-Hashemi, B., Li, Z., Rahman, S., & Morell, M. (2006). High-amylose wheat generated by RNA interference improves indices of large-bowel health in rats. *Proceedings of the National Academy of Sciences of the United States of America*, *103*(10), 3546-3551. https://doi.org/10.1073/pnas.0510737103

Ridout, M. J., Parker, M. L., Hedley, C. L., Bogracheva, T. Y., & Morris, V. J. (2003). Atomic force microscopy of pea starch granules : Granule architecture of wild-type parent, r and rb single mutants, and the rrb double mutant. *Carbohydrate Research*, *338*(20), 2135-2147. https://doi.org/10.1016/S0008-6215(03)00309-4

Ritte, G., Heydenreich, M., Mahlow, S., Haebel, S., Kötting, O., & Steup, M. (2006). Phosphorylation of C6- and C3-positions of glucosyl residues in starch is catalysed by distinct dikinases. *FEBS Letters*, *580*(20), 4872-4876. https://doi.org/10.1016/j.febslet.2006.07.085

Ritte, G., Lloyd, J. R., Eckermann, N., Rottmann, A., Kossmann, J., & Steup, M. (2002). The starch-related R1 protein is an alpha -glucan, water dikinase. *Proceedings of the National Academy of Sciences of the United States of America*, *99*(10), 7166-7171. https://doi.org/10.1073/pnas.062053099

Robin, J. P., Mercier, C., Charbonniere, R., & Guilbot, A. (1974). Lintnerized Starches. Gel Filtration and Enzymatic Studies of Insoluble Residues from Prolonged Acid Treatment of Potato Starch. *American Association of Cereal Chemists*, *51*, 389-405.

Roldán, I., Wattebled, F., Mercedes Lucas, M., Delvallé, D., Planchot, V., Jiménez, S., Pérez, R., Ball, S., D'Hulst, C., & Mérida, Á. (2007). The phenotype of soluble starch synthase IV defective mutants of *Arabidopsis thaliana* suggests a novel function of elongation enzymes in the control of starch granule formation. *The Plant Journal*, *49*(3), 492-504. https://doi.org/10.1111/j.1365-313X.2006.02968.x

Rongine De Fekete, M. A., Leloir, L. F., & Cardini, C. E. (1960). Mechanism of Starch Biosynthesis. *Nature*, *187*(4741), 918-919. https://doi.org/10.1038/187918a0

Rousselle, P., & Robert, Y. (1996). *La pomme de terre Production, amélioration, ennemis et maladies, utilisations*. INRA editions. http://sbiproxy.uqac.ca/login?url=http://international.scholarvox.com/book/45006985

Rydberg, U., Andersson, L., Andersson, R., Åman, P., & Larsson, H. (2001). Comparison of starch branching enzyme I and II from potato. *European Journal of Biochemistry*, *268*(23), 6140-6145. https://doi.org/10.1046/j.0014-2956.2001.02568.x

Saito, M., Tanaka, T., Sato, K., Vrinten, P., & Nakamura, T. (2018). A single nucleotide polymorphism in the "Fra" gene results in fractured starch granules in barley. *Theoretical and Applied Genetics*, *131*(2), 353-364. https://doi.org/10.1007/s00122-017-3006-1

Salaman, R. N. (1949). *The History and Social Influence of the Potato*. Cambridge University Press.

Santelia, D., Kötting, O., Seung, D., Schubert, M., Thalmann, M., Bischof, S., Meekins, D. A., Lutz, A., Patron, N., Gentry, M. S., Allain, F. H.-T., & Zeeman, S. C. (2011). The phosphoglucan phosphatase like sex Four2 dephosphorylates starch at the C3-position in Arabidopsis. *The Plant Cell*, *23*(11), 4096-4111. https://doi.org/10.1105/tpc.111.092155

Satoh, H., Nishi, A., Yamashita, K., Takemoto, Y., Tanaka, Y., Hosaka, Y., Sakurai, A., Fujita, N., & Nakamura, Y. (2003). Starch-branching enzyme I-deficient mutation specifically affects the structure and properties of starch in rice endosperm. *Plant Physiology*, *133*(3), 1111-1121. https://doi.org/10.1104/pp.103.021527

Satoh, H., Shibahara, K., Tokunaga, T., Nishi, A., Tasaki, M., Hwang, S.-K., Okita, T. W., Kaneko, N., Fujita, N., Yoshida, M., Hosaka, Y., Sato, A., Utsumi, Y., Ohdan, T., & Nakamura, Y. (2008). Mutation of the Plastidial α-Glucan Phosphorylase Gene in Rice Affects the Synthesis and Structure of Starch in the Endosperm. *The Plant Cell*, *20*(7), 1833-1849. https://doi.org/10.1105/tpc.107.054007

Schupp, N., & Ziegler, P. (2004). The relation of starch phosphorylases to starch metabolism in wheat. *Plant & Cell Physiology*, *45*(10), 1471-1484. https://doi.org/10.1093/pcp/pch170

Seo, B., Kim, S., Scott, M. P., Singletary, G. W., Wong, K., James, M. G., & Myers, A. M. (2002). Functional interactions between heterologously expressed starch-branching enzymes of maize and the glycogen synthases of Brewer's yeast. *Plant Physiology*, *128*(4), 1189-1199. https://doi.org/10.1104/pp.010756

Seung, D. (2020). Amylose in starch : Towards an understanding of biosynthesis, structure and function. *New Phytologist*, *228*(5), 1490-1504. https://doi.org/10.1111/nph.16858

Seung, D., Boudet, J., Monroe, J., Schreier, T. B., David, L. C., Abt, M., Lu, K.-J., Zanella, M., & Zeeman, S. C. (2017). Homologs of PROTEIN TARGETING TO STARCH Control Starch Granule Initiation in Arabidopsis Leaves. *The Plant Cell*, *29*(7), 1657-1677. https://doi.org/10.1105/tpc.17.00222

Seung, D., Lu, K.-J., Stettler, M., Streb, S., & Zeeman, S. C. (2016). Degradation of Glucan Primers in the Absence of Starch Synthase 4 Disrupts Starch Granule Initiation in Arabidopsis. *Journal of Biological Chemistry*, *291*(39), 20718-20728. https://doi.org/10.1074/jbc.M116.730648

Seung, D., Schreier, T. B., Bürgy, L., Eicke, S., & Zeeman, S. C. (2018). Two Plastidial Coiled-Coil Proteins Are Essential for Normal Starch Granule Initiation in Arabidopsis. *The Plant Cell*, *30*(7), 1523-1542. https://doi.org/10.1105/tpc.18.00219

Seung, D., & Smith, A. M. (2019). Starch granule initiation and morphogenesis—Progress in Arabidopsis and cereals. *Journal of Experimental Botany*, *70*(3), 771-784. https://doi.org/10.1093/jxb/ery412

Seung, D., Soyk, S., Coiro, M., Maier, B. A., Eicke, S., & Zeeman, S. C. (2015). PROTEIN TARGETING TO STARCH Is Required for Localising GRANULE-BOUND STARCH SYNTHASE to Starch Granules and for Normal Amylose Synthesis in Arabidopsis. *PLOS Biology*, *13*(2), e1002080. https://doi.org/10.1371/journal.pbio.1002080

Sevestre, F. (2020). *Mise en œuvre de l'édition génomique par CRISPR/Cas9 pour l'étude fonctionnelle des amidon-synthases chez la pomme de terre (Solanum tuberosum).*

Sevestre, F., Facon, M., Wattebled, F., & Szydlowski, N. (2020). Facilitating gene editing in potato : A Single-Nucleotide Polymorphism (SNP) map of the Solanum tuberosum L. cv. Desiree genome. *Scientific Reports*, *10*(1), 2045. https://doi.org/10.1038/s41598-020-58985-6

Sharma, M., Abt, M. R., Eicke, S., Ilse, T. E., Liu, C., Lucas, M. S., Pfister, B., & Zeeman, S. C. (2024). MFP1 defines the subchloroplast location of starch granule initiation. *Proceedings of the National Academy of Sciences*, *121*(3), e2309666121. https://doi.org/10.1073/pnas.2309666121

Sharma, S., Friberg, M., Vogel, P., Turesson, H., Olsson, N., Andersson, M., & Hofvander, P. (2023). Pho1a (plastid starch phosphorylase) is duplicated and essential for normal starch granule phenotype in tubers of Solanum tuberosum L. *Frontiers in Plant Science*, *14*, 1220973. https://doi.org/10.3389/fpls.2023.1220973

Shure, M., Wessler, S., & Fedoroff, N. (1983). Molecular identification and isolation of the Waxy locus in maize. *Cell*, *35*(1), 225-233. https://doi.org/10.1016/0092-8674(83)90225-8

Singh, A., Compart, J., AL-Rawi, S. A., Mahto, H., Ahmad, A. M., & Fettke, J. (2022). LIKE EARLY STARVATION 1 alters the glucan structures at the starch granule surface and thereby influences the action of both starch-synthesizing and starch-degrading enzymes. *The Plant Journal*, *111*(3), 819-835. https://doi.org/10.1111/tpj.15855

Smirnova, J., Fernie, A. R., & Steup, M. (2015). Starch Degradation. In Y. Nakamura (Éd.), *Starch* (p. 239-290). Springer Japan. https://doi.org/10.1007/978-4-431-55495-0_7

Song, K., Lee, D.-W., Kim, J., Kim, J., Guim, H., Kim, K., Jeon, J.-S., & Choi, G. (2021). EARLY STARVATION 1 Is a Functionally Conserved Protein Promoting Gravitropic Responses in Plants by Forming Starch Granules. *Frontiers in Plant Science*, *12*, 628948. https://doi.org/10.3389/fpls.2021.628948

Sonnewald, U., Basner, A., Greve, B., & Steup, M. (1995). A second L-type isozyme of potato glucan phosphorylase : Cloning, antisense inhibition and expression analysis. *Plant Molecular Biology*, *27*(3), 567-576. https://doi.org/10.1007/BF00019322

Stitt, M., & Zeeman, S. C. (2012). Starch turnover : Pathways, regulation and role in growth. *Current Opinion in Plant Biology*, *15*(3), 282-292. https://doi.org/10.1016/j.pbi.2012.03.016

Streb, S., Delatte, T., Umhang, M., Eicke, S., Schorderet, M., Reinhardt, D., & Zeeman, S. C. (2009). Starch Granule Biosynthesis in *Arabidopsis* Is Abolished by Removal of All Debranching Enzymes but Restored by the Subsequent Removal of an Endoamylase. *The Plant Cell*, *20*(12), 3448-3466. https://doi.org/10.1105/tpc.108.063487

Streb, S., & Zeeman, S. C. (2012). Starch metabolism in Arabidopsis. *The Arabidopsis Book*, *10*, e0160. https://doi.org/10.1199/tab.0160

Suh, D. S., Verhoeven, T., Denyer, K., & Jane, J. (2004). Characterization of Nubet and Franubet barley starches. *Carbohydrate Polymers*, *56*(1), 85-93. https://doi.org/10.1016/j.carbpol.2003.12.005

Sun, C., Sathish, P., Ahlandsberg, S., & Jansson, C. (1998). The Two Genes Encoding Starch-Branching Enzymes IIa and IIb Are Differentially Expressed in Barley. *Plant Physiology*, *118*(1), 37-49.

Szabo De Edelenyi, F., Julia, C., Courtois, F., Méjean, C., Péneau, S., Galan, P., Hercberg, S., & Kesse-Guyot, E. (2014). Starchy Food Consumption in French Adults : A Cross-Sectional Analysis of the Profile of Consumers and Contribution to Nutritional Intake in a Web-Based Prospective Cohort. *Annals of Nutrition and Metabolism*, *64*(1), 28-37. https://doi.org/10.1159/000358888

Szydlowski, N., Ragel, P., Hennen-Bierwagen, T. A., Planchot, V., Myers, A. M., Mérida, A., d'Hulst, C., & Wattebled, F. (2011a). Integrated functions among multiple starch synthases determine both amylopectin chain length and branch linkage location in Arabidopsis leaf starch. *Journal of Experimental Botany*, *62*(13), 4547-4559. https://doi.org/10.1093/jxb/err172

Szydlowski, N., Ragel, P., Hennen-Bierwagen, T. A., Planchot, V., Myers, A. M., Mérida, A., d'Hulst, C., & Wattebled, F. (2011b). Integrated functions among multiple starch synthases determine both amylopectin chain length and branch linkage location in Arabidopsis leaf starch. *Journal of Experimental Botany*, *62*(13), 4547-4559. https://doi.org/10.1093/jxb/err172

Szydlowski, N., Ragel, P., Raynaud, S., Lucas, M. M., Roldán, I., Montero, M., Muñoz, F. J., Ovecka, M., Bahaji, A., Planchot, V., Pozueta-Romero, J., D'Hulst, C., & Mérida, Á. (2009). Starch Granule Initiation in Arabidopsis Requires the Presence of Either Class IV or Class III Starch Synthases. *The Plant Cell*, *21*(8), 2443-2457. https://doi.org/10.1105/tpc.109.066522

Takaha, T., Yanase, M., Okada, S., & Smith, S. M. (1993). Disproportionating enzyme (4-alpha-glucanotransferase; EC 2.4.1.25) of potato. Purification, molecular cloning, and potential role in starch metabolism. *The Journal of Biological Chemistry*, *268*(2), 1391-1396.

Takeda, Y., Guan, H.-P., & Preiss, J. (1993). Branching of amylose by the branching isoenzymes of maize endosperm. *Carbohydrate Research*, *240*, 253-263. https://doi.org/10.1016/0008-6215(93)84188-C

Takeda, Y., & Hizukuri, S. (1982). Location of phosphate groups in potato amylopectin. *Carbohydrate Research*, *102*(1), 321-327. https://doi.org/10.1016/S0008-6215(00)88077-5

Tanaka, E., Ral, J.-P. F., Li, S., Gaire, R., Cavanagh, C. R., Cullis, B. R., & Whan, A. (2017). Increased accuracy of starch granule type quantification using mixture distributions. *Plant Methods*, *13*(1), 107. https://doi.org/10.1186/s13007-017-0259-2

Tetlow, I. J., Beisel, K. G., Cameron, S., Makhmoudova, A., Liu, F., Bresolin, N. S., Wait, R., Morell, M. K., & Emes, M. J. (2008). Analysis of Protein Complexes in Wheat Amyloplasts Reveals Functional Interactions among Starch Biosynthetic Enzymes. *Plant Physiology*, *146*(4), 1878-1891. https://doi.org/10.1104/pp.108.116244

Tetlow, I. J., & Bertoft, E. (2020). A Review of Starch Biosynthesis in Relation to the Building Block-Backbone Model. *International Journal of Molecular Sciences*, *21*(19), 7011. https://doi.org/10.3390/ijms21197011

Tetlow, I. J., Wait, R., Lu, Z., Akkasaeng, R., Bowsher, C. G., Esposito, S., Kosar-Hashemi, B., Morell, M. K., & Emes, M. J. (2004). Protein Phosphorylation in Amyloplasts Regulates Starch Branching Enzyme Activity and Protein–Protein Interactions. *The Plant Cell*, *16*(3), 694-708. https://doi.org/10.1105/tpc.017400

Thalmann, M., Pazmino, D., Seung, D., Horrer, D., Nigro, A., Meier, T., Kölling, K., Pfeifhofer, H. W., Zeeman, S. C., & Santelia, D. (2016). Regulation of Leaf Starch Degradation by Abscisic Acid Is Important for Osmotic Stress Tolerance in Plants. *The Plant Cell*, *28*(8), 1860-1878. https://doi.org/10.1105/tpc.16.00143

Tiwari, J. K., Buckseth, T., Challam, C., Zinta, R., Bhatia, N., Dalamu, D., Naik, S., Poonia, A. K., Singh, R. K., Luthra, S. K., Kumar, V., & Kumar, M. (2022). CRISPR/Cas Genome Editing in Potato : Current Status and Future Perspectives. *Frontiers in Genetics*, *13*, 827808. https://doi.org/10.3389/fgene.2022.827808

Toyosawa, Y., Kawagoe, Y., Matsushima, R., Crofts, N., Ogawa, M., Fukuda, M., Kumamaru, T., Okazaki, Y., Kusano, M., Saito, K., Toyooka, K., Sato, M., Ai, Y., Jane, J.-L., Nakamura, Y., & Fujita, N. (2016). Deficiency of Starch Synthase IIIa and IVb Alters Starch Granule Morphology from Polyhedral to Spherical in Rice Endosperm. *Plant Physiology*, *170*(3), 1255-1270. https://doi.org/10.1104/pp.15.01232

Tsai, C.-Y. (1974). The function of the Waxy locus in starch synthesis in maize endosperm. *Biochemical Genetics*, *11*(2), 83-96. https://doi.org/10.1007/BF00485766

Tuncel, A., Corbin, K. R., Ahn-Jarvis, J., Harris, S., Hawkins, E., Smedley, M. A., Harwood, W., Warren, F. J., Patron, N. J., & Smith, A. M. (2019). Cas9-mediated mutagenesis of potato starch-branching enzymes generates a range of tuber starch phenotypes. *Plant Biotechnology Journal*, *17*(12), 2259-2271. https://doi.org/10.1111/pbi.13137

Tyson, R. H., & Ap Rees, T. (1988). Starch synthesis by isolated amyloplasts from wheat endosperm. *Planta*, *175*(1), 33-38. https://doi.org/10.1007/BF00402879

Tyynelä, J., & Schulman, A. H. (1993). An analysis of soluble starch synthase isozymes from the developing grains of normal and shx cv. Bomi barley (Hordeum vulgare). *Physiologia Plantarum*, *89*(4), 835-841. https://doi.org/10.1111/j.1399-3054.1993.tb05293.x

Utsumi, Y., & Nakamura, Y. (2006). Structural and enzymatic characterization of the isoamylase1 homo-oligomer and the isoamylase1–isoamylase2 hetero-oligomer from rice endosperm. *Planta*, *225*(1), 75-87. https://doi.org/10.1007/s00425-006-0331-z

Utsumi, Y., Utsumi, C., Sawada, T., Fujita, N., & Nakamura, Y. (2011). Functional diversity of isoamylase oligomers : The ISA1 homo-oligomer is essential for amylopectin biosynthesis in rice endosperm. *Plant Physiology*, *156*(1), 61-77. https://doi.org/10.1104/pp.111.173435

Vamadevan, V., & Bertoft, E. (2015). Structure-function relationships of starch components. *Starch - Stärke*, *67*(1-2), 55-68. https://doi.org/10.1002/star.201400188

Van De Wal, M., D'Hulst, C., Vincken, J.-P., Buléon, A., Visser, R., & Ball, S. (1998). Amylose Is Synthesized in Vitro by Extension of and Cleavage from Amylopectin. *Journal of Biological Chemistry*, *273*(35), 22232-22240. https://doi.org/10.1074/jbc.273.35.22232

Van Harsselaar, J. K., Lorenz, J., Senning, M., Sonnewald, U., & Sonnewald, S. (2017). Genome-wide analysis of starch metabolism genes in potato (Solanum tuberosum L.). *BMC Genomics*, *18*, 37. https://doi.org/10.1186/s12864-016-3381-z

Vandenbrink, J. P., & Kiss, J. Z. (2019). Plant responses to gravity. *Seminars in Cell & Developmental Biology*, *92*, 122-125. https://doi.org/10.1016/j.semcdb.2019.03.011

Vandromme, C., Spriet, C., Dauvillée, D., Courseaux, A., Putaux, J., Wychowski, A., Krzewinski, F., Facon, M., D'Hulst, C., & Wattebled, F. (2019). PII1 : A protein involved in starch initiation that determines granule number and size in Arabidopsis chloroplast. *New Phytologist*, *221*(1), 356-370. https://doi.org/10.1111/nph.15356

Vandromme, C., Spriet, C., Putaux, J., Dauvillée, D., Courseaux, A., D'Hulst, C., & Wattebled, F. (2023). Further insight into the involvement of PII1 in starch granule initiation in Arabidopsis leaf chloroplasts. *New Phytologist*, *239*(1), 132-145. https://doi.org/10.1111/nph.18923

Veillet, F., Chauvin, L., Kermarrec, M.-P., Sevestre, F., Merrer, M., Terret, Z., Szydlowski, N., Devaux, P., Gallois, J.-L., & Chauvin, J.-E. (2019). The Solanum tuberosum GBSSI gene : A target for assessing gene and base editing in tetraploid potato. *Plant Cell Reports*, *38*(9), 1065-1080. https://doi.org/10.1007/s00299-019-02426-w

Verbeke, J., Penverne, C., D'Hulst, C., Rolando, C., & Szydlowski, N. (2016). Rapid and sensitive quantification of C3- and C6-phosphoesters in starch by fluorescence-assisted capillary electrophoresis. *Carbohydrate Polymers*, *152*, 784-791. https://doi.org/10.1016/j.carbpol.2016.07.057

Vitha, S., Yang, M., Sack, F. D., & Kiss, J. Z. (2007). Gravitropism in the starch excess mutant of Arabidopsis thaliana. *American Journal of Botany*, *94*(4), 590-598. https://doi.org/10.3732/ajb.94.4.590

Vrinten, P. L., & Nakamura, T. (2000). Wheat Granule-Bound Starch Synthase I and II Are Encoded by Separate Genes That Are Expressed in Different Tissues. *Plant Physiology*, *122*(1), 255-264.

Watson-Lazowski, A., Raven, E., Feike, D., Hill, L., Barclay, J. E., Smith, A. M., & Seung, D. (2022). Loss of PROTEIN TARGETING TO STARCH 2 has variable effects on starch synthesis across organs and species. *Journal of Experimental Botany*, *73*(18), 6367-6379. https://doi.org/10.1093/jxb/erac268

Wattebled, F., Dong, Y., Dumez, S., Delvallé, D., Planchot, V., Berbezy, P., Vyas, D., Colonna, P., Chatterjee, M., Ball, S., & D'Hulst, C. (2005). Mutants of Arabidopsis Lacking a Chloroplastic Isoamylase Accumulate Phytoglycogen and an Abnormal Form of Amylopectin. *Plant Physiology*, *138*(1), 184-195. https://doi.org/10.1104/pp.105.059295

Wattebled, F., Planchot, V., Dong, Y., Szydlowski, N., Pontoire, B., Devin, A., Ball, S., & D'Hulst, C. (2008). Further Evidence for the Mandatory Nature of Polysaccharide Debranching for the Aggregation of Semicrystalline Starch and for Overlapping Functions of Debranching Enzymes in Arabidopsis Leaves. *Plant Physiology*, *148*(3), 1309-1323. https://doi.org/10.1104/pp.108.129379

Weatherwax, P. (1922). A Rare Carbohydrate in Waxy Maize. *Genetics*, *7*(6), 568-572.

Weise, S. E., Weber, A. P. M., & Sharkey, T. D. (2004). Maltose is the major form of carbon exported from the chloroplast at night. *Planta*, *218*(3), 474-482. https://doi.org/10.1007/s00425-003-1128-y

Wychowski, A., Bompard, C., Grimaud, F., Potocki-Véronèse, G., D'Hulst, C., Wattebled, F., & Roussel, X. (2017). Biochemical characterization of Arabidopsis thaliana starch branching enzyme 2.2 reveals an enzymatic positive cooperativity. *Biochimie*, *140*, 146-158. https://doi.org/10.1016/j.biochi.2017.07.013

Xu, X., Dees, D., Dechesne, A., Huang, X.-F., Visser, R. G. F., & Trindade, L. M. (2017). Starch phosphorylation plays an important role in starch biosynthesis. *Carbohydrate Polymers*, *157*, 1628-1637. https://doi.org/10.1016/j.carbpol.2016.11.043

Yamaguchi, M., Kainuma, K., & French, D. (1979). Electron microscopic observations of waxy maize starch. *Journal of Ultrastructure Research*, *69*(2), 249-261. https://doi.org/10.1016/S0022-5320(79)90114-X

Yamanouchi, H., & Nakamura, Y. (1992). Organ Specificity of Isoforms of Starch Branching Enzyme (Q-Enzyme) in Rice. *Plant and Cell Physiology*, *33*(7), 985-991. https://doi.org/10.1093/oxfordjournals.pcp.a078351

Yan, H., Zhang, W., Wang, Y., Jin, J., Xu, H., Fu, Y., Shan, Z., Wang, X., Teng, X., Li, X., Wang, Y., Hu, X., Zhang, W., Zhu, C., Zhang, X., Zhang, Y., Wang, R., Zhang, J., Cai, Y., … Wan, J. (2024). Rice LIKE EARLY STARVATION1 cooperates with FLOURY ENDOSPERM6 to modulate starch biosynthesis and endosperm development. *The Plant Cell*, koae006. https://doi.org/10.1093/plcell/koae006

Yang, L., Machin, F., Wang, S., Saplaoura, E., & Kragler, F. (2023). Heritable transgene-free genome editing in plants by grafting of wild-type shoots to transgenic donor rootstocks. *Nature Biotechnology*. https://doi.org/10.1038/s41587-022-01585-8

Young, G.-H., Chen, H.-M., Lin, C.-T., Tseng, K.-C., Wu, J.-S., & Juang, R.-H. (2006). Site-specific phosphorylation of L-form starch phosphorylase by the protein kinase activity from sweet potato roots. *Planta*, *223*(3), 468-478. https://doi.org/10.1007/s00425-005-0103-1

Yu, T.-S., Zeeman, S. C., Thorneycroft, D., Fulton, D. C., Dunstan, H., Lue, W.-L., Hegemann, B., Tung, S.-Y., Umemoto, T., Chapple, A., Tsai, D.-L., Wang, S.-M., Smith, A. M., Chen, J., & Smith, S. M. (2005). Alpha-Amylase is not required for breakdown of transitory starch in Arabidopsis leaves. *The Journal of Biological Chemistry*, *280*(11), 9773-9779. https://doi.org/10.1074/jbc.M413638200

Yun, M.-S., & Kawagoe, Y. (2010). Septum Formation in Amyloplasts Produces Compound Granules in the Rice Endosperm and is Regulated by Plastid Division Proteins. *Plant Cell Physiol.*

Yun, M.-S., Umemoto, T., & Kawagoe, Y. (2011). (PDF) Rice Debranching Enzyme Isoamylase3 Facilitates Starch Metabolism and Affects Plastid Morphogenesis. *Plant And Cell Physiology*, *52*(6), 1068-1082. https://doi.org/10.1093/pcp/pcr058

Yusuph, M., Tester, R. F., Ansell, R., & Snape, C. E. (2003). Composition and properties of starches extracted from tubers of different potato varieties grown under the same environmental conditions. *Food Chemistry*, *82*(2), 283-289. https://doi.org/10.1016/S0308-8146(02)00549-6

Zeeman, S. C., Kossmann, J., & Smith, A. M. (2010). Starch : Its Metabolism, Evolution, and Biotechnological Modification in Plants. *Annual Review of Plant Biology*, *61*(1), 209-234. https://doi.org/10.1146/annurev-arplant-042809-112301

Zeeman, S. C., & Rees, T. A. (1999). Changes in carbohydrate metabolism and assimilate export in starch-excess mutants of Arabidopsis. *Plant, Cell & Environment*, *22*(11), 1445-1453. https://doi.org/10.1046/j.1365-3040.1999.00503.x

Zeeman, S. C., Thorneycroft, D., Schupp, N., Chapple, A., Weck, M., Dunstan, H., Haldimann, P., Bechtold, N., Smith, A. M., & Smith, S. M. (2004). Plastidial *α* -Glucan Phosphorylase Is Not Required for Starch Degradation in Arabidopsis Leaves But Has a Role in the Tolerance of Abiotic Stress. *Plant Physiology*, *135*(2), 849-858. https://doi.org/10.1104/pp.103.032631

Zeeman, S. C., Umemoto, T., Lue, W. L., Au-Yeung, P., Martin, C., Smith, A. M., & Chen, J. (1998). A mutant of Arabidopsis lacking a chloroplastic isoamylase accumulates both starch and phytoglycogen. *The Plant Cell*, *10*(10), 1699-1712. https://doi.org/10.1105/tpc.10.10.1699

Zhang, L., Li, N., Zhang, J., Zhao, L., Qiu, J., & Wei, C. (2022). The CBM48 domain-containing protein FLO6 regulates starch synthesis by interacting with SSIVb and GBSS in rice. *Plant Molecular Biology*, *108*(4-5), 343-361. https://doi.org/10.1007/s11103-021-01178-0

Zhang, W., Thieme, C. J., Kollwig, G., Apelt, F., Yang, L., Winter, N., Andresen, N., Walther, D., & Kragler, F. (2016). tRNA-Related Sequences Trigger Systemic mRNA Transport in Plants. *The Plant Cell*, *28*(6), 1237-1249. https://doi.org/10.1105/tpc.15.01056

Zhang, X., Colleoni, C., Ratushna, V., Sirghie-Colleoni, M., James, M. G., & Myers, A. M. (2004). Molecular characterization demonstrates that the Zea mays gene sugary2 codes for the starch synthase isoform SSIIa. *Plant Molecular Biology*, *54*(6), 865-879. https://doi.org/10.1007/s11103-004-0312-1

Zhang, X., Myers, A. M., & James, M. G. (2005). Mutations Affecting Starch Synthase III in Arabidopsis Alter Leaf Starch Structure and Increase the Rate of Starch Synthesis. *Plant Physiology*, *138*(2), 663-674. https://doi.org/10.1104/pp.105.060319

Zhang, X., Szydlowski, N., Delvallé, D., D'Hulst, C., James, M. G., & Myers, A. M. (2008). Overlapping functions of the starch synthases SSII and SSIII in amylopectin biosynthesis in Arabidopsis. *BMC Plant Biology*, *8*(1), 96. https://doi.org/10.1186/1471-2229-8-96

Zhao, S., Ren, Y., & Wei, C. (2023). Staining Starch with Iodine Solution. In C. Pellicciari, M. Biggiogera, & M. Malatesta (Éds.), *Histochemistry of Single Molecules* (Vol. 2566, p. 281-290). Springer US. https://doi.org/10.1007/978-1-0716-2675-7_23

Zhou, T., Zhang, L., Liu, Q., Liu, W., & Hu, H. (2021). Rheological behaviors and physicochemical changes of doughs reconstituted from potato starch with different sizes and gluten. *Food Research International*, *145*, 110397. https://doi.org/10.1016/j.foodres.2021.110397

Ziegler, G. R., Creek, J. A., & Runt, J. (2005). Spherulitic Crystallization in Starch as a Model for Starch Granule Initiation. *Biomacromolecules*, *6*(3), 1547-1554. https://doi.org/10.1021/bm049214p

List of figures

Figure 1: Potato plant anatomy. 23

Figure 2 : Schematic representation of the primary structure of O-glycosidic bonds between glucose residues of starch, including phosphate residues 31

Figure 3 : Starch structure 32

Figure 4: Composition and structure of starch granules 35

Figure 5 : Scanning electron microscopy of purified starch granules from different botanic origins....38

Figure 6 : Domain structure of Starch Synthases (SSs) from potato. 42

Figure 7 : The pathway of starch degradation in chloroplasts and the role of transient glucan phosphorylation....48

Figure 8 : Protein interaction network in *Arabidopsis thaliana* starch granule initiation....62

Figure 9 : Starch granules isolated from control and isoamylase mutant tubers 64

Figure 10 : Structures and conservation of ESV1 and LESV proteins....68

Figure 11 : Electromobility shift assays (EMSA) gels analyzing the interaction between ESV1 or LESV and starch glucans....69

Figure 12 : Location of ESV1 and LESV proteins 71

Figure 13 : Label free quantification of proteins following SDS- or thermolysin- treatment of potato tuber starch granules 72

Figure 14 : Conservation of ESV1 and LESV proteins in land plants and algae 73

Figure 15 : Starch turnover in leaves of *esv1* mutants. 74

Figure 16 : The *lesv* single mutant has a conditional mutant phenotype 76

Figure 17 : Starch Granule Morphology in *esv1* and *lesv* mutants and overexpressing plant 76

Figure 18 : Quantification of insoluble and soluble glucans from yeast strains expressing ESV1, LESV, or both proteins in the 28 and 29 genetic backgrounds (expression sets indicated above the strain number)....78

Figure 19 : Scanning electron microscopy images of insoluble glucans purified from yeast strains expressing ESV1 and LESV 78

Figure 20 : Glucan accumulation and turnover in plants overexpressing ESV1 and LESV in the *isa1isa2* background 79

Figure 21 : Glucan content of *isa1isa2, esv1, lesv*, and triple mutants. 80

Figure 22 : Model of the proposed ESV1 and LESV functions 82

Figure 23 : Phenotypic characterization of the *flo9* mutant.....84

Figure 24 : Impact of ESV1 and LESV on starch granule surface properties.....85

Figure 25 : Targeted mutagenesis of the LESV and ESV1 genes using CRISPR/Cas9 system.104

Figure 26 : PCR amplification of a 959 bp region of the *CAS9* gene in mutants.....104

Figure 27 : Label free quantification of proteins 107

Figure 28 : Potato growth and development.....108

Figure 29 : Carbohydrate quantification of wild-type and *lesv* (a) and *esv1* (b) mutants.....109

Figure 30 : Coloration of fried potato tuber slices and sugar content in wild-type and *lesv* and *esv1* mutant lines. 111

Figure 31: Starch granule granulomorphometry 113

Figure 32: Light microscopy of starch granules 114

Figure 33: Scanning Electron Microscopy of purified starch granules from wild type (WT), lesv and *esv1* mutants tubers 115

Figure 34 : Purified starch granules observed under polarized light.....117

Figure 35: Molecular structure of *lesv* starches 117

Figure 36: Molecular structure of *esv1* starches 118

Figure 37: Assay of phosphoester residues: ratio of total phosphoester residues (GxP) over total glucose residues (GxP/Glc), ratio of O-6-phosphoesters (G6P/Glc) and ratio of O-3-phosphoesters (G3P/Glc) over total glucose residues 119

Figure 38 : Enzymatic hydrolysis of starch by porcine pancreatic α-amylase (PPA) 121

Figure 39 : Pasting properties of starch analyzed using a Rapid Visco-Analyzer (RVA) 122

Figure 40 : Label free quantification of proteins 125

Figure 41 : Immunoblot analysis of LESV protein in the soluble and insoluble fractions of potato tubers 128

Figure 42 : Immunoprecipitation assay of LESV and ISA1 expressed in *Nicotiana benthamiana* leaves 130

Figure 43 : Principle of the yeast two-hybrid assay 132

Figure 44 : Yeast two hybrid assay showing LESV and ISA1 physical interaction 133

Figure 45 : Granulomorphometry of fractionated starch based on granule size 135

Figure 46 : Starch phosphorylation profile in size-fractionated granules from *lesv* mutants 136

Figure 47 : Tubers harvested at different stage of WT and *lesv-10* plants development 137

Figure 48 : Boxplot of starch granule granulometry along tuber growth 138

Figure 49 : Light microscopy images of purified starch granules extracted from tubers harvested after (a) seven, (b) eight, (c) nine, (d) ten, (e) eleven weeks of culture. 139

Figure 50 : Confocal microscopy images of leaf starch in wild-type (WT) and mutant plants. 140

Figure 51 : Scanning Electron Microscopy of purified starch granules from wild type (WT), lesv and *esv1* mutants leaves 141

Figure 52 : Starch granule diameter in *ss5* mutants 143

Figure 53 : Scanning Electron Microscopy of purified starch granules from *ss5* mutants and wild-type controls 144

Figure 54 : Amylose content of *ss5* mutants and control lines 144

Figure 55 : Proposed model for the functions of LESV and ESV1 in amyloplasts 152

Figure 56 : Regulation of starch granule initiation across plant species and tissues 158

Figure 57 : Workflow of the production of transgene-free gene-edited plants through grafting 170

Figure 58 : Plasmid construction for graft-mobile editing system. 171

Figure 59 : PCR amplification of a 959 bp region of the *CAS9* gene in mutants.....175

Figure 60 : Workflow of grafting and cultivation of transgenic scions.....176

Figure 61 : Cladogram of the proteins most closely related to *Solanum tuberosum* SS6 across major plant groups.....181

Figure 62 : Domain structure of Starch Synthases (SSs) from potato 182

Figure 63 : Electrophoretic profiles of ADP and ADP-glucose standards 184

Figure 64 : Linearity of ADP detection. (a) Electrophoretic profiles of ADP standards at different concentrations.....185

Figure 65 : GBSS activity assay.....186

Figure 66 : Purification of recombinant SS6 using Ni-NTA resin 192

Figure 67 : Enzymatic characterization of recombinant SS6 193

List of tables

Table 1 : Characteristics of the guide RNAs (gRNAs) targeting *LESV* and *ESV1* 103

Table 2 : Genotyping results of targeted mutagenesis in *LESV* and *ESV1* genes.....106

Table 3 : Differential Scanning Calorimetry (DSC) transition parameters of starch.....123

Table 4 : Proportion of small granules (SG) (<11 µm) in total starch granules volume and number.....134

Table 5 : Guide RNAs (gRNAs) targeting GBSS selected for grafted-mobile editing system .173

Annexes

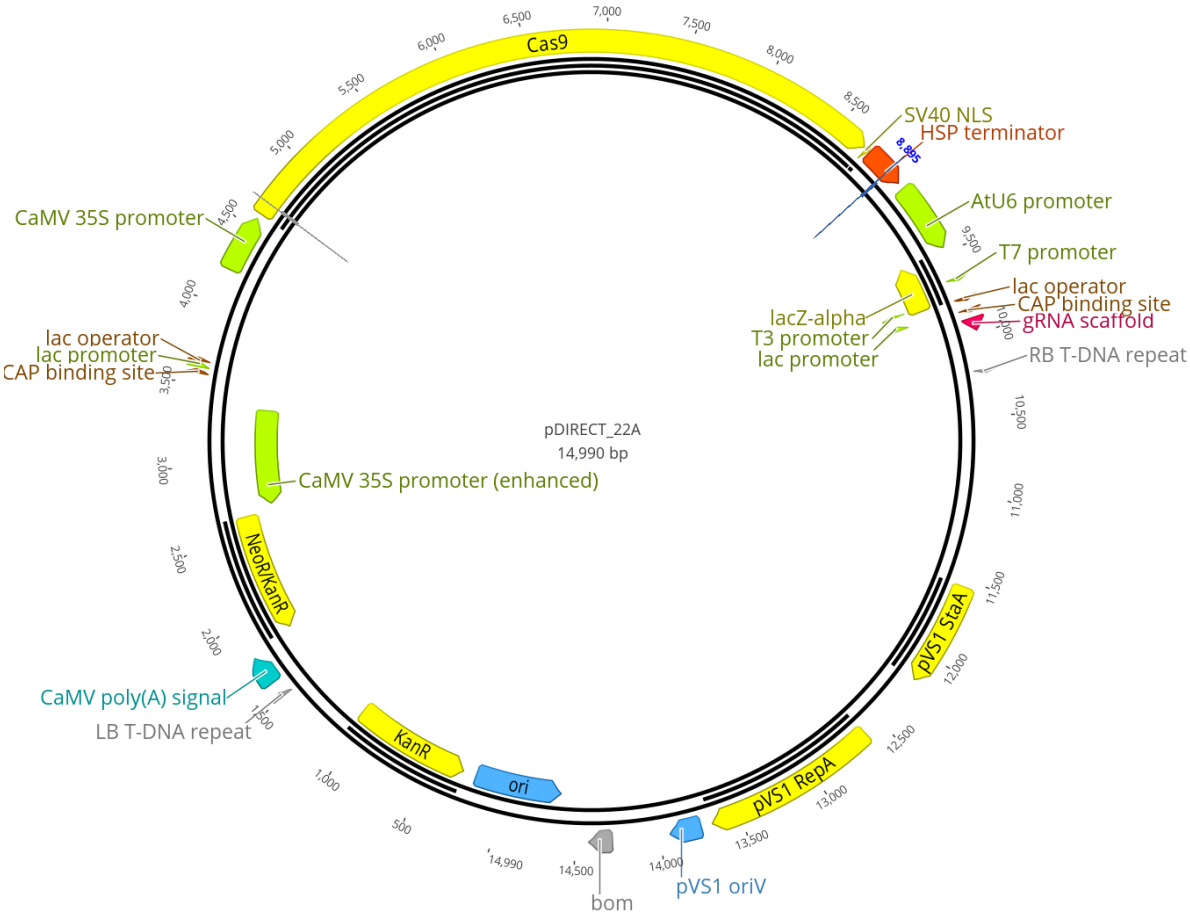

Annex 1 : Map of the pDIRECT_22A vector.

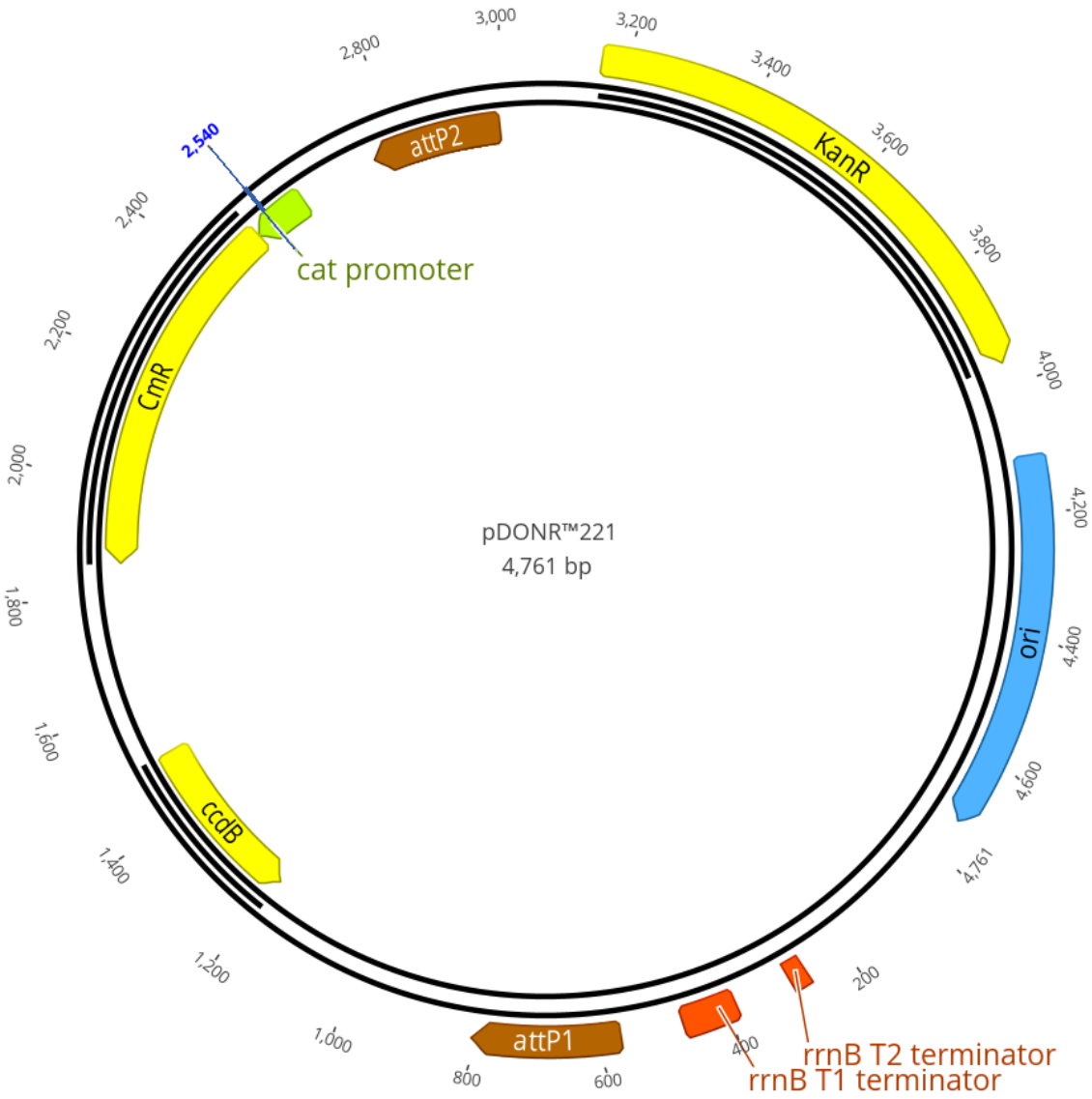

Annex 2 : Map of the pDONR221 entry vector.

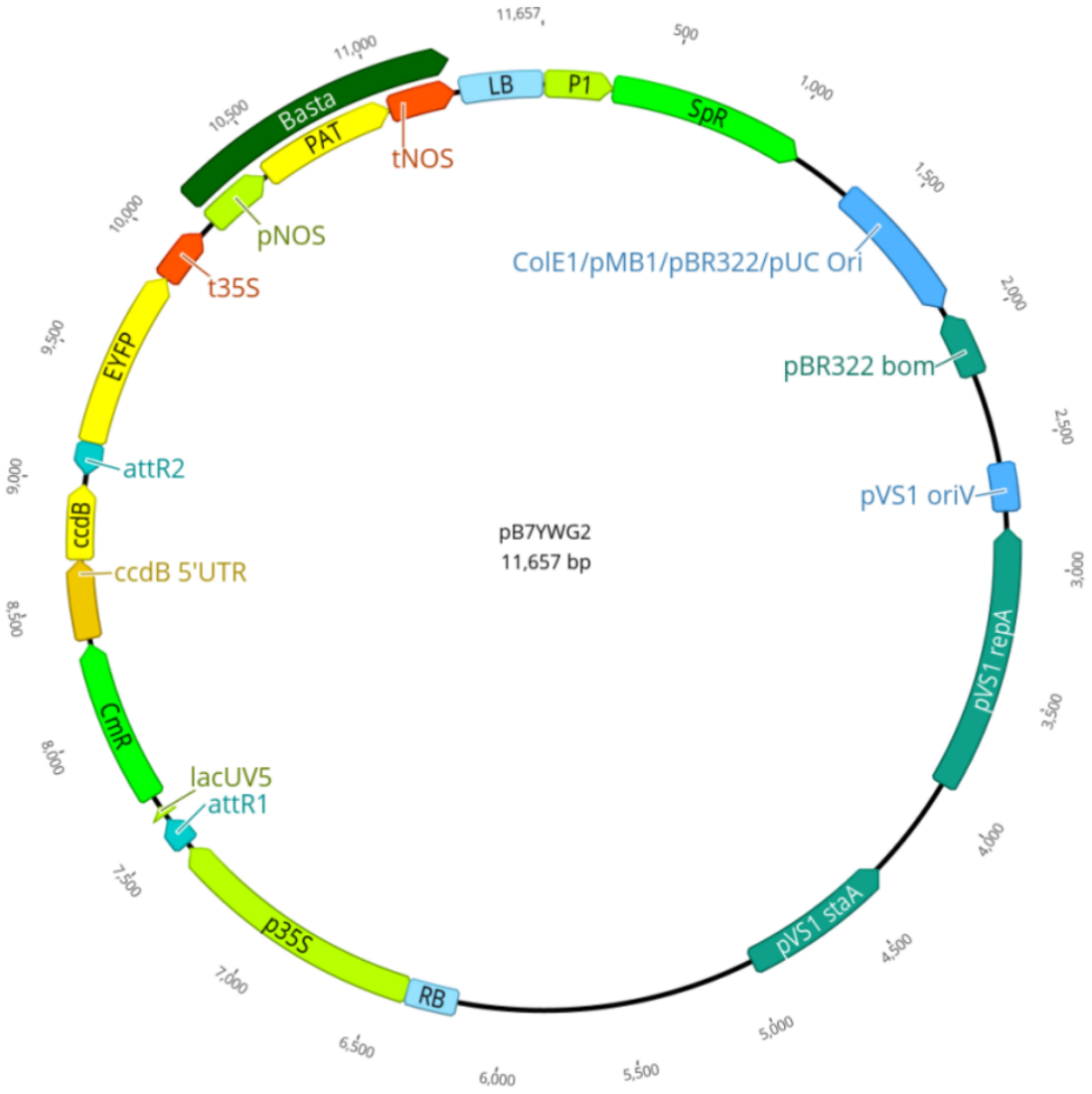

Annex 3 : Map of the pB7YWG2 destination vector.

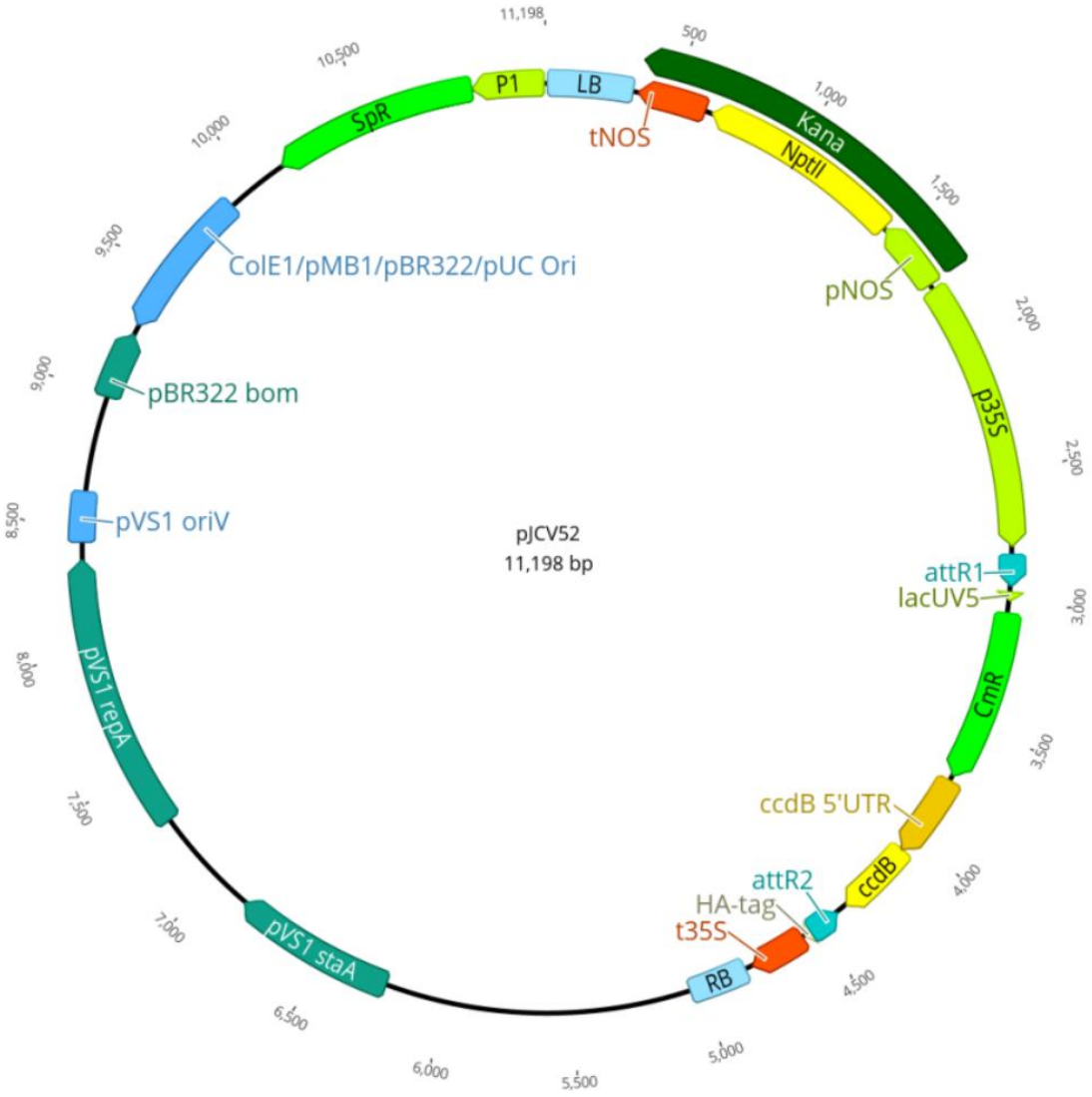

Annex 4 : Map of the pJCV52 destination vector.

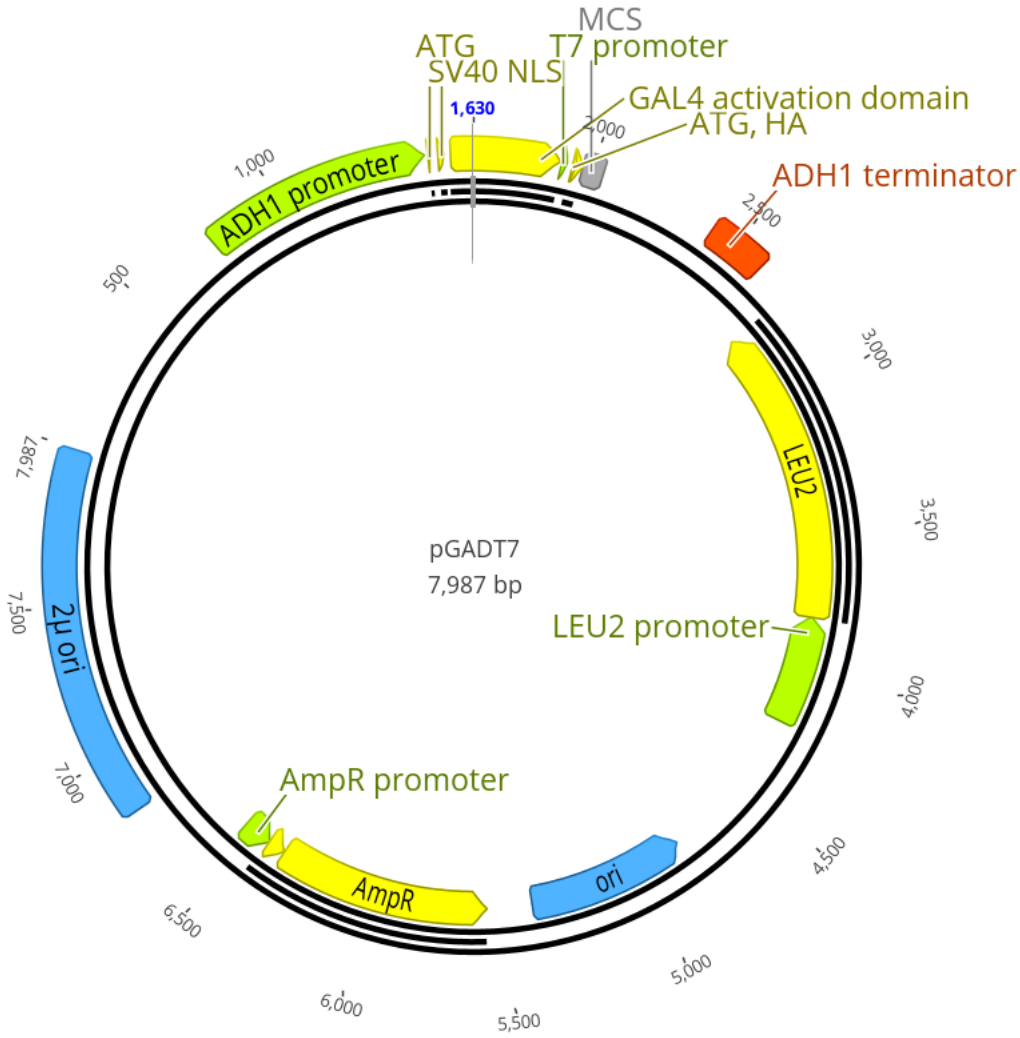

Annex 5 : Map of the pGADT7 destination vector containing the GAL4 activation domain.

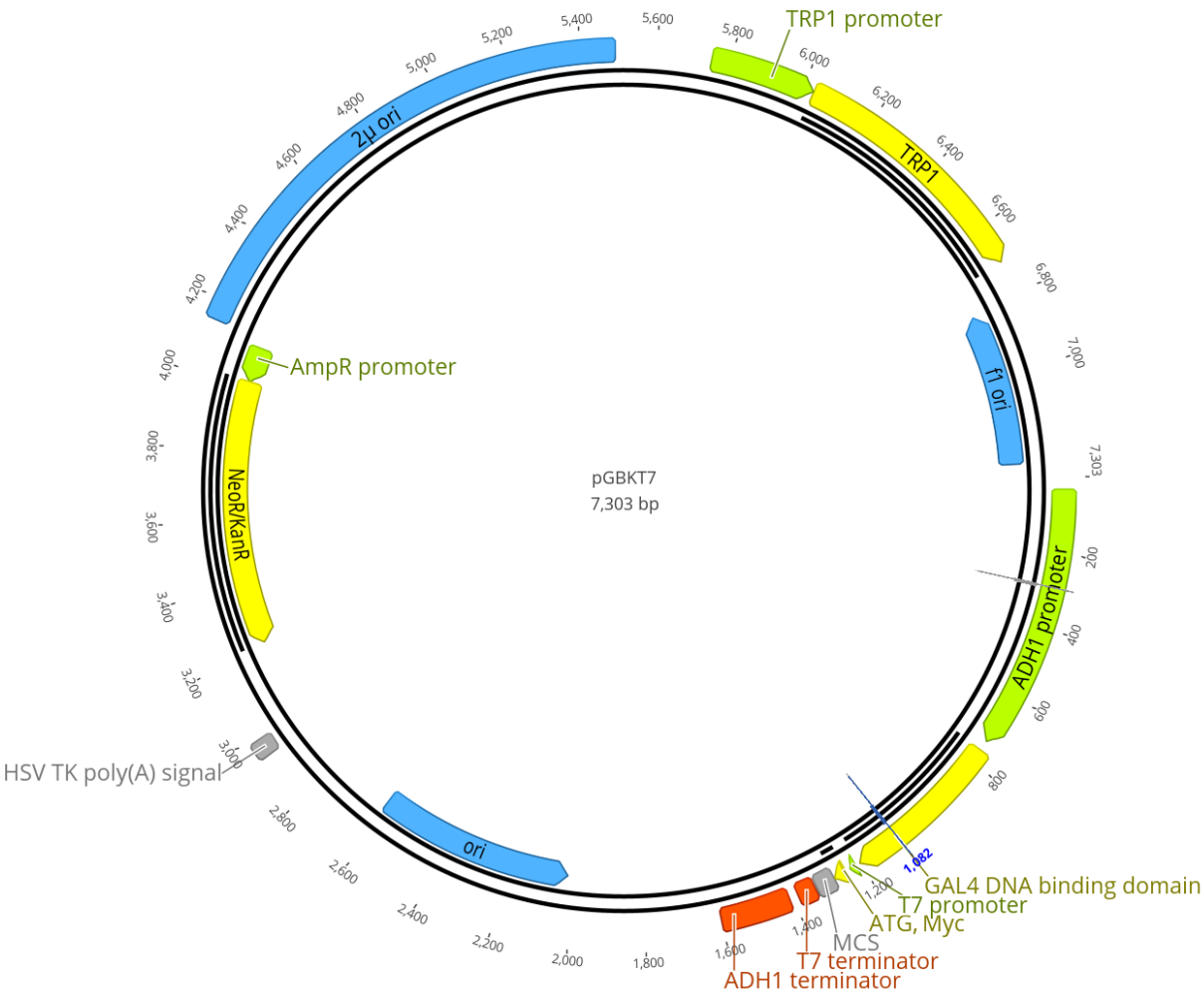

Annex 6 : Map of the pGBKT7 destination vector containing the GAL4 DNA binding domain.

Yellow color background indicates dMac3 sequence. Pink color background indicates SV40 NLS sequence. Light green color background indicates the C-terminal sequence of the *Cas9* gene. Red color background indicates gRNA scaffold. Light blue color background indicates $tRNA^{Met}$ (TLS1) sequences fused to Cas9 and gRNA scaffold.

>insert 1

CCTGCAGGTAGATCGCTCGAAGACTAAAGAGAGCTTTTTCATACCAAAGAAGTACAACAAAAGATTTGCTCCTCATTTTCTGAATCCTGGGACTCTCTAGCCTGTAGA
AGAAGAAAGGCAGGAATTTCAGCTCAAGAGAACAGATCACAATATTTACCCACGGCACTGTCTCGCAATATGGATTACAAGGACCACGACGGGGATTACAAGGACC
ACGACATTGATTACAAGGATGATGATGACAAGATGGCTCCGAAGAAGAAGAGGAAGGTTGGCATCCACGGTGCCAGCTGCGTCGAC

>insert 2

GGGACCCTAAGAAATACGGTGGTTTCGATTCTCCTACCGTGGCTTACTCTGTTCTCGTTGTGGCTAAGGTTGAGAAGGGAAAGAGTAAGAAGCTCAAGTCTGTTAAG
GAACTTCTCGGAATCACTATCATGGAAAGGTCATCTTTCGAGAAGAACCCAATCGATTTCCTCGAGGCTAAGGGATACAAAGAGGTTAAGAAGGATCTCATCATCAA
GCTCCCAAAGTACTCACTCTTCGAACTCGAGAACGGTAGAAAGAGGATGCTCGCTTCTGCTGGTGAGCTTCAAAAGGGAAACGAGCTTGCTCTCCCATCTAAGTACG
TTAACTTTCTTTACCTCGCTTCTCACTACGAGAAGTTGAAGGGATCTCCAGAAGATAACGAGCAGAAGCAACTTTTCGTTGAGCAGCACAAGCACTACTTGGATGAGA
TCATCGAGCAGATCTCTGAGTTCTCTAAAAGGGTGATCCTCGCTGATGCAAACCTCGATAAGGTGTTGTCTGCTTACAACAAGCACAGAGATAAGCCTATCAGGGAA
CAGGCAGAGAACATCATCCATCTCTTCACCCTTACCAACCTCGGTGCTCCTGCTGCTTTCAAGTACTTCGATACAACCATCGATAGGAAGAGATACACCTCTACCAAAG
AAGTGCTCGATGCTACCCTCATCCATCAGTCTATCACTGGACTCTACGAGACTAGGATCGATCTCTCACAGCTCGGTGGTGATTGAATTATCAGAGTGGCGCAGCGG
AAGCGTGGTGGGCCCATAACCCACAGGTCCCAGGATCGAAACCTGGCTCTGATCTCGAGATATGAAGATGAAGATGAAATATTTGGTGTGTCAAATAAAAAGCTTG
TGTGCTTAAGTTTGTGTTTTTTTCTTGGCTTGTTGTGTTATGAATTTGTGGCTTTTTCTAATATTAAATGAATGTAAGATCACATTATAATGAATAAACAAATGTTTCTAT
AATCCATTGTGAATGTTTTGTTGGATCTCTTCTGCAGCATATAACTACTGTATGTGCTATGGTATGGACTATGGAATATGATTAAAGATAAGGAGCTCCGGTGACGGA
CCCATGGCTTCGTTGAACAACGGAAACTCGACTTGCCTTCCGCACAATACATCATTTCTTCTTAGCTTTTTTTCTTCTTCTTCGTTCATACAGTTTTTTTTTGTTTATCAGC
TTACATTTTCTTGAACCGTAGCTTTCGTTTTCTTCTTTTTAACTTTCCATTCGGAGTTTTTGTATCTTGTTTCATAGTTTGTCCCAGGATTAGAATGATTAGGCATCGAAC
CTTCAAGAATTTGATTGAATAAAACATCTTCATTCTTAAGATATGAAGATAATCTTCAAAAGGCCCCTGGGAATCTGAAAGAAGAGAAGCAGGCCCATTTATATGGG
AAAGAACAATAGTATTTCTTATATAGGCCCATTTAAGTTGAAAACAATCTTCAAAAGTCCCACATCGCTTAGATAAGAAAACGAAGCTGAGTTTATATACAGCTAGAG
TCGAAGTAGTGATTAGAGGCAGGTGCCGCTACAGGGCGCGTCCCATTCGCCATTCAGGCTGCGCAACTGTTGGGAAGGGCGATCGGTGCGGGCCTCTTCGCTATTA
CGCCAGCTGGCGAAAGGGGGATGTGCTGCAAGGCGATTAAGTTGGGTAACGCCAGGGTTTTCCCAGTCACGACGTTGTAAAACGACGGCCAGTGAGCGCGCGTAA
TACGACTCACTATAGGGCGAATTGGGTACCGGGCCCCCCCTCGAGGTCCTCCAGCTTTTGTTCCCTTTAGTGAGGGTTAATTGCGCGCTTGGCGTAATCATGGTCATA
GCTGTTTCCTGTGTGAAATTGTTATCCGCTCACAATTCCACACAACATACGAGCCGGAAGCATAAAGTGTAAAGCCTGGGGTGCCTAATGAGTGAGCTAACTCACATT
AATTGCGTTGCGCTCACTGCCCGCTTTCCACCTGCGGTCGTTTTAGAGCTAGAAATAGCAAGTTAAAATAAGGCTAGTCCGTTATCAACTTGAAAAAGTGGCACCGAG
TCGGTGCATTATCAGAGTGGCGCAGCGGAAGCGTGGTGGGCCCATAACCCACAGGTCCCAGGATCGAAACCTGGCTCTGATAAAAAAAATTTTTTTCCCGGTGGCA
CTGGCCGTCGTTTTACAACGTCGTGACTGGGAAAACCCTGGCGTTACCCAACTTAATCGCCTTGCAGCACATCCCCCTTTCGCCAGCTGGCGTAATAGCGAAGAGGCC
CGCACCGATCGCCCTTCCCAACAGTTGCGCAGCCTGAATGGCGAATGCTAGAGCAGCTTGAGCTTGGATCAGATTGTCGTTTCCCGCCTTCAGTTTAAAC

Annex 7 : Plasmid construction for graft-mobile editing system.

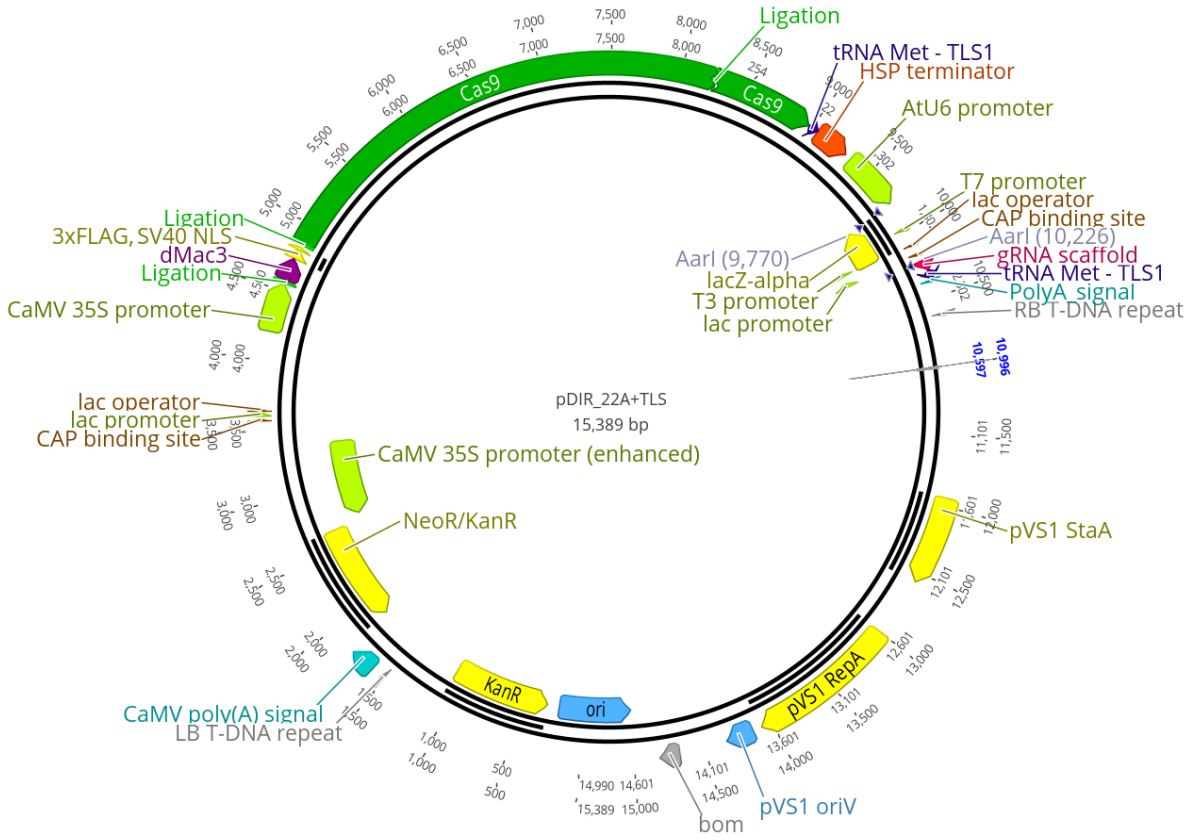

Annex 8 : Map of the plasmid construct used for graft-mobile editing system.

Annex 9 : Primers used in the mutants production and the characterization of the induced mutations.

Use of the primer	Sense	Sequence
Production of *lesv* mutant - sgRNA	Forward	5’- GATTGGAGTGGCATGAGAAATGGT -3’
	Reverse	5’- AAACACCATTTCTCATGCCACTCC -3’
Evaluation of the presence of the Cas9 gene	Forward	5’- CGCATCTCTCGGAACCTACC -3’
	Reverse	5’- GTCCTCCCCTCTCAGCCTTA -3’
Evaluation of the Cas9-induced mutation in *lesv*	Forward	5’- ATGGCCTATGAATGGGGTTT -3’
	Reverse	5’- GATGCCAGAGAAATGCTTCC -3’

WT

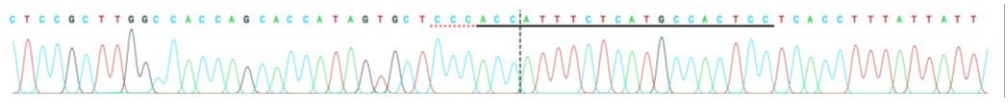

lesv-3

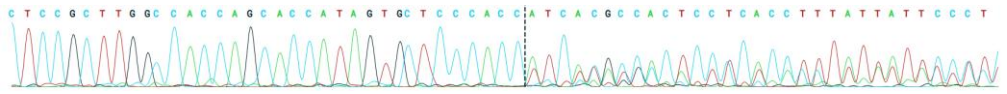

lesv-9

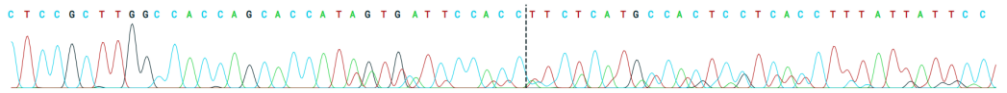

lesv-10

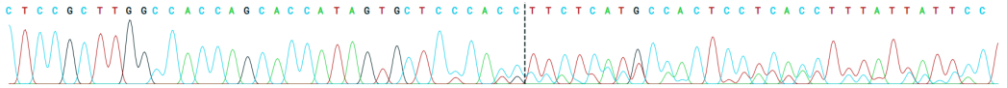

lesv-15

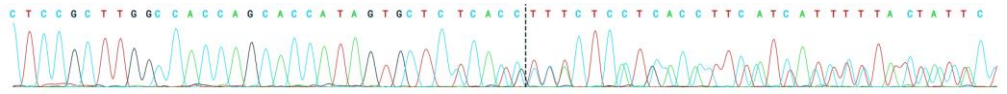

lesv-17

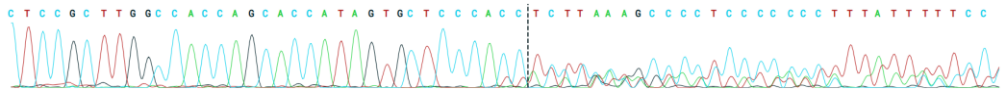

lesv-24

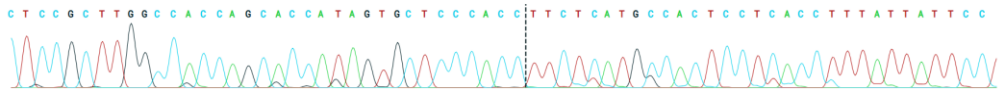

lesv-27

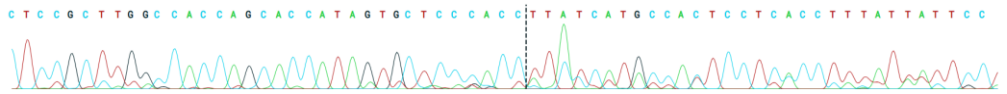

lesv-30

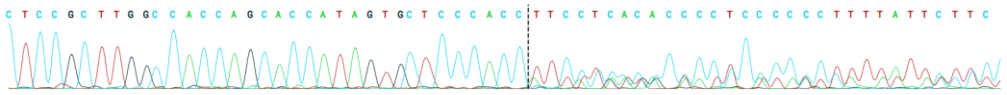

lesv-31

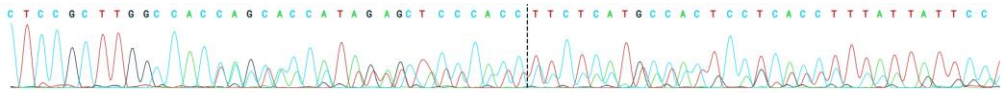

Annex 10 : Chromatograms of the *lesv* knockout lines. A window of 65 bp around the binding site of the gRNA is shown here, visualized using ICE Synthego. In WT, the gRNA is underlined in black, and the PAM motif is underlined in red dotted line. The Cas9 predicted cut site is presented in black dotted line. ICE Synthego allowed the separation of the superposed signals, corresponding to different alleles. The results of the ICE analysis are presented in Figure 25.

WT

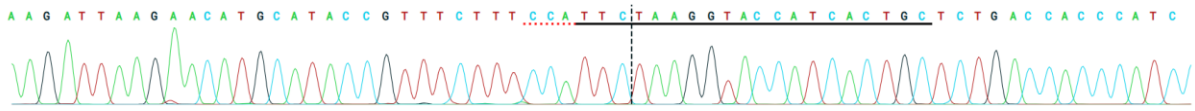

esv1-114

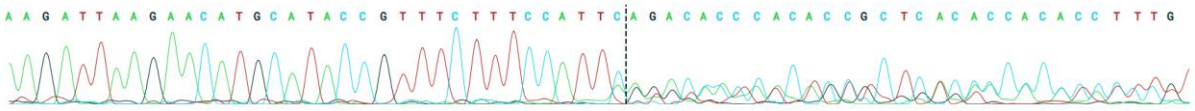

esv1-117

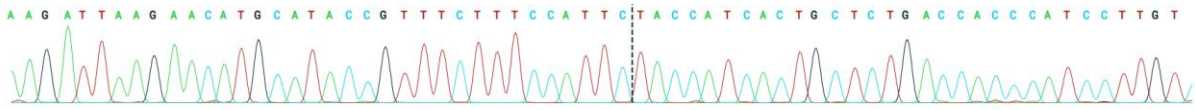

esv1-121

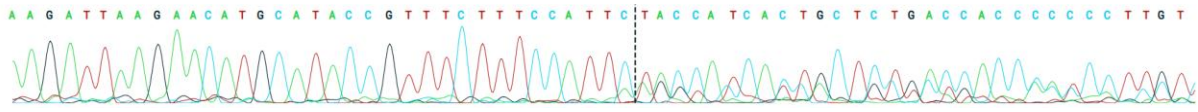

esv1-124

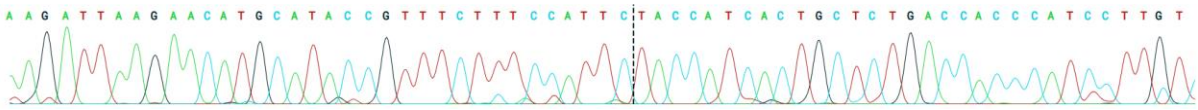

esv1-129

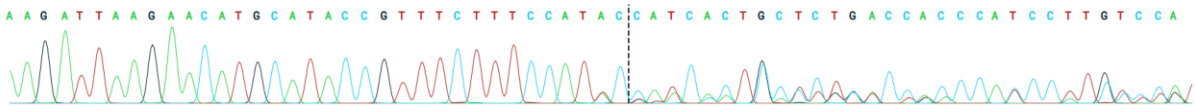

Annex 11 : Chromatograms of the *esv1* knockout lines. A window of 65 bp around the binding site of the gRNA is shown here, visualized using ICE Synthego. In WT, the gRNA is underlined in black, and the PAM motif is underlined in red dotted line. The Cas9 predicted cut site is represented by black vertical dotted lines. ICE Synthego allowed the separation of the superposed signals, corresponding to different alleles. The results of the ICE analysis are presented in Figure 25

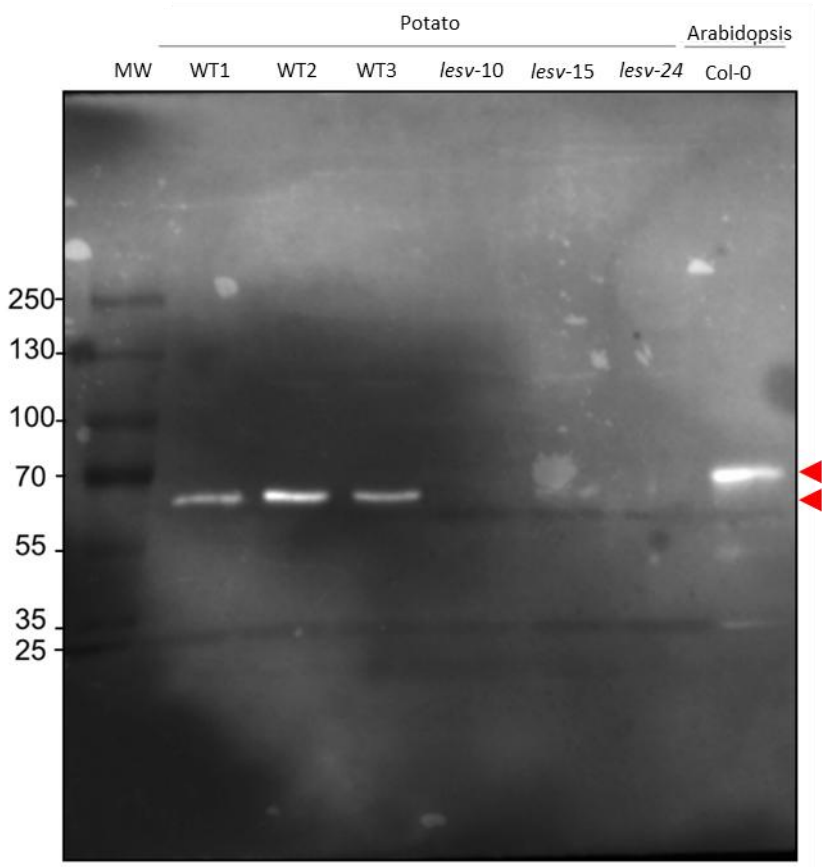

Annex 12 : Immunoblots of LESV protein in wild-type and *lesv* mutant potato plants, as well as in wild-type *Arabidopsis* plants. Potato tubers and *Arabidopsis* leaves were homogenized, and starch was purified by successive washes. The starch was washed five times with 2% (v/v) SDS and resuspended at a final concentration of 30 $g \cdot L^{-1}$. Samples were heated at 99°C for 15 minutes. LESV protein was detected using a polyclonal serum raised against *Arabidopsis* LESV (rabbit, 1:100). Detection was performed via chemiluminescence using a horseradish peroxidase (HRP)-conjugated anti-rabbit secondary antibody. The first lane corresponds to the molecular weight standard (in kDa).

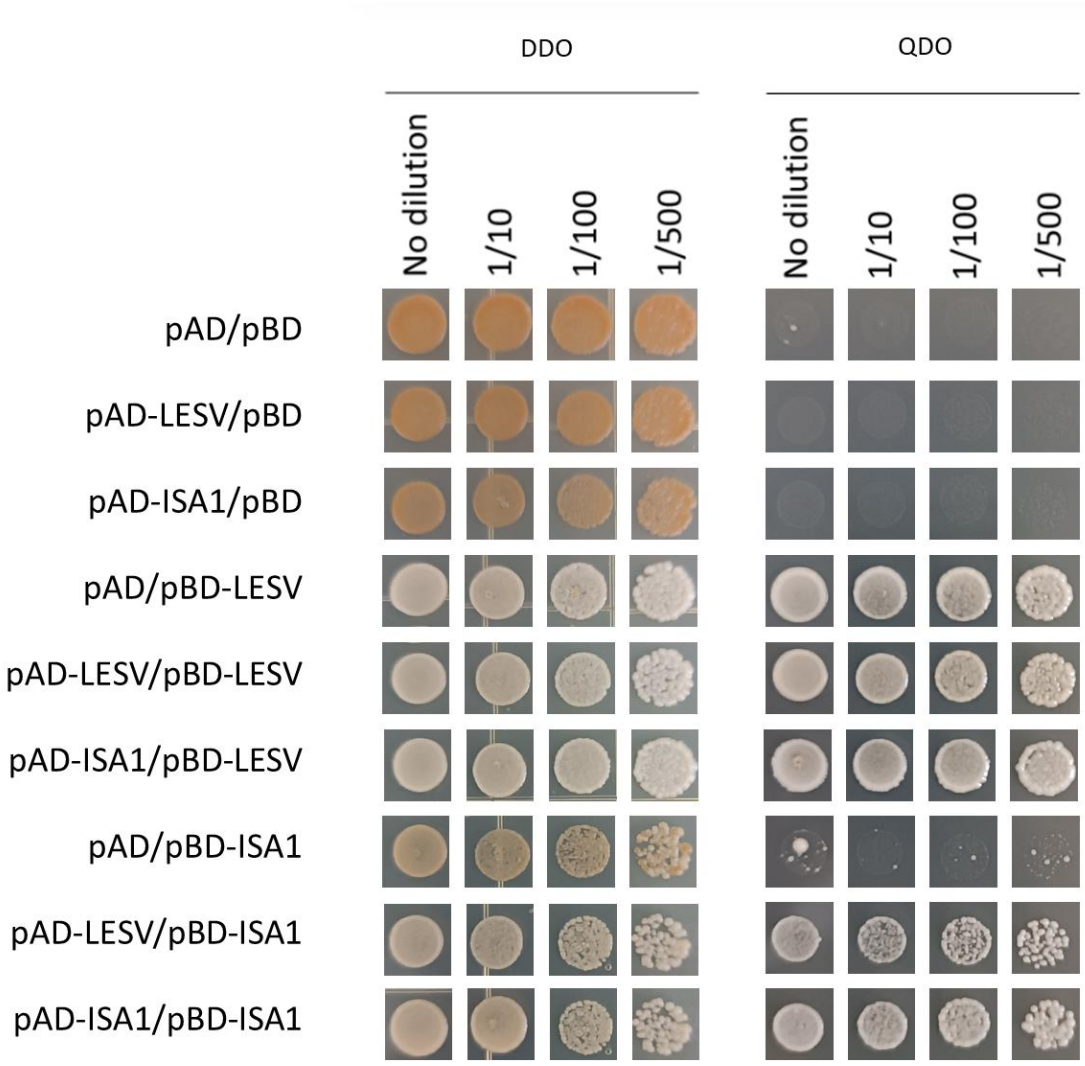

Annex 13 : Yeast two hybrid assay showing LESV and ISA1 physical interaction. Picture was taken after 5 days of growth. AD: activation domain (contained in pGADT7 vector); BD: DNA-binding domain (contained in pGBKT7 vector); DDO (Double Dropout Medium): control medium (SD/-Trp-Leu); QDO (Quadrule Dropout Medium): selective medium (SD/-Trp-Leu-His-Ade).

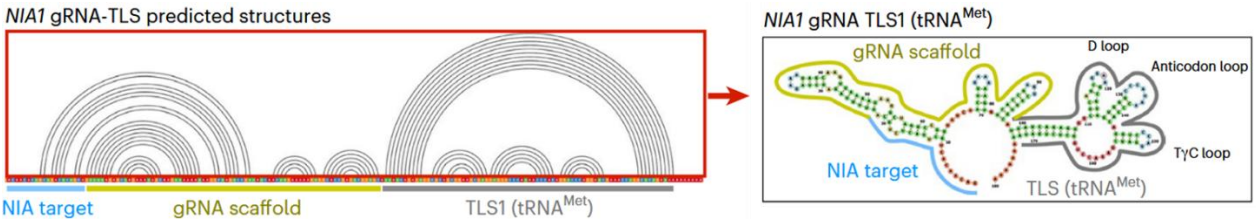

Annex 14: Predicted folding structures of the gNIA1-TLS and Cas9-TLS RNAs according to co-transcriptional folding. (Yang et al., 2023)

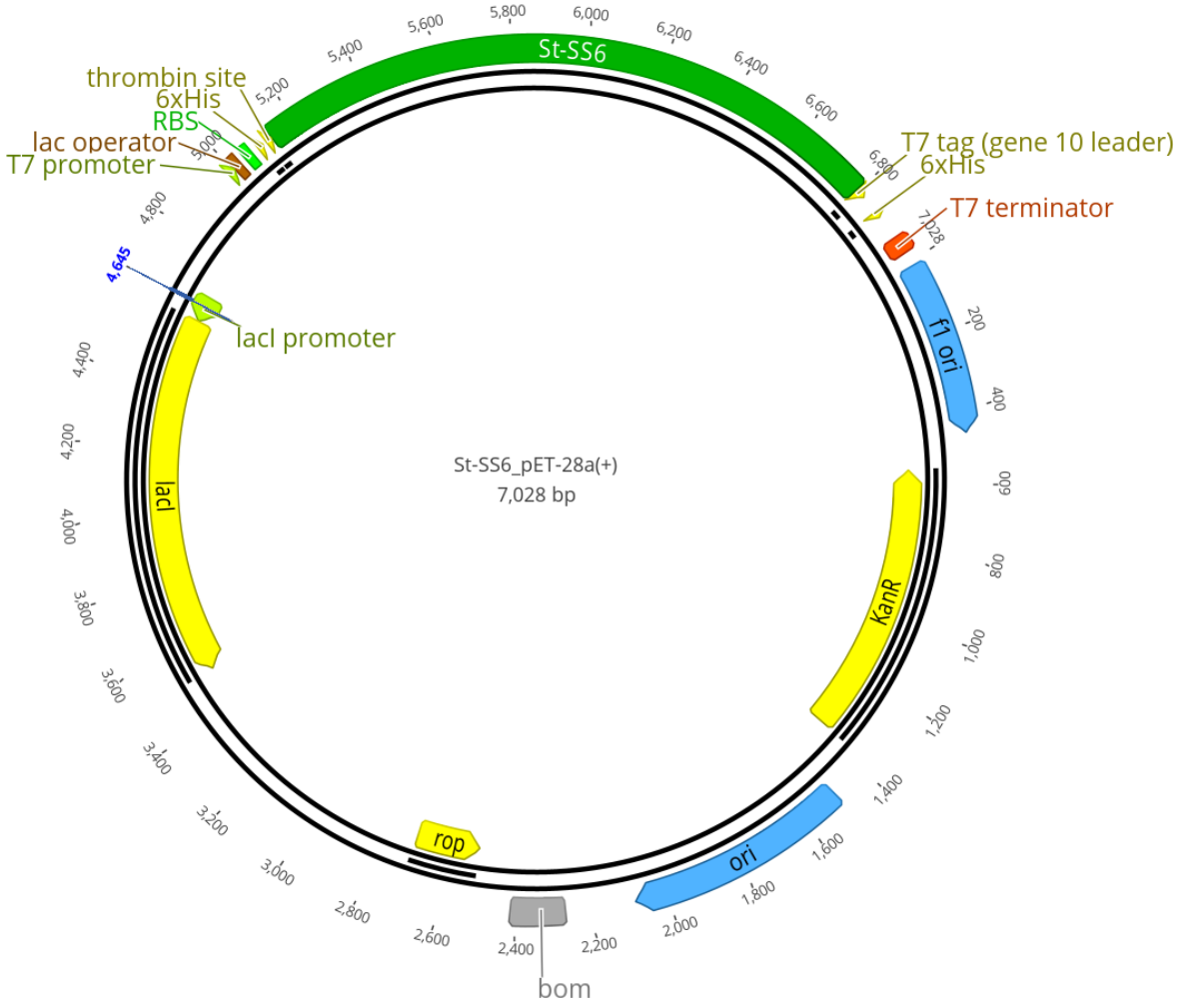

Annex 15 : Map of the plasmid construct used for production of SS6 recombinant protein.